PB98-110414

CONCEPTUAL ANALYSIS OF AN AESTHETIC BRIDGE BARRIER

30 JUL 97

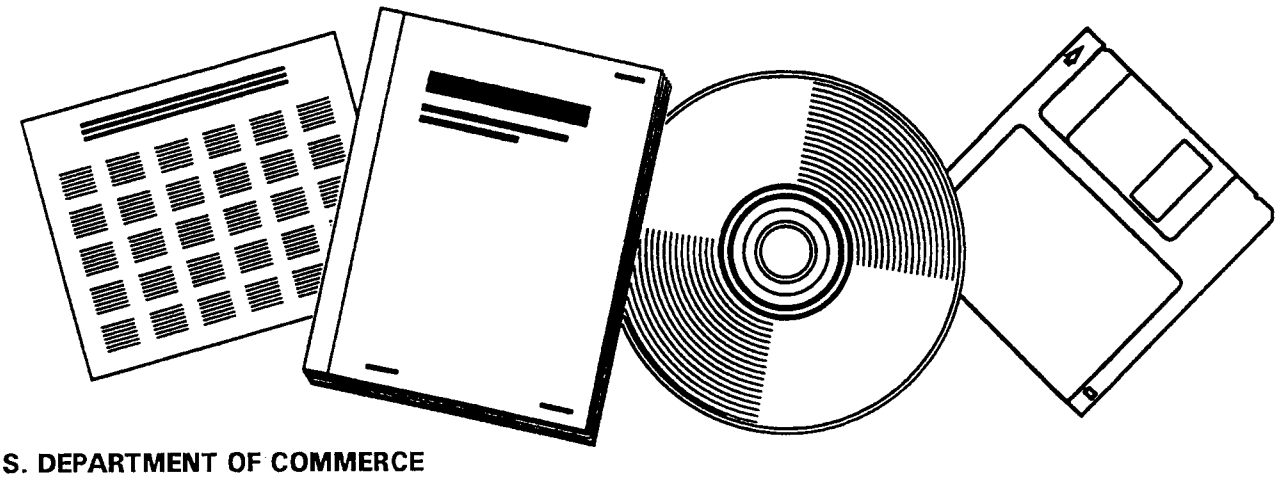

U.S. DEPARTMENT OF COMMERCE
National Technical Information Service

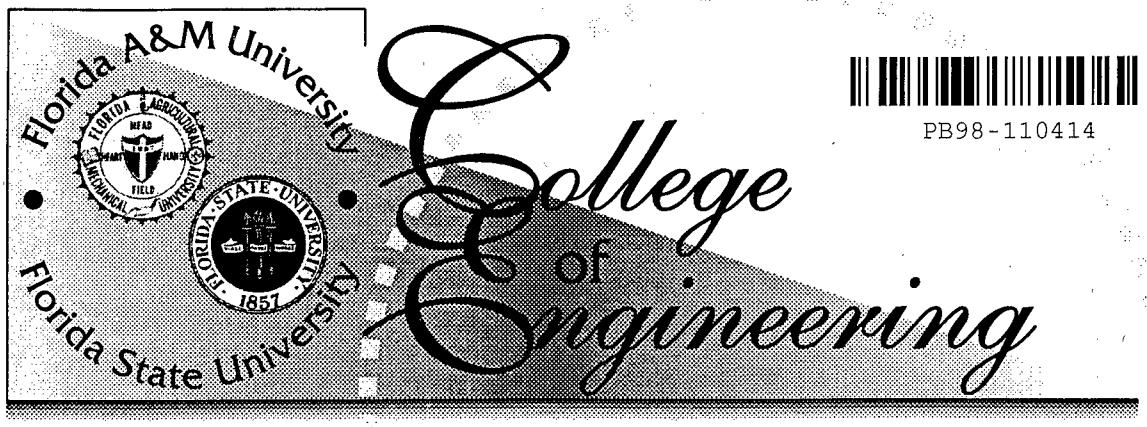

PB98-110414

Conceptual Analysis of an Aesthetic Bridge Barrier

Project Number: WPI-5010750

Final Report

submitted to

Dr. Moussa Issa, P.M.

Florida Department of Transportation

by

Dr. Jerry Wekezer, P.I.

Dr. Ireneusz Kreja

Mr. Chris Gilbert

FAMU-FSU College of Engineering

Tallahassee, Florida

July 30, 1997

Technical Report Documentation Page

1. Report No.	2. PB98-110414	3. Recipient's Catalog No.
WPI-5010750		

4. Title and Subtitle

Conceptual Analysis of an Aesthetic Bridge Barrier

5. Report Date: July 16, 1997

6. Performing Organization Code

8. Performing Organization Report No.

7. Author's
Dr. Jerry Wekezer, P.I.
Dr. Ireneusz Kreja
Mr. Chris Gilbert

9. Performing Organization Name and Address
FAMU-FSU College of Engineering
Civil Engineering Dept.
2525 Pottsdamer St.
Tallahassee, Fl 32310-6046

10. Work Unit No. (TRAIS)

11. Contract or Grant No.

13. Type of Report and Period Covered

12. Sponsoring Agency Name and Address
Florida Department of Transportation
605 Suwannee Street
Tallahassee, FL 32399-0450

14. Sponsoring Agency Code

15. Supplementary Notes
Prepared in cooperation with the US Department of Transportation and Federal Highway Administration

16. Abstract

This report presents computer crash test simulations used in the development of reinforced concrete bridge barriers. Three main categories of barriers are considered: Florida beam and post configuration, Texas T411 barrier, and Modified Standard Florida barrier. The finite element modeling of these barriers sufjected to vehicle impact loading is described in detail. Analysis is performed using LS-DYNAeD, a nonlinear, explicit, three-dimensional finite element code. All barrier models presented are impacted with the 2000kg vehicle model, developed by the Federal Highway Administration, at a speed of 100 km/hr and angle of 25 degrees. Results of simulations imclude impact sequences as well as plots of displacements, velocity and accelerations.

17. Key Words	18. Distribution Statement
LS-DYNA3D, Computer Impact Simulation, Aesthetic Bridge Barrier, Finite Element Modeling Analysis, FDOT Post and Beam, Dynamic Impact Analysis	No restriction This report is available to the public through the National Technical Information Service, Springfield, VA 22161

19. Security Classif. (of this report)	20. Security Classif. (of this page)	21. No. of Pages	22. Price
Unclassified	Unclassified	171	

Form DOT F 1700.7 (8-72)

DISCLAIMER

The opinions, findings, and conclusions expressed in this publication are those of the authors and not necessarily those of the Florida Department of Transportation or the U.S. Department of Transportation.

This publication was prepared in cooperation with the State of Florida Department of Transportation and the U.S. Department of Transportation.

ACKNOWLEDGEMENTS

A special thanks is extended to Dr. Moussa Issa, Dr. Mohsen Shahawy, and Mr. Jerry Potter for their assistance and guidance throughout this project.

Appreciation is also extended to Ms. Wendy J. Davis for her assistance in preparation of this document.

SI* (MODERN METRIC) CONVERSION FACTORS

APPROXIMATE CONVERSIONS TO SI UNITS

Symbol	When You Know	Multiply By	To Find	Symbol
	LENGTH			
in	inches	25.4	millimeters	mm
ft	feet	0.305	meters	m
yd	yards	0.914	meters	m
mi	miles	1.61	kilometers	km
	AREA			
in^2	square inches	645.2	square millimeters	mm^2
ft^2	square feet	0.093	square meters	m^2
yd^2	square yards	0.836	square meters	m^2
ac	acres	0.405	hectares	ha
mi^2	square miles	2.59	square kilometers	km^2
	VOLUME			
fl oz	fluid ounces	29.57	milliliters	mL
gal	gallons	3.785	liters	L
ft^3	cubic feet	0.028	cubic meters	m^3
yd^3	cubic yards	0.765	cubic meters	m^3
NOTE: Volumes greater than 1000 l shall be shown in m^3.				
	MASS			
oz	ounces	28.35	grams	g
lb	pounds	0.454	kilograms	kg
T	short tons (2000 lb)	0.907	megagrams (or "metric ton")	Mg (or "t")
	TEMPERATURE (exact)			
°F	Fahrenheit temperature	5(F-32)/9 or (F-32)/1.8	Celcius temperature	°C
	ILLUMINATION			
fc	foot-candles	10.76	lux	lx
fl	foot-Lamberts	3.426	candela/m^2	cd/m^2
	FORCE and PRESSURE or STRESS			
lbf	poundforce	4.45	newtons	N
lbf/in^2	poundforce per square inch	6.89	kilopascals	kPa

APPROXIMATE CONVERSIONS FROM SI UNITS

Symbol	When You Know	Multiply By	To Find	Symbol
	LENGTH			
mm	millimeters	0.039	inches	in
m	meters	3.28	feet	ft
m	meters	1.09	yards	yd
km	kilometers	0.621	miles	mi
	AREA			
mm^2	square millimeters	0.0016	square inches	in^2
m^2	square meters	10.764	square feet	ft^2
m^2	square meters	1.195	square yards	yd^2
ha	hectares	2.47	acres	ac
km^2	square kilometers	0.386	square miles	mi^2
	VOLUME			
mL	milliliters	0.034	fluid ounces	fl oz
L	liters	0.264	gallons	gal
m^3	cubic meters	35.71	cubic feet	ft^3
m^3	cubic meters	1.307	cubic yards	yd^3
	MASS			
g	grams	0.035	ounces	oz
kg	kilograms	2.202	pounds	lb
Mg (or "t")	megagrams (or "metric ton")	1.103	short tons (2000 lb)	T
	TEMPERATURE (exact)			
°C	Celcius temperature	1.8C + 32	Fahrenheit temperature	°F
	ILLUMINATION			
lx	lux	0.0929	foot-candles	fc
cd/m^2	candela/m^2	0.2919	foot-Lamberts	fl
	FORCE and PRESSURE or STRESS			
N	newtons	0.225	poundforce	lbf
kPa	kilopascals	0.145	poundforce per square inch	lbf/in^2

* SI is the symbol for the International System of Units. Appropriate rounding should be made to comply with Section 4 of ASTM E380.

(Revised September 1993)

TABLE OF CONTENTS

List of Figures

List of Tables

ABSTRACT

This report presents computer crash test simulations used in the development of reinforced concrete bridge barriers. This report discusses new possibilities of computer crash test simulations available today on workstation type computers. Three main categories of reinforced concrete bridge barriers are considered: Florida beam and post configuration, Texas T411 barrier, and the Standard Florida barrier. The finite element modeling of these barriers subjected to vehicle impact loading is described in detail. Analysis is performed using LS-DYNA3D, a nonlinear, explicit, three-dimensional finite element code. All barrier models presented are impacted with the 2000kg vehicle model, developed by the Federal Highway Administration, at a speed of 100 km/hr and angle of 25 degrees. Procedures and problems encountered in the assemblage of a vehicle impact situation are described. Results of simulations include impact sequences as well as plots of displacements, velocities and accelerations. Additionally, optimization tests of barrier geometry for a modification of the existing Standard Florida barrier are supplied, along with recommendations for design improvements and further design considerations for all barriers.

Chapter 1

INTRODUCTION

There is an ever-increasing need around the world for the development of safe, aesthetic, and efficient roadside safety features. As we progress into the twenty-first century, the size and number of vehicles on our nation's roadways continues to grow at an exponential rate. The design and purpose of these safety features is an area of debate. The barrier, sign post, etc. need to be strong enough to handle the impacting force. However, at the same time they need to absorb enough energy from the collision so that the vehicle is not redirected back into traffic. Often the latter can result in many more fatal accidents than if the vehicle was free to leave the roadway. Due to present deficiencies, some argue that roadside barriers should be eliminated.

In the past, the only method for testing and validating bridge barriers was a full-scale crash test. These tests often cost tens of thousands of dollars and provide seconds of data. Finite Element Methods are being utilized in computer crash simulations to determine the adequacy of many new and existing safety structures. Computer crash simulations are proving to be much more cost-effective and efficient.

Finite Element Method programs offer a tool of great potential in the design and development of roadside safety features as well as evaluation of existing features. This type of analysis can help to identify and correct problems before they are discovered in the field. Computer simulations also allow for the prediction of the likely outcome of a full-

scale crash test. Additionally, they can also include in the analysis those conditions that cannot be tested on a full-scale, such as braking and steering changes before impact.

At the present time, there is a cooperative group of seven Universities in the United States of America performing computer crash simulation to evaluate roadside safety features. These Universities include the University of Colorado, George Washington University, University of Iowa, University of Mississippi, University of Nebraska, Texas A&M University, and FAMU-FSU College of Engineering. Research varies from the development of finite element models of a wide range of guardrails to transformer and slip-base supports for sign poles.

History of Impact Simulation Programs

Many programs and computer applications used today had their beginnings as early as the 1960's. At that time, the high cost and scarce supply of computing facilities limited the focus of the research to military applications. Simple models today, such as a bullet penetrating a steel plate, would take many days of writing computer code and even longer for the actual computation time. Impact simulations have also been performed in the automobile industry since that time; however, the purpose of such simulations was the development of the vehicle models. Many of the problems with these programs being utilized for impact simulation revolved around the fact that the programs were not sophisticated enough to handle a problem with so many variables. In the 1980's, the Federal Highway Administration began to make an effort to focus on the development of accurate finite element models of roadside safety hardware.

DYNA3D was first released to the public by Lawrence Livermore National Laboratory (LLNL) in 1976. DYNA3D is an explicit three-dimensional finite element code for analyzing large displacement dynamic responses between two deformable bodies. Since 1980, several new versions of the program have been released, each with better features and fewer bugs than the previous version. LLNL continues work on the development of DYNA3D and new versions of the program are released periodically.

LS-DYNA3D was released by Livermore Software Technology Corporation (LSTC) as a derivative of the public domain DYNA3D. This version of the program supported the automotive applications of finite element software. New versions are always in development and the program's application and utilization is rapidly expanding. While computer simulations using finite element methods is a new concept, they are quickly becoming an important design tool for scientists and engineers all over the world.

Project Objective

The objective of this project is the development of nonlinear finite element models for analyzing bridge barrier design and indicate where further research is needed. In order to facilitate this research, three new, efficient, and aesthetic bridge barriers were selected for computer crash simulation. These barriers represent new models as well as modifications to previously tested rails. This research was performed as part of a cooperative research program with the Florida Department of Transportation (FDOT). The computer programs used were chosen due to availability and recognized use in the crash simulation field. The primary computer program used in this research is

LS-DYNA3D, an explicit three-dimensional finite element code for analyzing large displacement dynamic responses. The program allows for a number of different types of finite elements, from solid to shell to beam elements. A number of different types of elements can be listed in each of these categories. The program provides numerous material models for a variety of material properties including many different kinds of nonlinearity. A special feature of LS-DYNA3D exists in its contact algorithms, which allow the user to examine a broad range of interactions between two bodies. When used in conjunction with related pre- and post-processors, LS-INGRID and LS-TAURUS respectively, these programs can be powerful tools for any designer. Version 936 of LS-DYNA3D was used and the programs were run on a Sun Sparc20 workstation and a Sun ULTRA1 workstation at the FAMU-FSU College of Engineering in Tallahassee, Florida.

Aesthetic Rail Survey

As with any project of this nature, the first step is to perform a literature review of past efforts. In conducting this review, the Texas Transportation Institute (TTI) and the National Crash Analysis Center (NCAC) were contacted to acquire any suitable materials they may posses concerning aesthetic bridge barriers. The FDOT was also contacted for any relevant material that may already be known by the department. In addition to these primary agencies, numerous efforts and many other contacts were made in this search for a new, efficient, and aesthetic bridge rail.

- Several students working on computer impact simulations contributed sketches of

aesthetic bridge rails to be considered for computer crash simulation. The problem that arises is that aesthetics is a very subjective area and what is aesthetic to one person may not be to another.

- Another avenue that was explored with no avail was contacting the Architecture Department at Florida Agricultural & Mechanical University. Several efforts were made to contact professors from the department, who provided little assistance.
- Another similar effort made was to contact the Engineering Graphics class at the FAMU-FSU College of Engineering. Once again, the response was negative. The Engineering Graphics program generally focuses on mechanical engineering applications and the professor felt that the quantity and the quality of the response would probably not be useful for our application.
- The final effort made involved a contest focused towards the undergraduate engineering students at FAMU-FSU College of Engineering, but open to anyone who was interested. A flyer announcing a three hundred dollar prize was distributed throughout the college of engineering and the Florida Department of Transportation with hopes of creative response. A copy of this flyer can be seen in Appendix F of this report. Unfortunately the response to this contest was minimal.

Several aesthetic bridge barriers, which represented past models that might be considered for a retrofit design, were selected based on the survey and the literature review. These barriers represented a variety of styles and construction materials. These structures were presented in a meeting with the Florida Department of Transportation on July 3, 1996. The Florida Department of Transportation was represented by Dr. Moussa

Issa, Dr. Mohsen Shahawy, and Mr. Jerry Potter. FAMU-FSU College of Engineering was represented by Dr. Jerry Wekezer and Mr. Chris Gilbert. A copy of the materials presented at this meeting can be found in Appendix B.

The meeting produced the following potential barriers to be considered for modeling.

- Mr. Jerry Potter expressed interest in a beam and post type rail currently being utilized by the Florida Department of Transportation (see Figure 1-1). This is an older rail in use on many bridges. This rail is currently being replaced with Standart Florida Barriers; however, the FDOT is interested in a feasibility study of a retrofit design.

- The second barrier selected at this meeting was the Texas T411 Rail (see Figure 1-2). This is an aesthetic rail developed and tested at the Texas Transportation Institute. Problems, which have arisen with this rail, make it a good candidate for a retrofit design.

- The third barrier was selected at a December 16th meeting between Dr. Moussa Issa, Dr. Jerry Wekezer, and Chris Gilbert. This barrier is a modification of the existing Florida Barrier (see Figure 1-3). It was proposed that the overall height of the barrier be increased and voids in the top of the barrier be introduced to allow visibility.

A detailed analysis of presented simulations allowed for the formulation of several suggestions for possible improvements and on the direction of further needed research. There have not been any full-scale crash tests performed with the 2000P class vehicle on these barriers. A crash test would be the next step for validation of the numerical simulations.

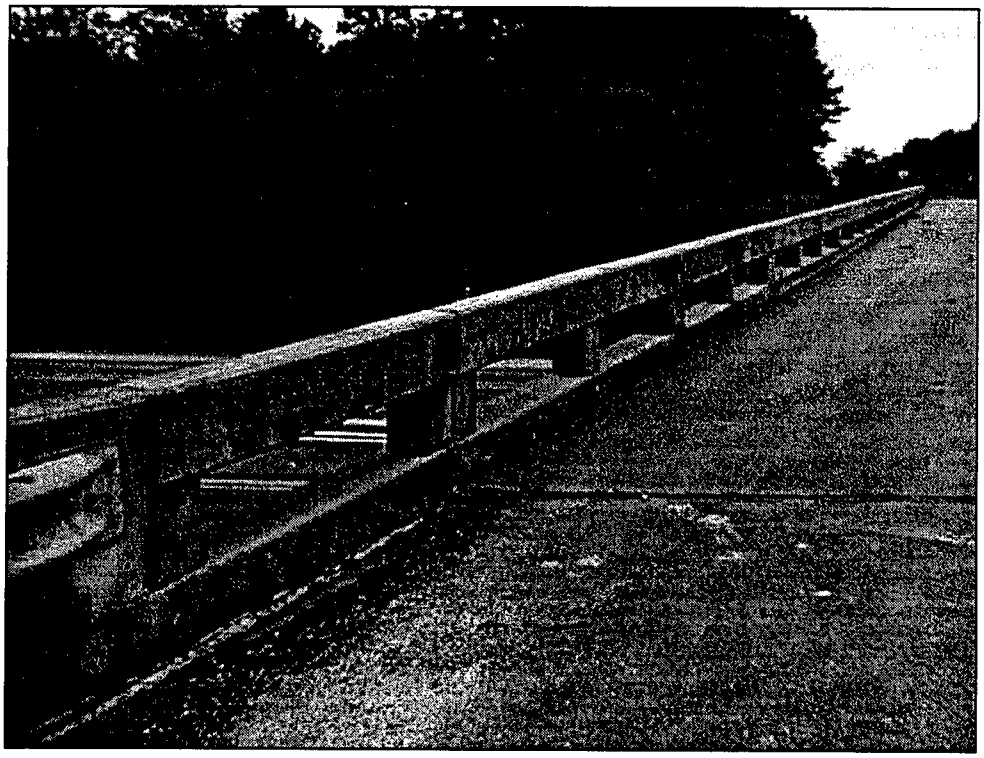

Figure1-1: Photograph of FDOT Beam and Post Rail

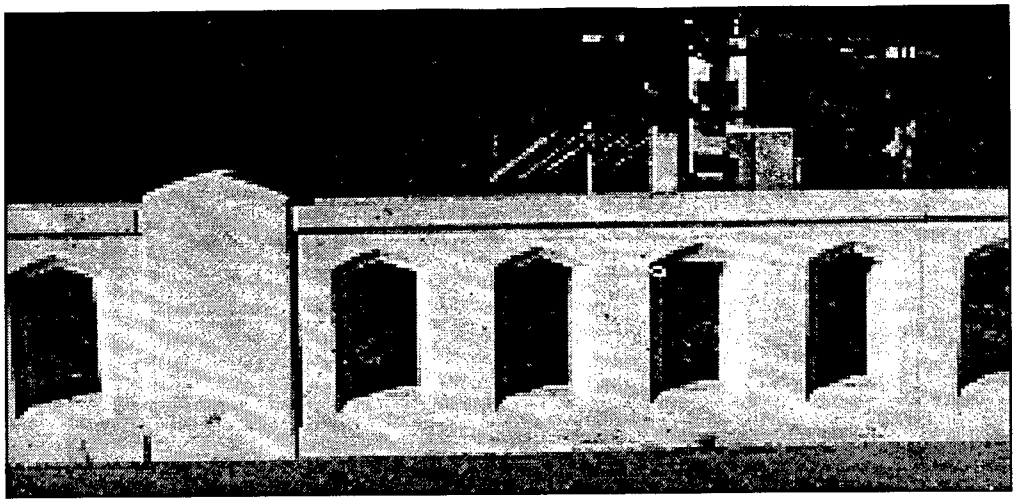

Figure 1-2: Photograph of Texas T411 Bridge Barrier [14]

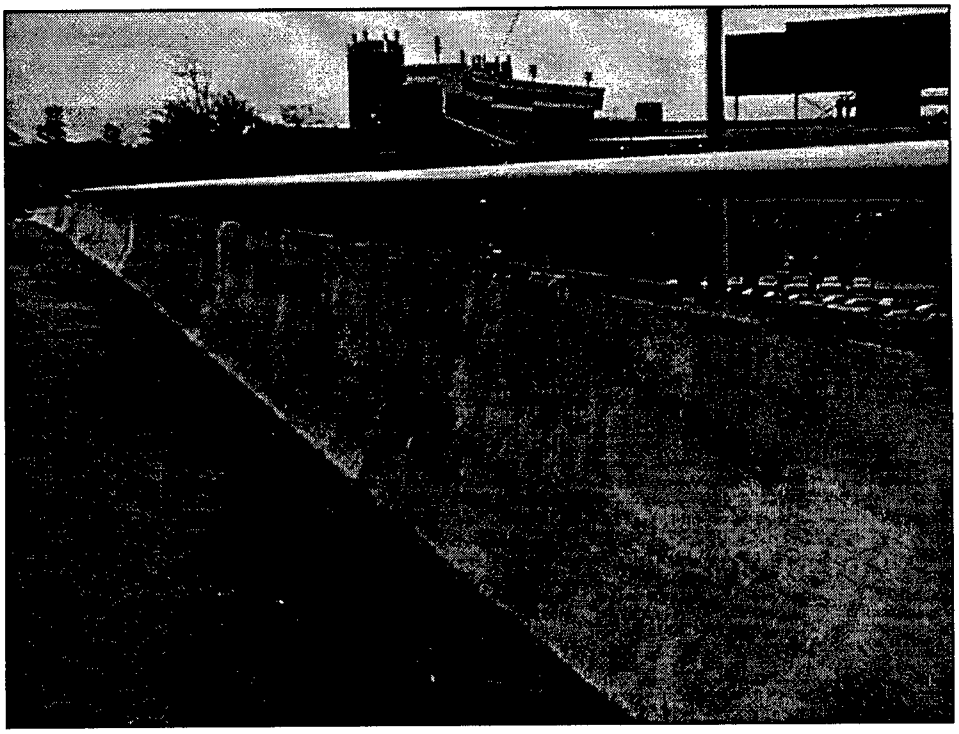

Figure 1-3: Photograph of Standard Florida Barrier with Aluminum Rail

Chapter 2

METHODS OF ANALYSIS

This chapter provides a brief overview of the numerical methods incorporated in this study.

Finite Element Analysis

This section introduces the concepts used in a finite element analysis. It does not attempt to provide a detailed explanation of the finite element method. There are many good sources of detailed explanations such as books by Bathe [31] and Zienkiewicz [32].

In the finite element analysis, a complex region defining a continuum is discretized into simple geometric shapes called finite elements. The material properties and the governing relationships are considered over these elements and expressed in terms of unknown values at element corners (nodes). Instead of solving the problem for the entire body in one operation, equations are formulated for each finite element. These equations are then combined to obtain the solution for the whole body.

Nonlinear, Explicit, Dynamic Problems

Vehicle crash analysis poses many dynamic problems due to nonlinearity. Nonlinearity problems arise in the material models, contact algorithm, and the geometrical deformations in the models. These problems are all considered in the solution.

We can start with a simple model of a single degree of freedom system presented in Figure 2-1. Figure 2-2 shows the free body diagram for the oscillator presented in Figure 2-1. D'Alembert's Principle states that a system may be set into a state of dynamic equilibrium by adding to the external forces a fictitious force which is commonly known as inertia force [39] (see Figure 2-2). One can notice that all forces acting in Figure 2-1 act in 2-2 in addition to an inertia force f_I. Summation of the horizontal forces acting in Figure 2-2 results in the equation of equilibrium:

$$f_I + f_D + f_{INT} = p(t) \tag{2-1}$$

In the case of a linear elastic system, the internal force can be replaced with an elastic force (f_s).

$$f_I + f_D + f_S = p(t) \tag{2-2}$$

With substitutions (see Table A-1) one can obtain the following equation of equilibrium:

$$m\ddot{u} + c\dot{u} + ku = p(t) \tag{2-3}$$

The adequate equation of dynamic equilibrium for a multi degree of freedom system can be given as:

$$M\ddot{U} + C\dot{U} + KU = P(t) \tag{2-4}$$

where M, C, and K are the mass, damping, and stiffness matrices and P is the vector of externally applied loads; and $\ddot{U}$, $\dot{U}$, and U are the displacement, velocity, and acceleration vectors, respectively.

For the nonlinear condition, this equation can be written as:

$$M\ddot{U} + C\dot{U} + f_{INT}(U) = P(t) \tag{2-5}$$

The Central Difference Method (see Figure 2-3) is applied in LS-DYNA3D for the integration of equations of motion.

In this method, it is assumed that the velocity can be expressed by the following approximation [31]:

$$\dot{U}_n = \frac{1}{2\Delta t}(U_{n+1} - U_{n-1}) \tag{2-6}$$

The acceleration is then obtained as:

$$\ddot{U}_n = \frac{1}{\Delta t}\left(\dot{U}_{n+1/2} - \dot{U}_{n-1/2}\right) = \frac{1}{\Delta t}\left(\frac{U_{n+1} - U_n}{\Delta t} - \frac{U_n - U_{n-1}}{\Delta t}\right) \tag{2-7a}$$

$$\ddot{U}_n = \frac{1}{(\Delta t)^2}(U_{n+1} - 2U_n + U_{n-1}) \tag{2-7b}$$

The displacement solution for time t + Δt is determined by considering the equation of equilibrium at time t.

$$M\ddot{U}_n + C\dot{U}_n + KU_n = P_n \tag{2-8}$$

The equations for $\ddot{U}$ and $\dot{U}$ can then be substituted to yield the following equation:

$$\left(\frac{1}{\Delta t^2}M+\frac{1}{2\Delta t}C\right)U_{n+1}=P_n-\left(K-\frac{2}{\Delta t^2}M\right)U_n-\left(\frac{1}{\Delta t^2}M-\frac{1}{2\Delta t}C\right)U_{n-1} \quad (2\text{-}9)$$

From this equation, U_{n+1} can be determined. This is referred to as explicit time integration because it is based on the equilibrium equation at time t_n. Other methods of integration base their solution on equilibrium equations at time $t + \Delta t$ and are commonly referred to as implicit time integration methods. The explicit approach is especially effective when it is implemented together with the lumped mass and damping matrices. With this approach, there is no need to form the global matrices. This feature makes the explicit method of integration particularly suitable for large problems.

The explicit time integration is classified as a conditionally stable method, i.e. a relatively small time step size should be used to obtain a valid solution [31]. In the central difference method, it is important to assure a proper time step Δt:

$$\Delta t \le \Delta t_{cr} = \frac{T_n}{\pi} \quad (2\text{-}10)$$

In this equation, T_n is the smallest period of the finite element assemblage.

Contact Algorithm

A unique feature of LS-DYNA3D exists in its contact algorithms, which allow the user to examine a broad range of interactions between two bodies. The main function of the contact algorithm is to provide a sliding interface with a closure and a separation between two bodies. The first step is to check for the possible penetration of the slave node through the master surface. No further action is performed for the slave node if it does not penetrate. If it penetrates, the interface force, f_i , is applied between the slave

node and its contact point on the master surface. The magnitude of this force is proportional to the value of the penetration, p, and the stiffness factor of the master segment, k_i:

$$f_i = -k_i \cdot p \tag{2-11}$$

with

$$k_i = \gamma \cdot \frac{K_i \cdot A_i^2}{V_i} \tag{2-12}$$

where γ is a scale factor for the interface stiffness (LS-DYNA3D manual [1] recommends to use value 0.10 to provide the stability of solution), K_i is the bulk modulus of the master body, with the V_i standing for the volume and A_i being the face area of the master element that contains the contact point. The more detailed description of the contact algorithm used in LS-DYNA3D can be found in [2].

2.4 Concrete Structures Modeling In LS-DYNA3D

LS-DYNA3D offers a broad range of material models in the explicit dynamic FEM analysis. There are 71 material models listed in LS-DYNA3D output file "d3hsp". After considering impact analysis of concrete structures, twelve material models were initially selected for a more detailed examination (see Table A-2). A more detailed literature study and some numerical experiments followed, allowing the authors to verify the practical applicability of those material models. The findings of this study ar as follows:

- Material no. 17 has been eliminated from the list because the description given in [1]

did not agree with the actual requirements of the program.

- Materials no. 84 & no. 85 have not been included in [1], and therefore the pattern of input data for those materials is unknown.
- Material no. 16 with the smeared reinforcement option provided the most accurate results.

The material properties used for material no. 16 are:

- Compressive strength, f_c' = 27.56 N/mm^2 (27.56 MPa = 4000 psi)
- Young modulus, E = 24838 N/mm^2 (24838 MPa = 3602447 psi)
- Poisson's ratio, ν = 0.180
- Mass density, $\rho = 2.4 \cdot 10^{-9}$ N·s^2/mm^4 ($2.25 \cdot 10^{-4}$ lb·s^2/in^4)
- Shear Modulus, G=10200N/mm^2 (10200 MPa = 1479385 psi)
- Percent reinforcement, p_r = 2.27%
- Tangent modulus reinforcement, ETAN=758.4
- Young modulus reinforcement, E = 206800 N/mm^2 (206800 Mpa = 29993804 psi)
- Poisson's ratio reinforcement, ν = 0.300
- Initial yield stress reinforcement, σ_y=413.7 N/mm^2

The DYNA3D users manual [3] gives a suggested stress strain relationship for material no. 16. For a mixture model of concrete with smeared reinforcement, the strain rate multiplier is taken form the load curve. This multiplier is a scaling factor for the actual yield stress of concrete. This relationship can be seen in Figure 2-4. The numbers specified by the DYNA3D user manual give results consistent for plain concrete [3]. This suggested stress-strain curve was used when modeling the FEM barriers.

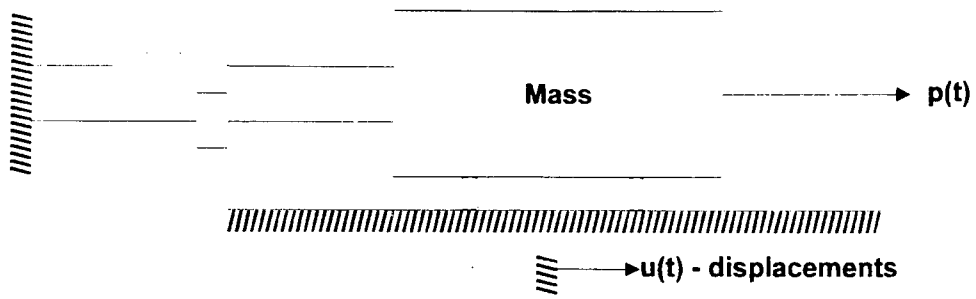

Figure 2-1: Single Degree of Freedom System

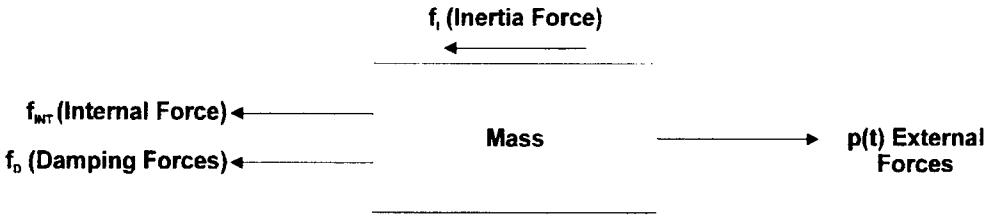

Figure 2-2: Forces acting on Mass

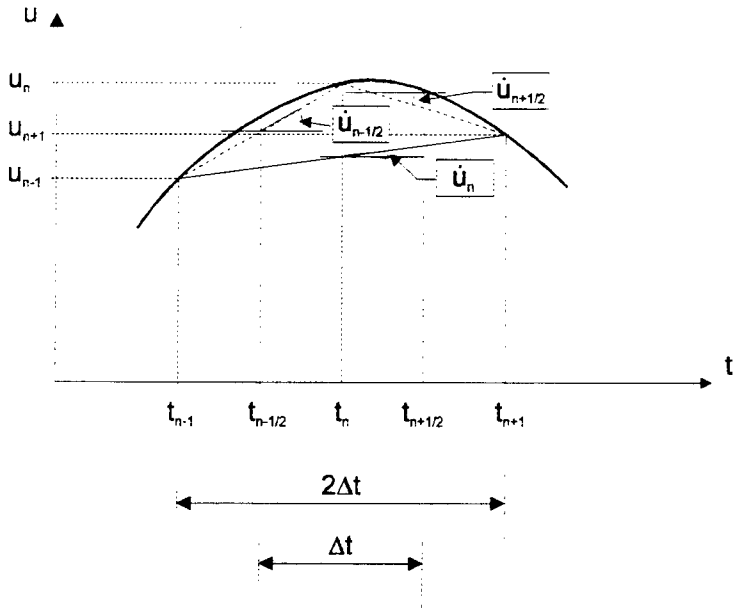

Figure 2-3: Central Difference Method

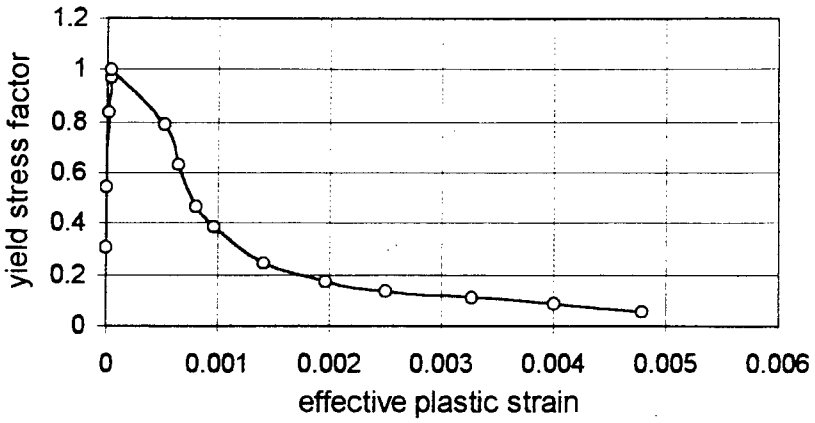

Figure 2-4: Assumed damage curve for material no. 16 (after [3])

CHAPTER 3

FINITE ELEMENT MODELS OF MOTOR VEHICLES

Finite element models of vehicles are increasingly being used in preliminary design analysis, component design, and vehicle crashworthiness evaluation, as well as roadside barrier design. Several vehicle models have been developed and continue to be built with the use of digitizers. Typically, models are created by digitizing surface geometry and storing data in AutoCAD IGES format. These files are then imported into PATRAN, where the finite element mesh can be assembled.

3.1 1991 GM Saturn

The first model developed specifically for roadside hardware analysis was a simple model of a 1991 GM Saturn [8]. The primary purpose of this model was to demonstrate the feasibility of the use of computational nonlinear finite element methods for transportation applications. The vehicle model was used to simulate frontal impacts with slipbase luminaire supports and rigid walls. The finite element model for this vehicle can be seen in Figure 3-1.

3.2 Honda Civic 1981

The next vehicle model developed was that of a 1981 Honda Civic. This vehicle was selected for finite element modeling due to its prevalent use in previous full-scale crash tests. To increase computational time, the front of the vehicle was represented by a dense mesh with a course mesh for the rear of the vehicle. This made the vehicle popular for frontal impact simulations. The model was developed by EASI Engineering and was subsequently refined by Lawrence Livermore National Laboratory (LLNL). The finite element model of this vehicle can be seen in Figure 3-2.

3.3 820C - Ford Festiva 1990

The 820C model represents a generic compact vehicle and is modeled after a 1990 Ford Festiva (see Figure 3-3). This model was developed by the Federal Highway Administration and can be down-loaded from the Internet homepage of the NCAC [30]. The vehicle contains between 4,900 to 5,200 elements depending on the mesh chosen for the front wheels (see Figure 3-4). This vehicle model is slightly lighter than the specifications set by NCHRP Report 350 for an 820C vehicle. NCHRP Report 350 [22] defines an 820C vehicle as having a mass of 820 kg, while the model only has a mass of 706 kg. It should be noted that the 820C vehicle model was originally created and validated for head-on frontal impact with a rigid pole. With this being the case, the developers of the vehicle model were not primarily concerned with the detailed modeling

of the vehicle sides, the suspension system, or the effects of tire friction. Though these factors may not have a significant influence on the response of the vehicle during a head on collision with a rigid barrier, they have a considerable effect upon the vehicle's response during a redirectional impact. [18]

3.4 1991 Ford Taurus

A finite element model of a 1991 Ford Taurus (see Figure 3-5) is available from the National Highway Traffic Safety Administration (NHTSA) homepage, [30]. This model has been used in a variety of crash simulations including:

- Off-set frontal vehicle to vehicle impacts
- frontal rigid wall impacts
- frontal narrow object impacts
- occupant compartment intrusion studies.

One can notice that this is a very detailed model and is too large to be applied on workstation type computers.

3.5 2000P - Chevrolet 2500 Truck

For the purposes of this study, the finite element model of a Chevrolet C-2500 truck was used for all impact simulations. This model was developed by the National Crash Analysis Center in Washington D.C. This model represents the 2000P class of vehicles (see Figure 3-6 and 3-7) referenced in NCHRP Report 350 [22] (see Appendix

B). The model is free to the public and can be down-loaded from the Internet homepage of the NCAC [30]. The vehicle is "ready to go" as is from this location with the exception of geometric relation to the barrier and initial velocity. In addition to these modifications, an accelerometer (see Appendix C.4) is defined at the center of gravity of the vehicle for a common point of comparison.

The model was developed specifically to address vehicle safety issues for roadside hardware design. The vehicle is a regular-cab, fleetside long-box C-2500 with a total length of 5.4 meters and a wheelbase of 3.34 meters with a mass of 2000 kg. The reduced model consists of 10,723 nodes, 8,721 shell elements, 34 beam elements, 337 hexahedron elements and 37 different material models. There are three material types including: Elastic with 9 components, Rigid with 4 components, and Piecewise Linear Isotropic Plastic with 24 components.

This vehicle was selected for all impact simulations for a variety of reasons:

- To date, this model is the most comprehensive and is generally recognized as an accurate finite element model of a vehicle.
- The majority of the tests specified in NCHRP Report 350 [22] require crash tests with both the 820C and the 2000P vehicles. The 2000P vehicle is the larger of the two vehicles and successful simulations between it and the barrier typically illustrates a good barrier design relative to strength requirements. The simulation with the 820C vehicle should still be performed to assure there are no excessively high ridedown accelerations when a relatively smaller vehicle impacts the barrier.

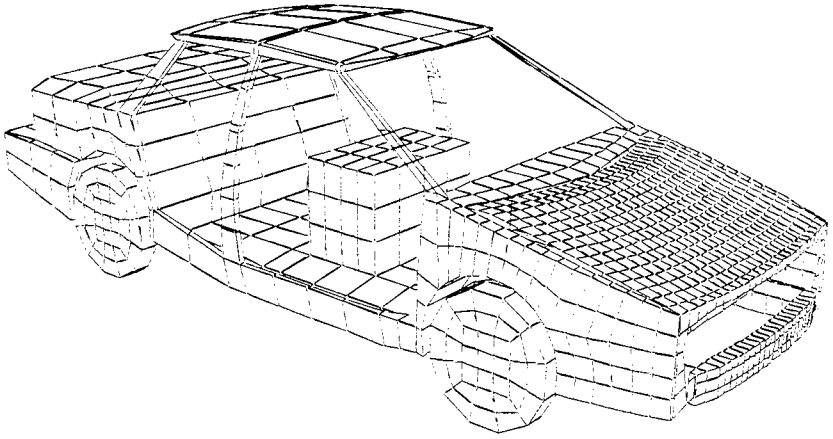

Figure 3-1: FEM of 1991 Saturn [8]

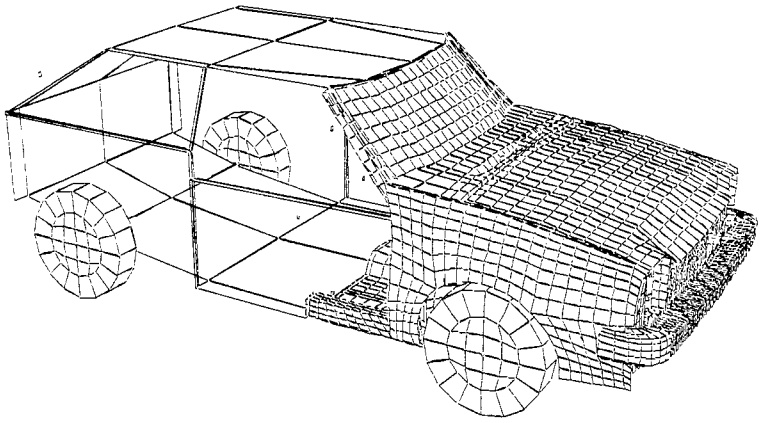

Figure 3-2: FEM of 1981 Honda Civic

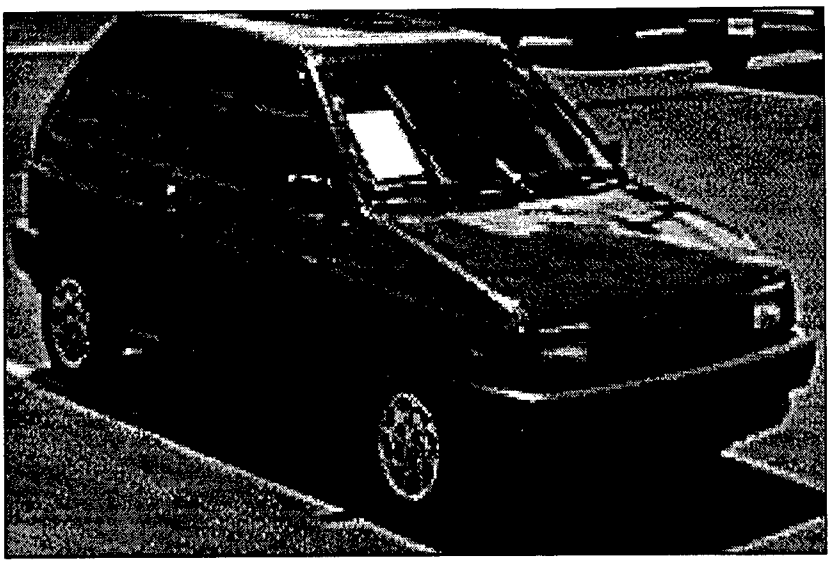

Figure 3-3: Photograph of Ford Festiva

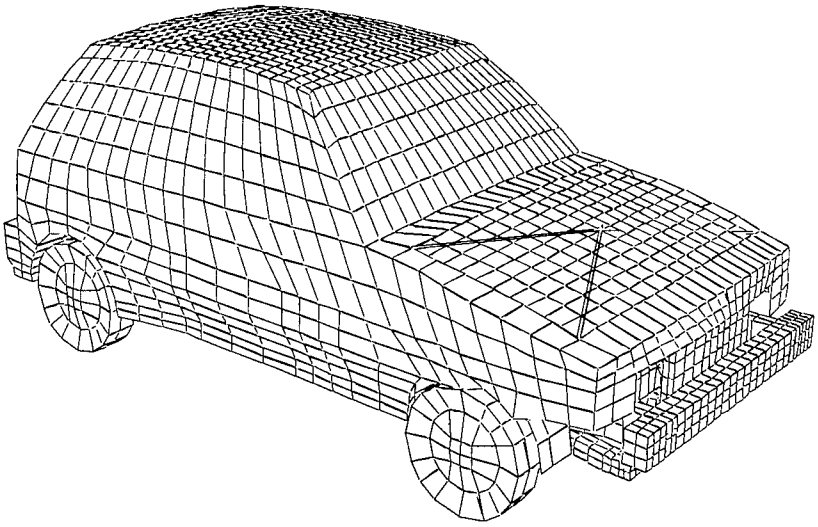

Figure 3-4: Finite Element Model of 820C Vehicle

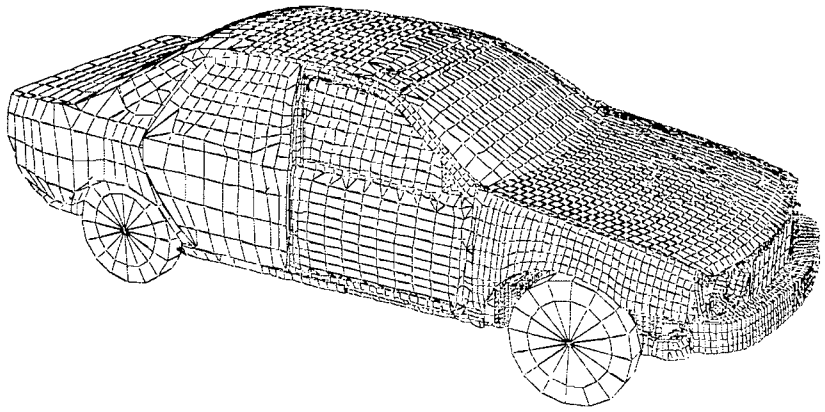

Figure 3-5: FEM of 1991 Ford Taurus

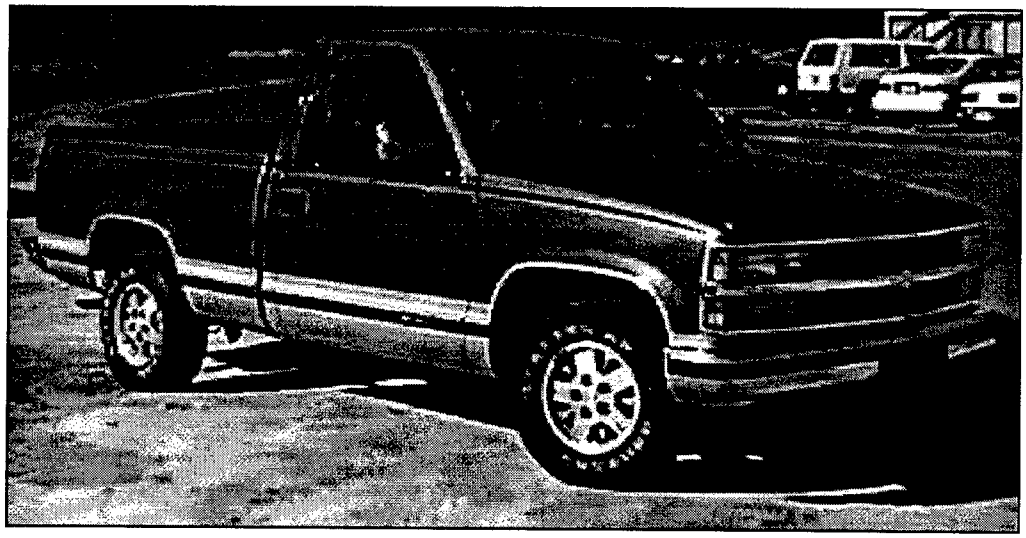

Figure 3-6: Photograph of C-2500 Chevrolet Truck

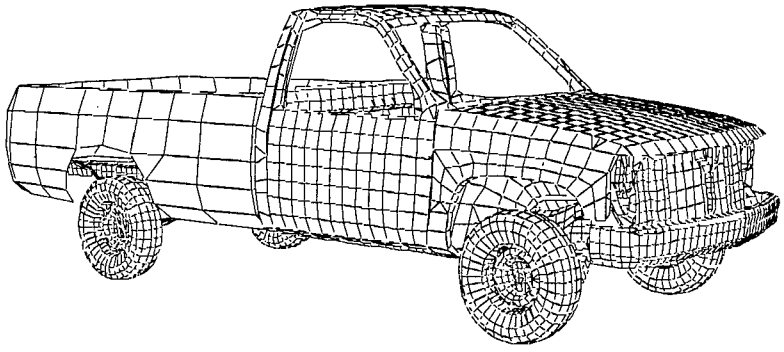

Figure 3-7: FEM of 2000P Vehicle Model

CHAPTER 4

FDOT BEAM AND POST RAIL

The FDOT Beam and Post rail (see Figure 1-1) is a reinforced concrete rail currently in use throughout the State of Florida. This bridge rail was originally developed in the early 1970's. The Florida Department of Transportation is currently replacing these barriers with the Standard Florida Barrier (see Figure 1-3). No full scale crash tests have been performed on this rail and the computer simulation results may lead to a retrofit design of the barrier or reiterate the removal of these barriers from the roadways.

4.1 Description of Rail

The barrier is composed of a beam or rail running parallel to the ground connected by posts at 1.524 m to 2.1336 m (5 to 7 feet) intervals depending upon the bridge superstructure. The common problem area with "rail and post" type barriers is the snagging effect commonly observed between the post and the vehicle. In addition to the normal guidelines for determining the adequacy of these rails, there are several specifications concerning ridedown accelerations. These guidelines are presented in NCHRP Report 350 [22].

4.2 Finite Element Models

The finite element model (FEM) of this rail is developed by first creating the initial geometry of the cross section view of the barrier. This cross section is then meshed with surface quad elements, which make a two-dimensional plane (see Figure 4-1). This plane is then extruded into the Z-direction to give the three dimensional view of the final rail seen in Figure 4-2. The concrete material is modeled with the use of solid hex-8 elements with the smeared model of reinforcing steel. The density of the finite element mesh assumed for the barrier is determined by several factors:

- The capacity of the computer (for workstation version of LS-DYNA3D, the total number of elements in the whole model <vehicle + barrier> cannot exceed 35,000);
- Reasonable computational time, (the smaller the size of elements, the smaller the maximum time step as determined from the stability requirements of the central difference method <see Fig 2-3>);
- The density of the finite element mesh used in the vehicle model (the contact algorithm prefers the adequate mesh density of two objects in contact).
- A maximum aspect ratio of 2 was used for the mesh in all models.

4.2.1 FDOT Beam and Post

Two models of this rail were developed for crash simulation with the 2000P truck model (Figures 4-2 & 3). The first model created with posts space at 1.524 m (5 feet) and the entire barrier was modeled as continuous. It was later decided to introduce a 19.05 mm (3/4 inch) expansion joint at 9.144 m (30 feet) intervals and increase the post spacing to 1.8288 m (6 feet). The second model consisted of two 9.144 m (30 feet) sections.

4.2.1.1 FDOT Beam and Post without Expansion Joint

This rail is comprised of 23,170 solid elements and is 18.593 m (61 feet) long. Results of computer simulations can be seen in section 6.4 of this report.

The material model used for this rail was material 16 with smeared reinforcement. The parameters for this material are presented below. These parameters represent a combination of the description presented in [3] and the actual constants used by the Florida Department of Transportation [41].

- Tensile cutoff, σ_f = 2.586 Mpa (375 psi)
- Cohesion, a_0 = 6.464 Mpa (938 psi)
- Pressure hardening coefficient, a_1 = 0.3333
- Pressure hardening coefficient, a_2 = 0.01289 mm^2/N ($8.88 \cdot 10^{-5}$ in^2/lb)
- Cohesion for failed material, a_{0f} = 2.586 Mpa (375 psi)
- Pressure hardening coefficient for failed material, a_{1f} = 1.5
- Damage scaling factor, b_1 = 1.25
- Damage curve
- Equation of State (EOS)
- Effective plastic strain (EPS 1-16)
- Effective stress (ES 1-16)

4.2.1.2 FDOT Beam and Post with Expansion Joints

This rail finite element model is constructed of 23,656 solid elements and is 18.916 m (62 feet) long. The results of computer simulations for this model can be seen in section 4.5 and Appendix A of this report.

4.2.2 Modified FDOT Beam and Post Rail

Reducing the existing snagging effect is the main objective for the Modified FDOT Beam and Post rail. A W-Beam type rail (see Figure 4-5) is constructed over the front of the posts to reduce the interaction between the post and the vehicle. A cross-section of the resulting combination barrier can be seen in Figure 4-6. The standard W-beam is used in several different barriers and can vary slightly in dimensions. Once again, two finite element models were created (one with expansion joints and a second without joints). The same concrete material properties were used as above (see section 4.2.1.1).

4.2.2.1 Modified FDOT Beam and Post without Expansion Joints

The finite element model of this 15.545 m (51 feet) rail (see Figure 4-7)) is composed of 20,238 solid elements and 2,853 shell elements. The bolted connection between the concrete post and the W-beam is modeled as an elastic-plastic spring. After computer simulations, unrealistic deformations were observed in these elements, therefore modifications of this connection model were made in the development of the Modified FDOT Beam and Post with Expansion Joints model (see Section 4.2.2.2). The results of computer simulations for this model are presented in section 4.5 and in Appendix A of this report.

4.2.2.2 Modified FDOT Beam and Post with Expansion Joints

The finite element model of this rail (see Figure 4-8) is comprised of 21,414 solid elements and 3,123 shell elements. The length of this barrier is 17.087 m (56 feet). As stated earlier, a more detailed investigation into the connection model between the

concrete post and the W-beam was considered.

It is assumed that the real W-beam is connected to the concrete post with the steel bolts of diameter equal to 8 mm (5/16 inch). The limit tension force, S_n, for such a connection is taken after [34] to be 20,000 N. Consequently, the limit shear force, S_s, is estimated according to the relation:

$$S_s = \frac{S_n}{\sqrt{3}} = \frac{20{,}000}{\sqrt{3}} = 11{,}547 \text{ N}$$

The models of constrained connections available in Ls-dyna3d contain the *CONSTRAINED_SPOTWELD type connection that can be used with a brittle failure criterion:

$$\left(\frac{|f_n|}{S_n}\right)^2 + \left(\frac{|f_s|}{S_s}\right)^2 \geq 1$$

where f_n and f_s are the normal, and shear interface force, respectively. The examination of the bolt connection as reported in [34] and supported with the practical experience suggests rather ductile than brittle form of damage. To make the model capable to represent a pre-failure elastic behavior, an additional grid of four beam elements has been introduced to link the spotweld to four nodes of the W-beam FE model. Computer simulations can be seen in sections 4.4, 4.5, and Appendix A of this report. Although 8 mm bolts were initially selected for analysis, they did not perform well and a 16 mm (5/8 inch) bolted connection is recommended.

4.3 Computer Crash Simulations - Summary

All simulations are between the FDOT and the Modified FDOT Beam and Post and the

2000P Chevrolet Pickup vehicle model traveling at 100 km/hr with a 25 degree angle of impact. For all of the simulations the coefficients of friction between the vehicle and barrier are μ_{static}=0.35 and $\mu_{dynamic}$=0.3. The coefficients of friction between the vehicle and the ground are μ_{static}=0.6 and $\mu_{dynamic}$=0.5. The time duration of the simulations is 0.125 sec. The point of impact for the barriers without expansion joints is at the center of the post, and 152 mm (6 in.) from the post for the barriers with expansion joints.

4.4 Simulations 4-2 and 4-4: Impact Sequences

Simulation 4-2 is an impact between the Modified FDOT Beam and Post without expansion joints and the 2000P vehicle model. Comparing the impact sequences of simulation 4-1 (Figures A-1a&b) to simulation 4-2 (Figures A-2a&b), one can notice an improvement in the redirection of the truck with the Modified FDOT Beam and Post. From the top view in Figure A-2b, one can notice that the vehicle is beginning to yaw properly towards the front face of the barrier and that the tires of the truck do not loose contact with the ground surface until the final stages. The simulation was terminated after 0.105 seconds as the W-beam appeared to have served its purpose in that snagging of the post was substantially reduced. Figures A-2a and A-2b appear to illustrate a relatively smooth redirection of the vehicle; however, a more detailed analysis (see section 4.5) shows that this barrier does not meet the criteria set forth in NCHRP Report 350 [22].

Simulation 4-3 (see Figures A-3a&b) is similar to Simulation 4-1. Simulation 4-4 is an impact between the Modified FDOT Beam and Post with expansion joints and the 2000P vehicle model. Figures A-4a&b appear to illustrate a relatively smooth redirection

of the vehicle. There is great similarity between simulation 4-4 and simulation 4-2. The main difference is the failure of the connection between the barrier and the w-beam. The top views of Figure A-4a show that the vehicle is beginning to yaw properly towards the front face of the barrier along with failure of several of the bolted connections between the concrete post and the w-beam. Severe damage to the w-beam can be observed at midspan between two posts. From FigureA-4b, one can notice the end bolt has broken, and the w-beam seems to be wrapping around the truck counter-clockwise and falling to the ground.

4.5 Analysis of Results: Simulations 4-1 through 4-4

The output given by the accelerometer defined in Appendix C.4 was analyzed graphically. For simulations 4-1 and 4-2, the first graph (Figure A-5) represents the displacement of the vehicle. The coordinate system for displacement is in the global coordinate system (see Figure 4-9). The values represent the displacement of the truck's center of gravity with respect to the whole system. The distance measured represents how far the car travels with respect to the barrier. The X-direction is defined positive normal to the front face of the barrier, the Y-direction is defined positive normal to the ground (towards the sky), and the Z-direction is defined positive along the guardrail opposite the direction the vehicle is moving.

The Z displacement shows that the vehicle has traversed a greater distance along the barrier when the Modified FDOT Beam and Post Rail was used as compared to the FDOT Beam and Post. This is due to the presence of the W-beam, which eliminated the snagging effect and facilitated a smoother redirection of the vehicle

The next graph (Figure A-6) shows the time history plots for X, Y, and Z velocities respectively. All velocity outputs are in the local coordinate system as specified in the accelerometer definition. The vehicle is initially moving 100km/hr in the X-direction.

The velocity shows that the rate at which the vehicle came to rest was much less severe with the addition of the W-beam. The Z velocity shows where the vehicle severely snagged the post causing the vehicle to loose contact with the ground (negative Z-direction). This effect was greatly reduced with the Modified FDOT Beam and Post Rail.

The time history plots for the acceleration in the X, Y, and Z direction (Figures A-7 through A-9) are also taken at the center of gravity of the vehicle in the global coordinate system. A 10 ms average is also used due to the averaging done to full-scale crash test data. NCHRP Report 350 [22] reports that all accelerations should be evaluated by averaging values over a 10ms period. Comparing this averaging to the actual accelerations, one can notice the smoothing effect the averaging has on the graph. This method reports a more reasonable result of what is actually felt by the occupant in the vehicle. There is a considerable decrease in acceleration observed with the addition of a W-beam.

Simulations 4-3 and 4-4 have similar output data for displacement, velocity, and acceleration. This data can be seen in Figures A-10 through A-14. Maximum values for all four simulations are given in Table 4-1.

Figures A-15 and A-16 present the correlation between the impact simulations and the longitudinal acceleration (local X-direction) for simulations 4-1 and 4-2. One can

notice three primary acceleration peaks, points A, B, and C. Point A, corresponds to the initial point of contact between the bumper of the truck and the rail of the barrier. Point B represents the combined effect of contact between the tire and the bumper of the truck model with the barrier. Point C represents the action between the tire and the frame of the truck.

Figures A-17 and A-18 present the correlation between the impact simulations and the longitudinal acceleration (local X-direction) of the accelerometer at the center of gravity of the truck for simulations 4-3 and 4-4.

Examining Figure A-17, one can notice three primary peaks of longitudinal acceleration, points A, B, and C. Point A corresponds to the initial point of contact between the tire of the truck model and the continuous bottom rail. Point B represents contact between the bumper of the truck and the post of the barrier model. Point C corresponds to the action between the tire of the vehicle and the post of the barrier.

Studying Figure A-18, four major peaks of longitudinal acceleration can be identified: points A, B, C, and D. Point A represents the moment of contact between the bumper of the vehicle and the rail of the barrier. Point B illustrates the contact between the tire of the truck and the bottom beam at the ground level. Point C represents the contact between the tire and the post of the barrier. This point corresponds to the maximum deceleration of the center of gravity of the truck model. The maximum peak on the graph averaged to a lower 10 ms average acceleration due to the short duration of time for the spike. Point D corresponds to the contact between the tire and the frame of the truck.

In the following, the concern is focused on the upper beam of the post and beam

concrete barrier. One can expect, that the extreme conditions for this 1829 mm (6 feet) span beam occur when the large normal force resulted from the truck impact acts at the midspan of the beam. Examining the sequence of X-displacement fringes, it was found that such conditions can be related to the time, t = 0.039 seconds. The fringes of the X-displacements at that configuration are presented in Figure A-19. Recalling that the global X-direction is defined as positive when directed normal outwards the front face of the barrier, the extreme negative displacement should be in the midspan at the top fiber. The displacements at the top of the barrier vary from about -1.5 mm at the post to the extreme value -4.4 mm in the mid span.

Figure A-20 illustrates the fringe plot of the Z-stress at time t = 0.039 seconds. Analyzing this plot, one can clearly notice the compression zone on the front face of the barrier and the tension zone in the rear face of the barrier. The maximum compressive stress in the top rail of the barrier is -21.24 MPa, while the maximum tensile stress on the rear face of the barrier is 12.51 MPa. At first glance one can conclude that the level of the tension stress is out of range for the concrete. This statement is correct; however, one should also remember that material 16 represents the reinforced concrete. The concept of the smeared reinforcement used in LS-DYNA3D assumes that the limit stress level for the reinforced concrete, f_{rc}, is taken as [4-1]

$$f_{rc} = \frac{100 - p_r}{100} f_c + \frac{p_r}{100} f_s \qquad (4\text{-}1)$$

where f_c is the limit stress for the concrete, f_s represents the yield stress in steel, and p_r stands for the percentage of the reinforcement. Assuming for tension, f_c = 2.586 MPa, f_s = 413.7 MPa (neglecting the strain hardening) and p_r = 2.27 one can obtain f_{rc} = 12.1

MPa. Additionally, the strain rate effect should be included which, for the average strain rate equal to 0.3, gives the stress multiplier over 1.3.

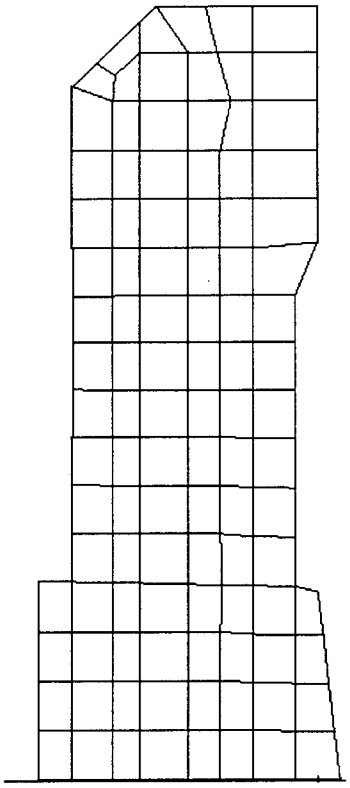

Figure 4-1: 2-D Cross Section View of FEM of FDOT Beam and Post Rail

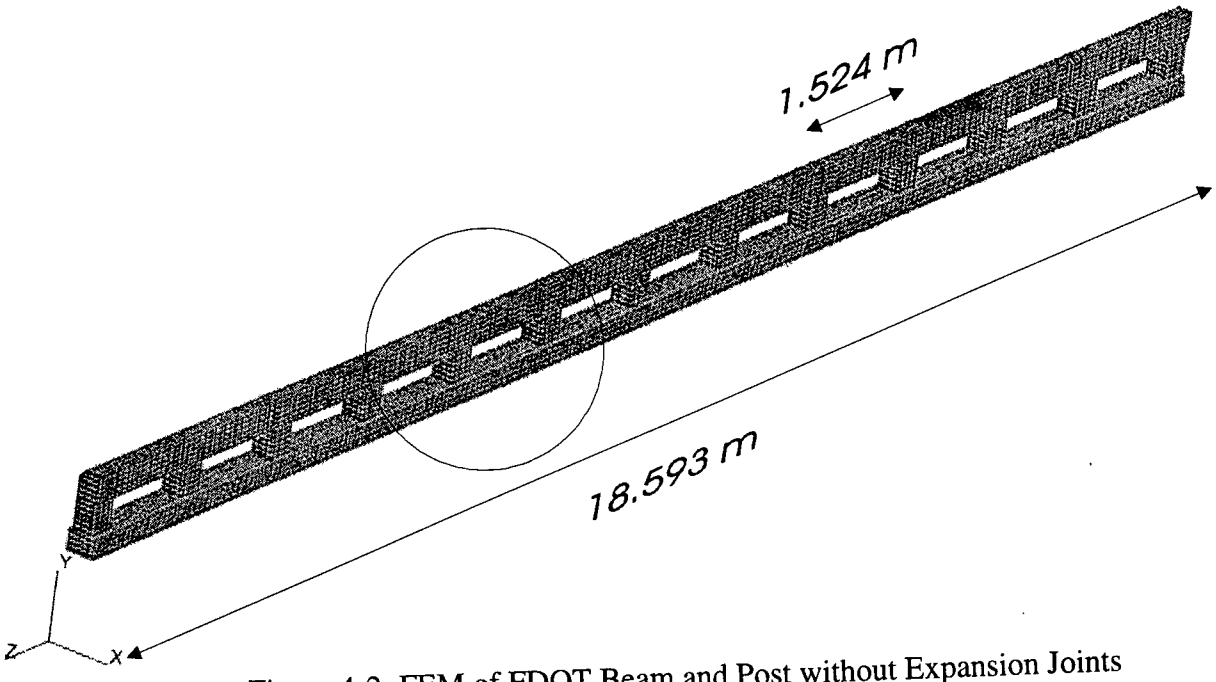

Figure 4-2: FEM of FDOT Beam and Post without Expansion Joints

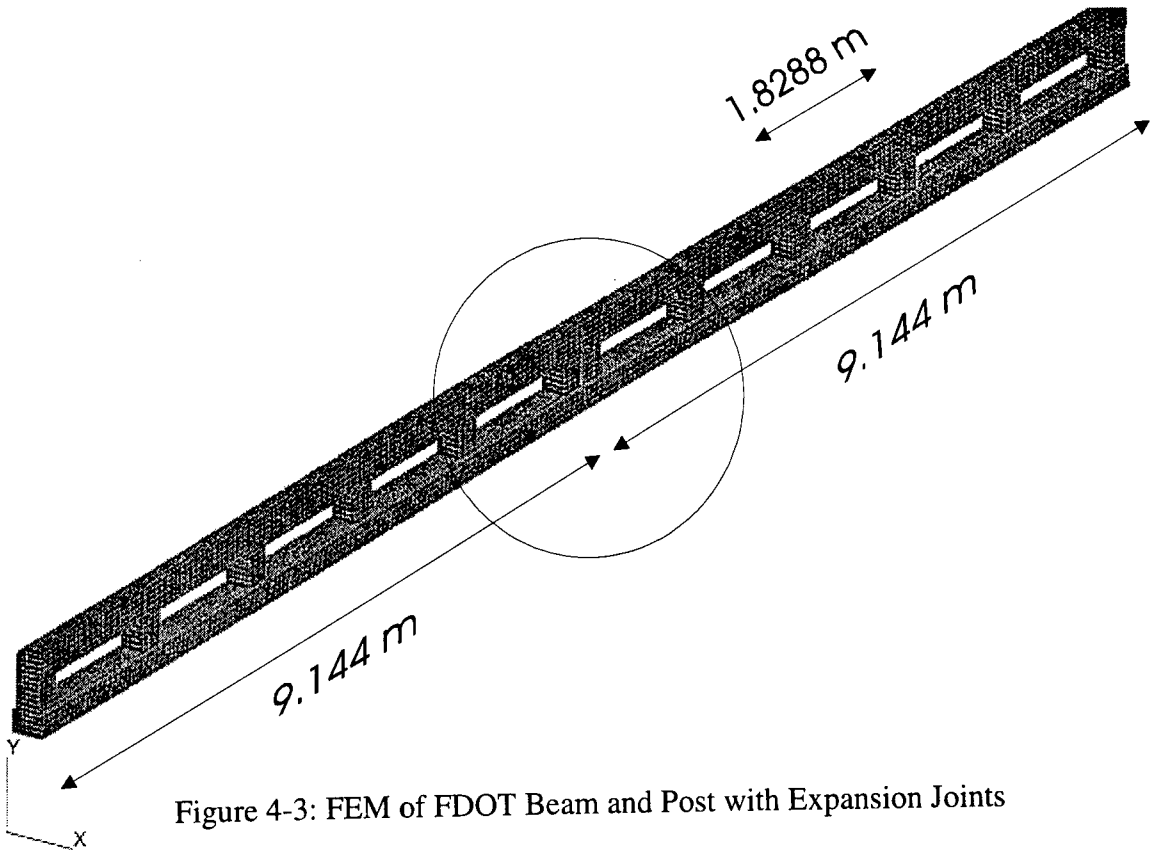

Figure 4-3: FEM of FDOT Beam and Post with Expansion Joints

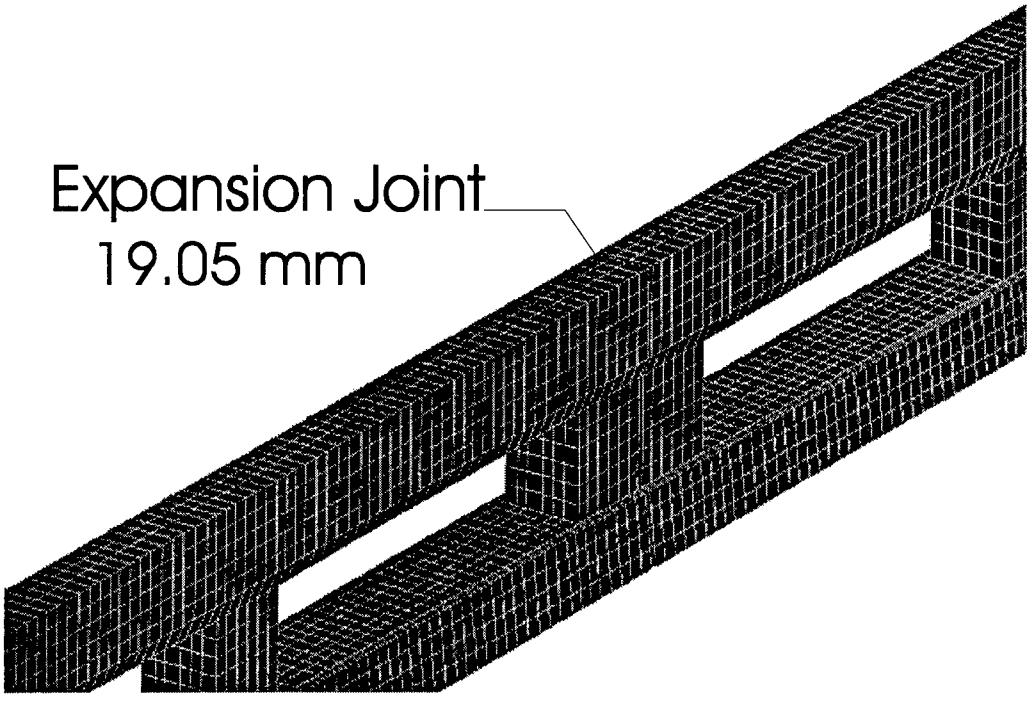

Figure 4-4: Zoom View of FEM of FDOT Beam and Post with Expansion Joints

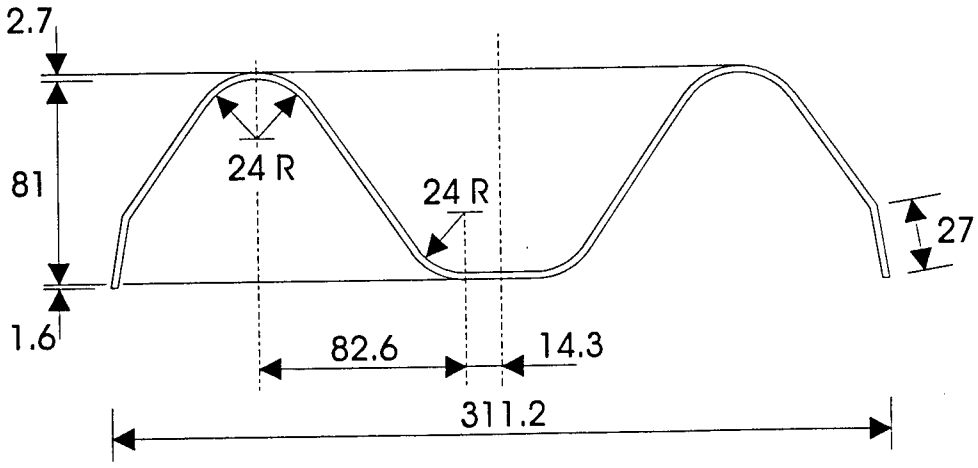

Figure 4-5: Cross sectional details of W-beam

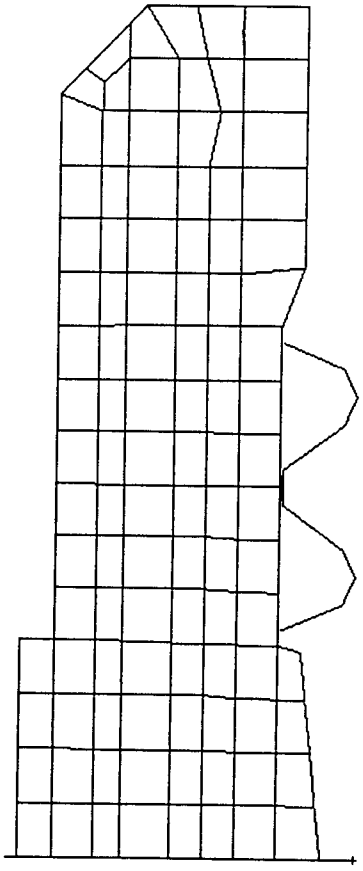

Figure 4-6: Cross-Section view of FEM of Modified FDOT Beam and Post

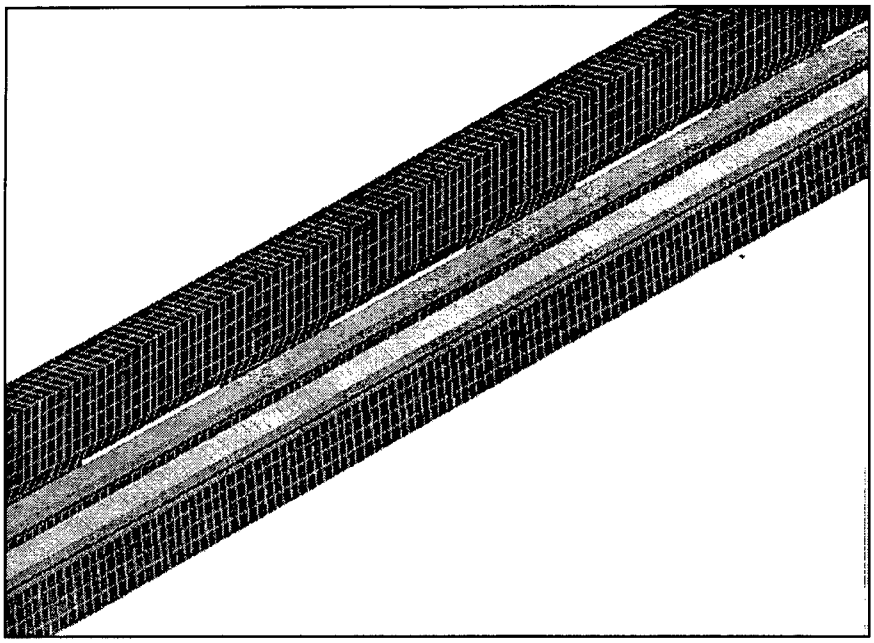

Figure 4-7: Zoom View of FEM of Modified FDOT Beam and Post without Expansion Joints

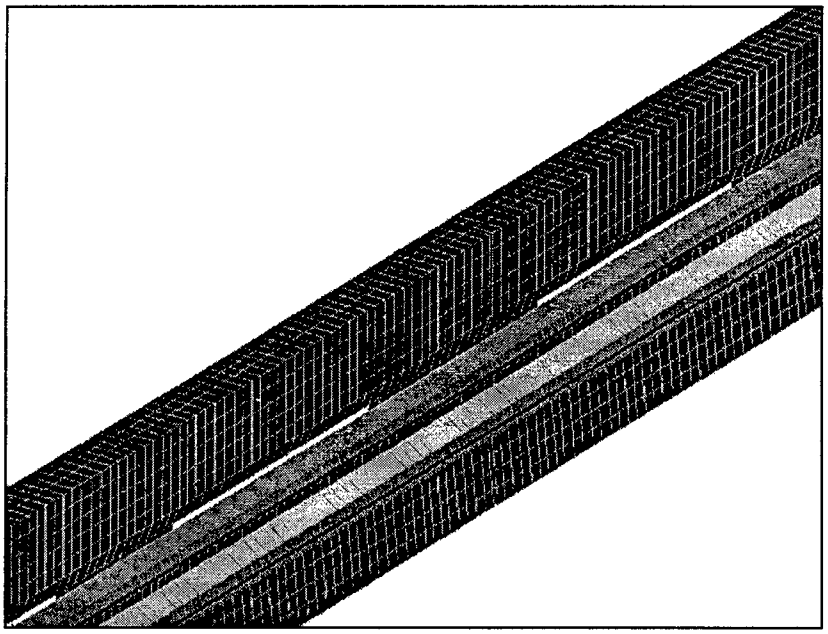

Figure 4-8: Zoom View of FEM Modified FDOT Beam and Post with Expansion Joints

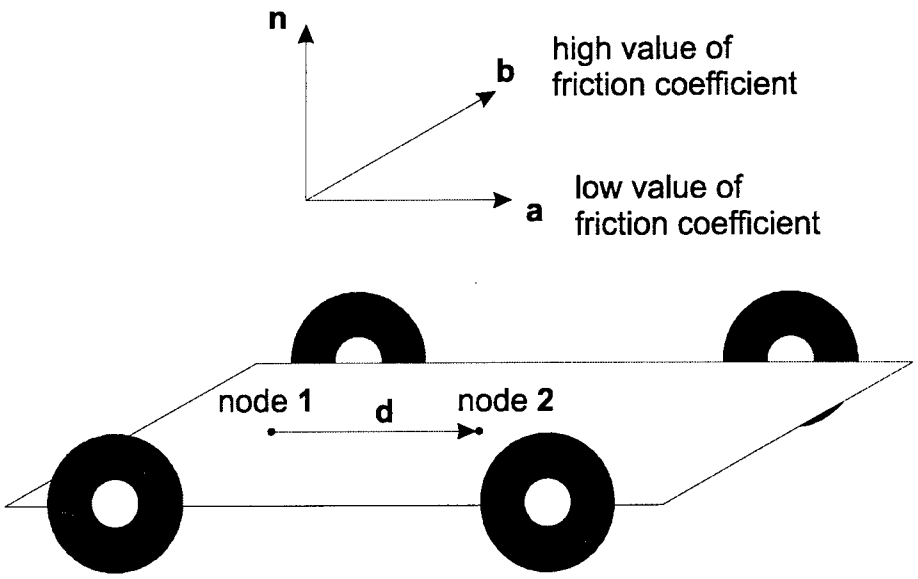

a = direction the vehicle is moving
b = perpendicular to the direction of motion
$\mu_{sa} = 0.0$ (free rolling)
$\mu_{ka} = 0.0$ (free rolling)
$\mu_{sb} = 0.6$ (static)
$\mu_{kb} = 0.5$ (dynamic)

Figure 4-9: Coordinate System of the Vehicles Center of Gravity

CHAPTER 5

TEXAS T411 BRIDGE BARRIER

The Texas T411 Bridge Rail was suggested around 1990 as a result of the search for an aesthetic reinforced concrete bridge barrier. This rail was evaluated in crash tests performed at the Texas Transportation Institute [14]. A photograph of the rail at the Texas Transportation Institute used for the full scale crash tests can be viewed in Figure 1-2. This rail was crash tested in accordance with NCHRP Report 230 [36]; however, this is now out of date as NCHRP Report 350 [22] was developed and implemented in 1993 and the barrier should now be tested according to the new standards established by [22]. Two full scale crash tests were performed on the rail; Test 10 with a 4,500-lb vehicle striking the barrier at 60 mph, at 25 degrees, and Test S13 with an 1,800-lb vehicle at 60 mph, at 20 degrees.

5.1 Description of Texas T411 Bridge Barrier

The dimensions of the guard fence are 812.8 mm high by 304.8 mm thick (32 in. high by 12 in. thick) with 203.2 mm by 457.2 mm (8 in. by 18 in.) high openings spaced

at 457.2 mm (18 in.) center to center [14]. This rail is suggested as appropriate for an urban environment.

5.2 Finite Element Models

The finite element model of this rail was developed in a similar fashion to the FDOT Beam and Post Rail. The lengths of the models presented in this chapter are smaller than that of the other barriers considered. This is due to the complex geometry of the rail, which made a dense cross-sectional mesh necessary. The material model used for this rail is material 16 with smeared reinforcement (see section 4.2.1.1).

5.2.1 Texas T411 Bridge Barrier

The finite element model can be seen in Figures 5-1 and 5-2. This rail is composed of 24,416 solid elements and is 12.014 m (40 feet) long. The results of computer simulations for this model are presented in section 5.4 and Appendix A.

5.2.2 Modified Texas T411 Bridge Barriers

The full scale crash tests showed that the primary problem with the Texas T411 barrier was the excessively high ridedown accelerations due to the snagging effect of the hollow sections of the rail. In order to correct this problem, modifications have been made to the rail to eliminate the hollow sections in the bottom of the barrier.

5.2.2.1 Modified Texas T411 Bridge Barrier # 1

This barrier is identical to the Texas T411 Bridge Barrier with the exception that the bottom 425.45 mm (16 3/4 inch) of the barrier has been filled with concrete. It was expected that this modification may stimulate improved interaction between the solid concrete section and the vehicle bumper and will allow for a more smooth redirection of the vehicle. The finite element model for this rail can be seen in Figures 5-3 and 5-4. This rail is comprised of 25,028 solid elements and is 10.642 m (35 feet) long. The results of computer simulations for this model are presented in section 5.4 and in Appendix A.

5.2.2.2 Modified Texas T411 Bridge Barrier # 2

A second model of the modified barrier was developed by increasing the overall height of the barrier to 1067 mm (42 inches) and translating the voids to the upper region of the rail. In this model, the bottom of the voids are at a height of 609.6 mm (24 inches). This modification was made to assure that there would be no action between the bumper or the tire of the vehicle and the cavity in the barrier. The finite element model of this barrier can be seen in Figures 5-5 and 5-6. This rail is constructed of 25,836 solid elements and is 6.985 m (23 feet) long. Contact type 5a was used on this model. Simulation and comparison revealed that the less complex type 5a behaved similar to the previously use type 13. The results of computer crash simulations for this model can be seen in section 5.4 and Appendix A.

5.3 Computer Crash Simulations - Summary

All of the computer crash simulations were between the Texas T411 Bridge Barrier or Modified Texas T411 Bridge Barrier and the 2000P Chevrolet Pickup traveling at 100 km/hr with a 25 degree angle of impact. The points of impact are at the midspan of the barrier, and the impact duration time is 0.105 sec. The coefficients of friction between the vehicle and the barrier are $\mu_{static} = 0.35$ and $\mu_{dynamic} = 0.3$. The coefficients of friction between the vehicle and the ground are $\mu_{static} = 0.6$ and $\mu_{dynamic} = 0.5$. The last two are for the transverse direction only.

5.4 Simulations 5-1 through 5-3:Impact Sequences

Simulation 5-1 (see Figures A-21a&b) represents an impact between the Texas T411 Bridge Barrier and the 2000P vehicle model. Figure A-21a shows that there is a contact between the tire and the frame of the truck. The front view shows the beginning of the snagging effect between the tire and the post of the barrier, along with large deformations to the front panel and the hood of the truck. The final frame of Figure A-21b is a clear indication of the snagging effect between the tire and the post of the rail. At this moment, the truck has completely lost contact with the ground and the rear of the truck is rotating away from the front face of the guardrail. This will lead to extremely high values of ridedown acceleration of the center of gravity of the truck. This is contrary to the smooth redirection typically desired for concrete bridge barriers.

Simulation 5-2 (see Figures A-22a&b) represents an impact between the Modified Texas T411 Bridge Barrier # 1 and the 2000P vehicle model. It can be noticed that the tire of the vehicle no longer snags, as the post of the barrier has been eliminated from the model; however, the new problem observed is the action between the bumper of the truck and the void in the barrier. With the Modified Texas T411 Barrier # 1, the void is located at approximately the same height as the bumper of the vehicle. This will cause the bumper of the vehicle to "ride" in the opening in the barrier, and allow it to snag on the far face of the void. Figures A-22a and A-22b appear to illustrate a relatively smooth redirection of the vehicle; however, a more detailed analysis (see section 5.5) shows that this barrier does not meet the criteria set forth in NCHRP Report 350 [22].

Simulation 5-3 (see Figures A-23a&b) mimics an impact between the Modified Texas T411 Bridge Barrier # 2 and the 2000P vehicle model. Slight deformations are apparent in the bumper and driver's side panel. The front view shows the start of the snagging effect between the hood of the truck and the rear face of the void in the barrier. In Figure A-23b one can notice the tire of the truck has become flush with the lower surface of the barrier. Severe damage to the hood and the driver's side panel of the truck is noticed. Initially, this sequence appears to illustrate good containment and redirection of the vehicle; however, upon a further detailed analysis the barrier, it can be noticed that the barrier does not satisfy the requirements of NCHRP Report 350 [22]. The snagging effect between the tire and the bumper of the truck with the post of the rail have now been replaced by the contact between the hood and driver's side front panel of the truck with the rear face of the void in the barrier.

5.5 Analysis of Results: Simulations 5-1 through 5-3

Figures A-24 to A-35 represent the output of the accelerometer defined in Chapter C.4. All outputs follow the same coordinate system as defined for the FDOT Beam and Post. The displacements and accelerations are in the global coordinate system, and the velocities are in the local coordinate system.

Figures A-24 through A-26 represent the displacement of the vehicle with respect to the whole system. Figure A-24 shows that the X-displacement of the accelerometer for simulations 5-2&3 is smaller than that for simulation 5-1. During simulation 5-1, the vehicle did not hug to the rail as it did in the modified barriers due to the snagging of the post. The drastic difference in the Y-displacement (see Figure A-25) is due to the fact that in simulation 5-1, the vehicle lost contact with the ground surface, while in simulations 5-2&3, the vehicle remained relatively close to the ground.

Figures A-27 through A-29 represent the velocity of the vehicle. Figure A-27 shows the rate at which the vehicle came to rest was much less severe with the addition of the concrete parapet. The point at which the two curves begin to separate corresponds to the action between the tire of the vehicle and the post of the Texas T411 Bridge Barrier. After 0.10 seconds, the velocity in the X-direction of the accelerometer of the truck was almost zero. Recalling that the accelerometer is located at the center of gravity of the vehicle, one can expect this result as the truck is rotating counter-clockwise away from the front face of the barrier around this point.

Figures A-32 through A-35 represent the accelerations of the vehicle's center of gravity. One can notice the decrease in acceleration with the addition of the concrete parapet in the Modified Texas T411 Barrier # 1 & 2. This is to be expected due to the

fact that the vehicle snagged on the post and moved away from the front face of the barrier. The acceleration in the Z-direction is the most important to observe, as it is in the longitudinal direction of the barrier. Figures A-32 and 35 show the largest improvement with the Modified Texas T411 Bridge Barriers, but it does not meet the requirements of NCHRP Report 350 [22].

Figures A-36 through A-38 present the correlation between the impact simulations and the time history plot of longitudinal acceleration of the center of gravity of the truck for simulations 5-1 through 5-3.

Examining Figure A-36, one can notice three primary peaks of acceleration: points A, B, and C. Point A corresponds to the initial point of contact between the post of the guardrail and the tire of the vehicle model with simultaneous contact between the bumper and the next post of the barrier. The geometry of this barrier does not appear to allow for a smooth redirection of the 2000P class vehicle. Point B corresponds to the impact between the tire and the frame of the truck. Point C represents the action between the barrier and the bumper of the truck model. At this point in time, the vehicle is beginning to rotate counter-clockwise, which initiates contact between the front of the bumper and the face of the barrier. All of the 10 ms average accelerations are in excess of the limiting 20 g's as suggested by the NCHRP Report 350 [22].

Studying Figure A-37, again three peaks of acceleration can be observed, points A, B, and C. Point A represents the moment of contact between the bumper of the vehicle and the void in the barrier. Point B illustrates the contact between the bumper and the tire of the vehicle model. Point C once again represents the action between the barrier and the bumper. The results of this simulation show a vast improvement over the

maximum 10 ms average longitudinal acceleration of simulation 5-1; however, the results obtained for simulation 5-2 are still in excess of the requirements of [22]. The problem of the contact between the tire and the post is solved with the Modified Texas T411 barrier # 1, yet the contact between the bumper and the post is serious enough to disqualify this barrier.

Examining Figure A-38, one can notice three primary peaks of Z-acceleration, points A, B, and C. Point A corresponds to the combined effect of contact between the tire and the barrier and the contact of the hood of the vehicle with the void in the barrier. Points B and C are the combination of contact between several of the components in the truck model as well as action between the barrier and the vehicle.

NCHRP Report 350 sets a –20 g limit for the maximum allowable longitudinal acceleration for this simulation [22]. The accelerations in the longitudinal direction of the vehicle are well in excess of the limit. This barrier does not satisfy the requirements of [22] due to its sharp geometric properties, which facilitate the snagging effect.

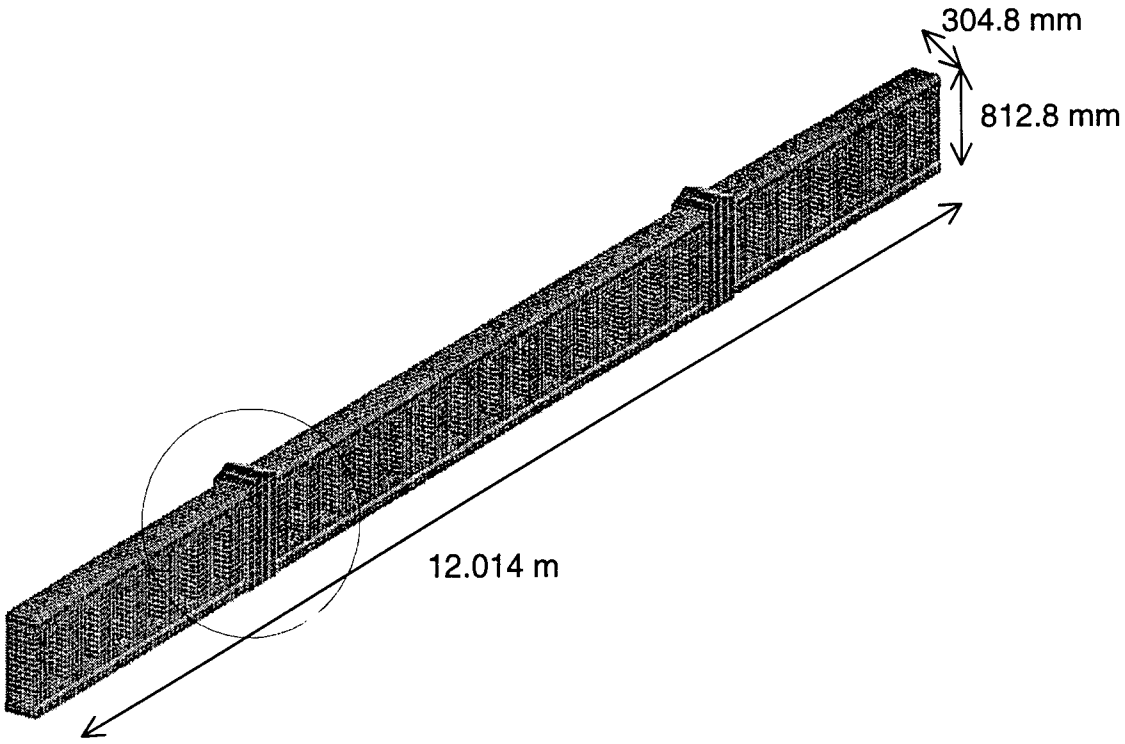

Figure 5-1: FEM of Texas T411 Barrier

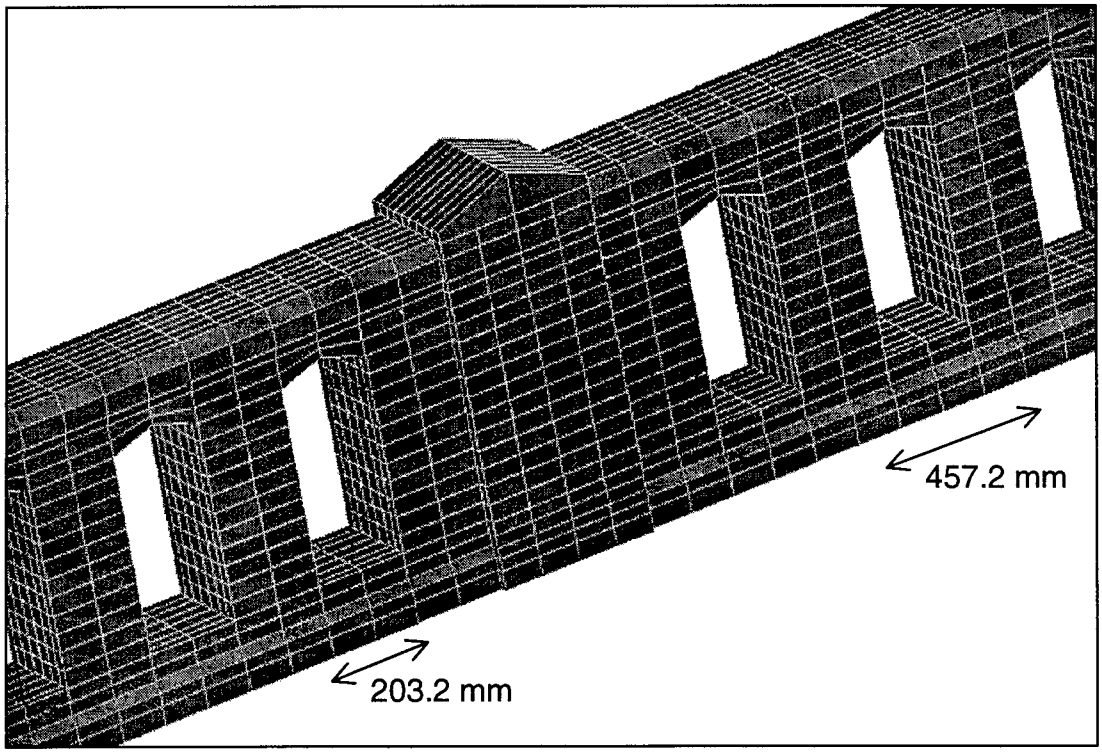

Figure 5-2: Zoom view FEM of Texas T411 Barrier

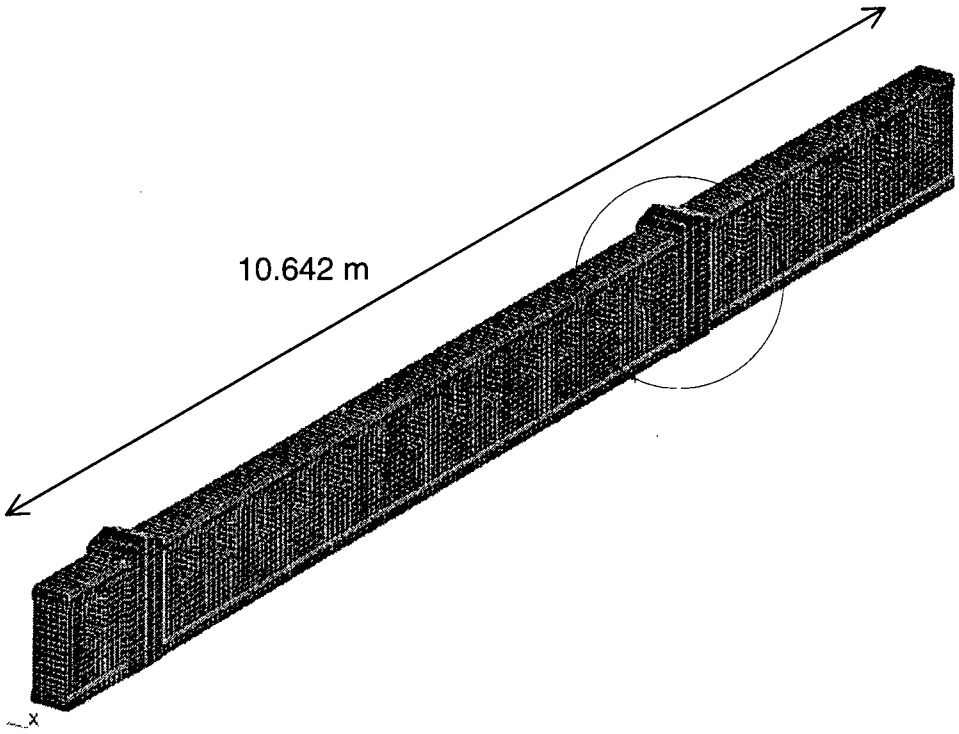

Figure 5-3: FEM of Modified Texas T411 Bridge Barrier # 1

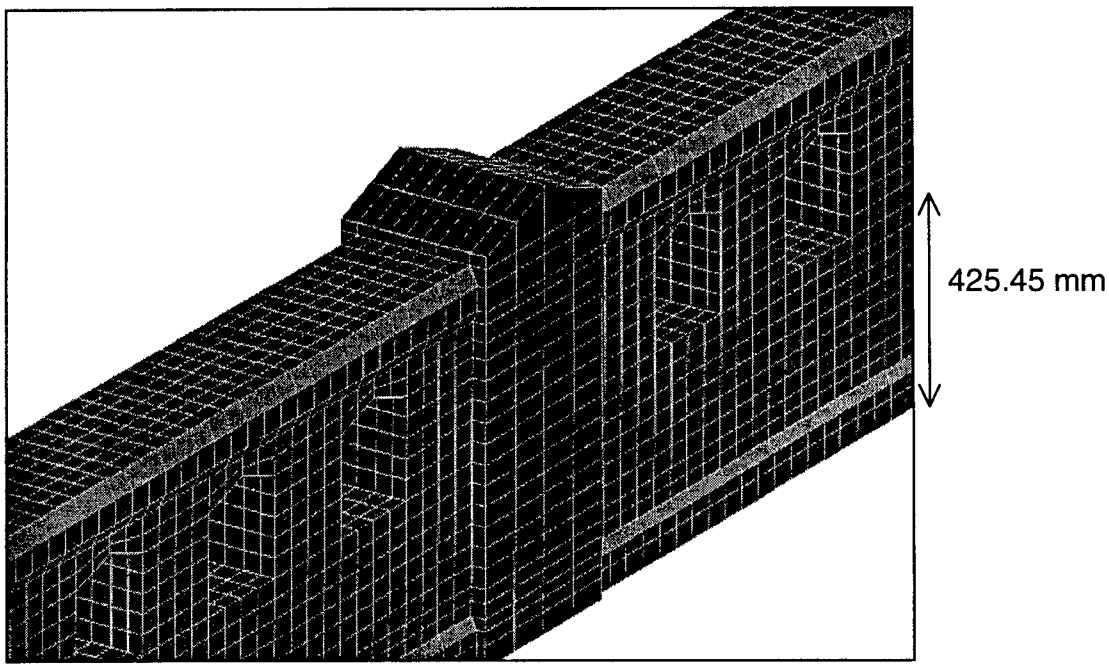

Figure 5-4: Zoom view of FEM of Modified Texas T411 Bridge Barrier # 1

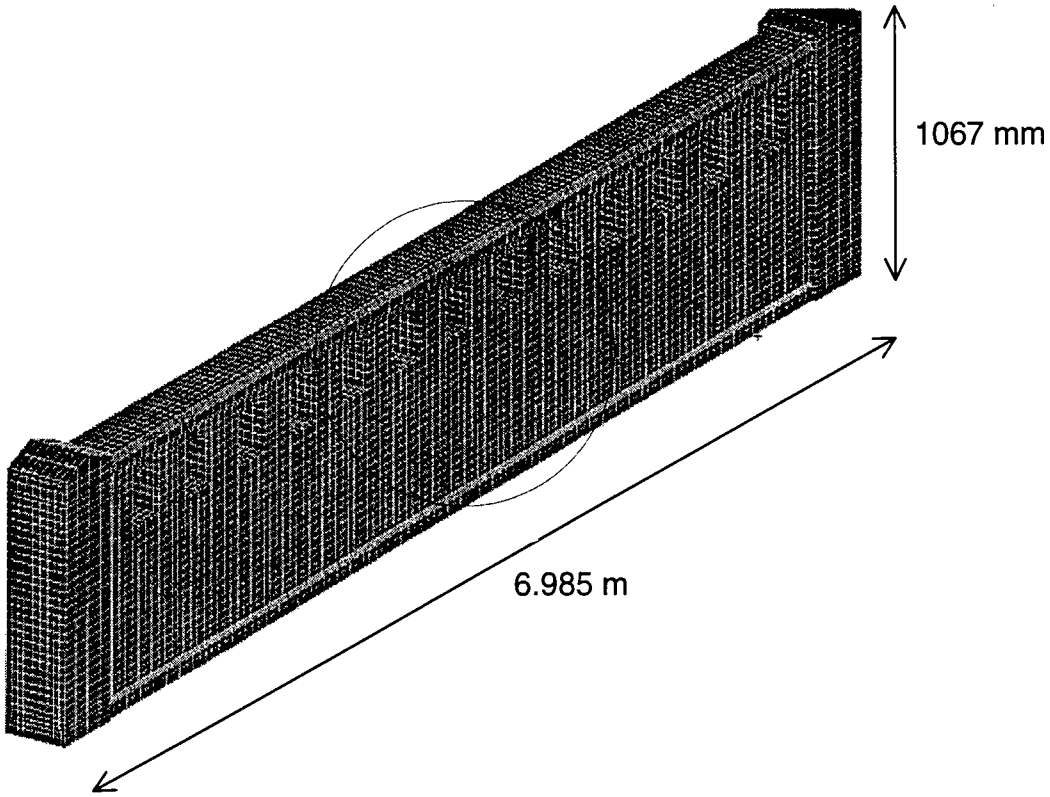

Figure 5-5: FEM of Modified Texas T411 Bridge Barrier # 2

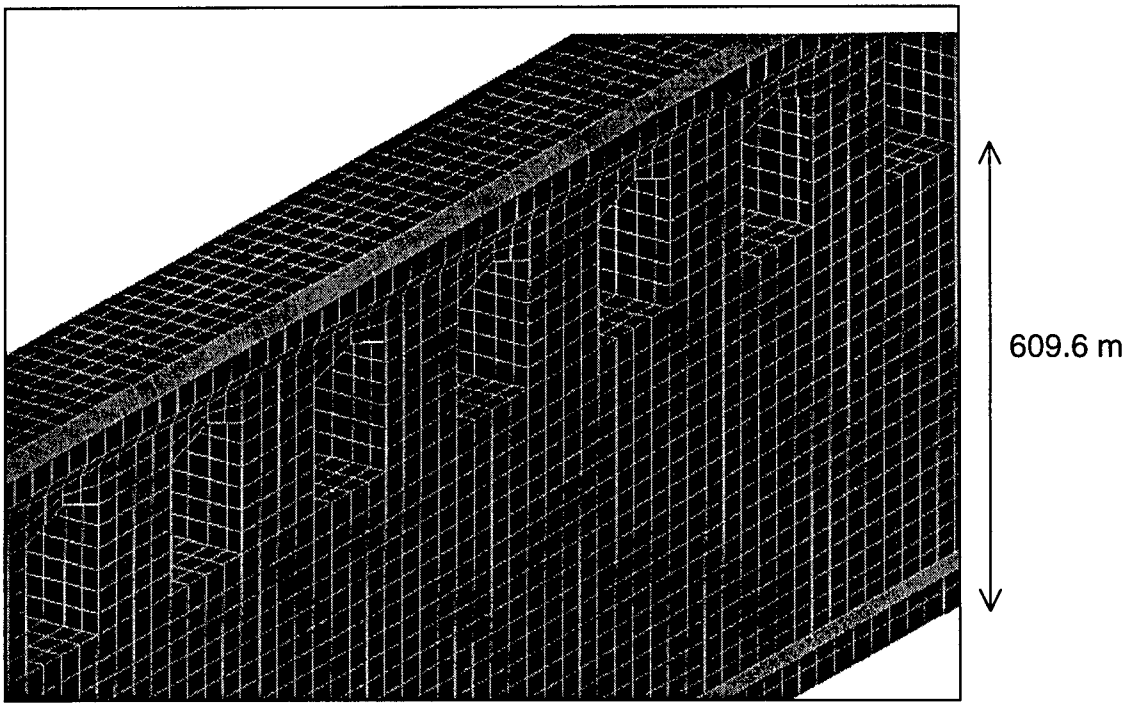

Figure 5-6: Zoom View of FEM of Modified Texas T411 Bridge Barrier # 2

CHAPTER 6

MODIFIED STANDARD FLORIDA BARRIER

The Standard Florida Barrier (see Figure 1-3) has become one of the most popular barriers on our nations' highways. The primary purpose of the proposed revisions was to improve the aesthetics of the Standard Florida Barrier by the inclusion of equally distributed openings. The Modified Standard Florida Barrier is a new concept based on modifications of a previous design, thus there are no full scale crash tests available.

6.1 Description of Modified Standard Florida Barrier

The modifications to the existing Standard Florida Barrier involved raising the overall height of the rail to 1067 mm (42 inches) and introducing 203 mm by 914.4 mm (8 inch by 36 inch) voids in the middle to upper region of the rail. The location of these voids was determined through a series of optimization tests suggested by the FDOT and presented in section 6.2.

6.2 Optimization of Geometry

Three barriers were developed with the height from the ground to the bottom of the void varying from 508 mm to 609.6 mm (20 inches to 24 inches). All barriers were 8.23 meters (27 feet) long with voids 203 mm high by 914.4 mm long (8 inches high and 36 inches long), the difference being in the location of the bottom of the void with respect to the ground surface. A series of simulations were performed to determine the minimum height to locate a cavity in a Standard Florida Barrier to avoid a snagging effect. The

barrier with the void 609.6 mm (24 inches) above the ground proved to be the best option. Figure 6-1 shows the finite element model of this barrier.

6.3 Finite Element Model

The Modified Standard Florida Barrier (see section 8.1) was the final barrier model developed. Once again, this rail model was developed in a similar fashion to the FDOT Beam and Post Rail.

6.3.1 Modified Standard Florida Barrier

The finite element model of this rail is constructed of 23,992 solid elements and is 20.422 m (67 feet) long. The material model used for this rail is material 16 with smeared reinforcement (same as FDOT Beam and Post Rail - see Chapter 4). The finite element model of this rail can be seen in Figures 6-2 and 6-3. The results of computer simulations for this model are presented in section 6.4.

6.4 Computer Crash Simulations - Summary

The computer crash simulation was set up between the Modified Standard Florida Barrier and the 2000P Chevrolet Pickup. The 2000P vehicle model was traveling at 100 km/hr with a 25 degree angle of impact. The point of impact was at midspan of the barrier. The coefficients of friction were the same as for the Texas T411 barrier (see Chapter 5). The time duration of the simulation was 0.200 sec.

6.5 Simulation 6-1: Impact Sequences

Simulation 6-1 represents an impact between the Modified Standard Florida Barrier and the 2000P vehicle model. Analyzing Figure A-39a, it can be noted that the bumper of the vehicle has come into contact with the barrier. It can also be noted that the tire of the vehicle climbs the front face of the barrier, which has a slight incline. The deformations in the hood become apparent. Analyzing the top views of Figure A-39a, one can notice the truck is beginning to rotate towards the front face of the barrier as is expected. In Figure A-39b, the passenger's side front tire of the vehicle appears to loose contact with the ground surface ending up flush with the front face of the barrier. Overall, Figures A-39a and A-39b illustrate good containment and a smooth redirection of the vehicle.

6.6 Analysis of Results: Simulation 6-1

Figures A-40 to A-44 represent the output of the accelerometer defined in Appendix C.4 for simulation 6-1. The coordinate systems for the displacements, velocities, and accelerations are the same as defined in Chapter 4.

Figure A-40 illustrates a displacement of the truck with respect to the barrier. The curve in the X-direction corresponds to the yawing effect on the vehicle.

Figure A-41 represents the velocity of the vehicle. Comparing the Y-velocities to the Y-direction velocities obtained for previous barriers, these values are within reason. It can be noted that the Z-velocity is almost negligible. This is to be expected because the vehicle does not appear to rapidly lose contact with the ground.

Figures A-42 to A-44 represent the accelerations as provided by the accelerometer. The accelerations in the Y-direction are presented in Figure A-43. Initial

observation of this plot shows a maximum acceleration of almost 80 g's; however, after 10 ms averaging, this value is reduced to around 25 g's. This is due to the fact that the duration of the spike is very small. NCHRP Report 350 documents that spikes with a duration of less than 0.007 s are not critical and should be averaged from the pulse [22].

Figure A-45 presents the time history plot of accelerations in the longitudinal direction of the truck (local X-direction) with the correlation to the impact sequences for simulation 6-1. Four primary acceleration peaks have been identified, points A, B, C, and D. Point A corresponds to the initial contact between the tire of the truck and the barrier. Analyzing point B, one can notice the contact between the bumper of the truck and the barrier. The maximum longitudinal acceleration can be observed at Point C. This point corresponds to the combined effect of the contact between the bumper and the tire of the truck with the barrier. Point D corresponds to contact between the tire of the truck and the frame of the truck.

Figure A-46 represents the state of stress at the time step identified by the maximum normal deflection as related to the maximum impact force for the Modified Standard Florida Barrier. This value corresponds to the time t=0.042 seconds. At this moment, the maximum deflection is equal to 0.92 mm. The corresponding fringes of the Y-stress (Figure A-47) are characterized by the tension region at the fixed support below the area of impact. Figure A-48 illustrates the state of the Z-stress in the barrier at the time t=0.042 seconds. Here, the region of impact is related to compressive stresses from the range between 0 and –8.89 MPa.

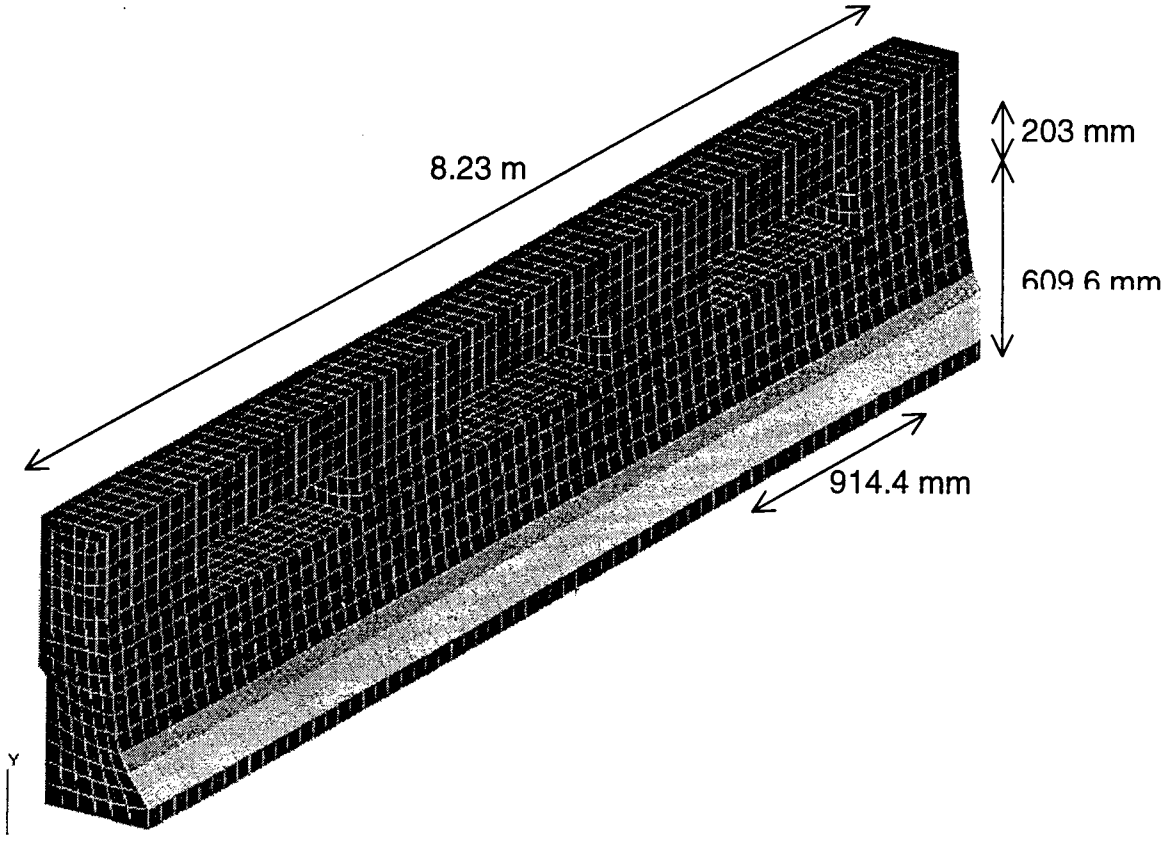

Figure 6-1: FEM of Modified Standard Florida Barrier

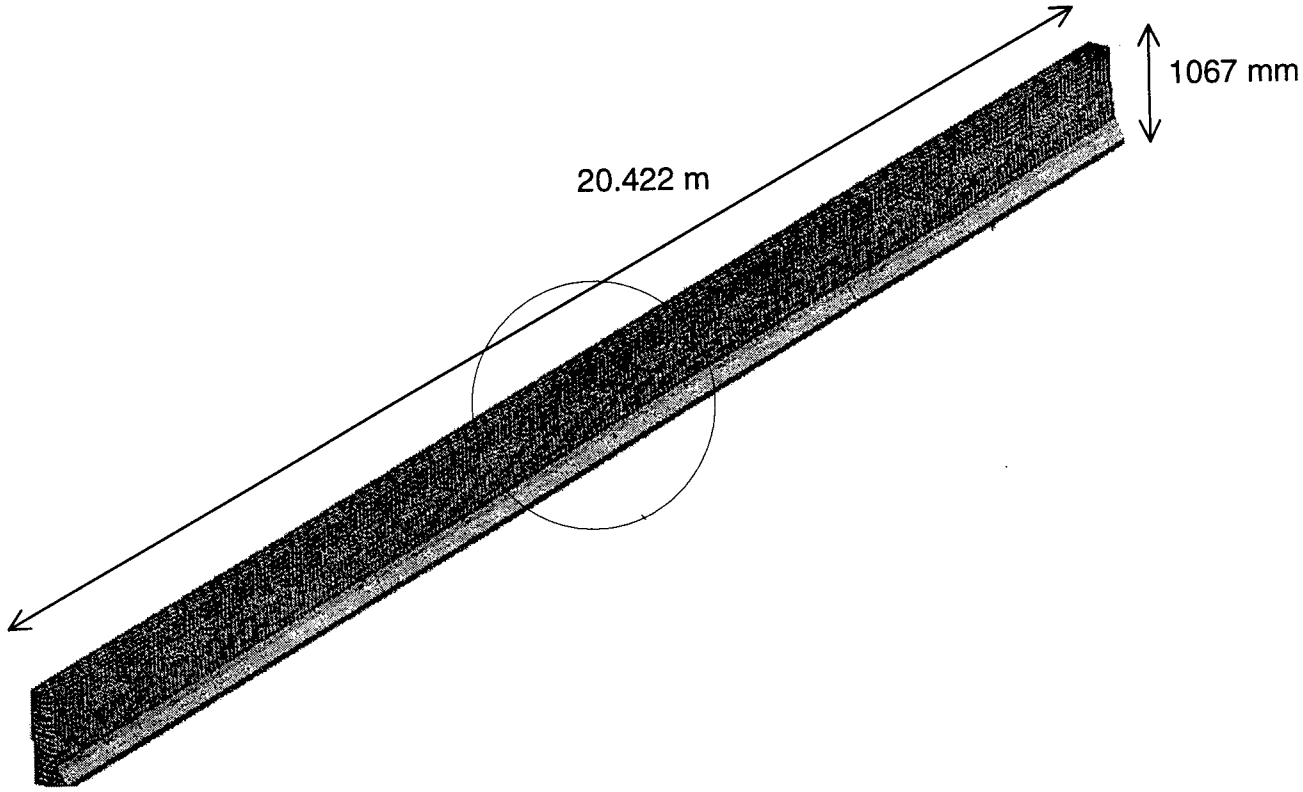

Figure 6-2: FEM of Modified Standard Florida Barrier

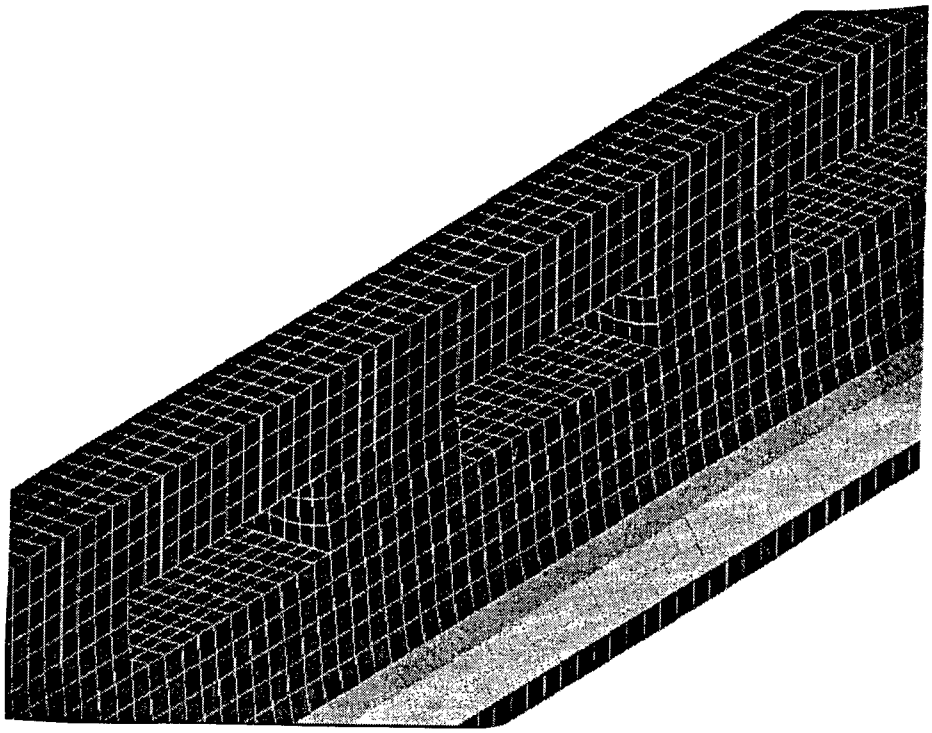

Figure 6-3: Zoom View of FEM of Modified Standard Florida Barrier

Chapter 7

SUMMARY AND CONCLUSIONS

This report discussed a method and procedure for the use of computer crash simulations in the design and development of reinforced concrete bridge barriers. With the recent advances in computational power, detailed analysis of large problems is becoming available through finite element methods.

Computer crash simulations were performed on three main categories of reinforced concrete bridge barriers: Beam and post type configuration, Texas T411 aesthetic barrier, and the Modified Standard Florida barrier. After computer simulations using LS-DYNA3D, problem areas were identified along with recommendations for further design improvements. Table 7-1 compares the three barrier's longitudinal accelerations. The longitudinal accelerations are the most crucial with respect to occupant safety [22]. It should be noted that none of the three previously mentioned barriers have been evaluated through a full-scale impact with the 2000P vehicle and the next step for validation of the numerical simulations presented in this report should be full-scale crash tests.

A valuable retrofit design was proposed and evaluated for the existing FDOT Beam and Post Rail. The addition of the W-beam to the front of the posts facilitated a much smoother containment and redirection of the vehicle. The first two barriers were constructed of a continuous concrete section with post spacing of 1.524 m (5 feet) on center and elastic-plastic springs were used to model the bolted connection between the

post and the w-beam. It was later discovered that while the spacing of the posts is dependent upon the superstructure and commonly is1.524 m (5 feet), it is more typical to find the posts spaced at 2.1336 m (7 feet) on center. In addition to the distance between the posts, a 19.05 mm (3/4 inch) expansion joint every 9.144 m (30 feet) was included in the final model. Finally, a complete new bolt model was implemented in the final modified barrier (see section 4.2.2.2). It was fond that the four-spring model bolt connection used in simulation 4-2 produced excessively high elongation of the springs without failure. The previous statements lead directly to the development of simulations 4-3 and 4-4. The results of the longitudinal deceleration of the FDOT Beam and Post with expansion joints can be viewed in Figures A-17 and A-18. The maximum deceleration after 10 ms averaging for simulation 4-4 was 23 g's. Although, this barrier did not meet the requirements of NCHRP Report 350 [22], the barrier showed very good potential and full-scale crash tests might indicate permissible ridedown accelerations as the computer simulations only indicate a most likely outcome. A full-scale crash test would therefore be recommended.

Several modifications were made and evaluated for the Texas T411 Bridge barrier; however, none of the simulations with these modified barriers produced results that were comparable with the standards of NCHRP Report 350 [22]. At this point in the study of this barrier, further research and modifications are needed to develop and adequate design for use on our nations highways. The geometry of this barrier contains many sharp edges and corners, which create snagging problems with the geometry of the 2000P vehicle. It should be noted that both the Modified Texas T411 # 1 and # 2, may not have problems

with other vehicles, as the bumper of the 2000P truck is generally higher than many other vehicles.

Numerical optimization simulations were performed for the Modified Standard Florida Barrier. These simulations determined the best placement of a 203 mm by 914.4 mm (8 inch by 36 inch) opening with regards to an impact with the 2000P class vehicle. The results from these simulations determined that a minimum height of 609.6 mm (24 inches) from the ground to the bottom of the void performed the best. These conclusions lead directly to the development of the Modified Standard Florida Barrier # 1. A second barrier was developed with an overall height of 1067mm (42 inches). The voids were translated to the upper region of the rail. This barrier was not presented because it produced data that was almost identical to Barrier #1. Simulations produced results with accelerations greater than the acceptable 20 g's after averaging. This barrier concept is an excellent candidate for use as a new, efficient, and aesthetic barrier; however, further investigation will be necessary to provide longitudinal accelerations within the guidelines of NCHRP Report 350[22]. Alterations, which may illustrate improved behavior, include altering the size of the void, the location of the void, and the overall height of the barrier. Further tests may need to be performed with different vehicles because these numerical simulations are strongly dependent upon the height of the vehicle from the ground surface and especially the height of the bumper from the ground.

The numerous computer crash simulations performed in this research lead to the development of some general guidelines to follow for the design and development of reinforced concrete bridge barriers. All the barriers presented in this project are some

variation on the basic concept of a concrete beam (top and bottom) connected with vertical posts between them. While this concept is appealing for aesthetic purposes, problems arise in dealing with the contact between the vehicle and the post. Figure 9-1 illustrates the most efficient use of this barrier. If it is at all possible, one should try to avoid the vertical pilasters. If they are necessary, attempt to place the post close to the rear of the section to avoid contact with oncoming vehicles. A further modification to the FDOT Beam and Post rail might be to consider a change to the concepts of Figure 7-1. After the completion of a work of this magnitude, it is quite typical for a project of such a complex nature to lead to a set of directions of any further necessary research, which can be identified.

One should list here the following items:

- It should be noted that the longitudinal accelerations of the center of gravity of the vehicle exceed the requirements of NCHRP Report 350 [22] for all impact simulations. With this in mind it should be considered that the results presented in this report represent the extreme conditions of a 2000 kg vehicle traveling at 100 km/hr impacting a virtually rigid barrier at 25 degrees. In reality, it will be very seldom that all of these conditions will occur simultaneously.

- The location of the initial point of impact is an area of special concern. NCHRP Report 350 provides specific guidelines for the determination of the "critical impact point." In reality, the vehicle could impact the barrier at any location, which would yield different results. Simulations not presented in this report illustrated that the initial point of impact plays a very strong influence on the overall results obtained, and many times, the critical impact point reported by NCHRP Report 350[22], did not yield the most severe collision.

One can also construct a following list of expectations for the improved tools used in the computer crash simulation:

- Another important place to look for possible improvements is in the model of the vehicle, especially the proper modeling of the wheels with tires and the system of suspension. In angle type impacts, the wheels very often come into contact with

elements of the barriers producing the snagging effect. It seems obvious that the final, huge deformations of the truck obtained in simulations 7-1 and 7-3 are unrealistic due to too strong wheels and their suspension in the FEM model of the truck. In a real crash wheels would be damaged and/or separated from a vehicle. It should be stressed, however, that the required improvements would not influence the initial part of mentioned simulations, i.e. they can correct only the post-snagging phase of those simulations.

- It would be requested to develop and implement a wider variety of vehicle models for impact simulations at varying speeds and angles of impact. At this time, this is probably the most limiting aspect of vehicle impact simulation. Automobile manufactures can change the geometry of their vehicle fleet very quickly, which often presents problems for roadside safety devices designed and constructed twenty years ago. A key example to this problem is minivans and sport utility vehicles, which now represent approximately 10 percent of the vehicle population [42]. No crash tests between minivans and roadside hardware have been performed, and there is no data available for how this fleet of vehicles will perform under such conditions.

Longitudinal acceleration g's

	Actual	10 ms averaging
Modified FDOT Beam and Post with expansion joints (simulation 4-4)	-32	-23
Modified Texas T411 Bridge Barrier #1 (simulation 5-2)	-90	-45
Modified Texas T411 Bridge Barrier #2 (simulation 5-3)	-70	-40
Modified Standard Florida Barrier (simulation 6-1)	-70	-46

Table 7-1: Longitudinal Accelerations

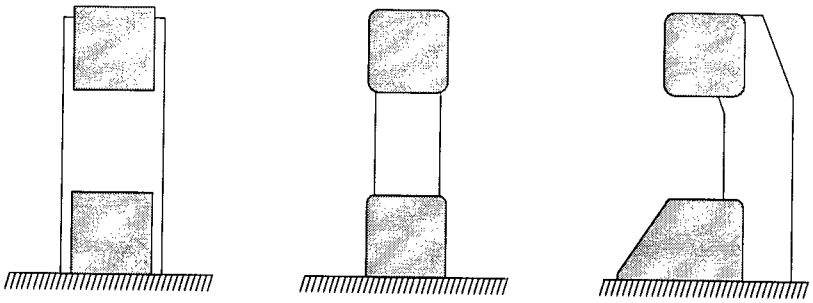

Figure 7-1: Simplified concepts of bridge barriers

CHAPTER 8

REFERENCES

[1] "LS-DYNA3D User's Manual (Nonlinear Dynamic Analysis of Structures in Three Dimensions)", Livermore Software Technology Corporation, August 1, 1995, Version 936

[2] J. O. Hallquist, "LS-DYNA3D Theoretical Manual", LSTC Report 1018 Revision 3, April 1994

[3] R. G. Whirley and B. E. Engelmann, "DYNA3D, A Nonlinear, Explicit, Three-Dimensional Finite Element Code For Solid and Structural Mechanics - User Manual", Lawrence Livermore National Laboratory, UCRL-MA-107254, November 1993

[4] K. Cichocki, private communications, October - November 1996

[5] S. C. C. Bathe, "The effect of impact loading on prestressed and ordinary reinforced concrete beams', National Building Studies, Research Paper 35, Her Majesty's Stationery Office, London 1961

[6] M. Issa, private communications, November 1996

[7] R. J. Roark and W. C. Young, "Formulas for Stress and Strain", McGraw-Hill Book Company, 1982

[8] J. W. Wekezer, M. S. Oskard, R. W. Logan and E. Zywicz, "Vehicle Impact Simulation", *Journal of Transportation Engineering*, ASCE, Vol. 119, No. 4, July/August 1993

[9] N. Jones, "Structural Impact", Cambridge Univ Press, 1989

[10] CRASH-L -The DYNA3D Crashworthiness Analysis Discussion List, archive available at http://www.ccad.uiowa.edu/~mhray/Crash-l

[11] T. Krauthammer, A. Assadi-Lamouki and H. M. Shanaa, "Analysis of impulsively loaded reinforced concrete structural elements - II. Implementation", *Computers & Structures*, Vol. 48, No. 5, pp. 861-871, 1993

[12] K. Cichocki, G. Maier and U. Perego, "Analysis of damages due to underwater explosions on a hybrid structure", *Int. Journal for Engineering Analysis and Design*, Vol. 1, pp. 341-361, 1994

[13] J. Du, A. S. Kobayashi and N. M. Hawkins, "FEM Dynamic Fracture Analysis of Concrete Beams", *Journal of Engineering Mechanics*, ASCE, Vol. 115, No. 10, pp. 2136-2149, 1989

[14] Hirsch, T.J., C.E. Buth, and D.L. Kaderka, "Aesthetically Pleasing Concrete Beam-and-Post Bridge Rail." *Transportation Research Record 1258*, Transportation Research Board, Washington D.C., 1990.

[15] Hirsch, T.J., C.E. Buth, W.L. Campise, and D.L. Kaderka, "Aesthetically Pleasing Concrete Beam and Post Bridge Rail: Texas Type T411." *Research Report 1185-1*, Texas Transportation Institute, Texas A&M University, College Station, Texas, March 1989.

[16] M.H. Ray, *Aesthetic Bridge Rails and Guardrails*, produced for the Federal Highway Administration, 1992 (video).

[17] M.H. Ray and J.E. Bryden, "Summary Report on Selected Aesthetic Bridge Rails and Guardrails." Federal Highway Administration, FHWA-SA-92-051, Washington, D.C., 1992.

[18] Plaxico, C.A., R.M. Hackett, and W. Uddin. "Simulation of a Vehicle Impacting a Modified T *Meeting*, January 12-16, 1997, Washington D.C.

[19] Bronstad, M.E., J.D. Michie, and J.D. Mayer, Jr. "Performance of Longitudinal Traffic Barriers." *National Cooperative Highway Research Program*, Transportation Research Board, Washington D.C., 1987.

[20] Beason, W. Lynn, T.J. Hirsch, and John C. Cain. "A Low-Maintenance, Energy-Absorbing Bridgerail." *Transportation Research Record 1065*, Transportation Research Board, Washington D.C., 1986.

[21] Hirsch, T.J., W.L. Fairbanks, and C.E. Buth. "Concrete Safety Shape with Metal Rail onTop to Redirect 80,000-lb. Trucks." *Transportation Research Record 1065*, Transportation Research Board, Washington, D.C., 1986.

[22] Ross, H.E., D.L. Sicking, R.A. Zimmer, and J.D. Michie. "Recommended Procedures for the Safety Performance Evaluation of Highway Features." *National Cooperative Highway Research Program Report 350*, Transportation Research Board, Washington D.C., 1993.

[23] Ranzo, Alessandro. "Development ofTraffic Barriers in Italy." *Transportation Research Cirular #341,* Transportation Research Board, Washington D.C., 1988.

[24] Michie, Jarvis D., and Maurice E. Bronstad. "Highway Guardrails: Safety Feature or Roadsid Research Board, Washington D.C., 1994.

[25] Bullard, D. Lance, Wanda L. Menges, and C. Eugene Buth. "Development of Combination Pedestrian-Traffic Bridge Railings." *Transportation Research Record 1468,* Transportation Research Board, Washington D.C., 1994.

[26] Mak, King K., Don J. Gripne, and Charles F. McDevitt. "Single-Slope Concrete Bridge Rail." *Transportation Research Record 1468,* Transportation Research Board, Washington D.C., 1994.

[27] Hirsch, T.J. and Perry Romere. "Crash Test of Modified Texas C202 Bridge Rail." *Transportation Research Record 1258,* Transportation Research Board, Washington D.C., 1990.

[28] Buth, C.E., T.J. Hirsch, and C.F. McDevitt. "Performance Level 2 Bridge Railings." *Transportation Research Record 1258,* Transportation Research Board, Washington D.C., 1990.

[29] Transportation Research Board. *Bridge Aesthetics Around the World,* Transportation Research Board National Research Council, Washington D.C., 1991.

[30] National Crash Analysis Center Internet Homepage, available at http://gwuva.jwu.edu/ncac/

[31] Bathe, Klaus-Jurgen. *Finite Element Procedures,* Prentice Hall,Englewood Cliffs, New Jersey, 1996.

[32] Zienkiewicz, O.C. and Taylor, R.L. *The Finite Element Method,* Fourth Edition, McGraw-Hill Book Company, London, 1989.

[33] Wekezer, J.W. *Finite Element Modeling of Motor Vehicles. Protocol for Developing INGRID Data Input Decks for DYNA3D Computer Code.* Technical Report No. FHWA-RD-94-153, U.S. Department of Transportation, FHWA, Washington, D.C., 1994.

[34] Hendricks, Bart. *Finite Element Modeling of the G2 Guardrail.* Master of Science Thesis. Florida State University. Spring 1996.

[35] AASHTO, "Guide Specification for Bridge Railings," American Association of State Highway and Transportation Officials, Washington, D.C. (1989).

[36] Michie, J.D., "Recommended Procedures for the Safety Performance Evaluation of Highway Apputenances," *NCHRP Report 230,* Transportation Research Board, Washington, D.C. (March 1981)

[37] Limpert, Rudolf. *Motor Vehicle Accident Reconstruction and Cause Analysis.* Third Edition. The Michie Company, Charlottesville, Virginia. 1989.

[38] Warner, Charles, Grefory Smith, Michael James and Geoff Germane, "Friction Applications in Accident Reconstruction." *International Congress and Exposition,* Detroit, Michigan. February, 1983.

[39] Paz, Mario. *Structural Dynamics: Theory and Computation.* Third Edition. Chapman & Hall, New York, New York. 1991.

[40] Hendricks, Bart and Jerry Wekezer, "Finite Element Modeling of G2 Guardrail," *Transportation Research Record 1528,* Transportation Research Board, Washington, D.C. 1996.

[41] Garcia, Antonio, Structural detail contained in memorandum to District Structures Design Engineers, Subject: *"Crash Tested Bridge Railings."* April 25, 1991.

Appendices A through F

APPENDIX A

Table A-1: Summary of Nomenclature for Single Degree of Freedom System

Variable	Nomenclature
Inertia Force	$f_I = m\ddot{u}$
Damping Force	$f_D = c\dot{u}$
Elastic Force	$f_S = ku$
Acceleration	$\ddot{u} = \frac{d^2u}{dt^2}$
Velocity	$\dot{u} = \frac{du}{dt}$
Mass	m
Damping Coefficient	c
Stiffness of Spring	k

Table A-2: First selection of material models for concrete modeling in LS-DYNA3D

Material No. in LS-DYNA3D	Material Model Name in LS-DYNA3D	Available description	
		in User's Manual [1]	in Theoretical Manual [2]
1	isotropic	x	x
3	elasto-plastic (von Mises)	x	x
5	soil and crushable foam model	x	x
12	isotropic elastic-plastic	x	x
13	elastic-plastic with failure	x	x

Table A-2: (cont.)

14	crushable foam with failure	x	x
16	pseudo tensor geological model	x	
17	elasto-plastic with fracture	x	
25	soil cap model by Taylor	x	
78	soil/concrete	x	
84	RS strainrate sensitive concrete		
85	reinforced concrete (AEA Winfrith, 1990)		

time = 0.000 sec

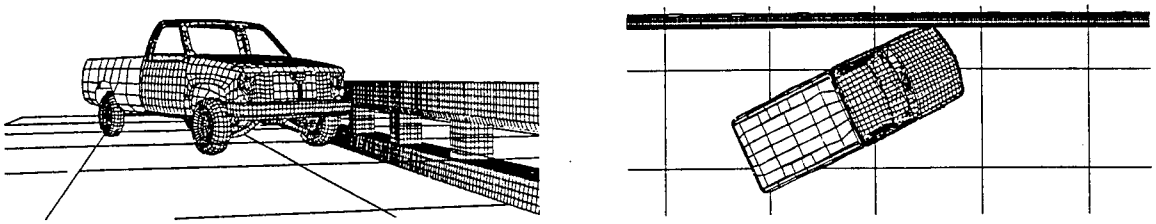

time = 0.015 sec

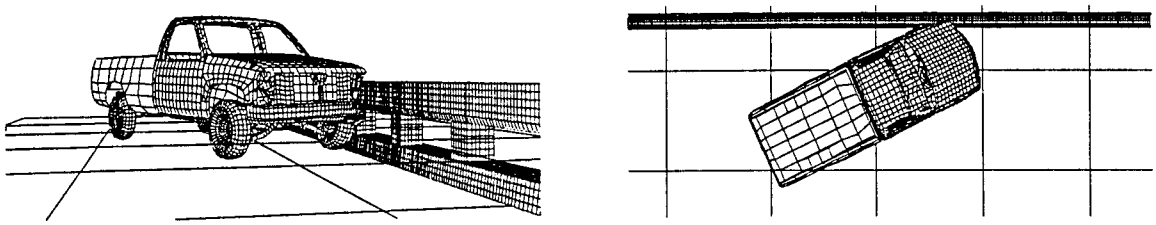

time = 0.030 sec

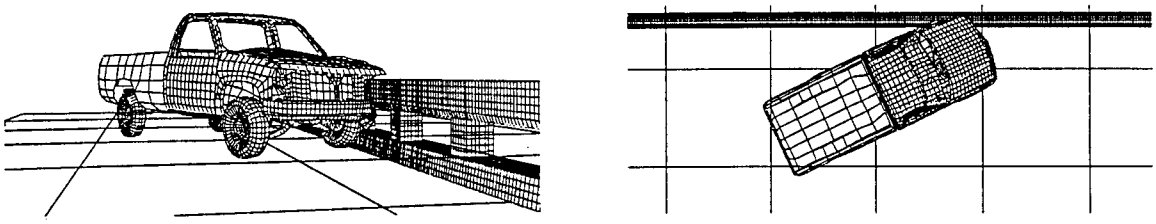

time = 0.045 sec

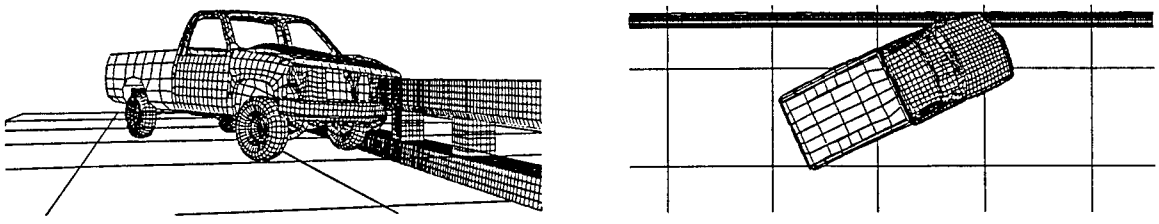

Figure A-1a: Simulation 4-1

time = 0.060 sec

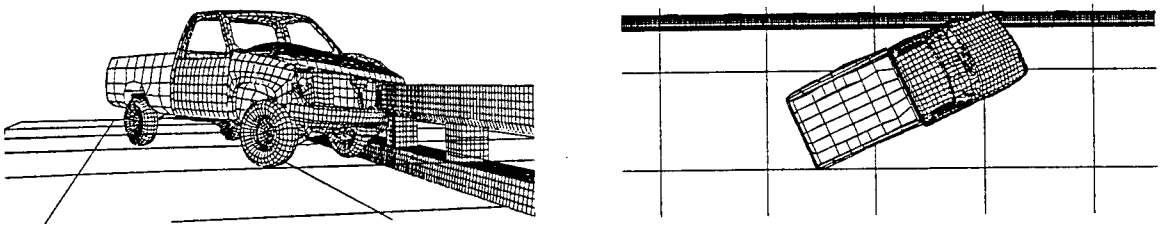

time = 0.075 sec

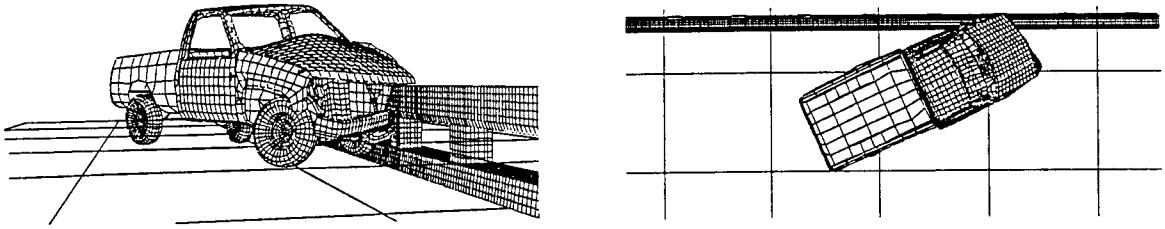

time = 0.090 sec

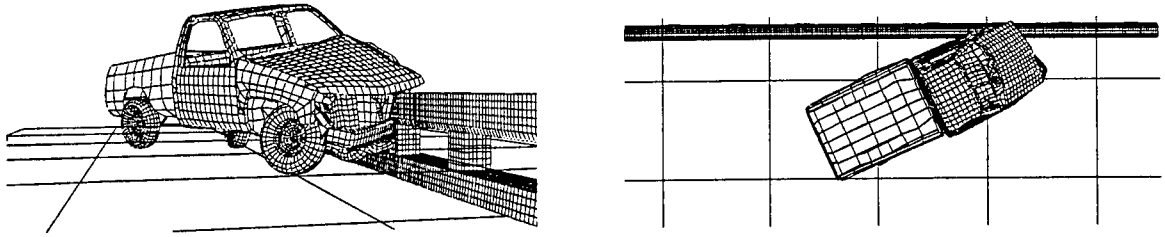

time = 0.105 sec

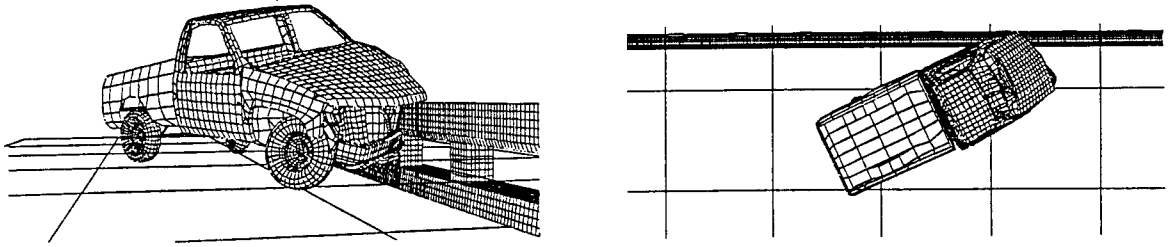

Figure A-1b: Simulation 4-1 cont.

time = 0.000 sec

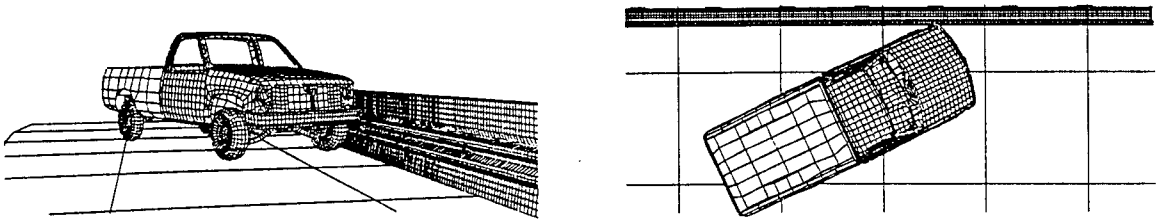

time = 0.015 sec

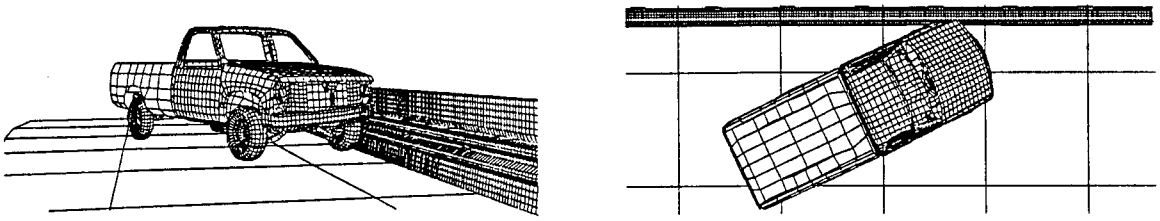

time = 0.030 sec

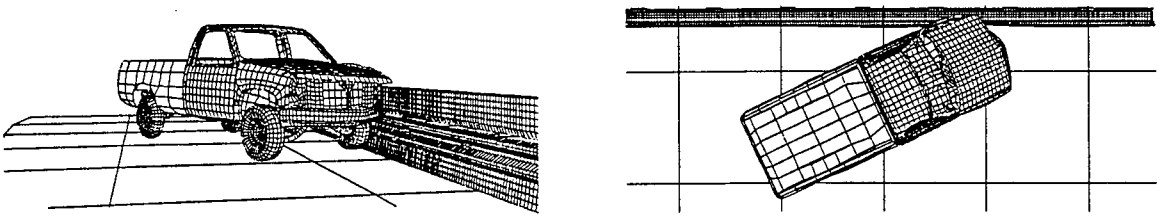

time = 0.045 sec

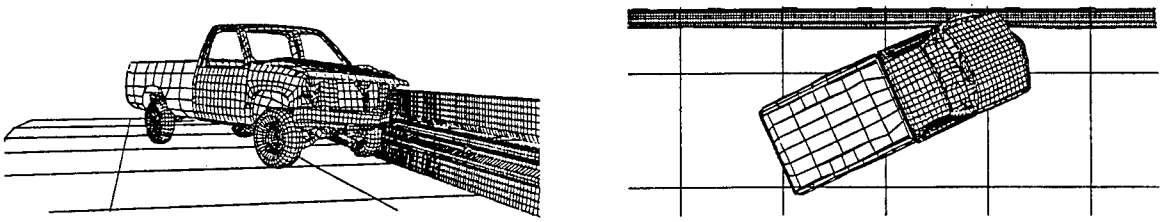

Figure A-2a: Simulation 4-2

time = 0.060 sec

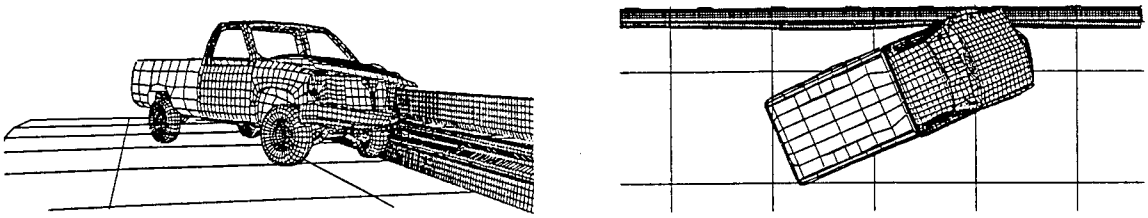

time = 0.075 sec

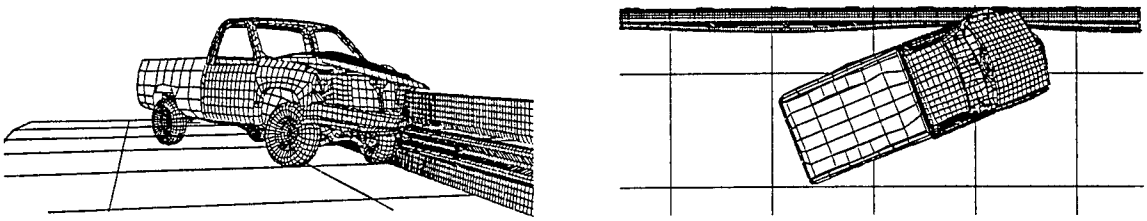

time = 0.090 sec

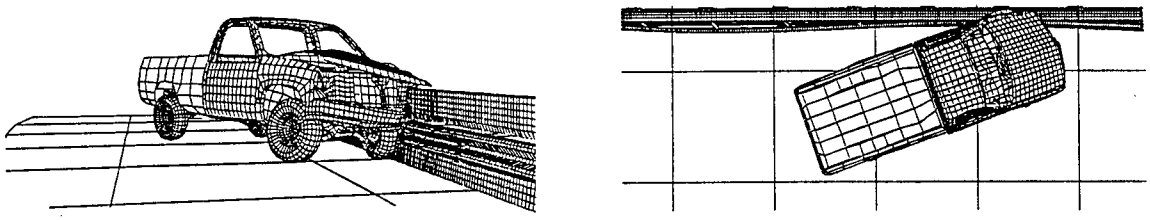

time = 0.105 sec

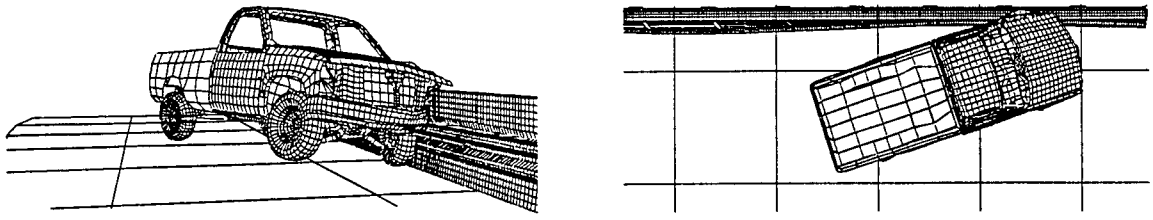

Figure A-2b: Simulation 4-2 cont.

time = 0.000 sec

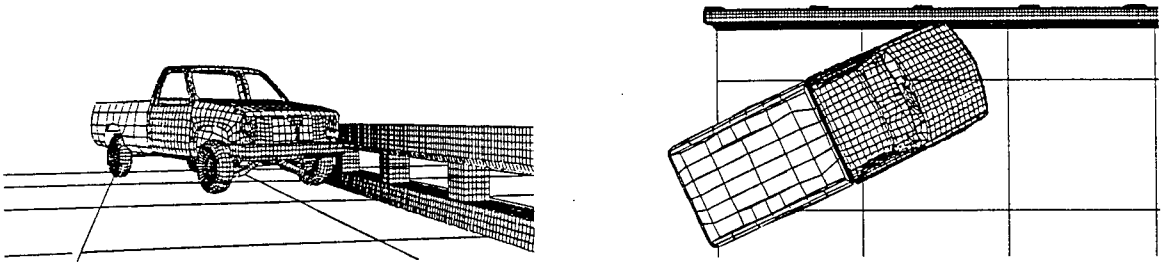

time = 0.015 sec

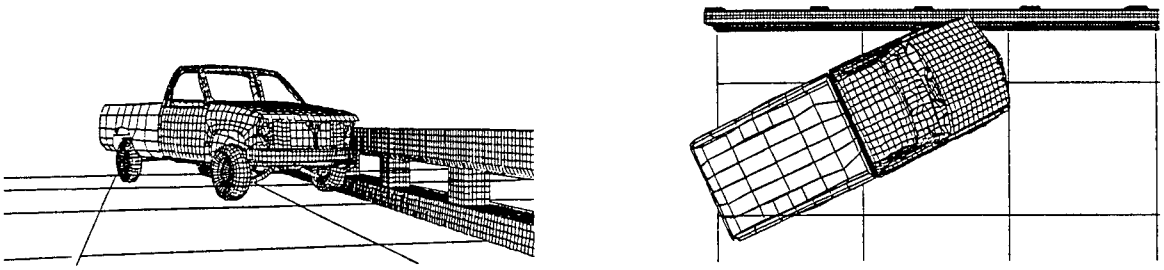

time = 0.030 sec

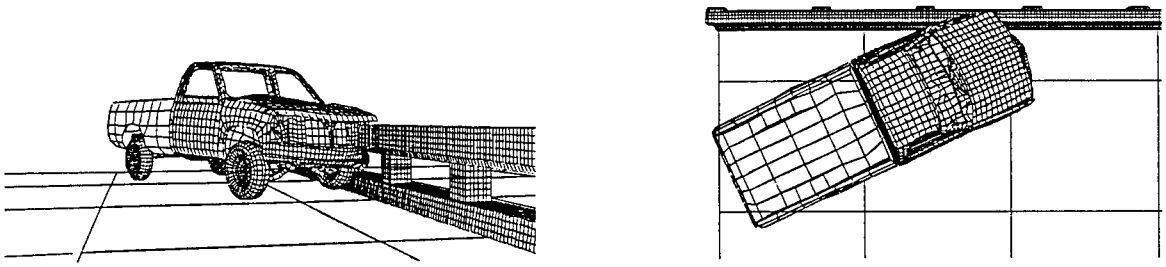

time = 0.045 sec

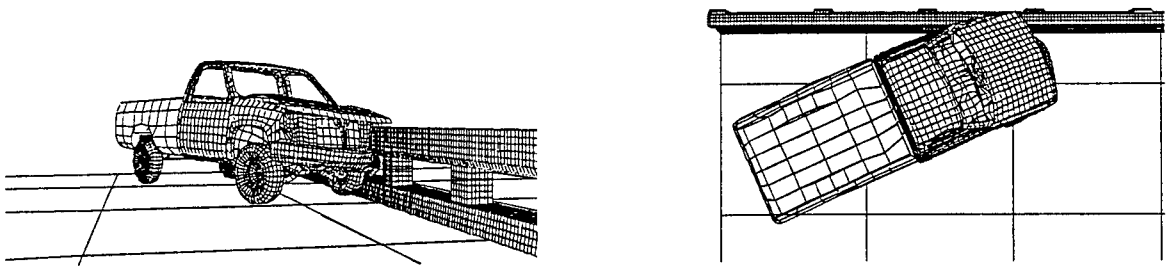

Figure A-3a: Simulation 4-3

time = 0.060 sec

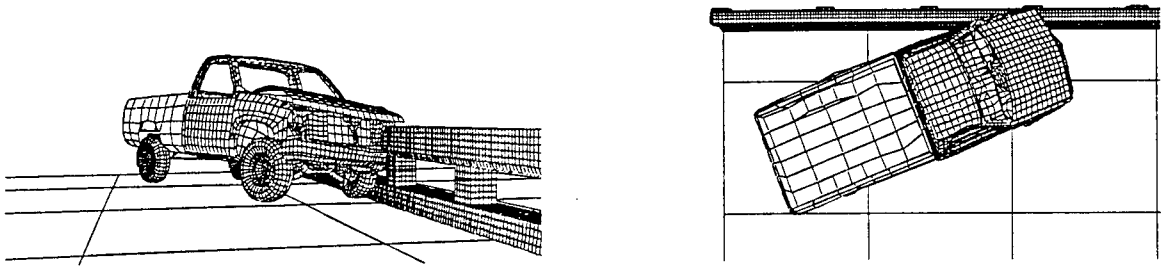

time = 0.075 sec

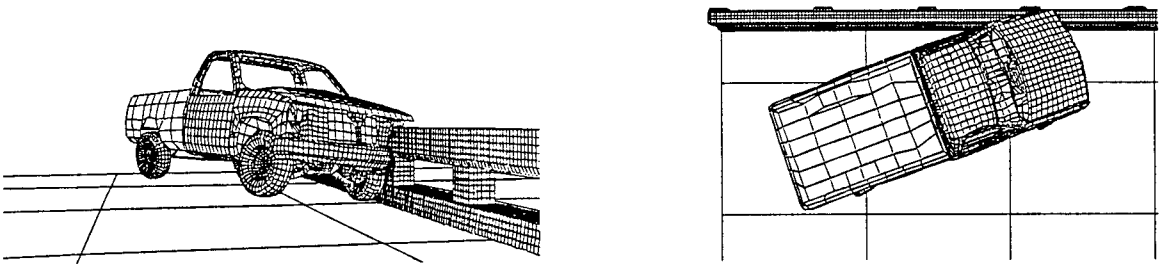

time = 0.090 sec

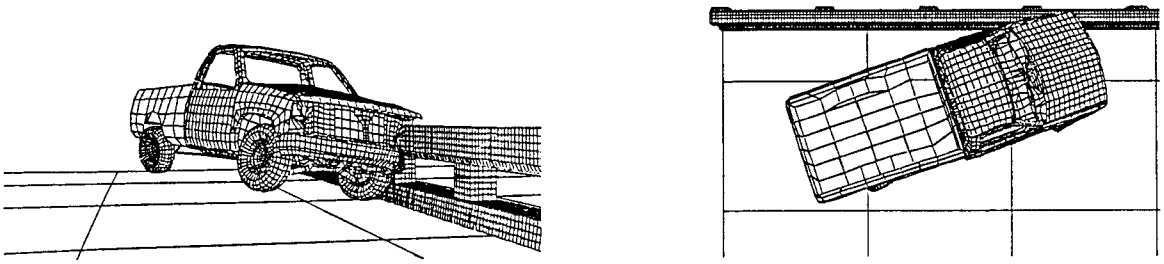

time = 0.105 sec

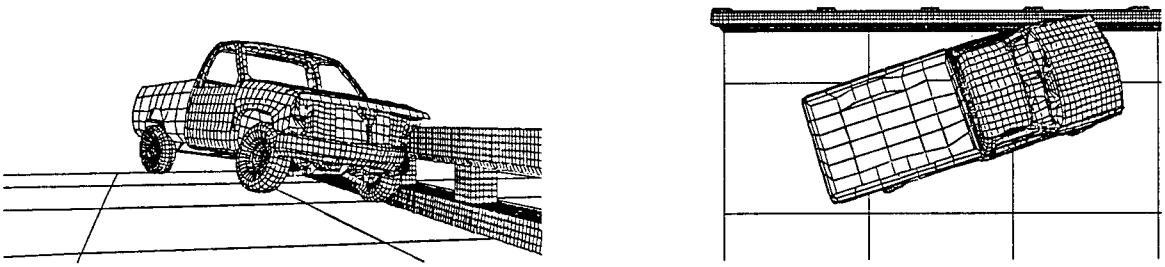

Figure A-3b: Simulation 4-3 cont.

time = 0.000 sec

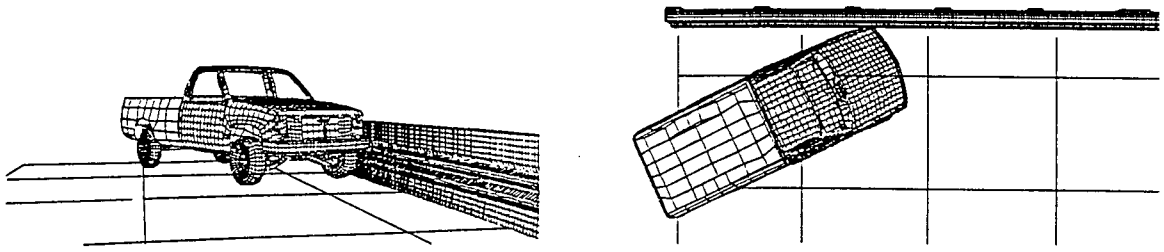

time = 0.030 sec

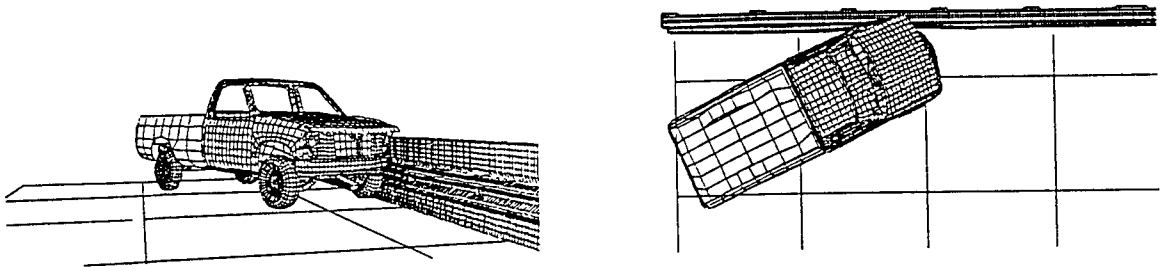

time = 0.060 sec

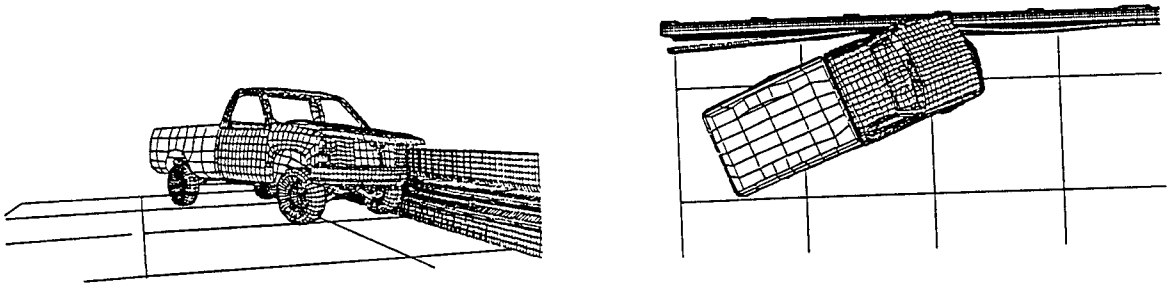

time = 0.090 sec

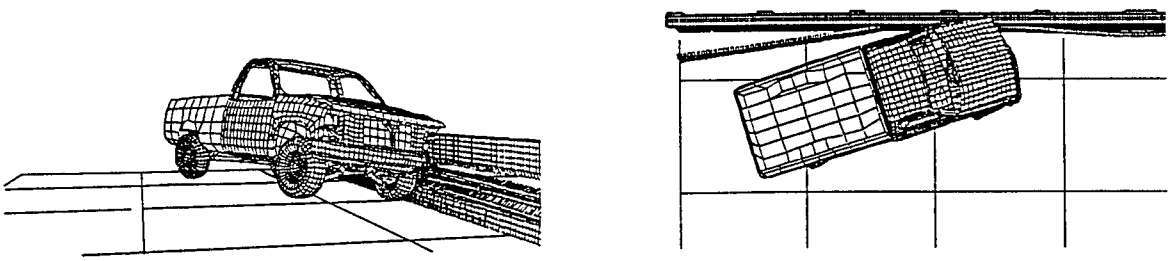

Figure A-4a: Simulation 4-4

time = 0.120 sec

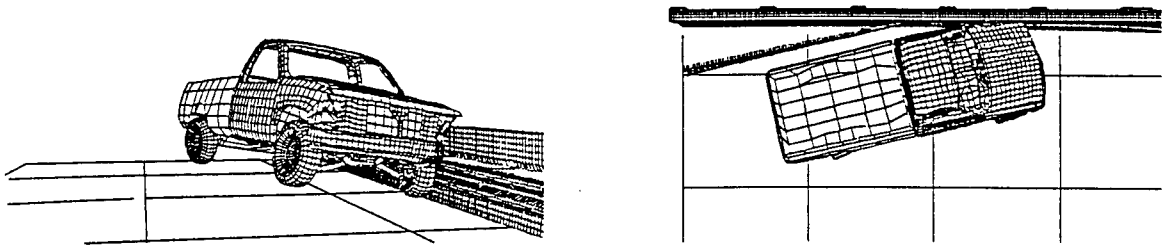

time = 0.150 sec

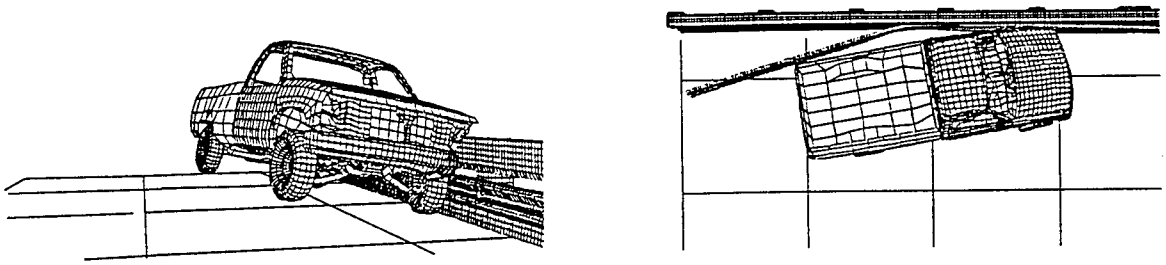

time = 0.180 sec

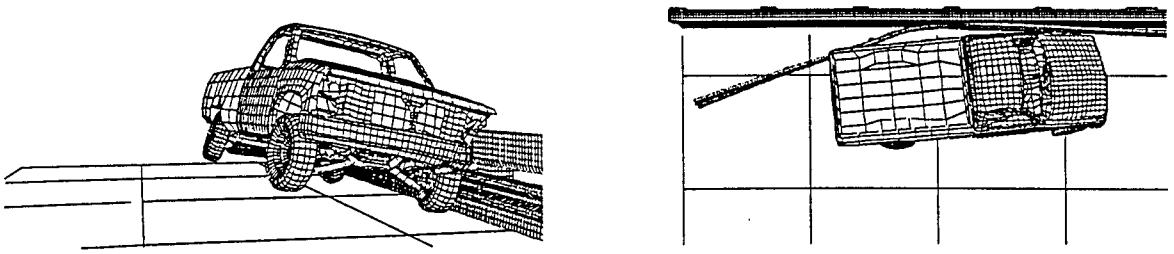

time = 0.210 sec

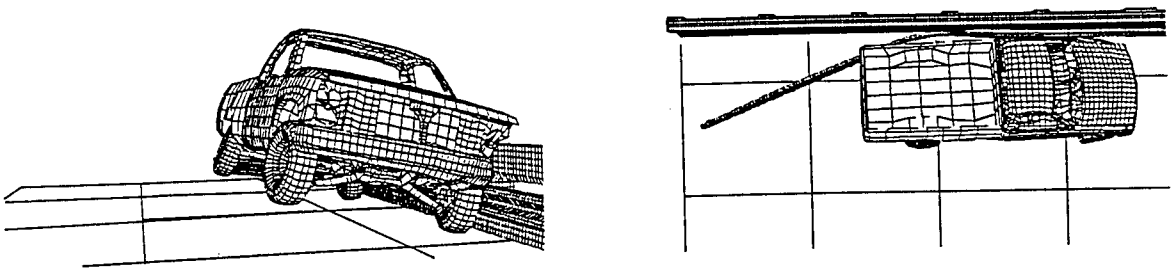

Figure A-4b: Simulation 4-4 cont.

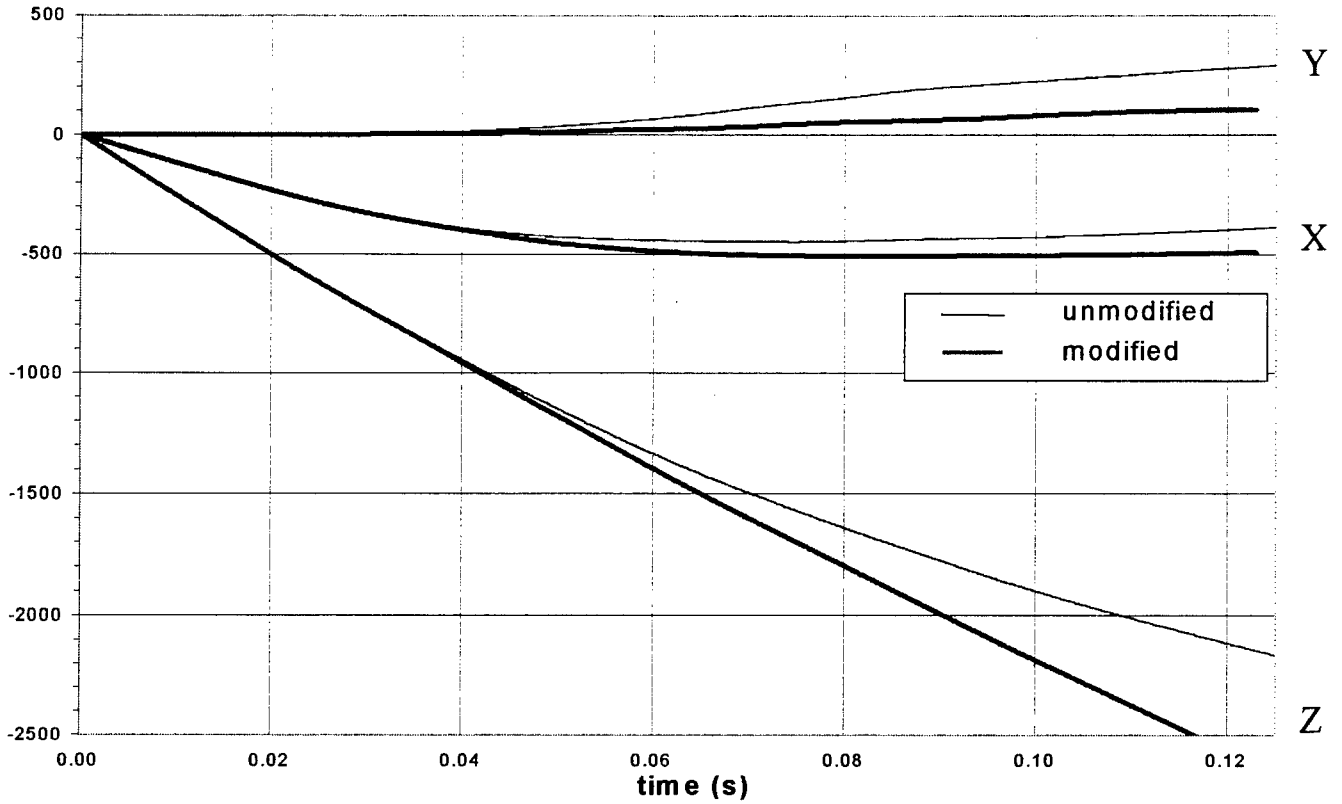

Figure A-5: Global displacement of the car's C.G. with respect to the barrier vs. time (Simulation 4-1&2)

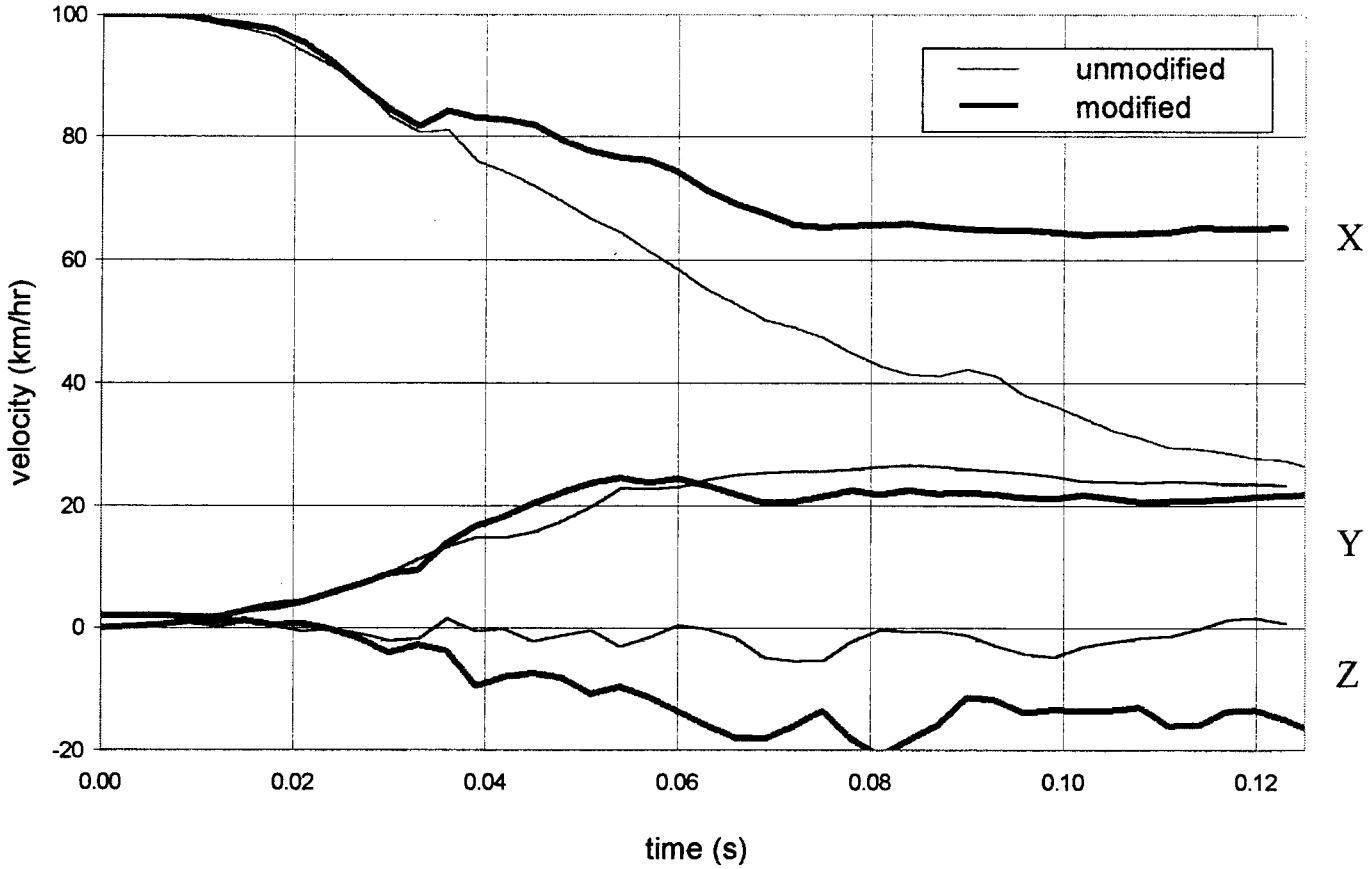

Figure A-6: Local velocity vs. time (Simulation 4-1&2)

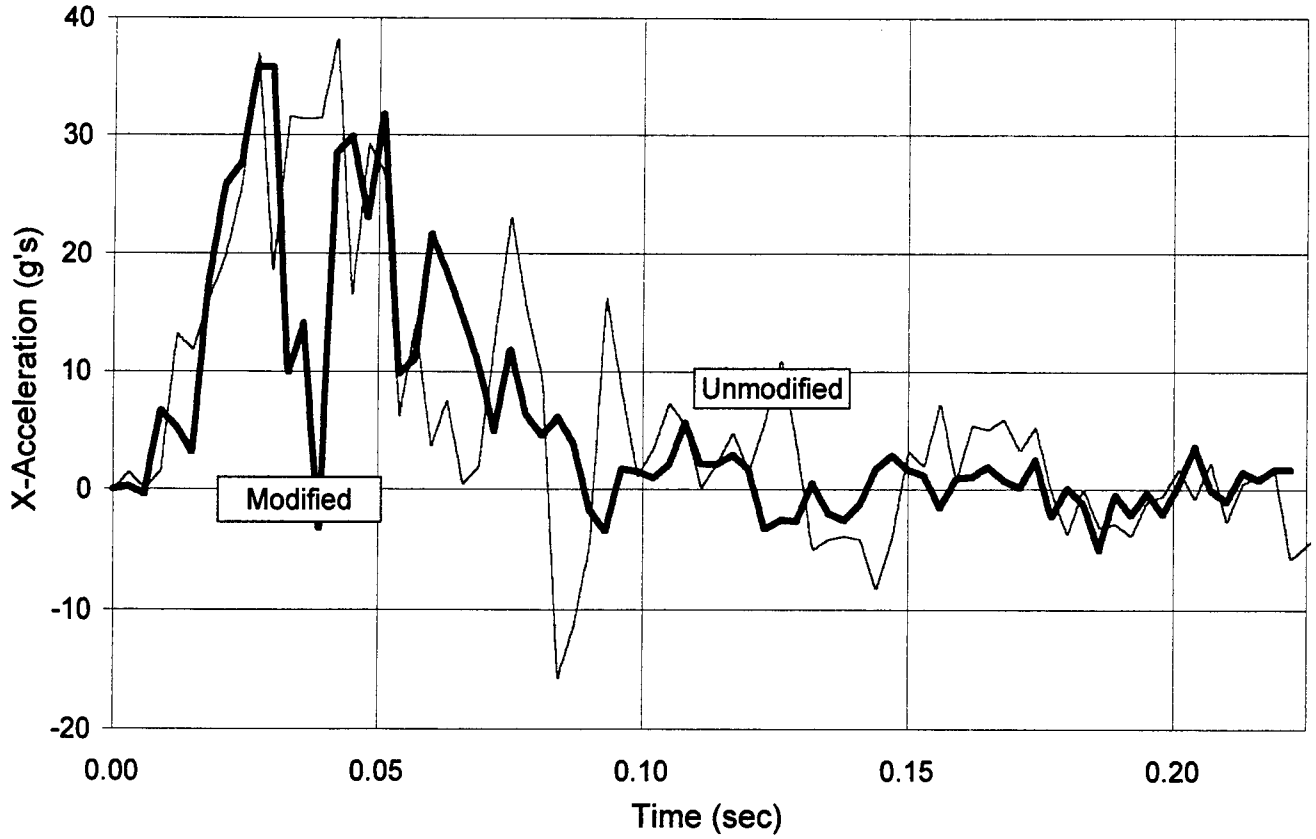

Figure A-7a: Global X-acceleration vs. time (Simulation 4-1&2)

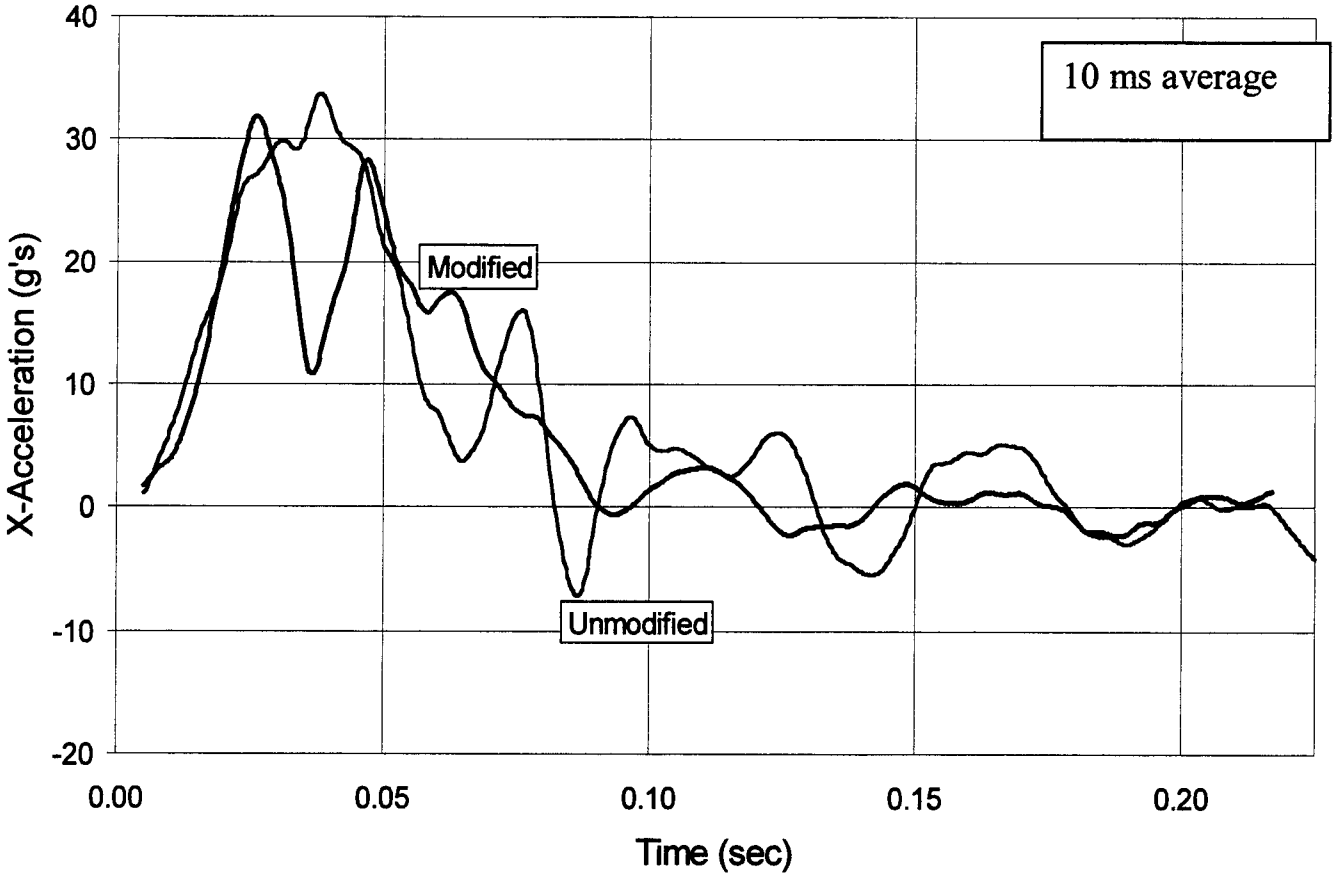

Figure A-7b: 10ms average of X-acceleration (Simulation 4-1&2)

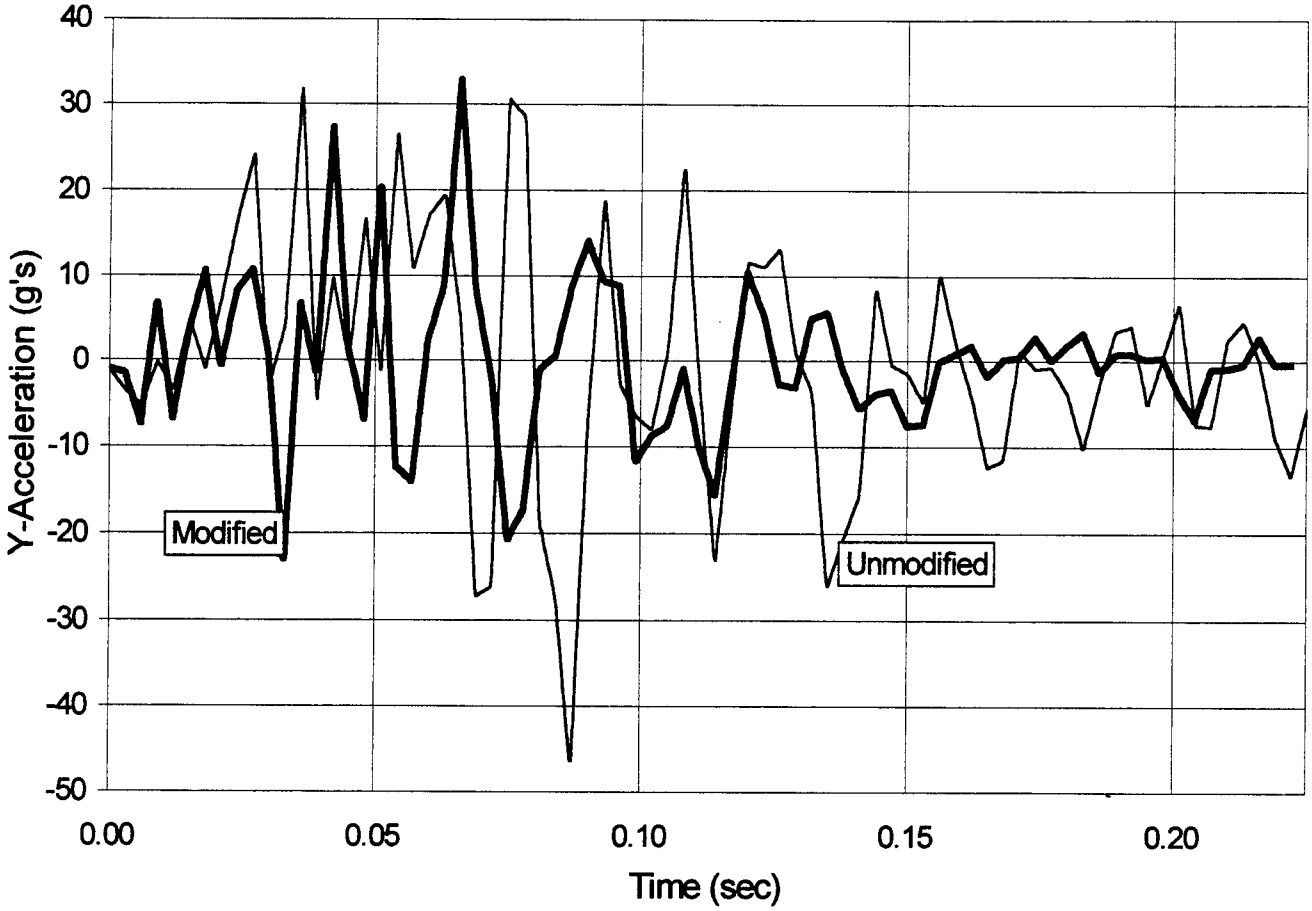

Figure A-8a: Global Y-acceleration vs. time (Simulation 4-1&2)

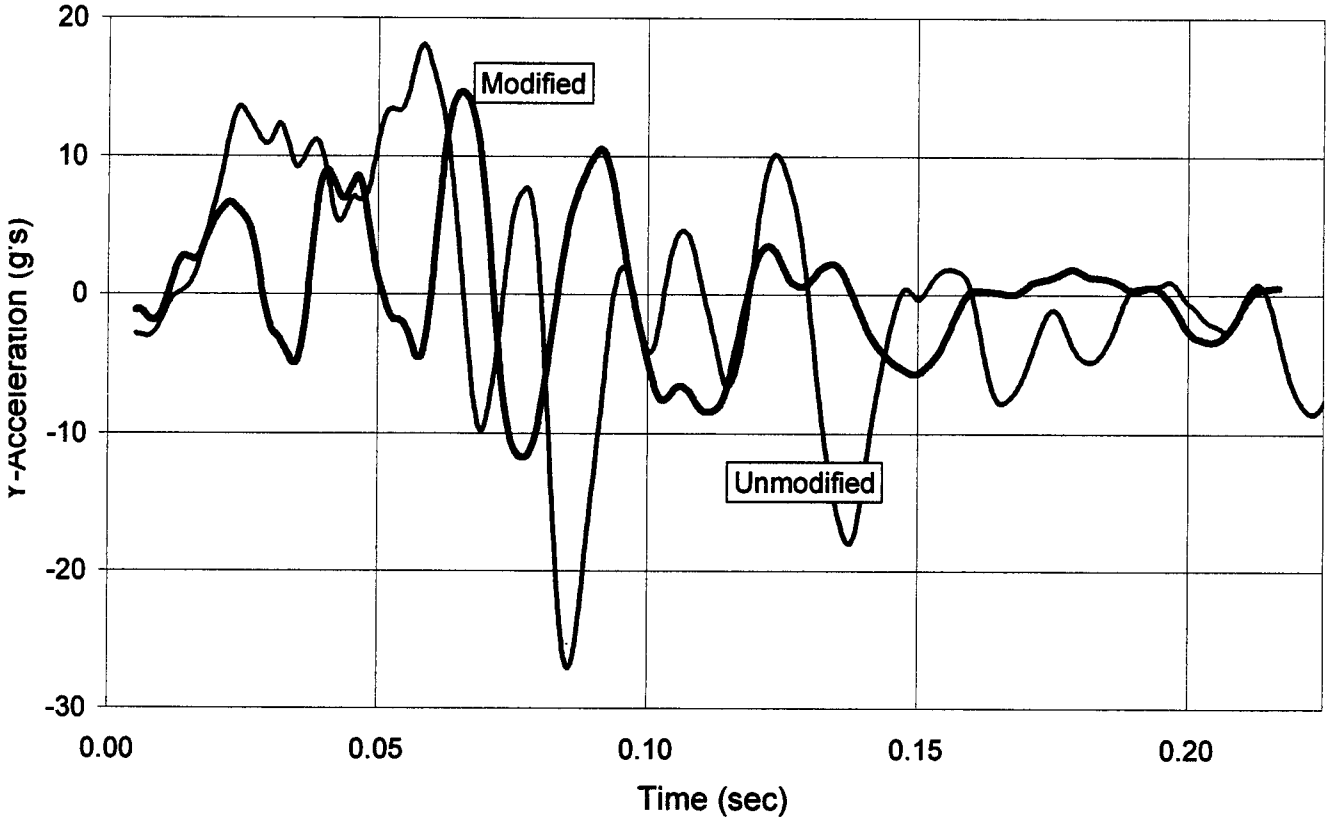

Figure A-8b: 10ms average of Y-acceleration (Simulation 4-1&2)

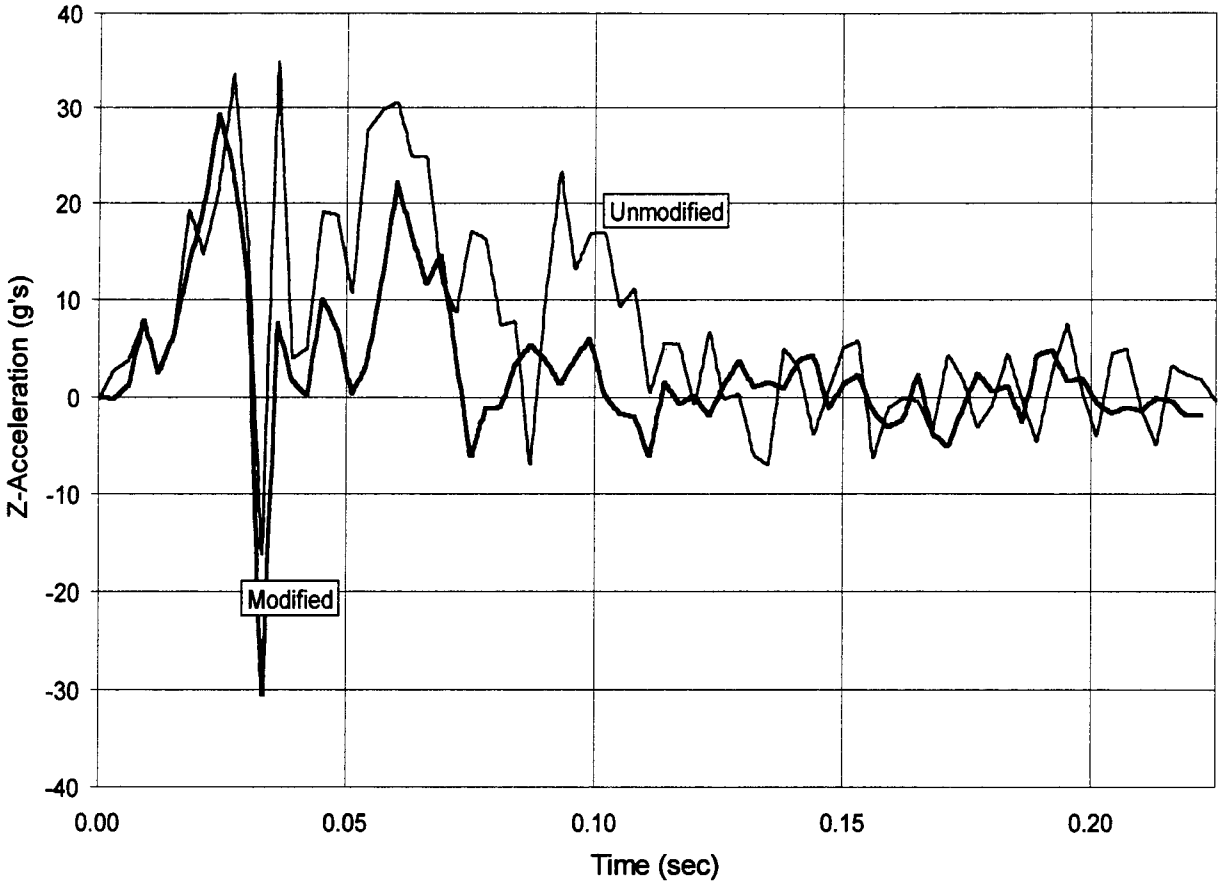

Figure A-9a: Global Z-acceleration vs. time (Simulation 4-1&2)

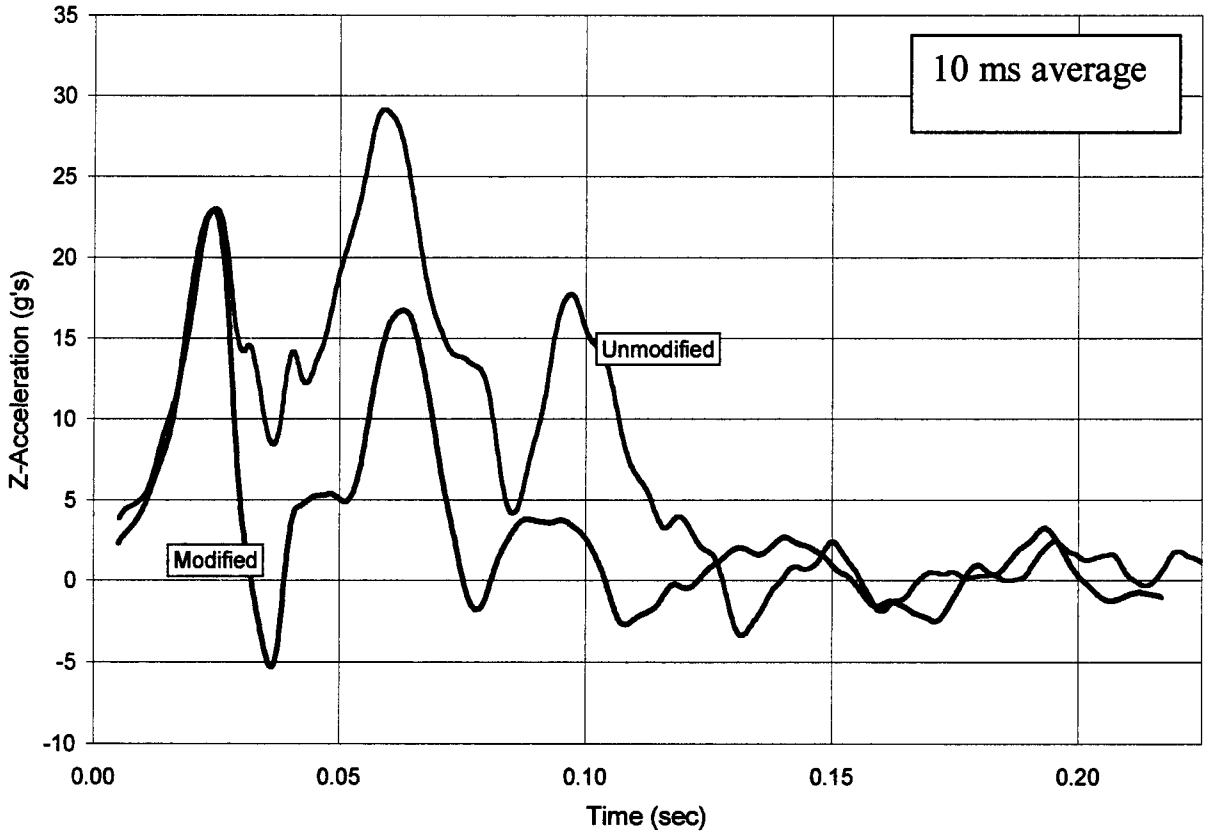

Figure A-9b: 10ms average of Z-acceleration (Simulation 4-1&2)

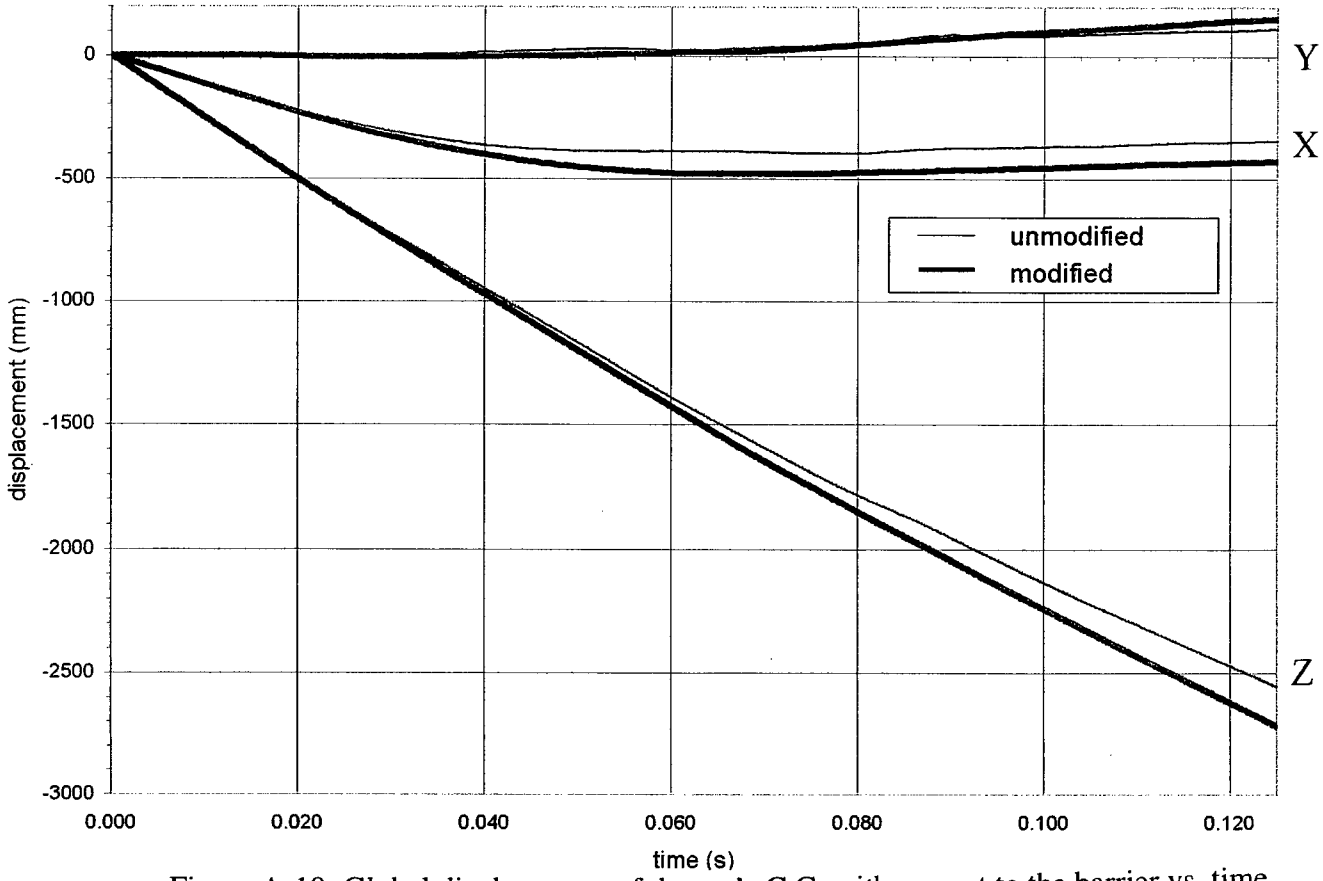

Figure A-10: Global displacement of the car's C.G. with respect to the barrier vs. time (Simulation 4-3&4)

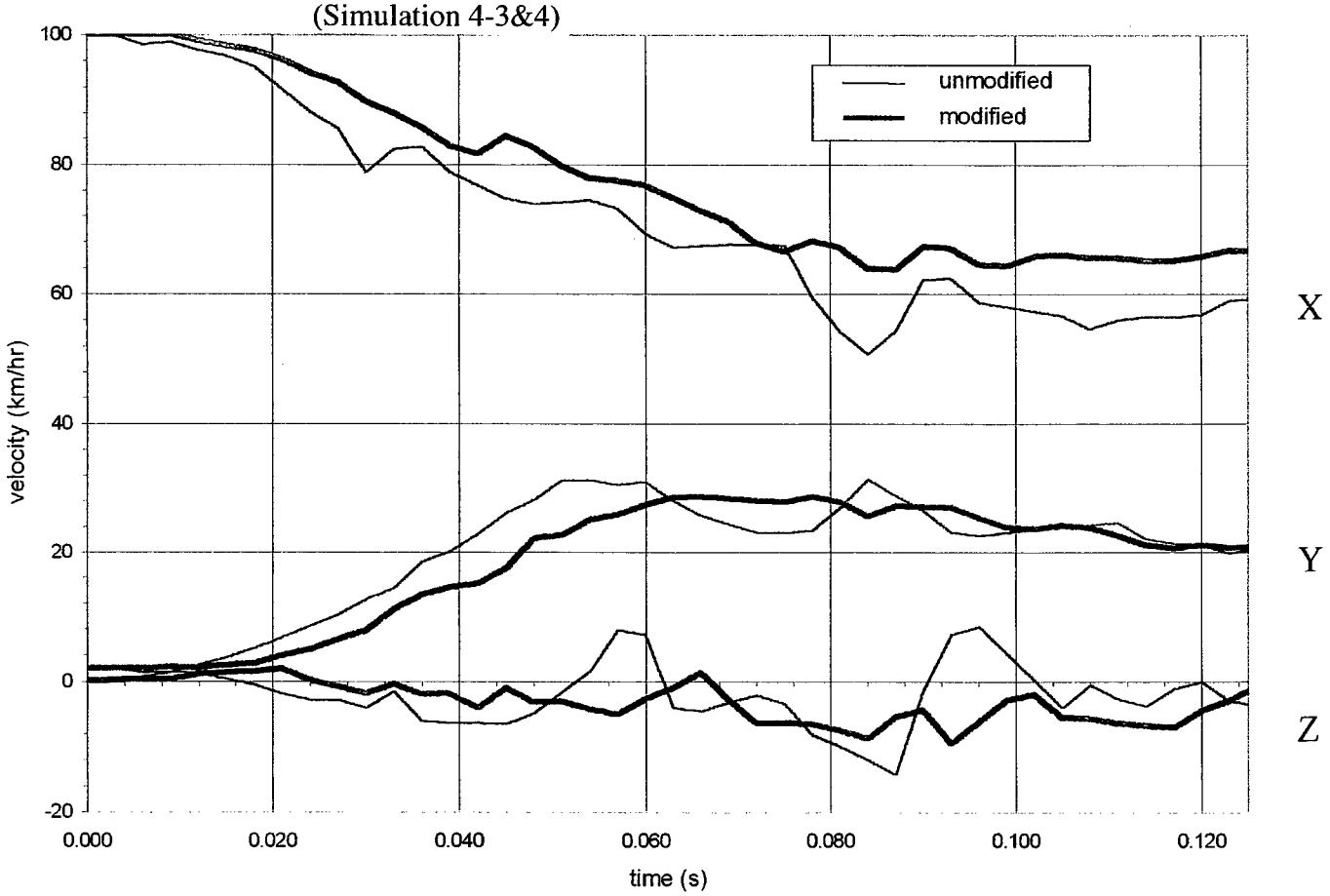

Figure A-11: Local velocity vs. time (Simulation 4-3&4)

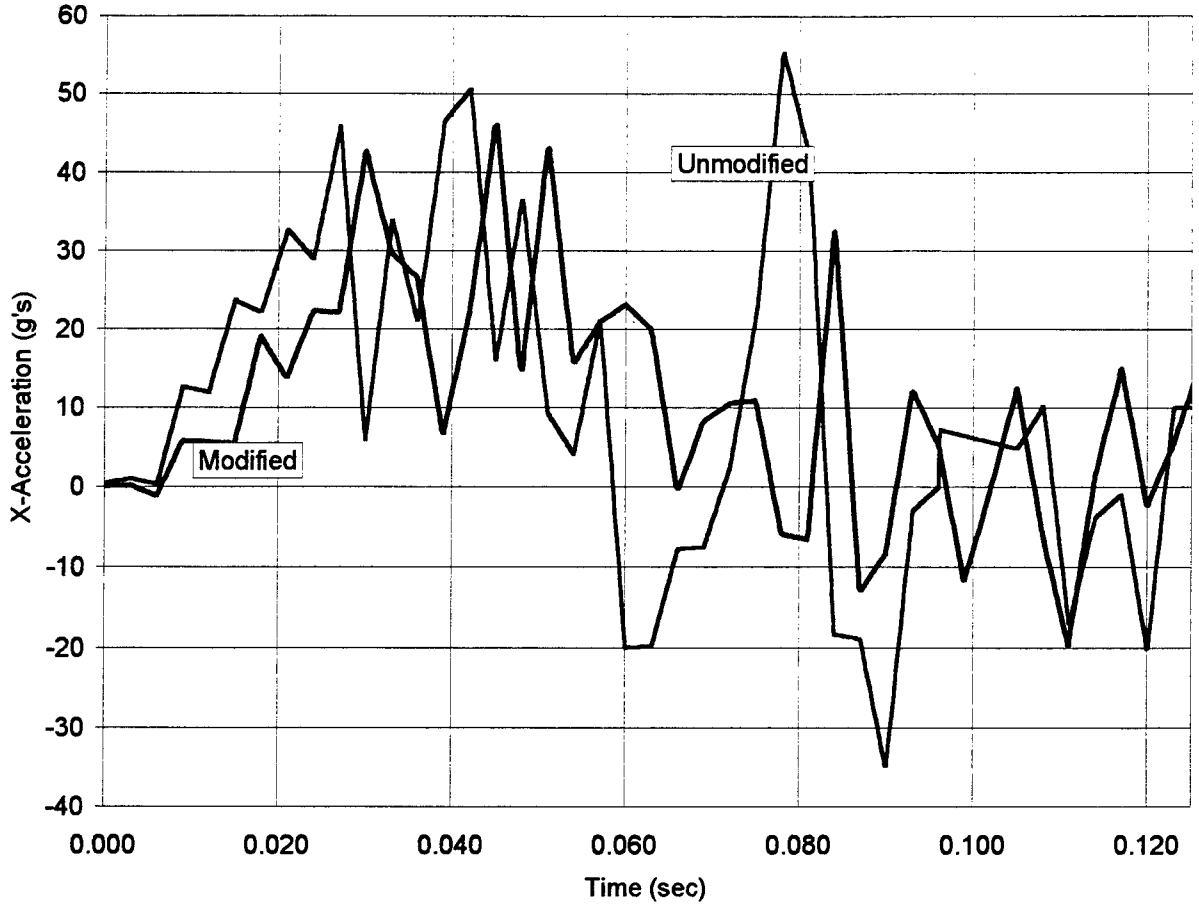

Figure A-12a: Global X-acceleration vs. time (Simulation 4-3&4)

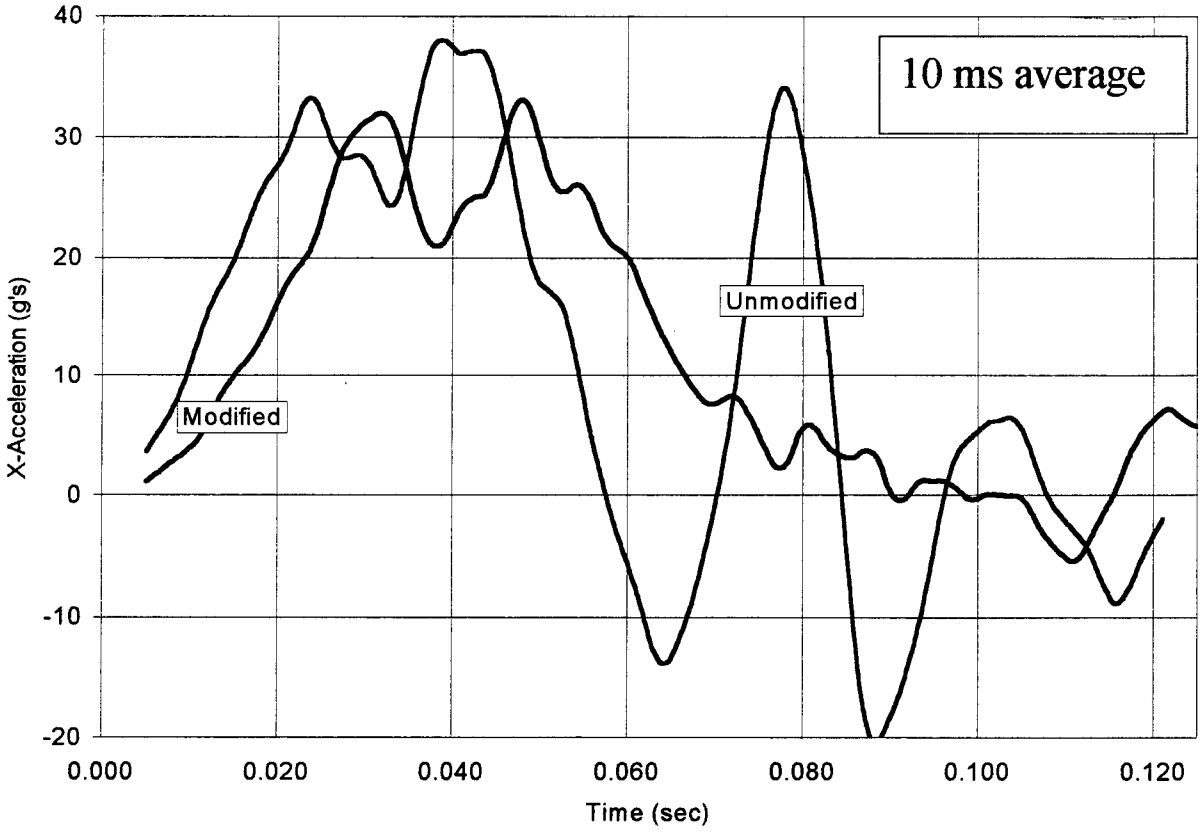

Figure A-12b: 10ms average of X-acceleration (Simulation 4-3&4)

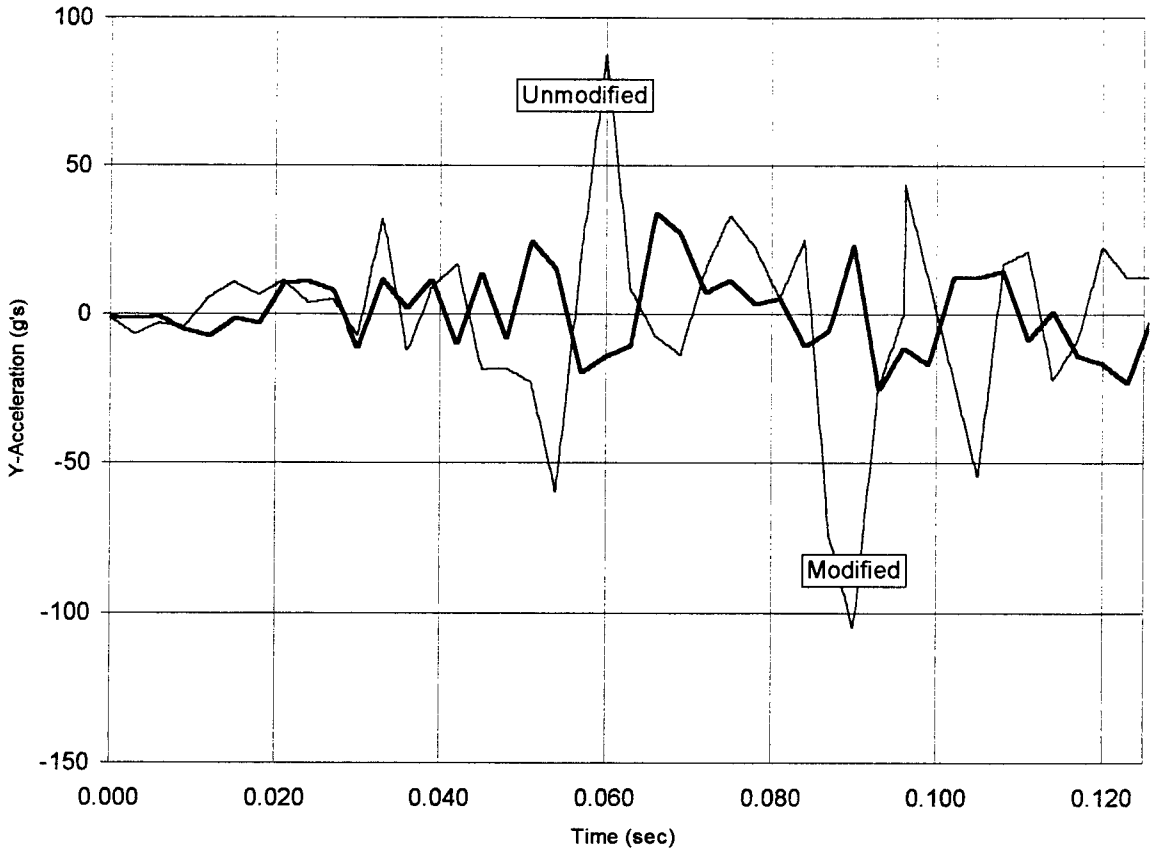

Figure A-13a: Global Y-acceleration vs. time (Simulation 4-3&4)

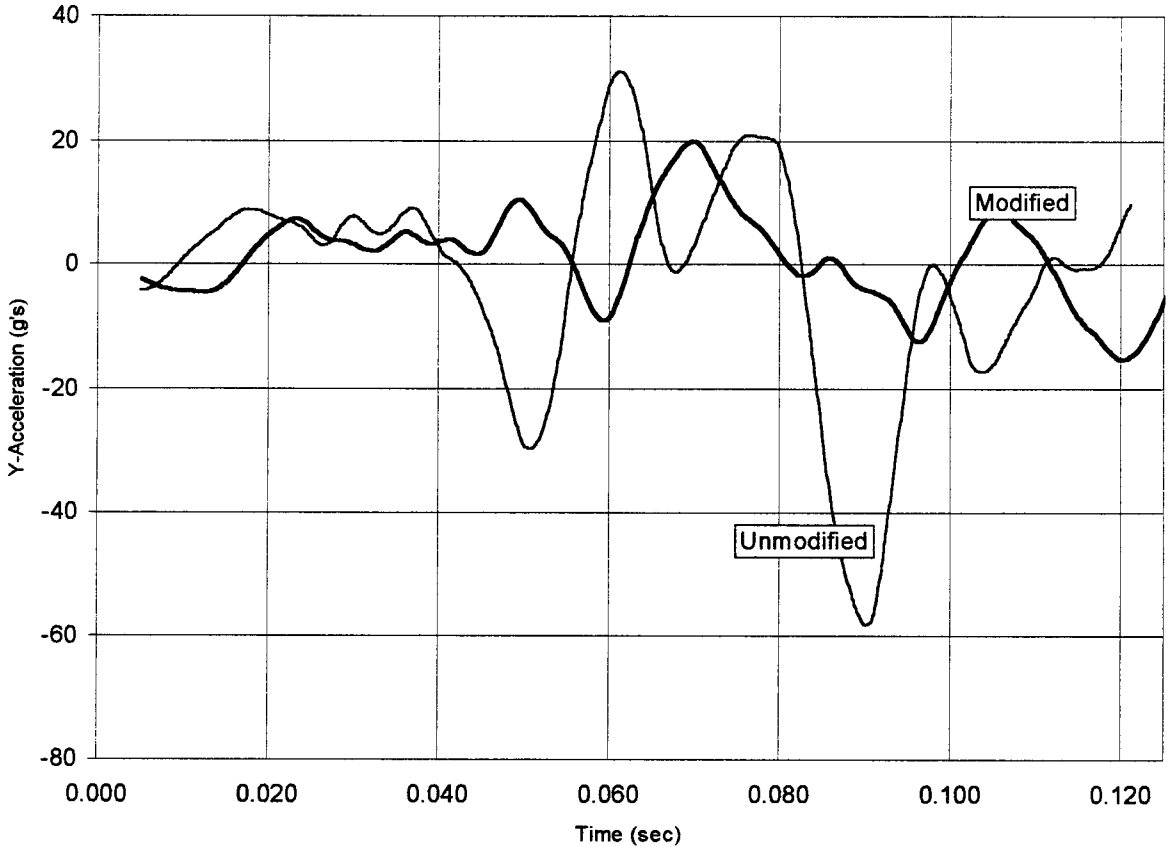

Figure A-13b: 10ms average of Y-acceleration (Simulation 4-3&4)

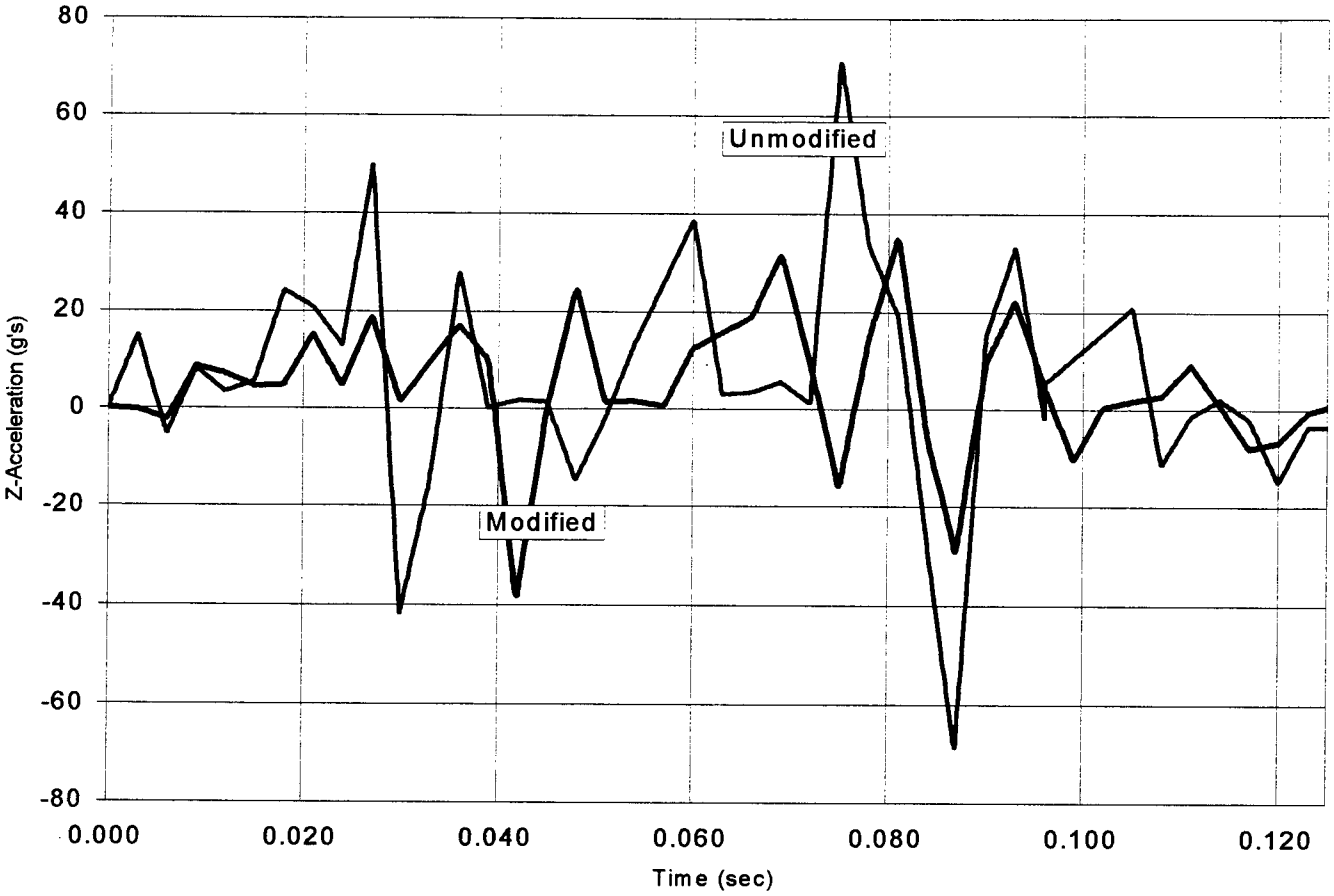

Figure A-14a: Global Z-acceleration vs. time (Simulation 4-3&4)

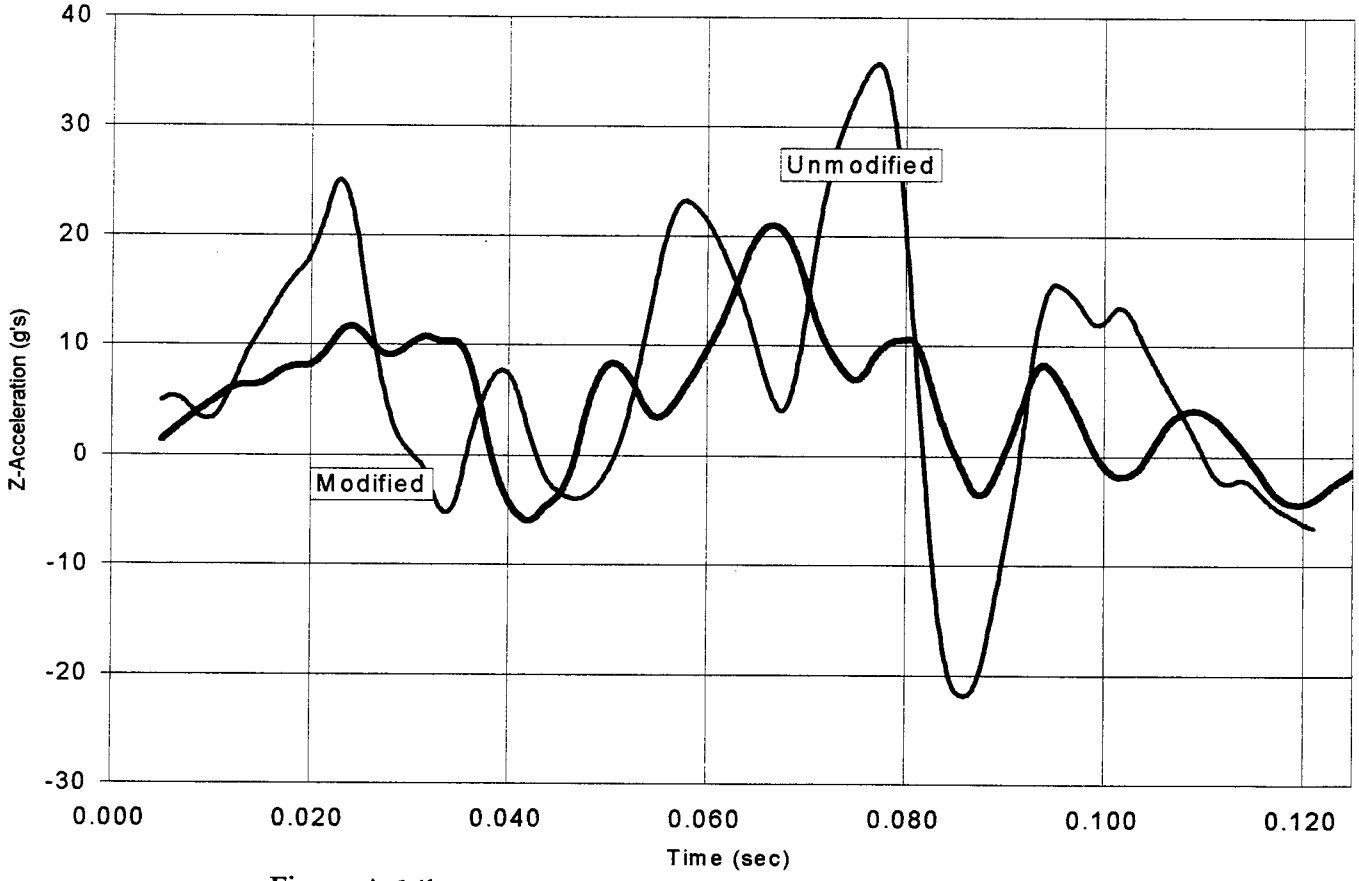

Figure A-14b: 10ms average of Z-acceleration (Simulation 4-3&4)

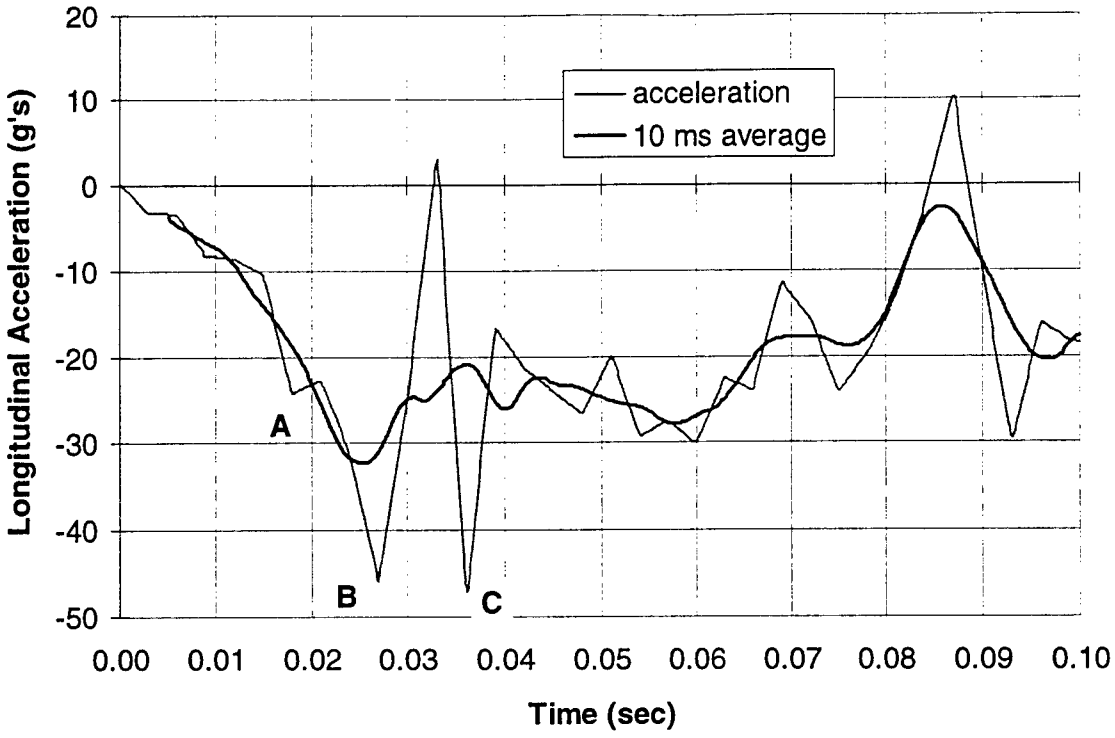

Point **A** - time t = 0.018 s

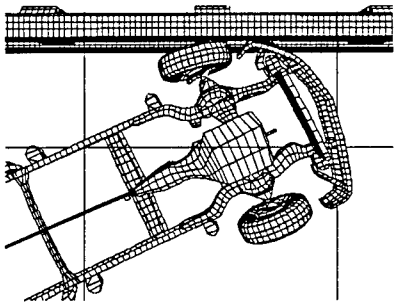

Point **B** - time t = 0.027 s

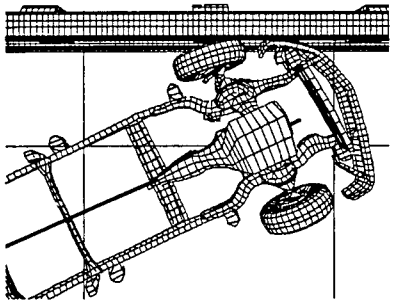

Point **C** - time t = 0.036 s

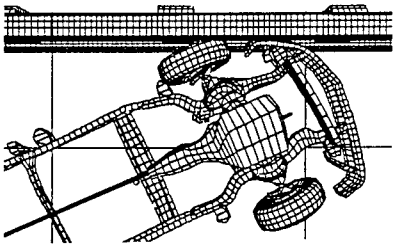

Figure A-15: Longitudinal accelerations (Simulation 4-1) correlation to acceleration peaks

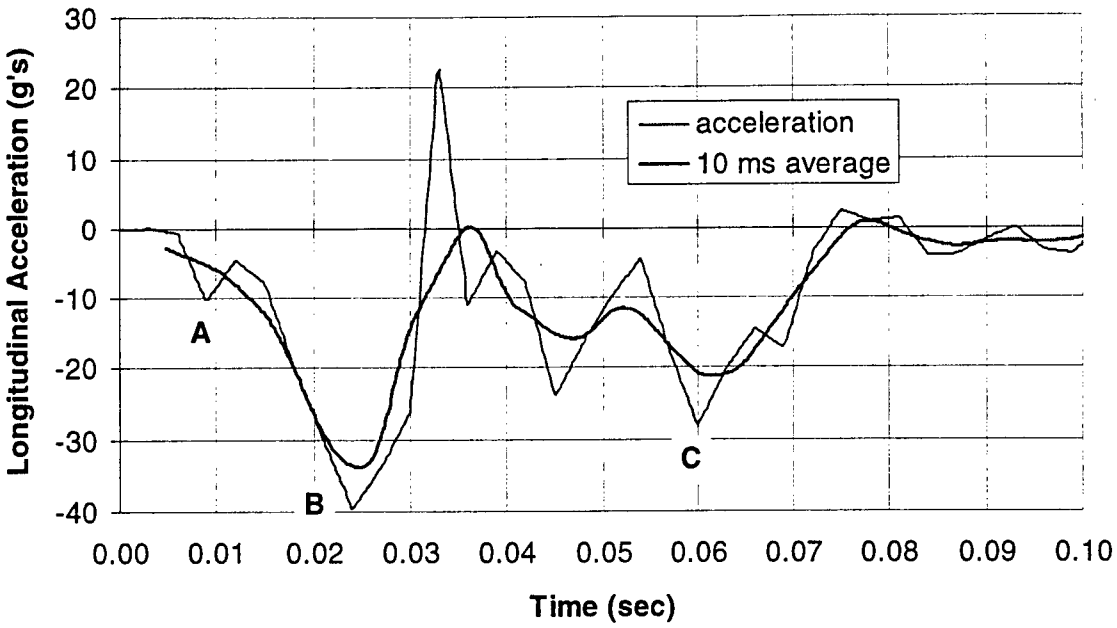

Point **A** - time t = 0.009 s

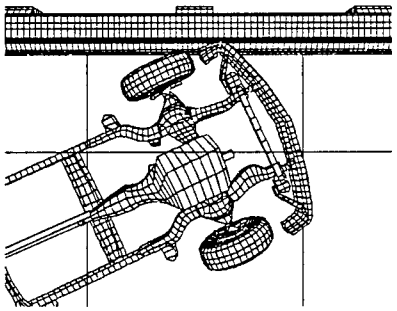

Point **B** - time t = 0.024 s

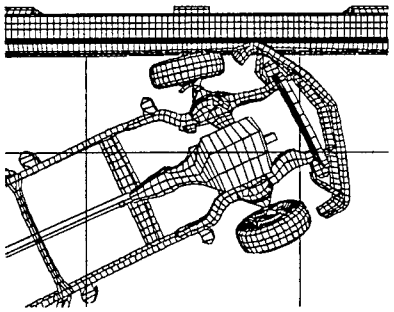

Point **C** - time t = 0.060 s

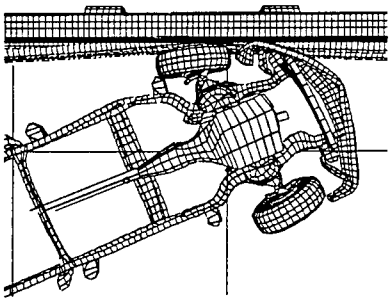

Figure A-16: Longitudinal accelerations (Simulation 4-2) correlation to acceleration peaks

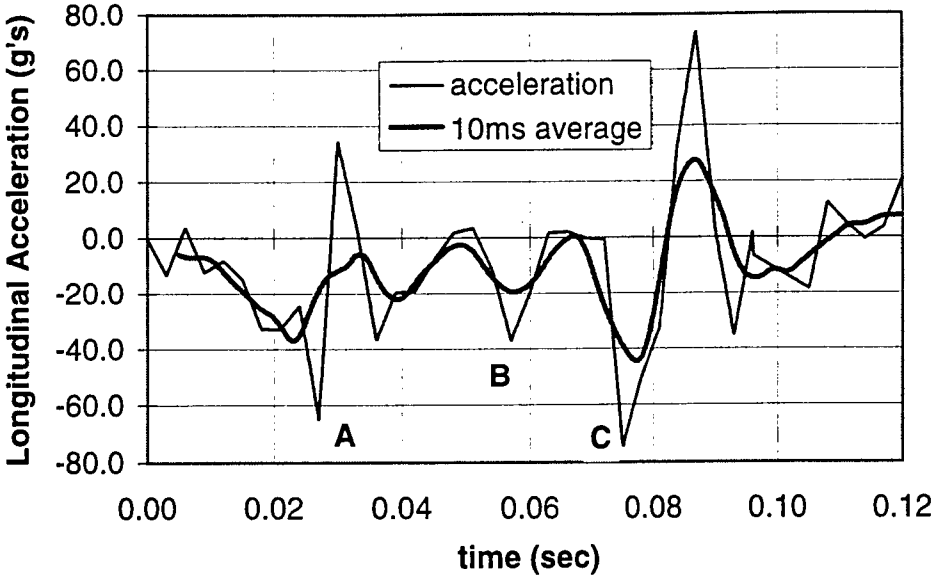

Point **A** - time t = 0.027 s

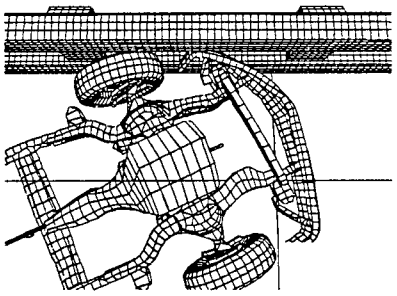

Point **B** - time t = 0.057 s

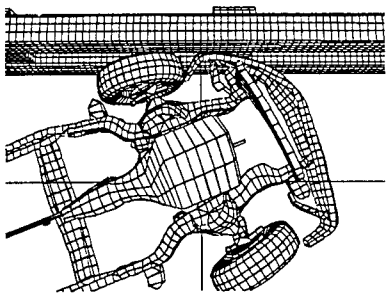

Point **C** - time t = 0.075 s

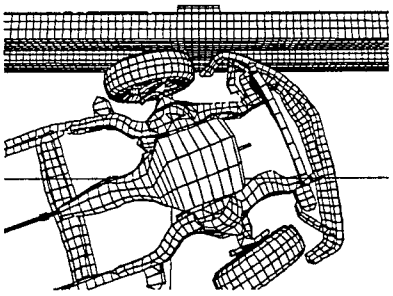

Figure A-17: Longitudinal accelerations (Simulation 4-3) correlation to acceleration peaks

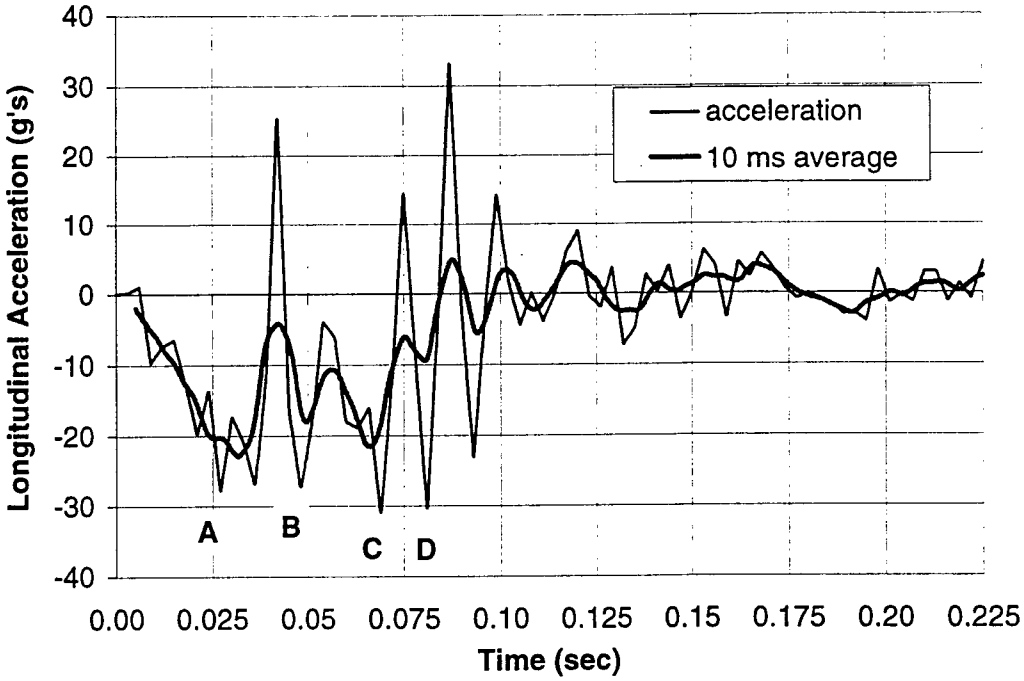

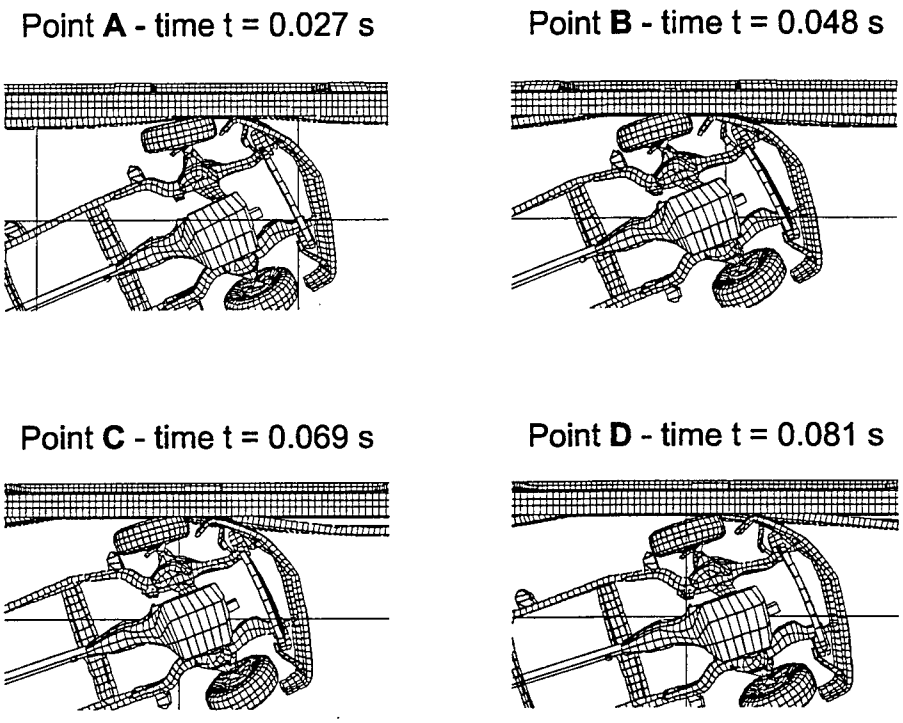

Figure A-18: Longitudinal accelerations (Simulation 4-4) correlation to acceleration peaks

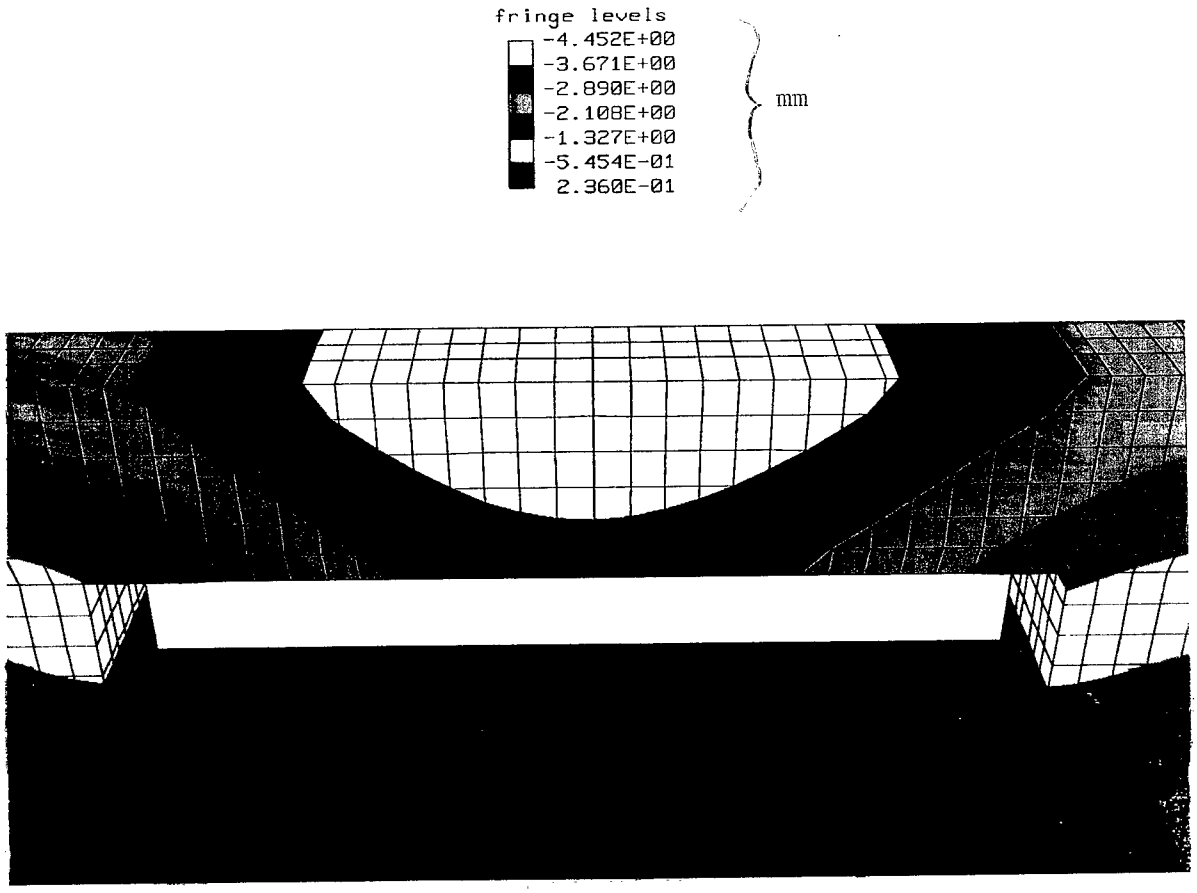

Figure A-19: Fringes of X-displacement (simulation 4-3) (mm)

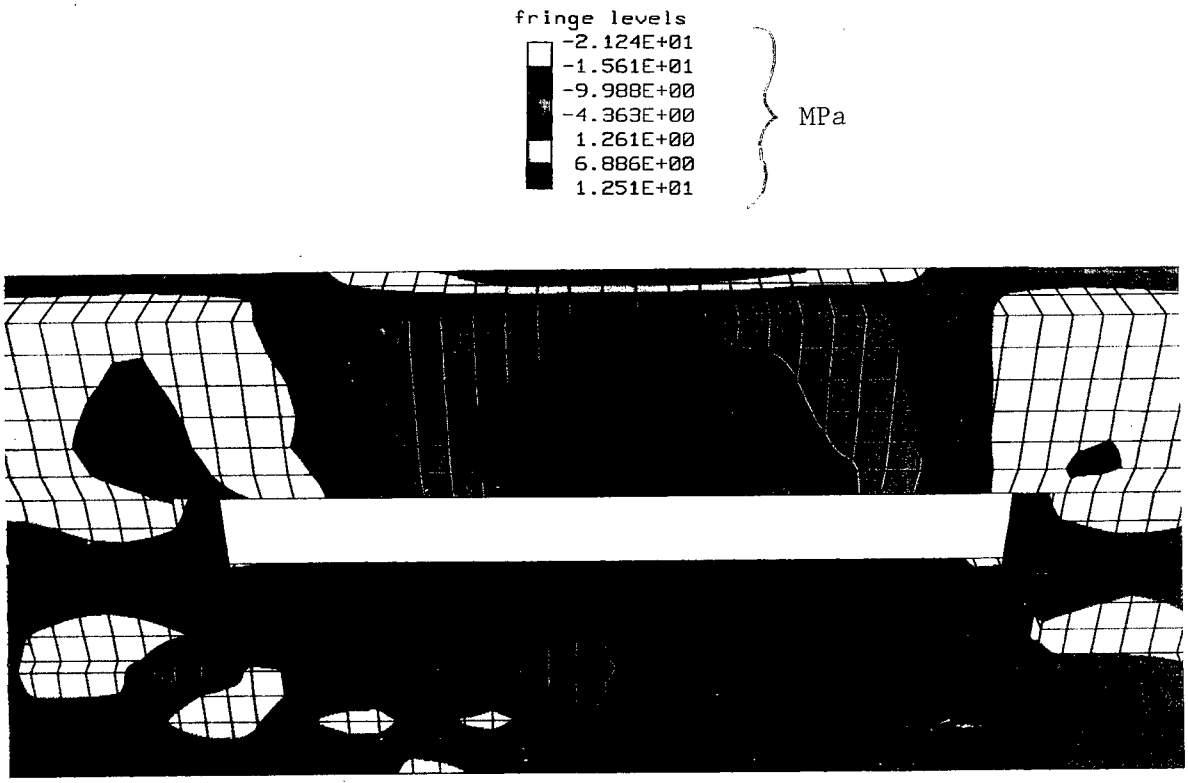

Figure A-20: Fringes of Z-Stress (simulation 4-3) (MPa)

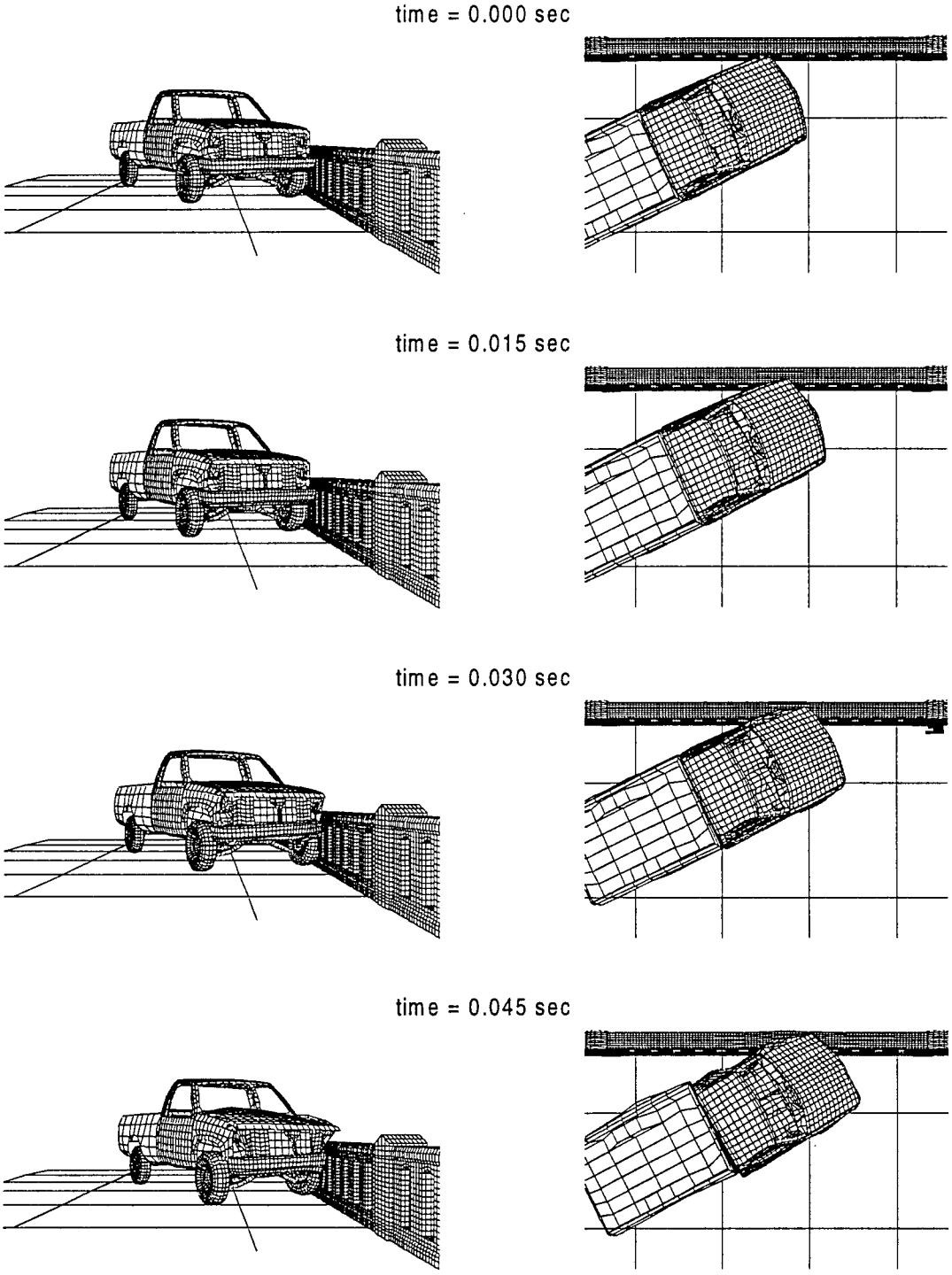

Figure A-21a: Simulation 5-1

time = 0.060 sec

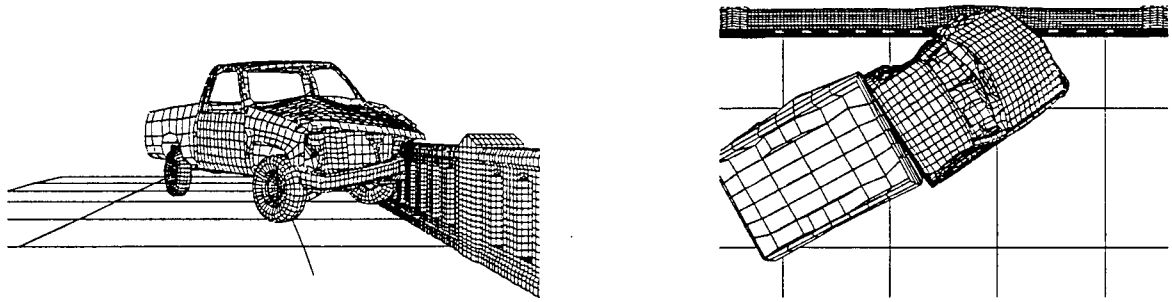

time = 0.075 sec

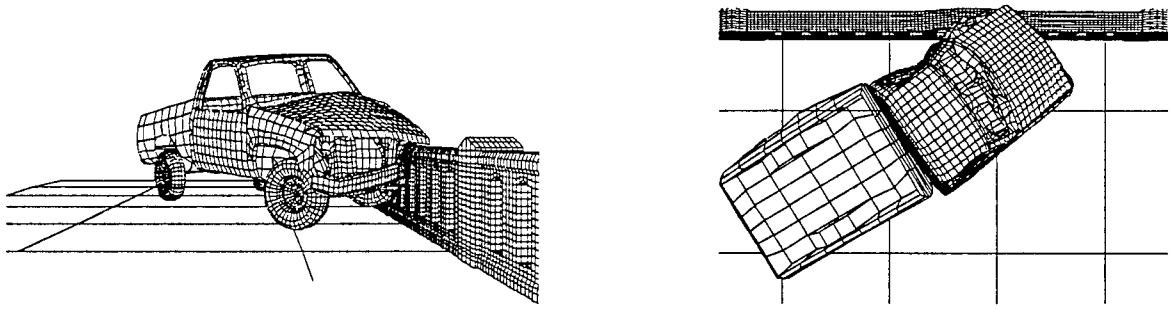

time = 0.090 sec

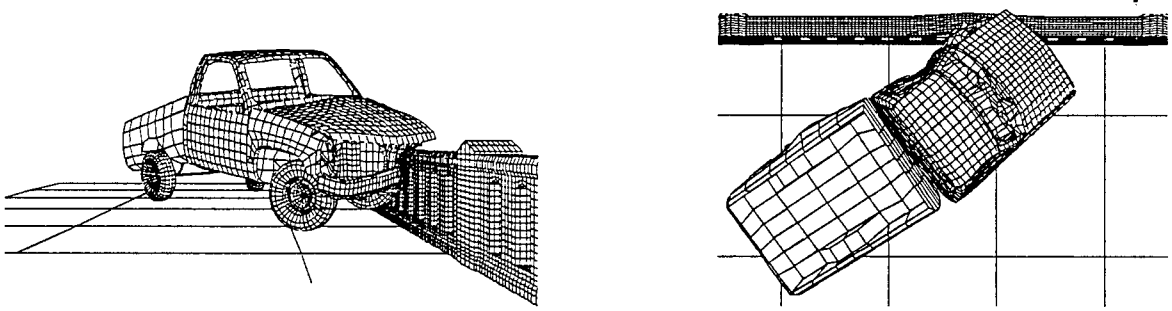

time = 0.105 sec

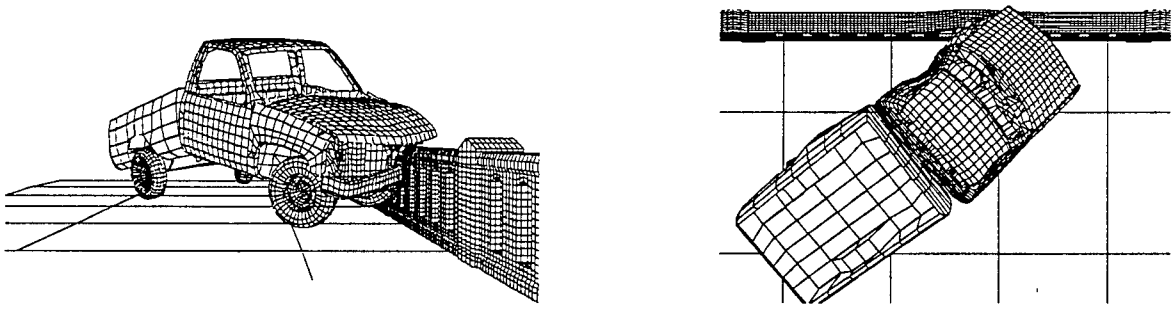

Figure A-21b: Simulation 5-1 cont.

time = 0.000 sec

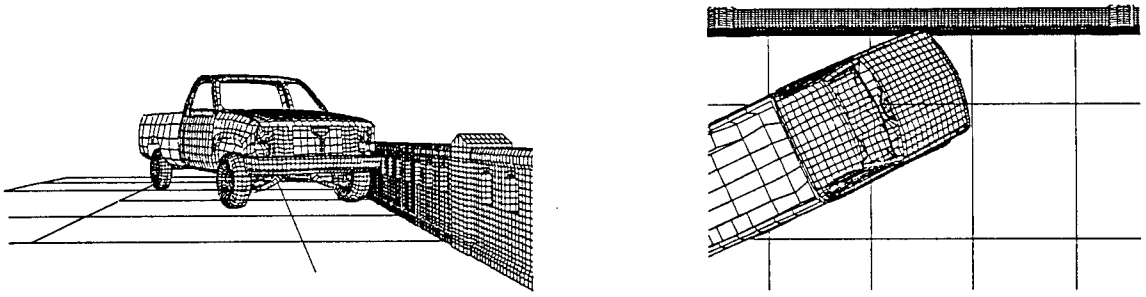

time = 0.015 sec

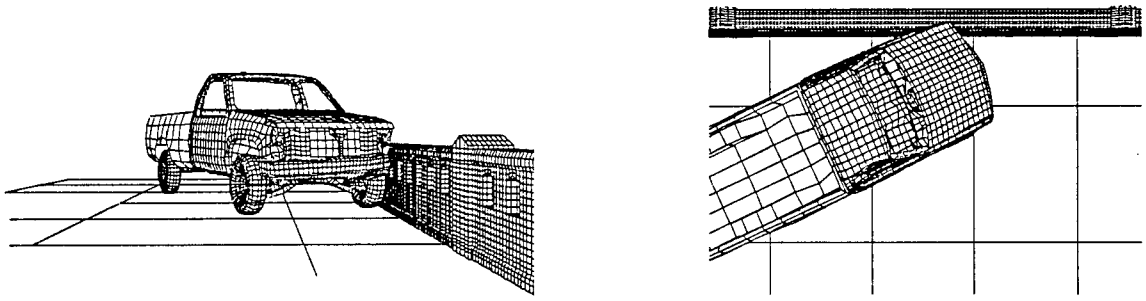

time = 0.030 sec

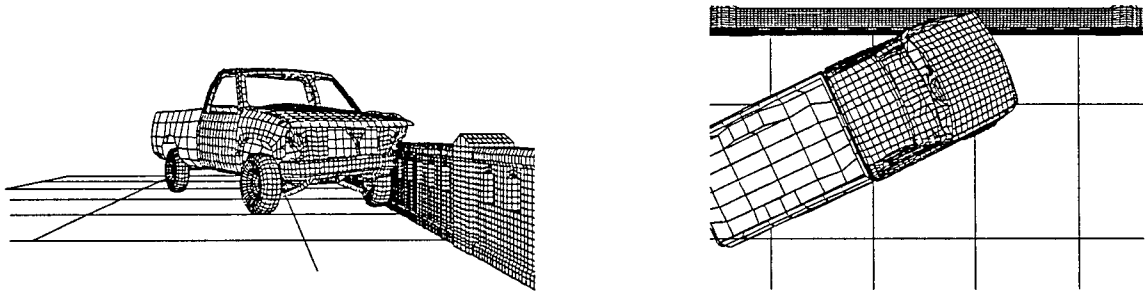

time = 0.045 sec

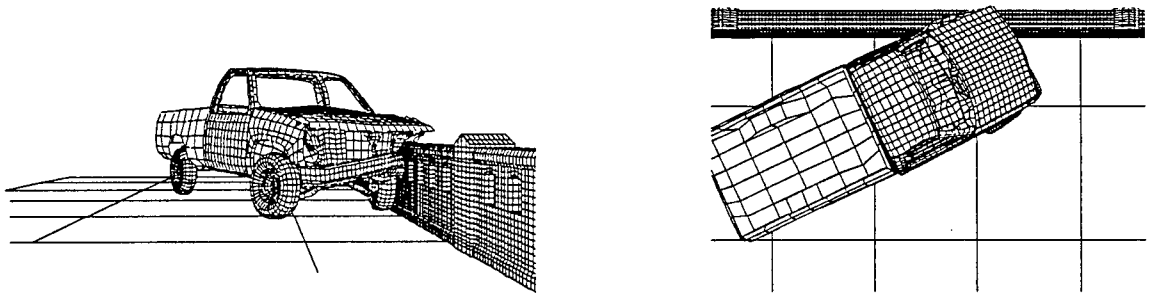

Figure A-22a: Simulation 5-2

time = 0.060 sec

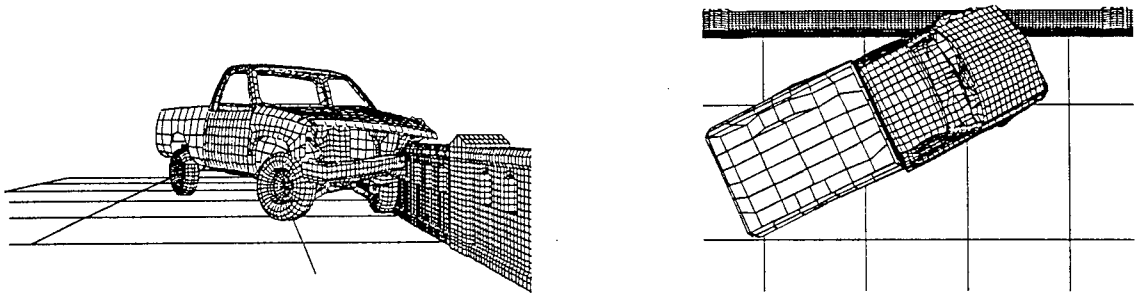

time = 0.075 sec

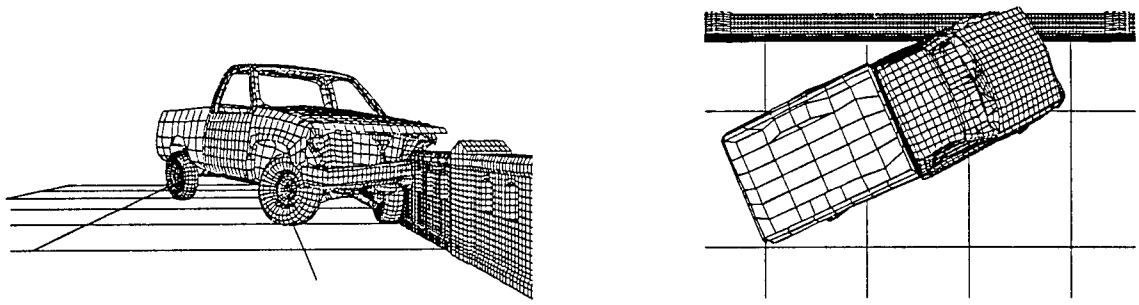

time = 0.090 sec

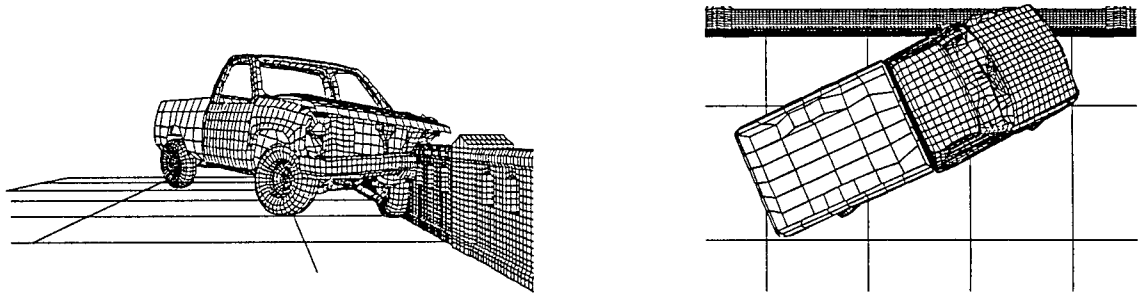

time = 0.105 sec

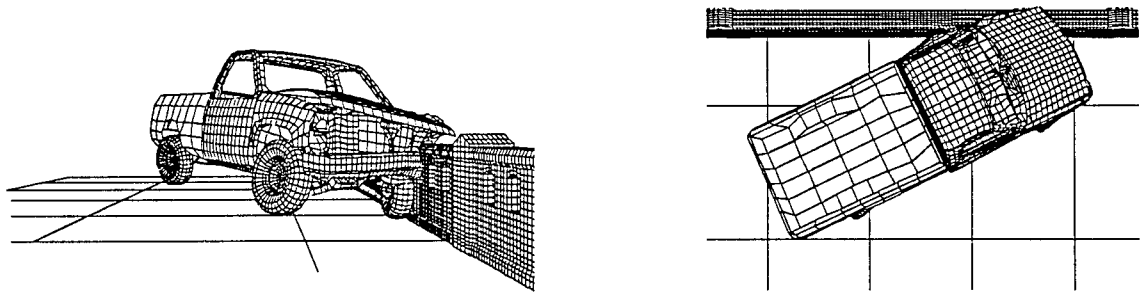

Figure A-22b: Simulation 5-2 cont.

time = 0.000 sec

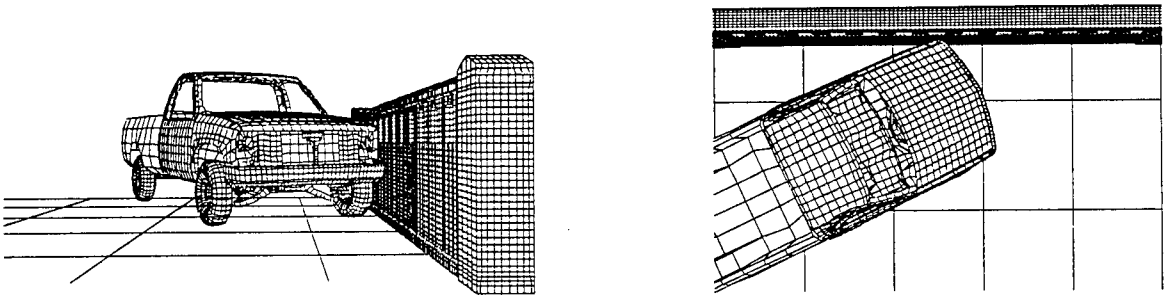

time = 0.015 sec

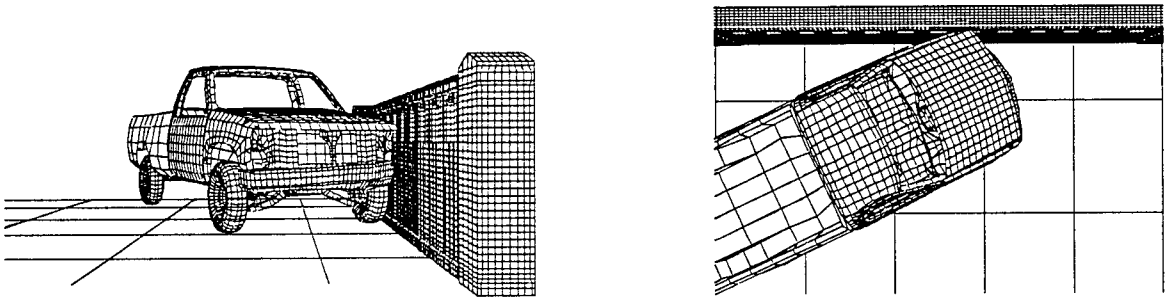

time = 0.030 sec

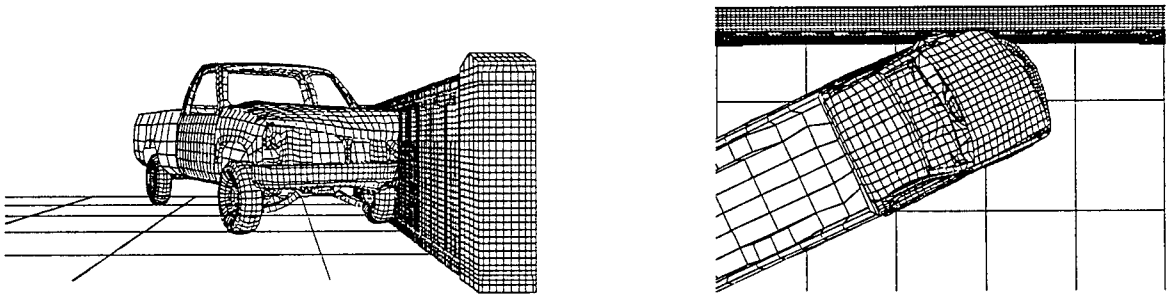

time = 0.045 sec

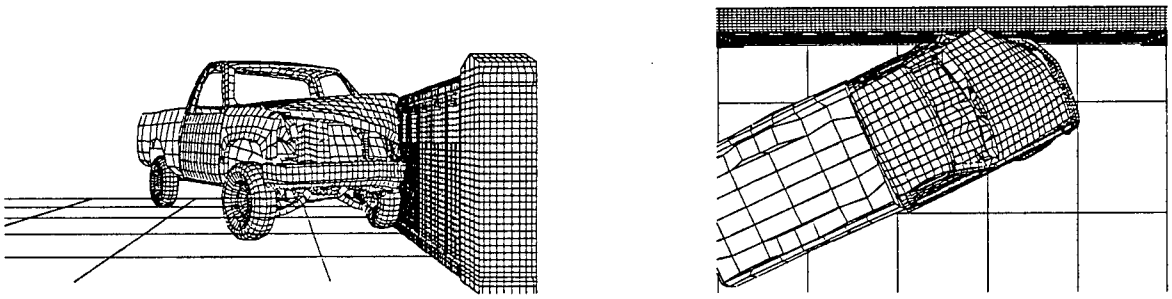

Figure A-23a: Simulation 5-3

time = 0.060 sec

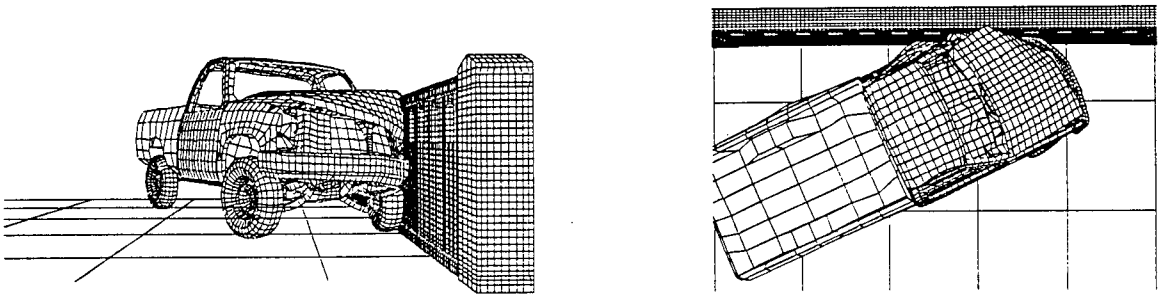

time = 0.075 sec

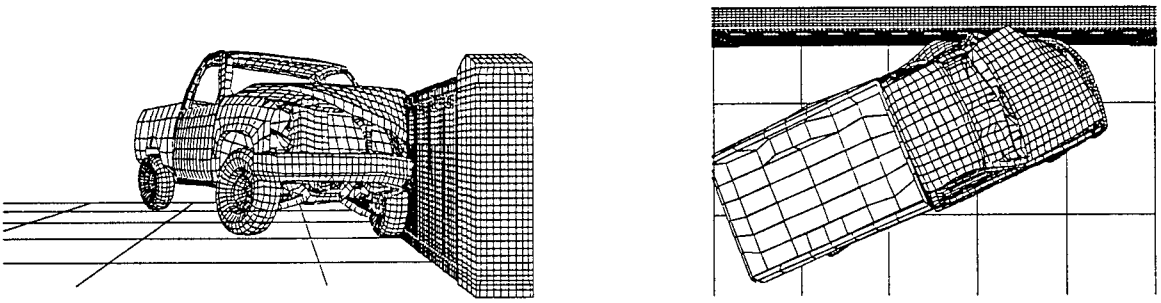

time = 0.090 sec

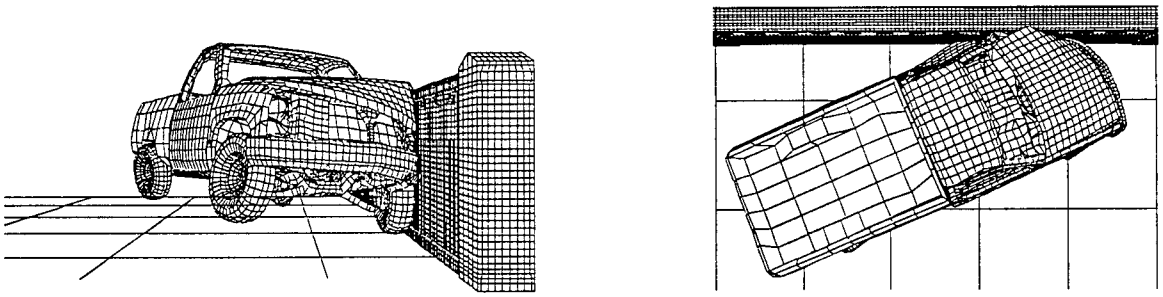

time = 0.102 sec

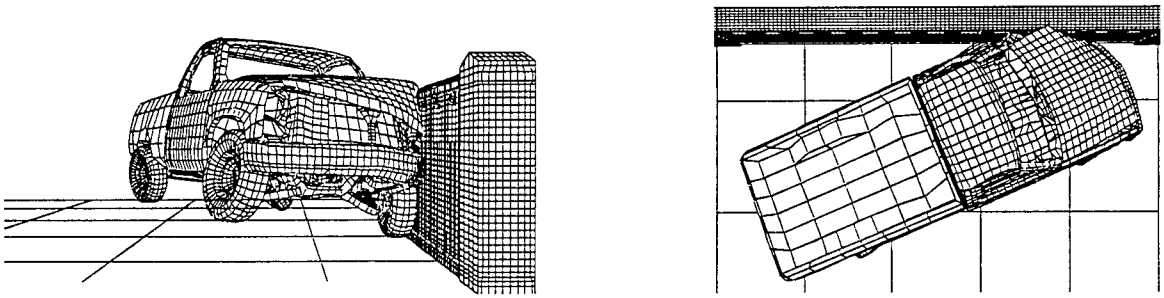

Figure A-23b: Simulation 5-3 cont.

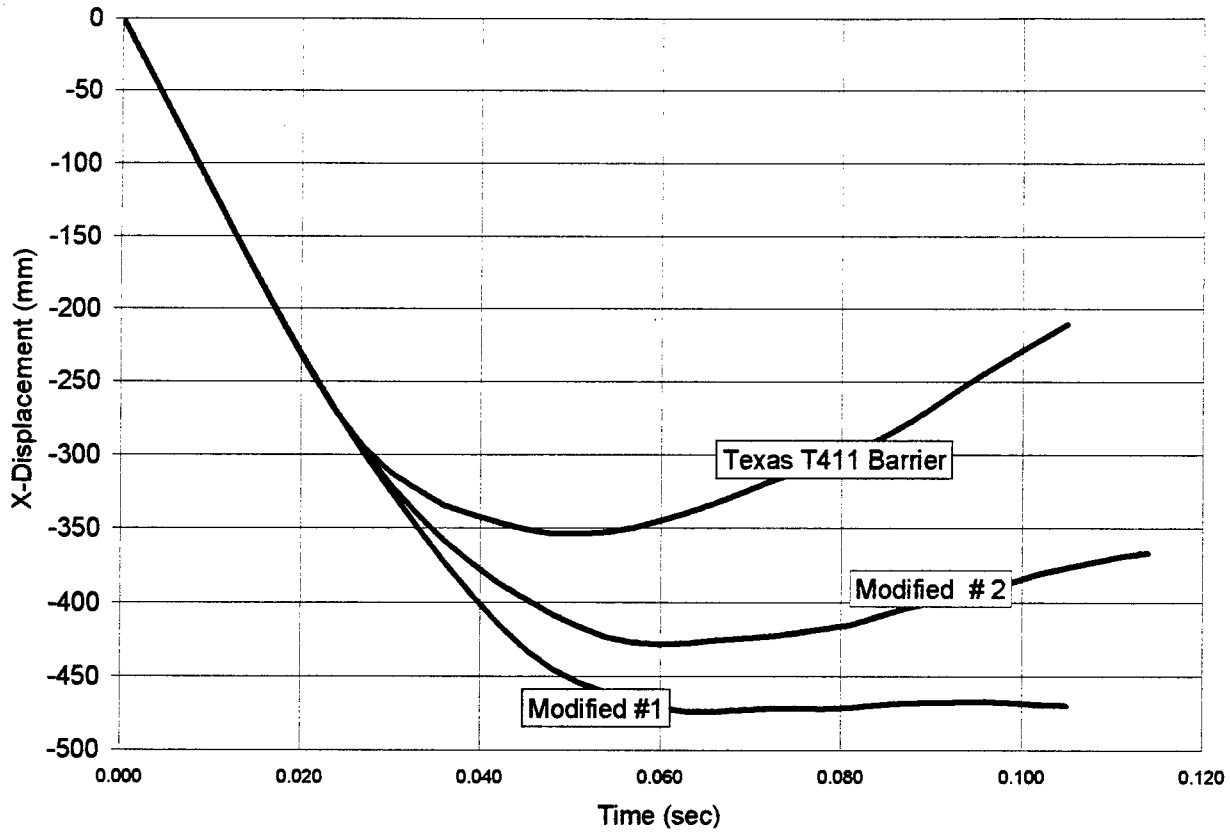

Figure A-24: Global X-displacement of the car's C.G. with respect to the barrier vs. time (Simulation 5-1,2&3)

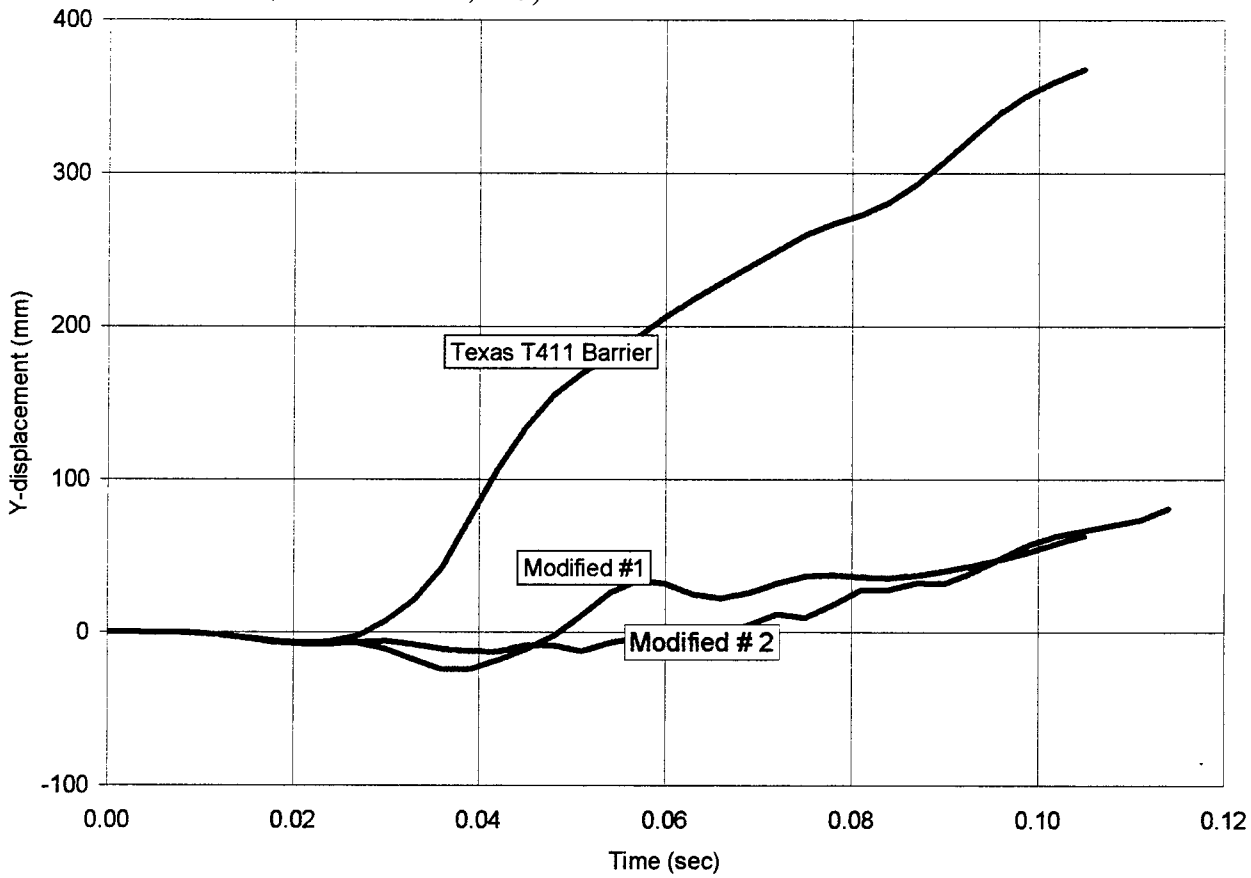

Figure A-25: Global Y-displacement of the car's C.G. with respect to the barrier vs. time (Simulation 5-1,2&3)

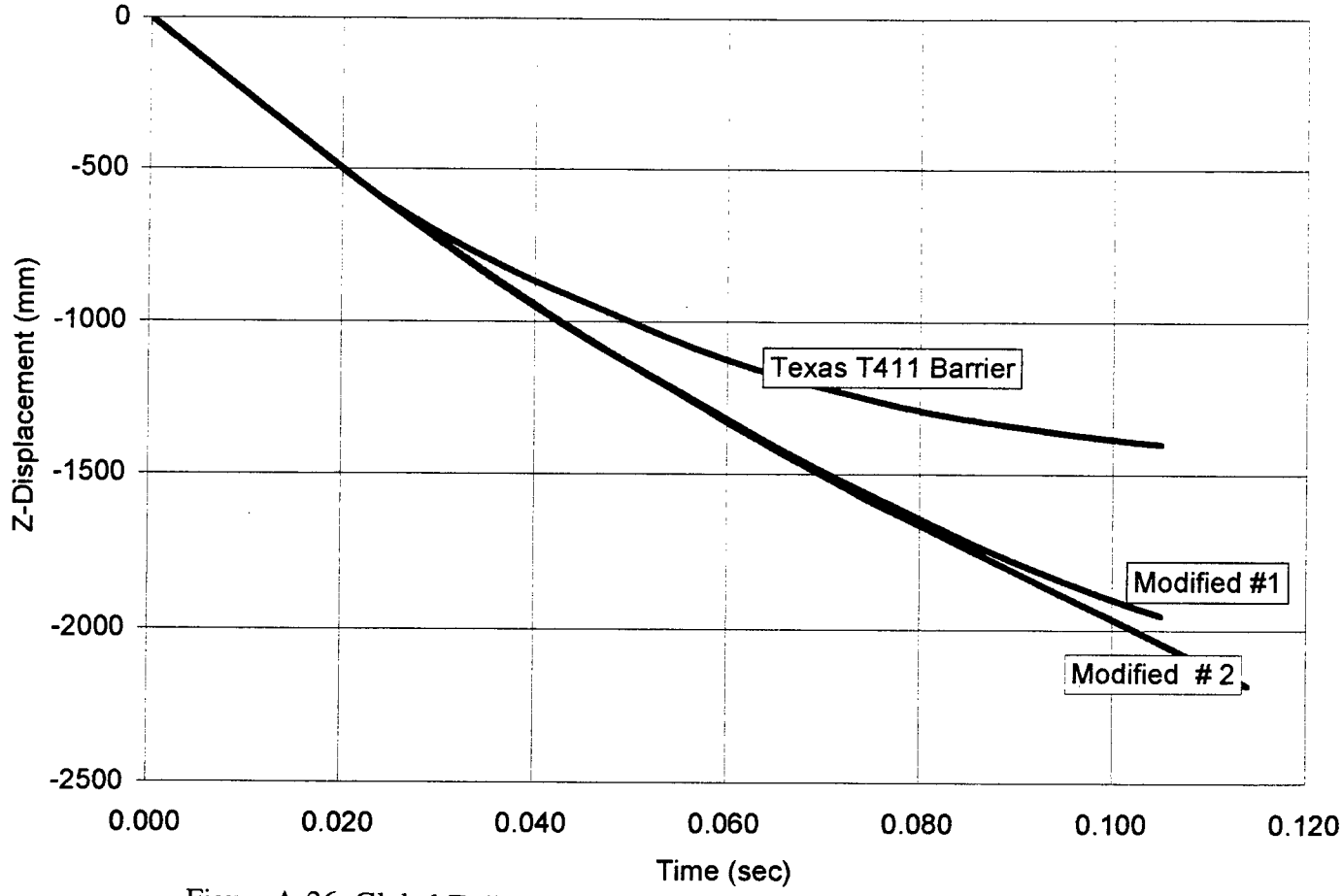

Figure A-26: Global Z-displacement of the car's C.G. with respect to the barrier vs. time (Simulation 5-1,2&3)

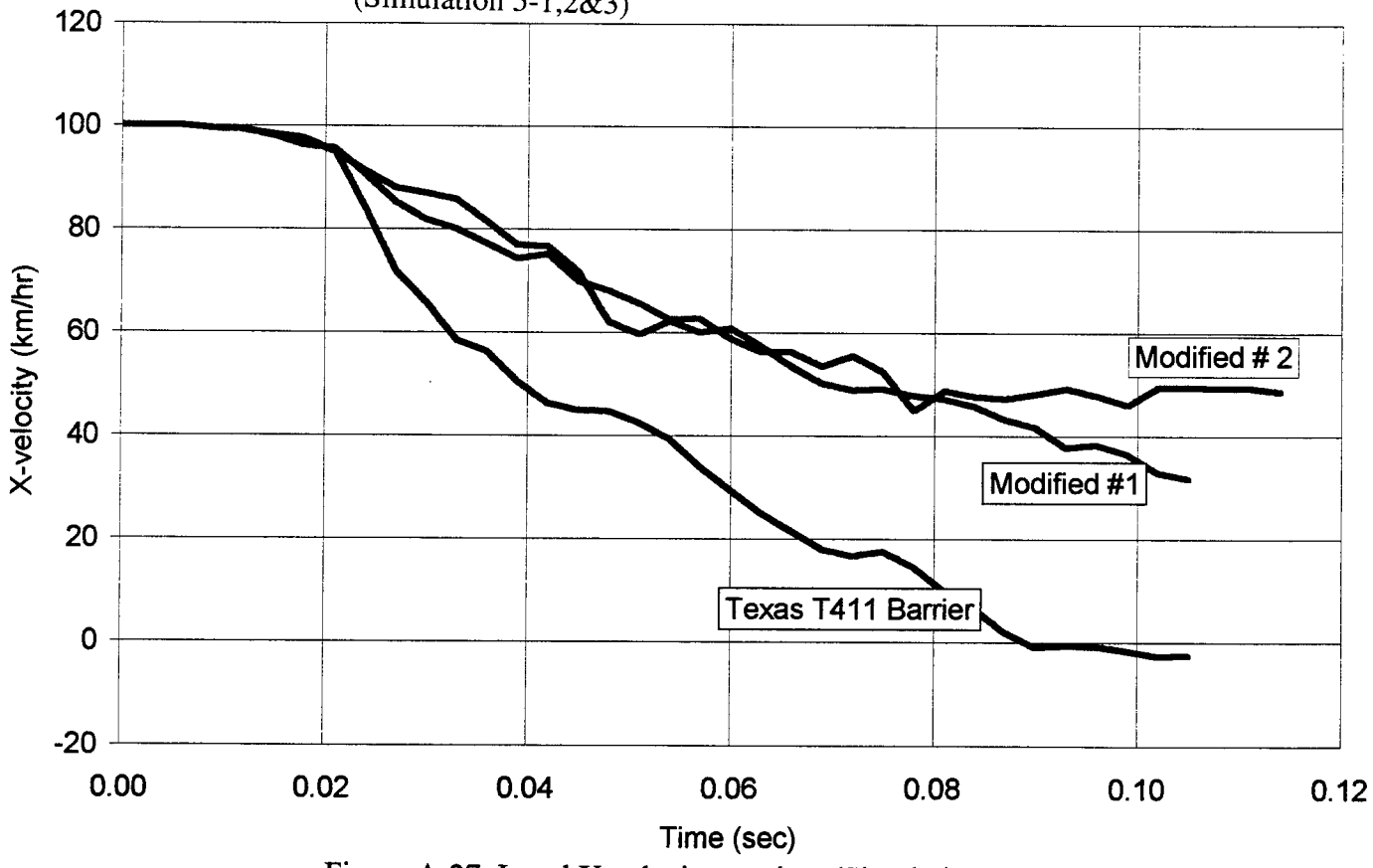

Figure A-27: Local X-velocity vs. time (Simulation 5-1,2&3)

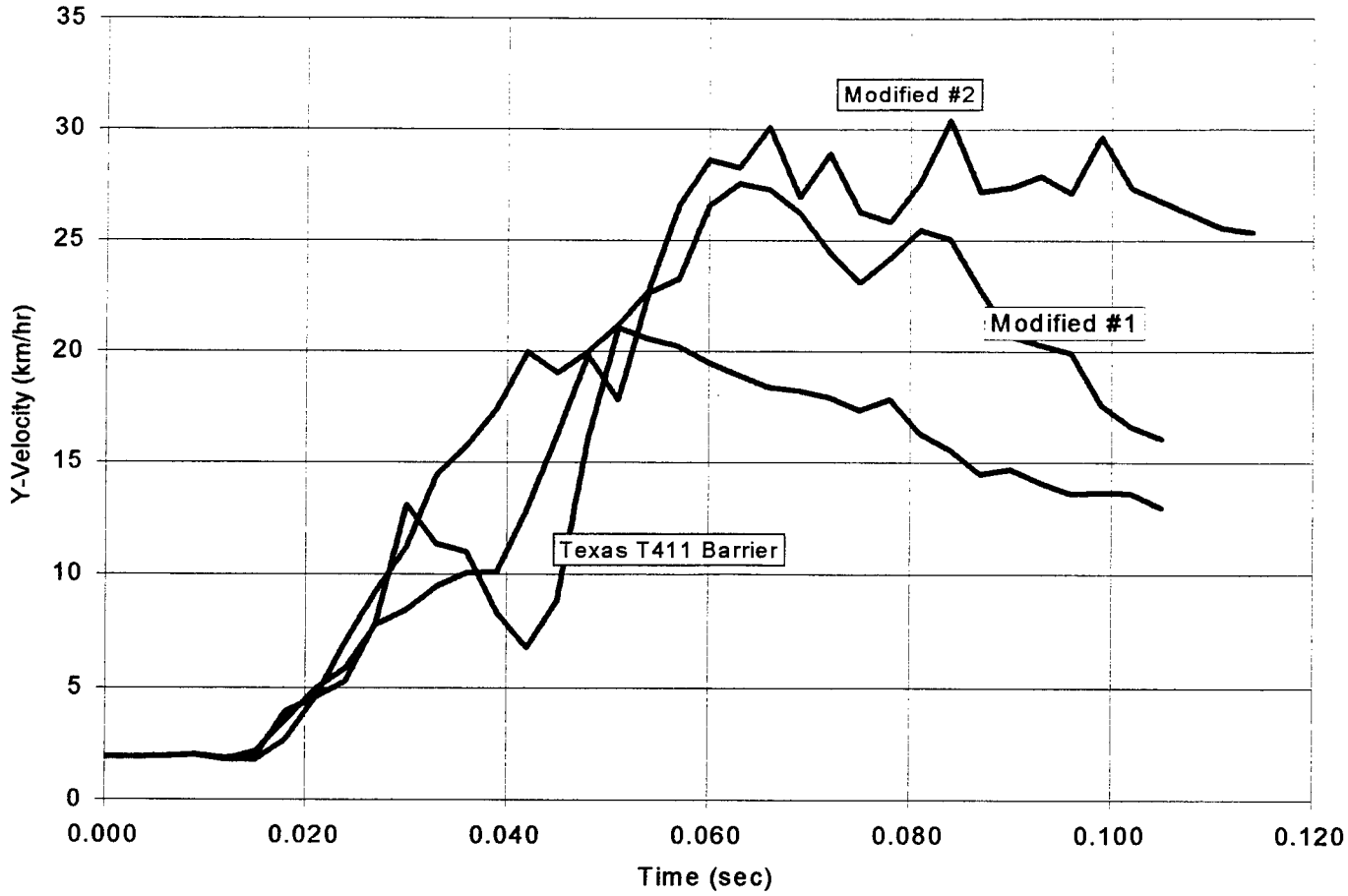

Figure A-28: Local Y-velocity vs. time (Simulation 5-1,2&3)

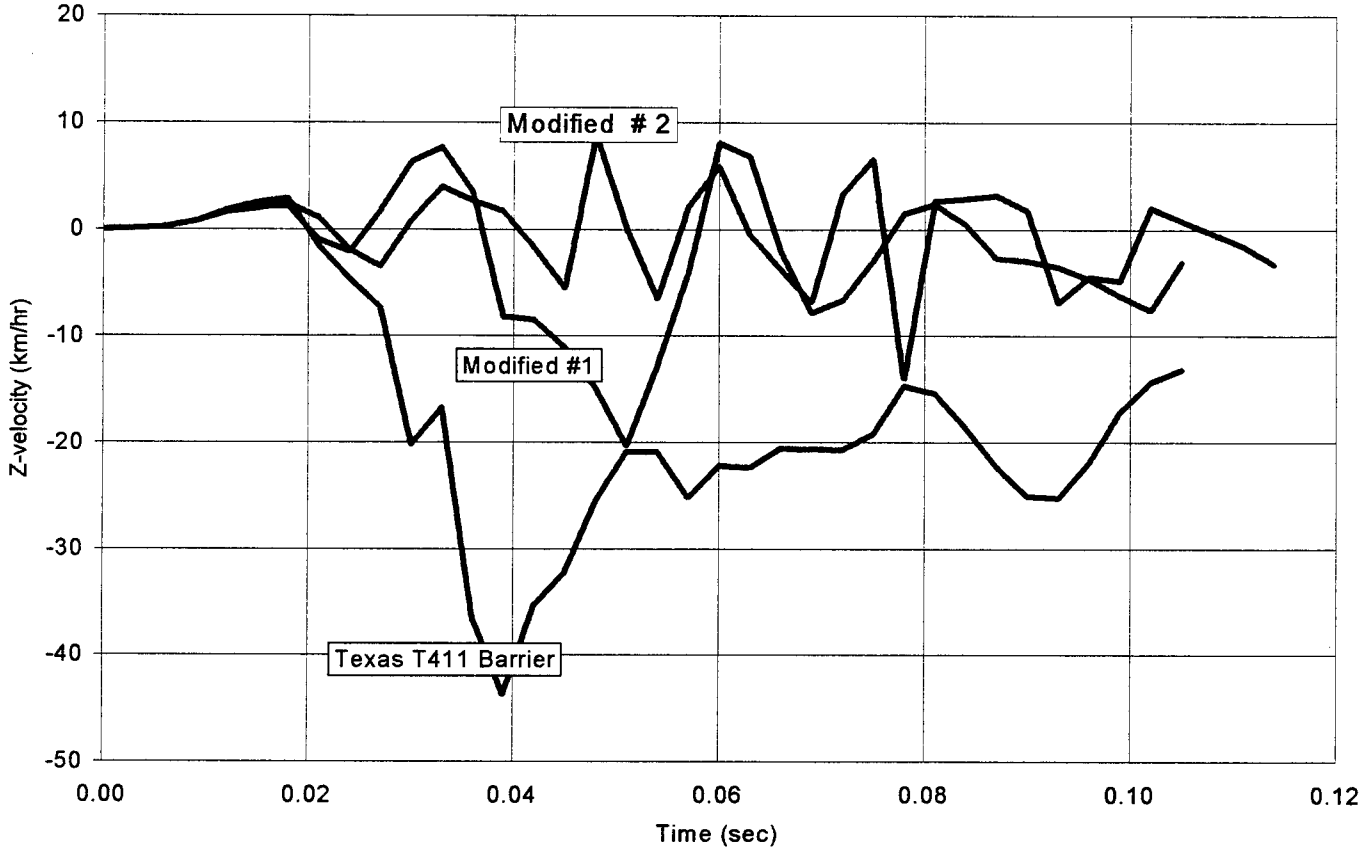

Figure A-29: Local Z-velocity vs. time (Simulation 5-1,2&3)

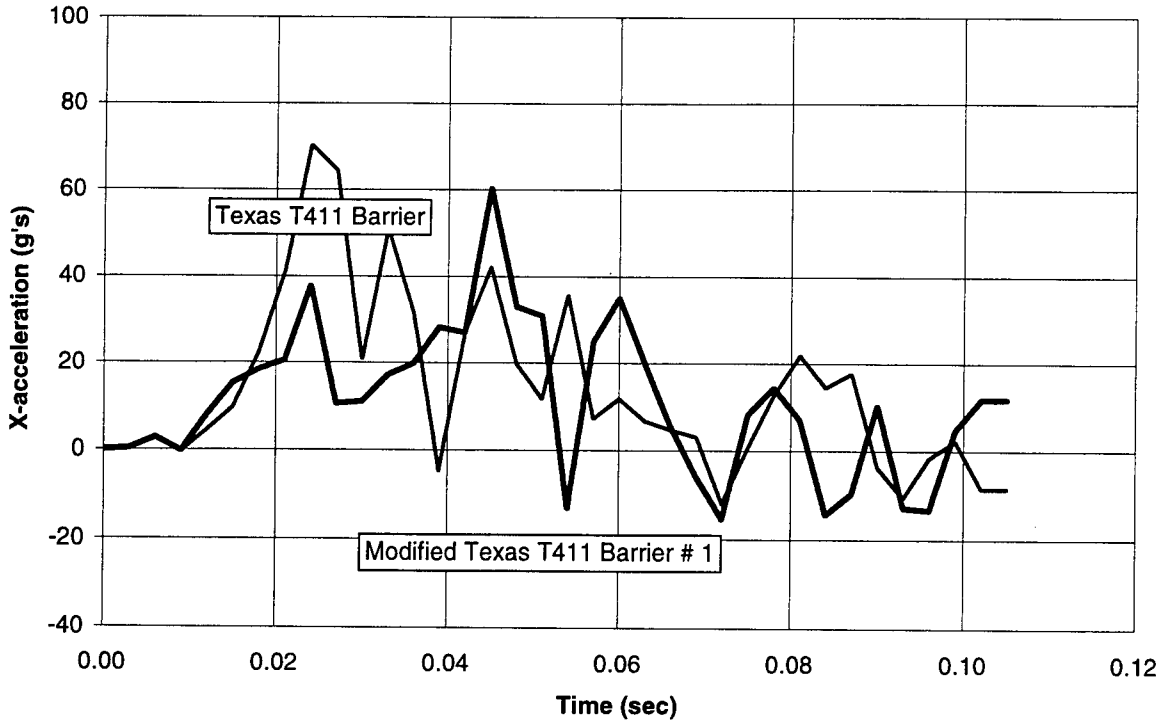

Figure A-30a: Global X-acceleration vs. time (Simulation 5-1&2)

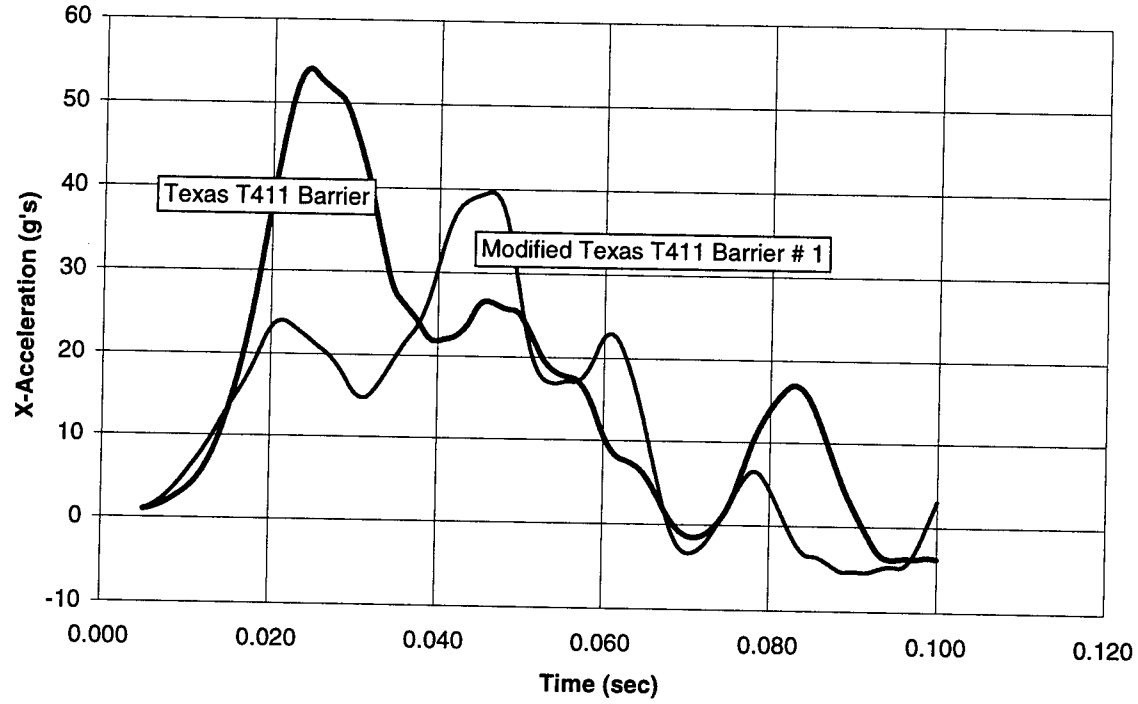

Figure A-30b: 10ms average of X-acceleration (Simulation 5-1&2)

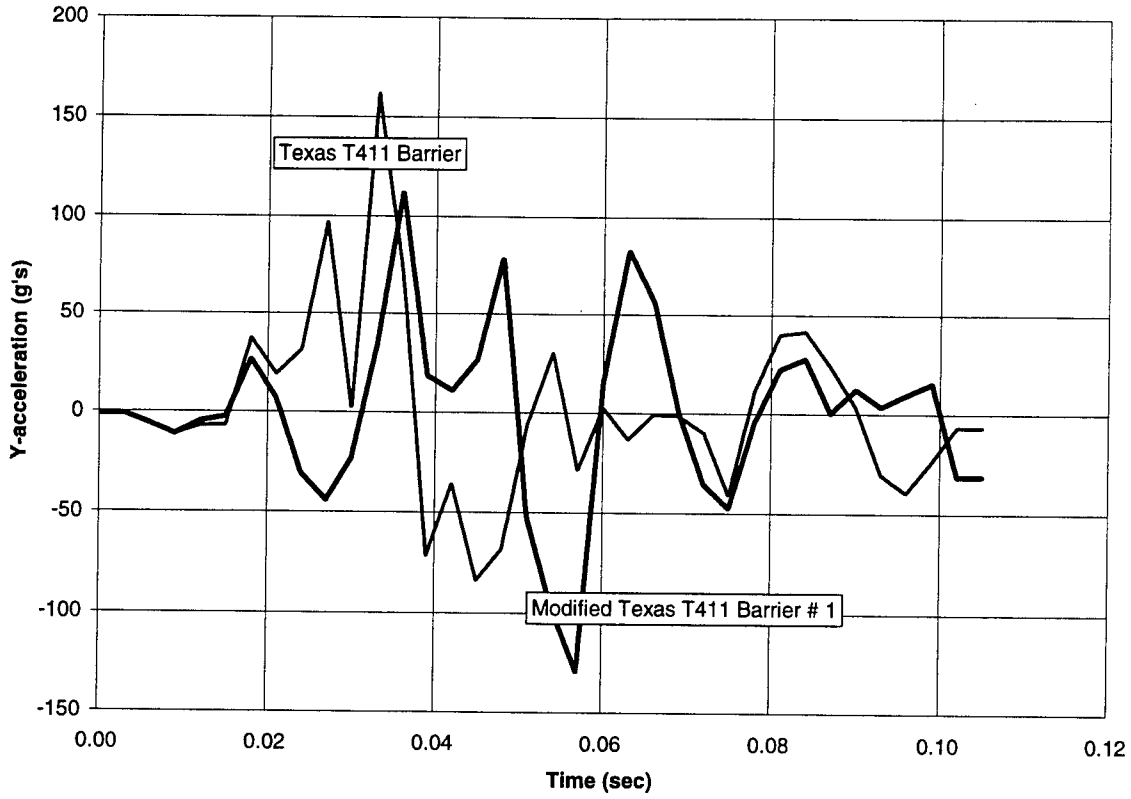

Figure A-31a: Global Y-acceleration vs. time (Simulation 5-1&2)

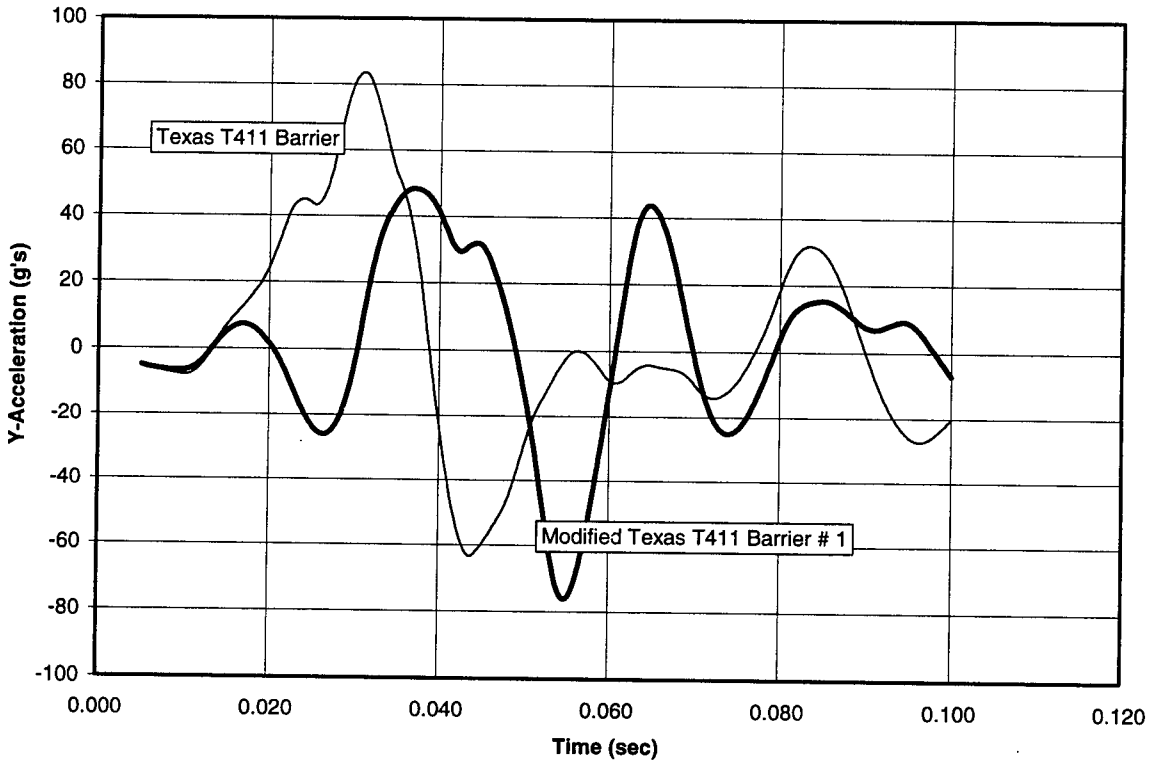

Figure A-31b: 10ms average of Y-acceleration (Simulation 5-1&2)

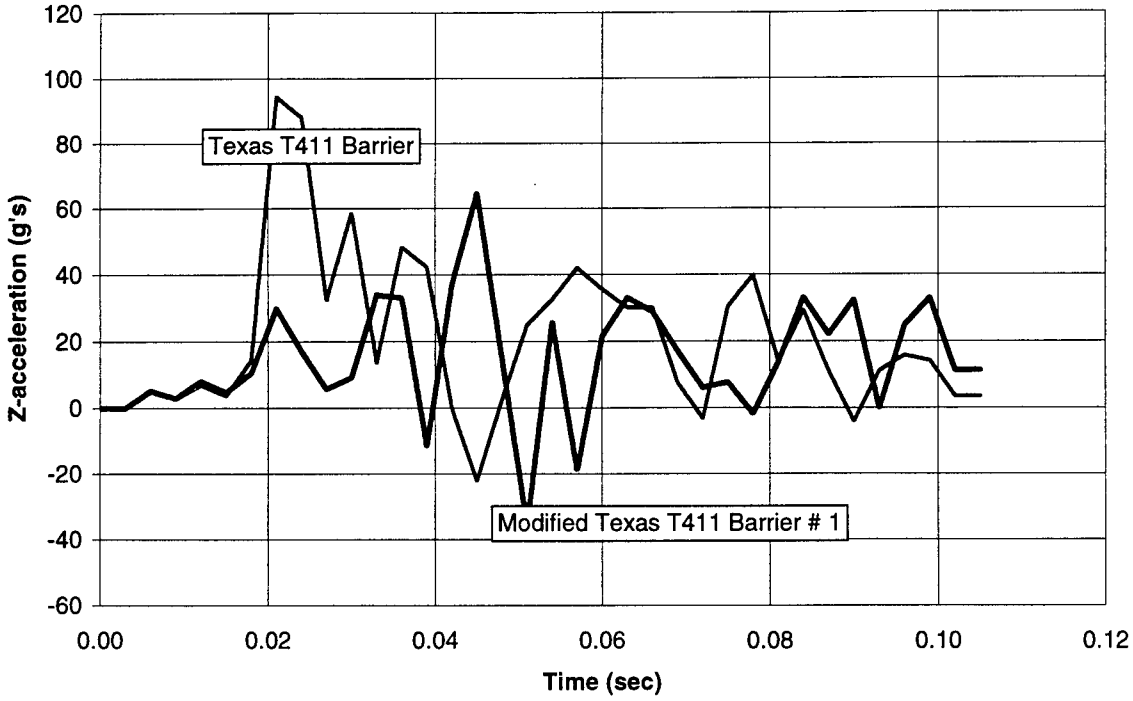

Figure A-32a: Global Z-acceleration vs. time (Simulation 5-1&2)

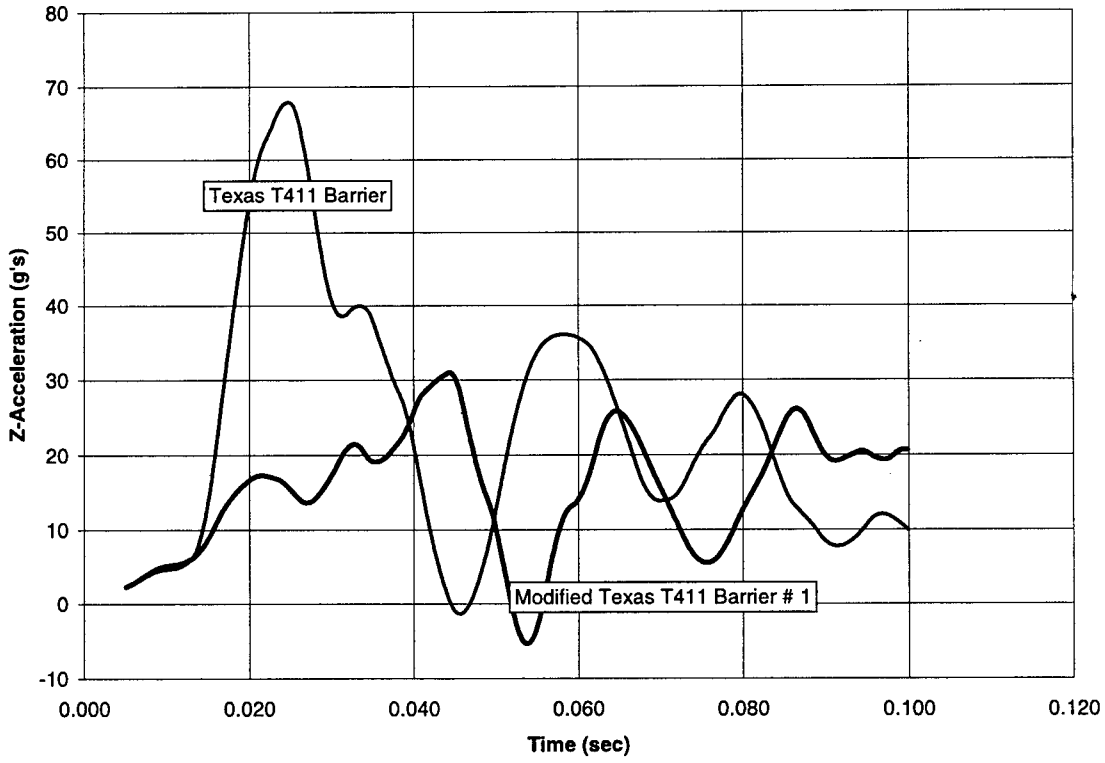

Figure A-32b: 10ms average of Z-acceleration (Simulation 5-1&2)

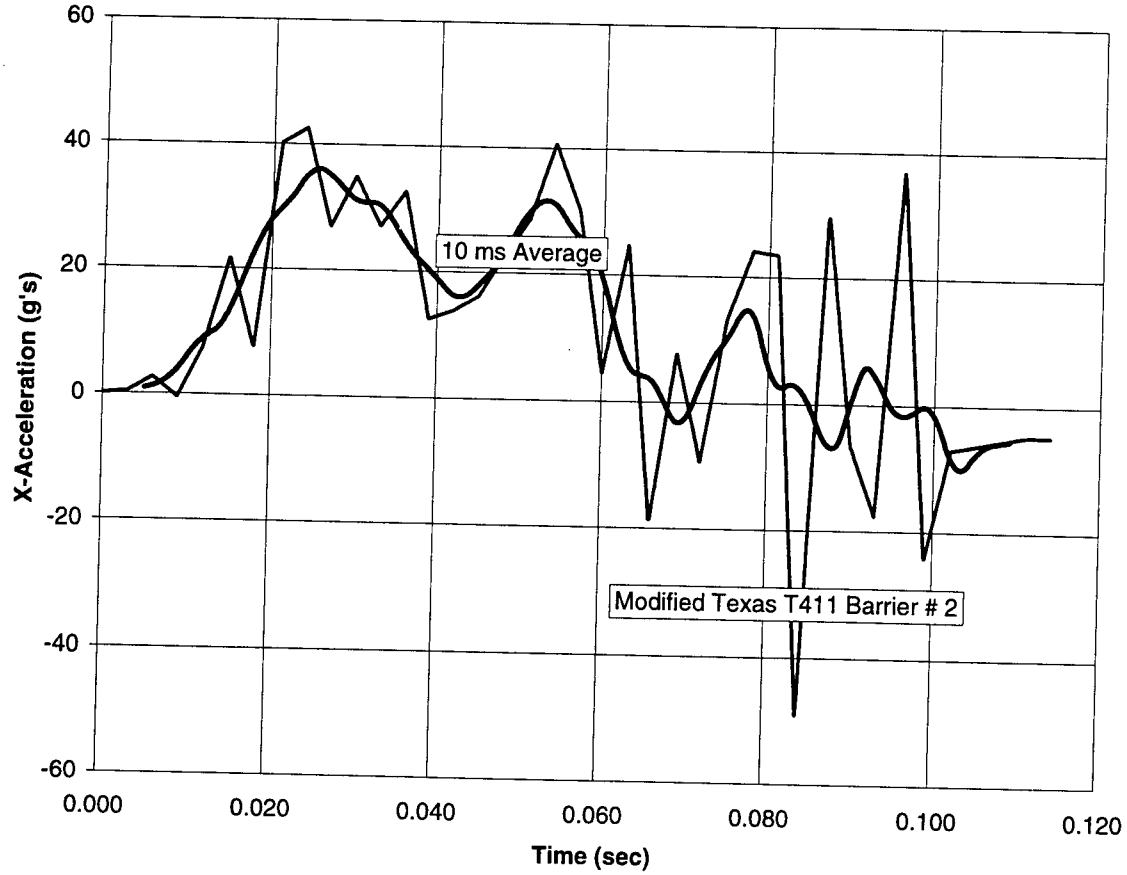

Figure A-33: Global X-acceleration vs. time (Simulation 5-3)

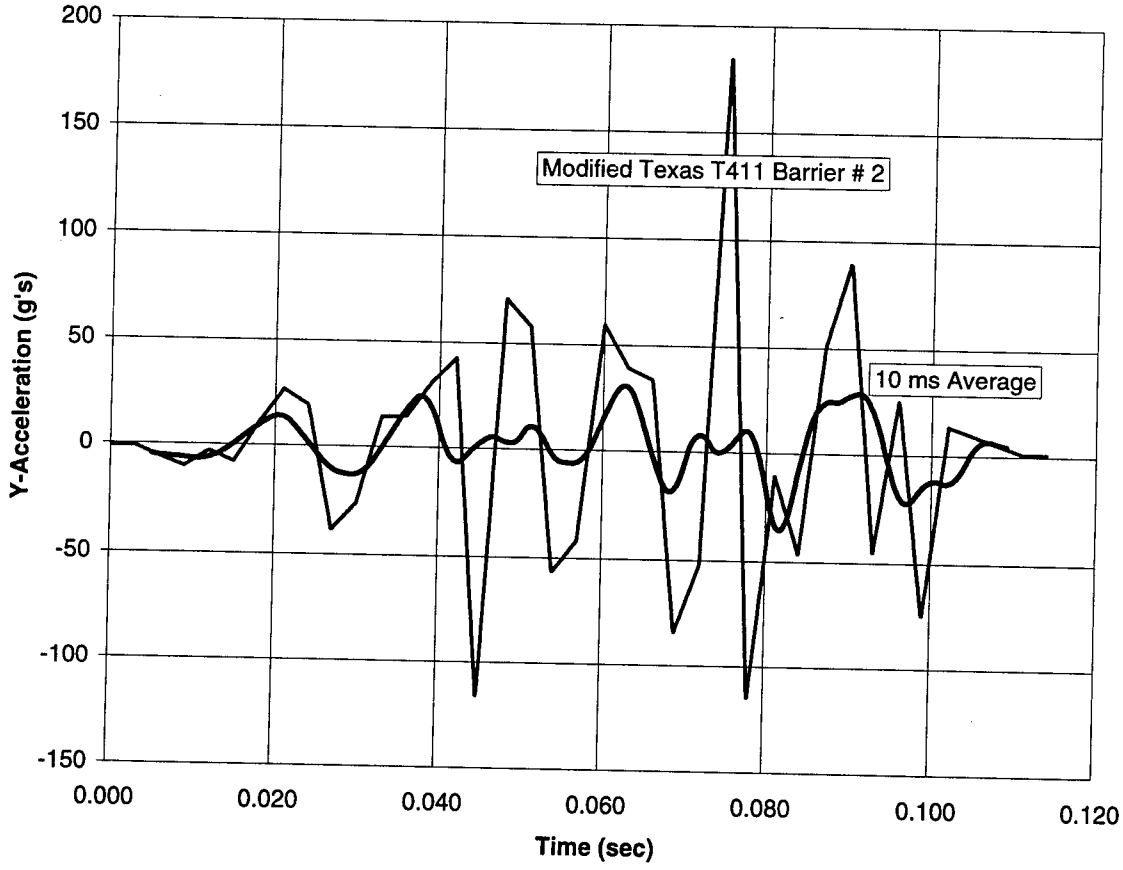

Figure A-34: Global Y-acceleration vs. time (Simulation 5-3)

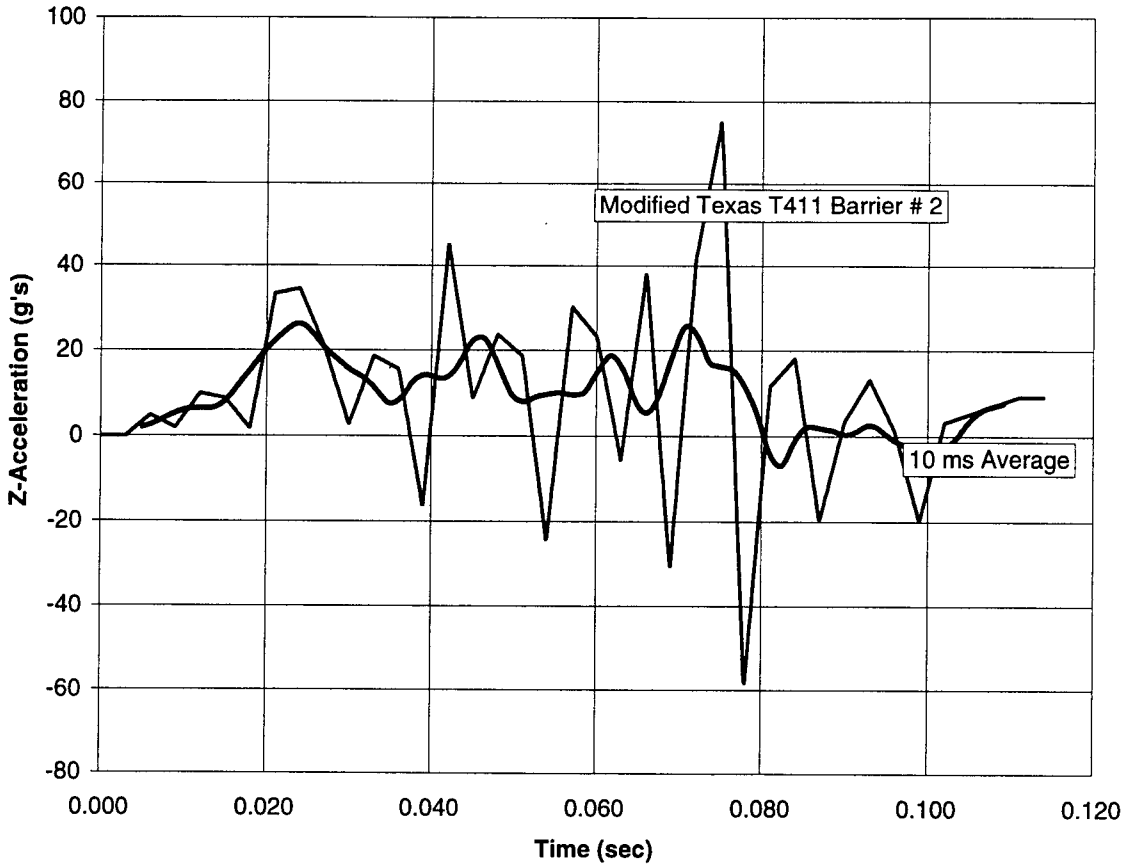

Figure A-35: Global Z-acceleration vs. time (Simulation 5-3)

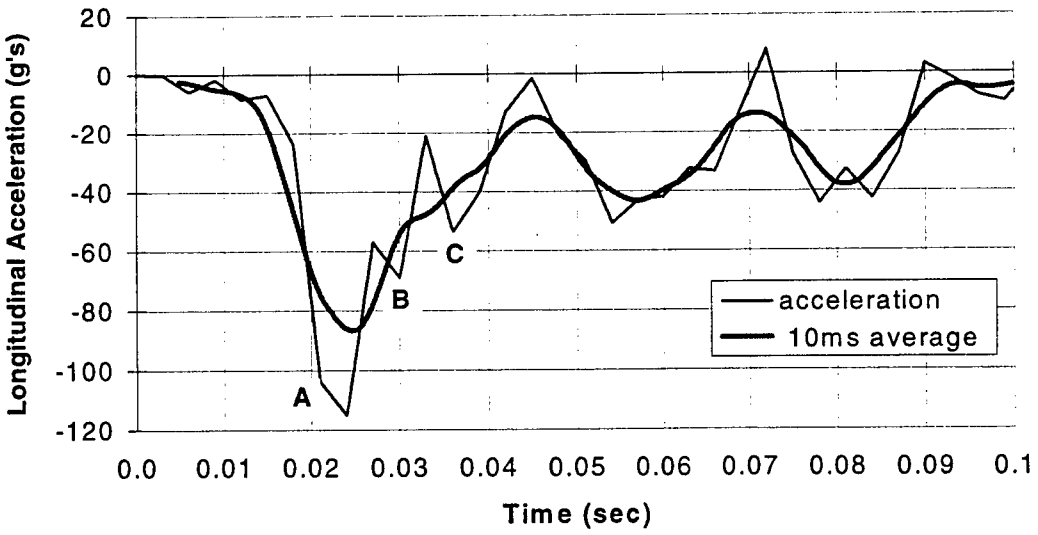

Point **A** - time t = 0.021 s

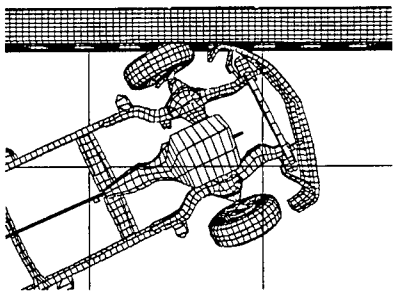

Point **B** - time t = 0.030 s

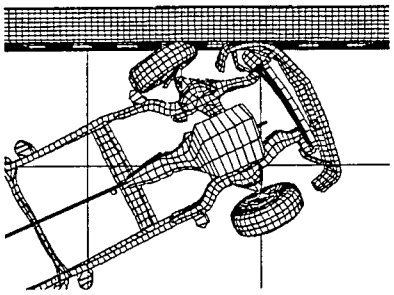

Point **C** - time t = 0.036 s

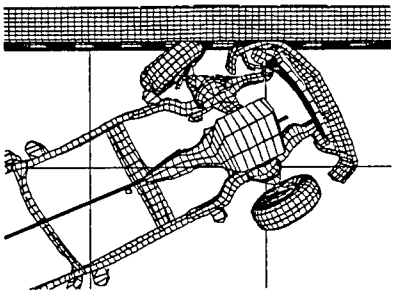

Figure A-36: Longitudinal accelerations (Simulation 5-1) correlation to acceleration peaks

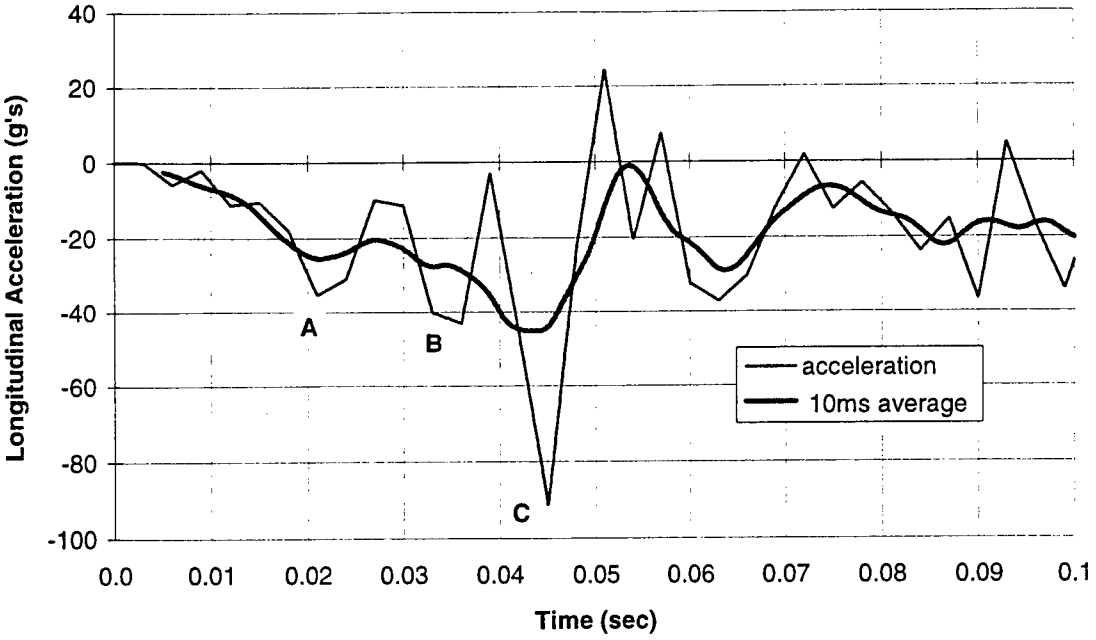

Point **A** - time t = 0.021 s

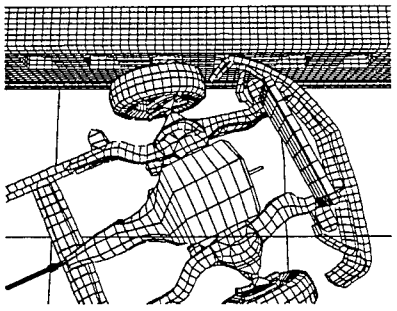

Point **B** - time t = 0.033 s

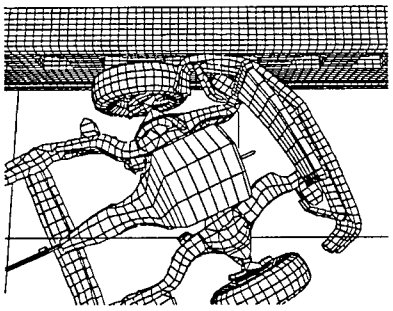

Point **C** - time t = 0.045 s

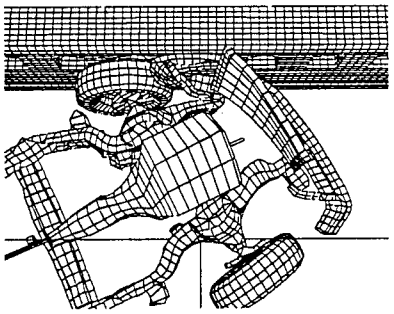

Figure A-37: Longitudinal accelerations (Simulation 5-2) correlation to acceleration peaks

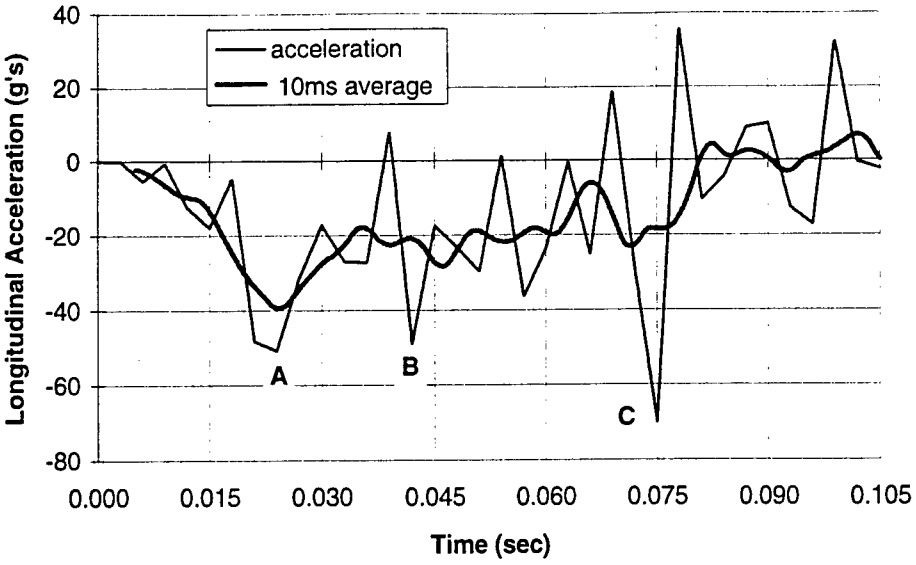

Point **A** - time t = 0.024 s

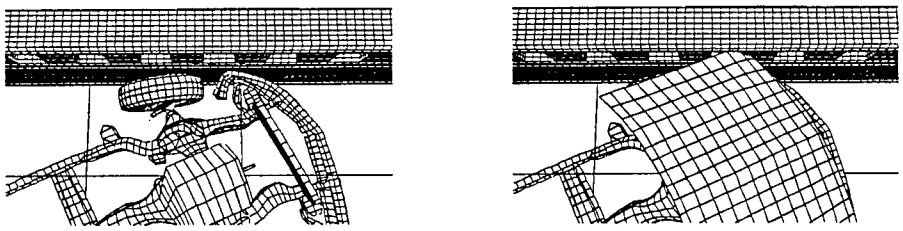

Point **B** - time t = 0.042 s

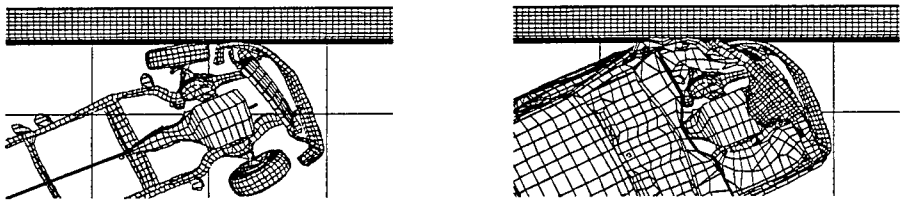

Point **C** - time t = 0.075 s

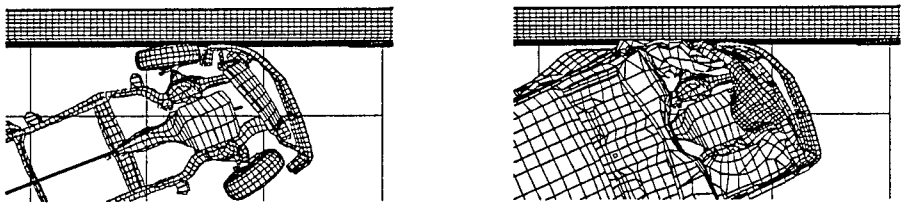

Figure A-38: Longitudinal accelerations (Simulation 5-3)
correlation to acceleration peaks

time = 0.000 sec

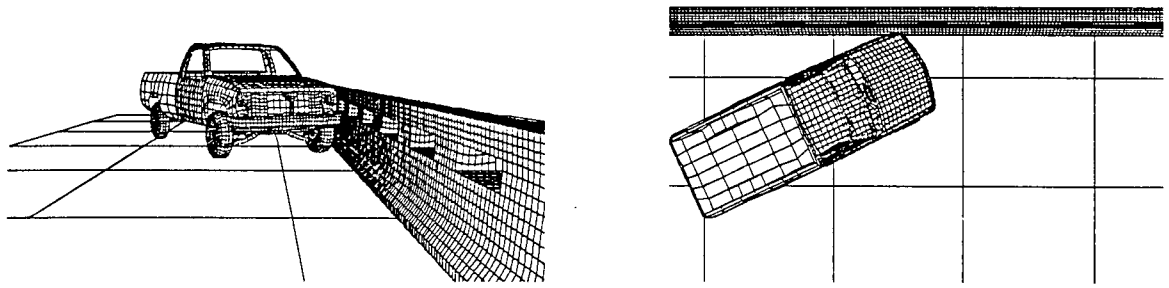

time = 0.030 sec

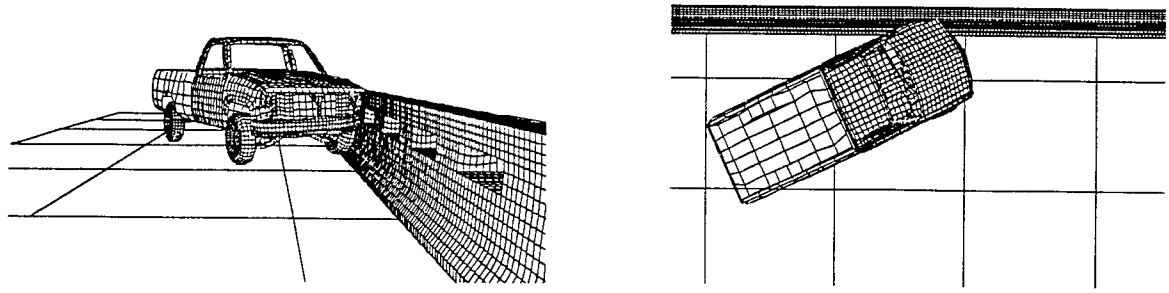

time = 0.060 sec

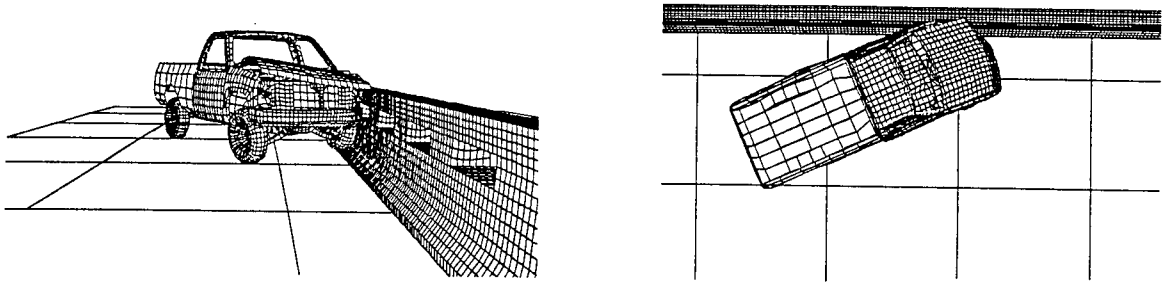

time = 0.090 sec

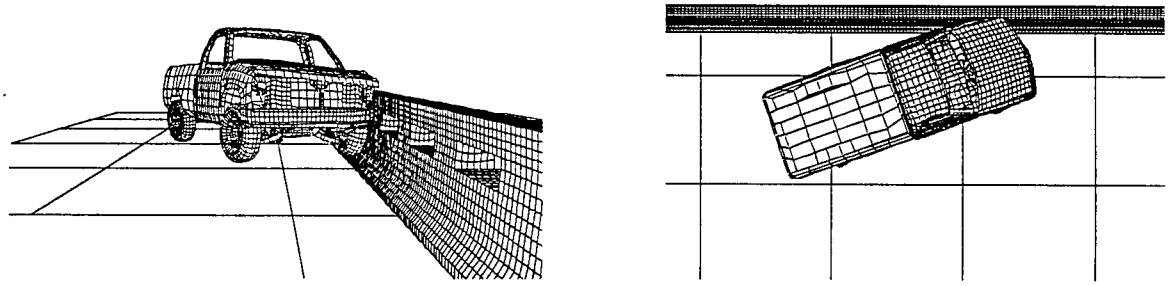

Figure A-39a: Simulation 6-1

time = 0.120 sec

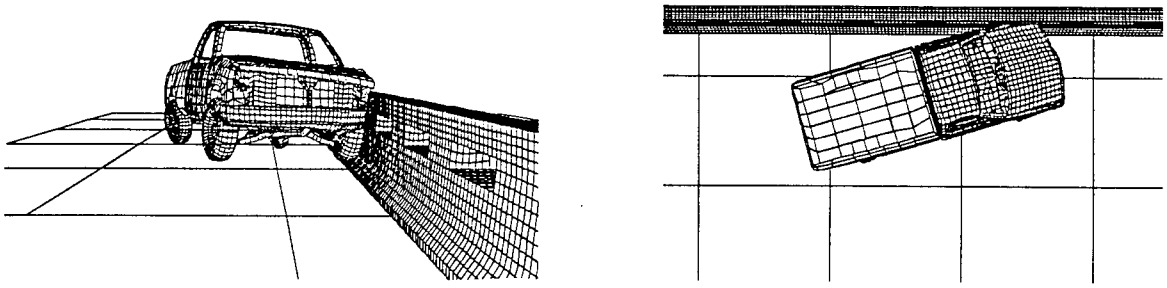

time = 0.150 sec

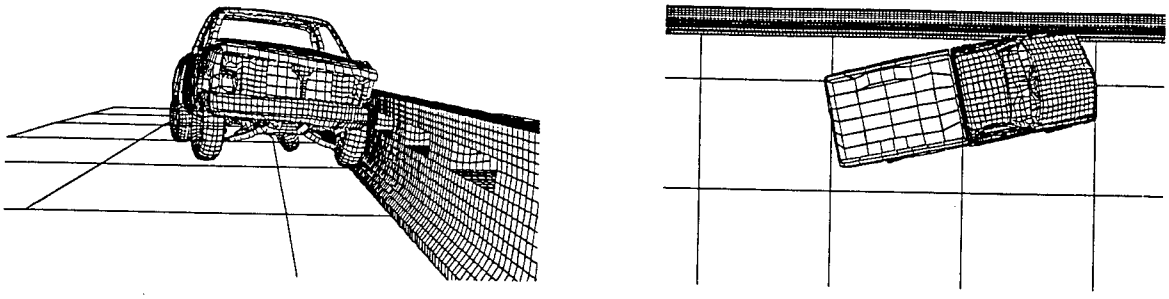

time = 0.180 sec

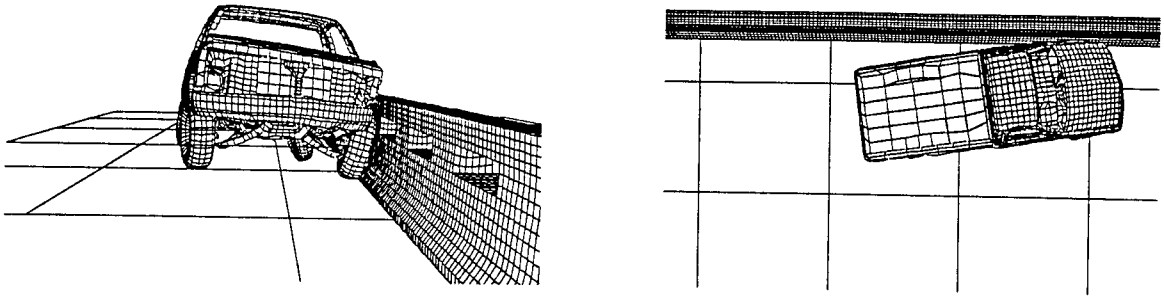

time = 0.207 sec

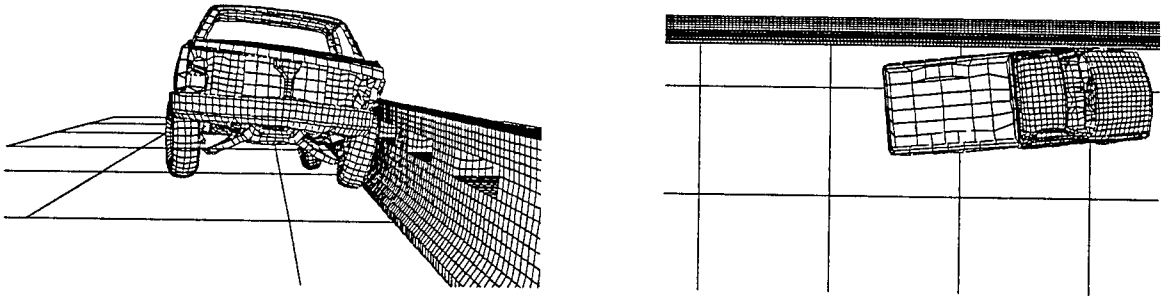

Figure A-39b: Simulation 6-1 cont.

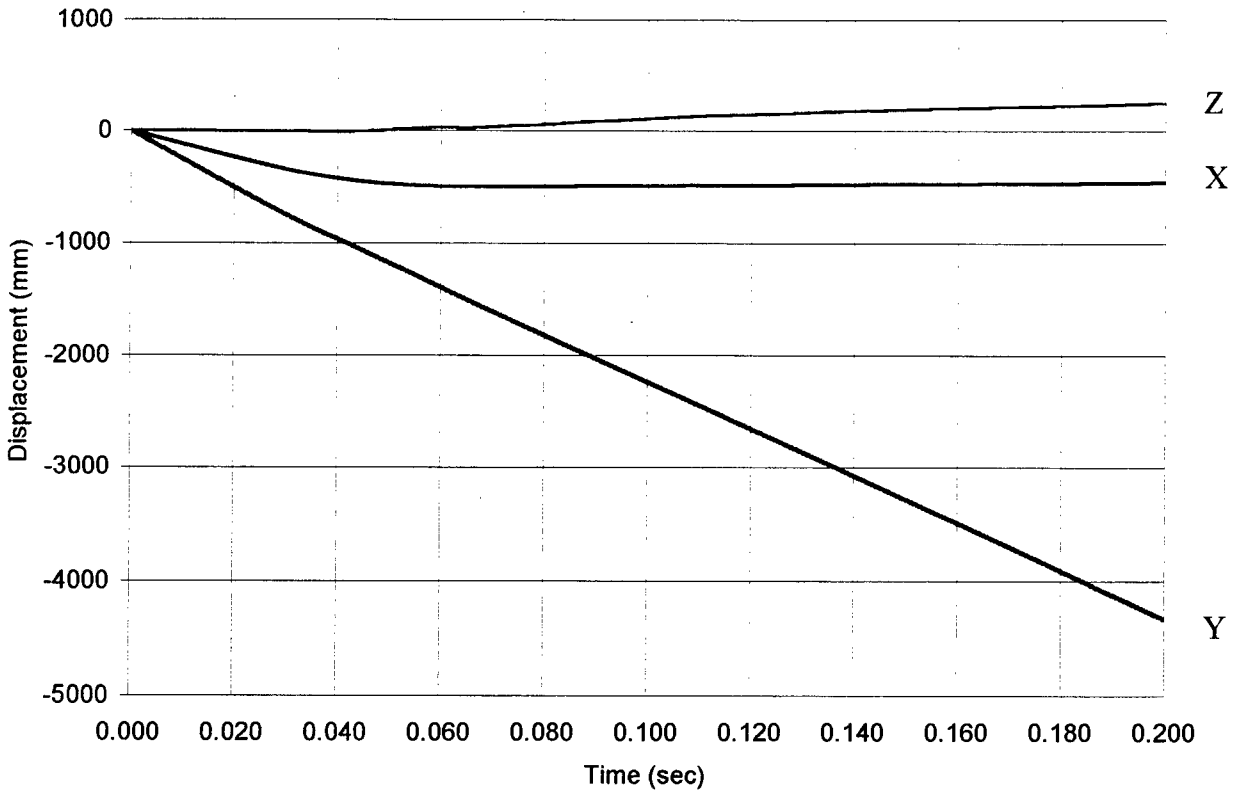

Figure A-40: Global displacement of the car's C.G. with respect to the barrier vs. time (Simulation 6-1)

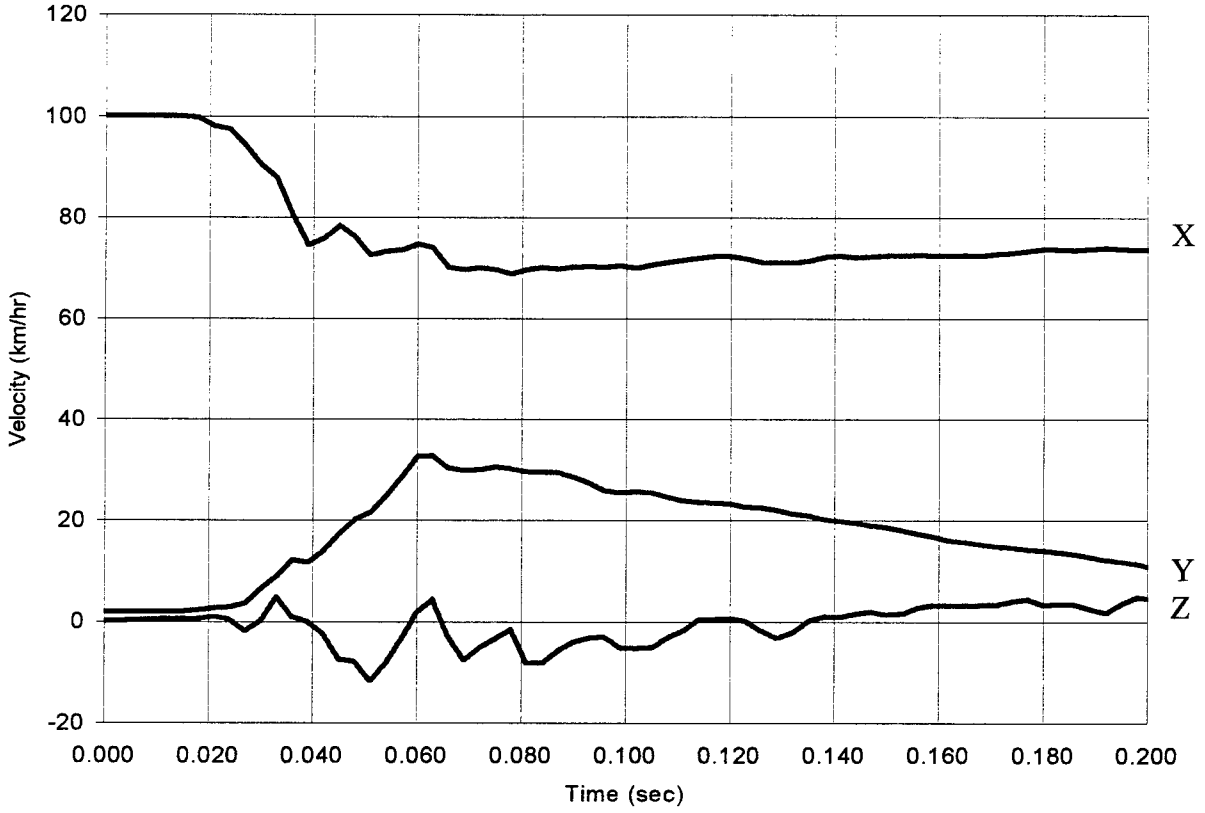

Figure A-41: Local velocity vs. time (Simulation 6-1)

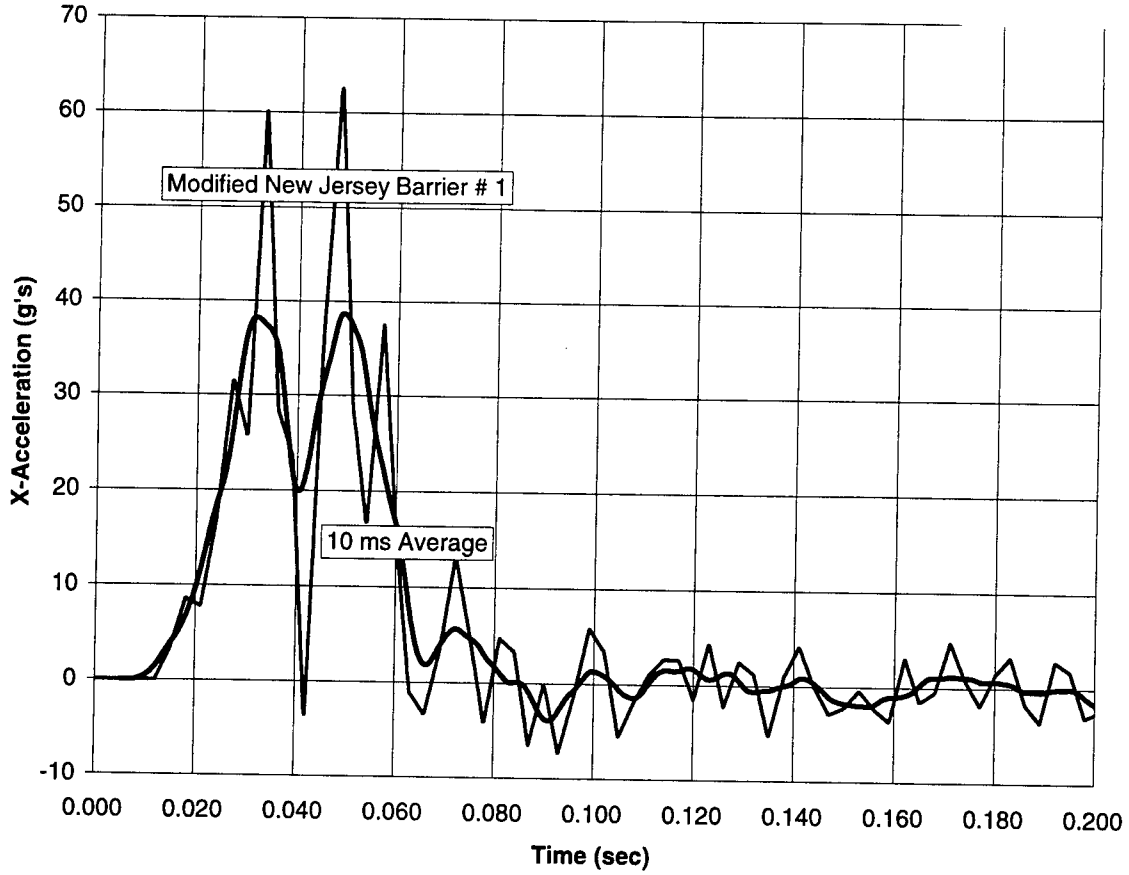

Figure A-42: Global X-acceleration vs. time (Simulation 6-1)

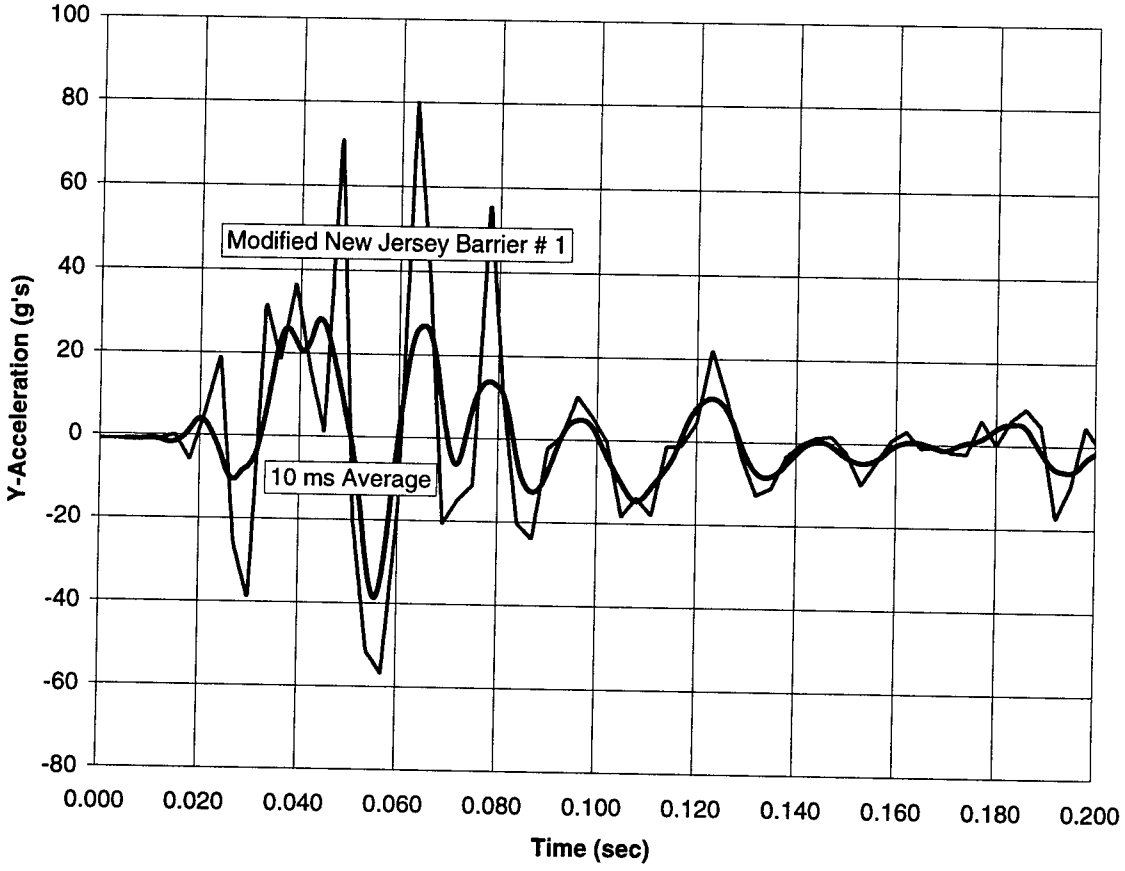

Figure A-43: Global Y-acceleration vs. time (Simulation 6-1)

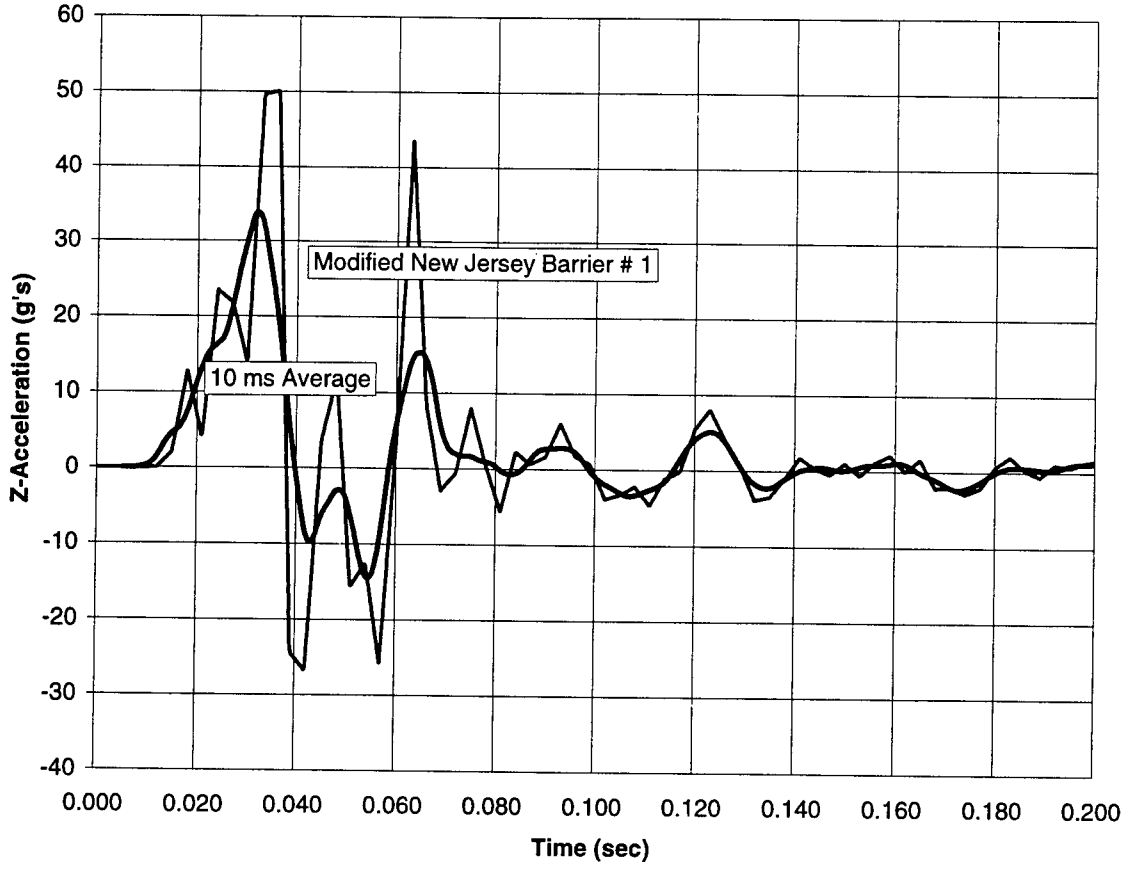

Figure A-44: Global Z-acceleration vs. time (Simulation 6-1)

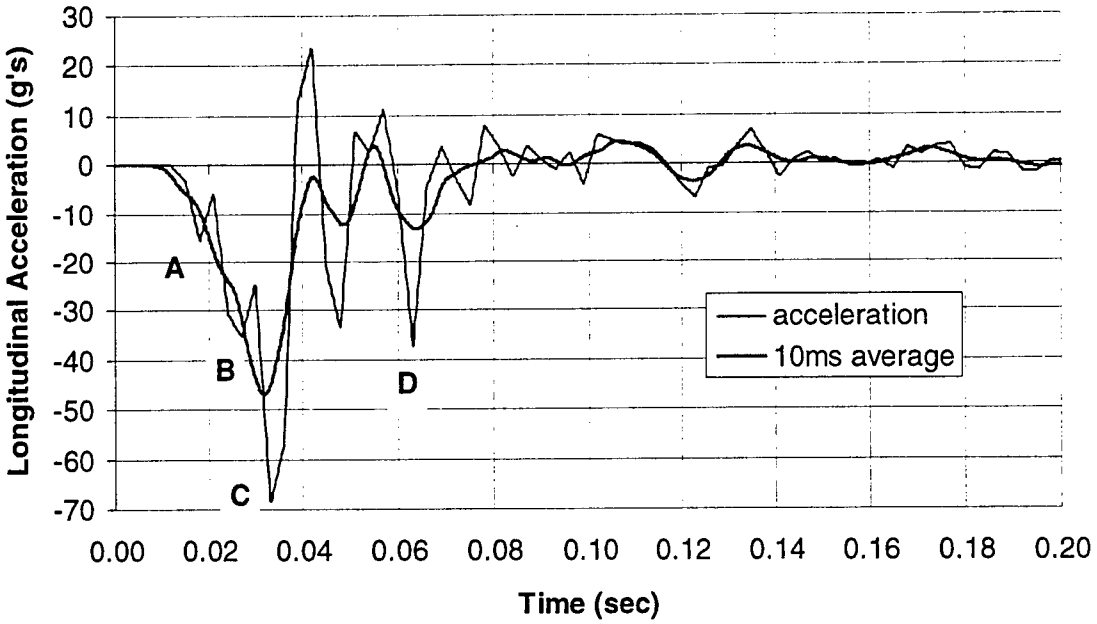

Point **A** - time t = 0.018 s

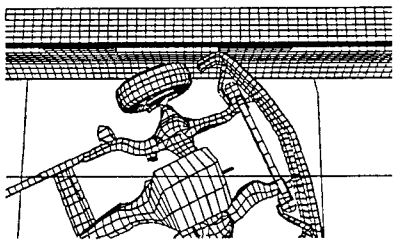

Point **B** - time t = 0.027 s

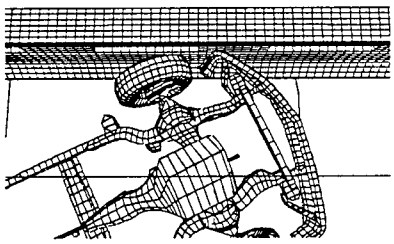

Point **C** - time t = 0.033 s

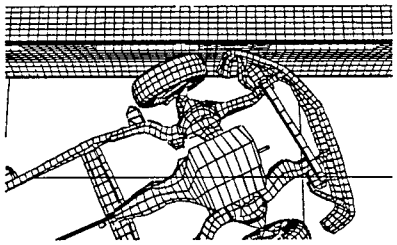

Point **D** - time t = 0.063 s

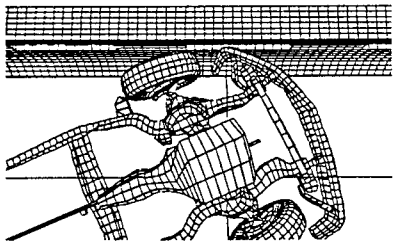

Figure A-45: Longitudinal accelerations (Simulation 6-1) correlation to acceleration peaks

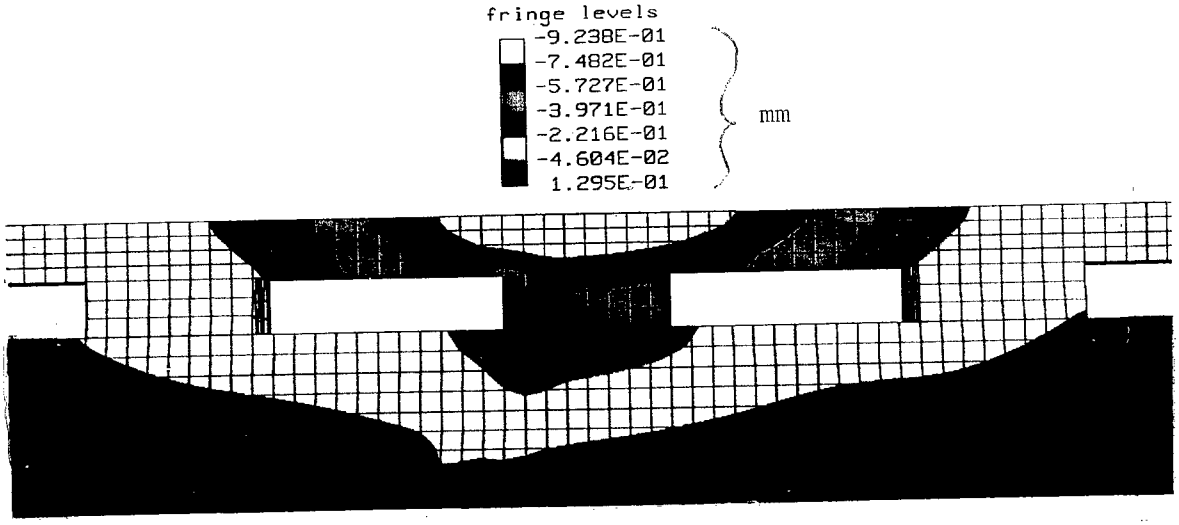

Figure A-46: Fringes of X-displacement (Simulation 6-1) (mm)

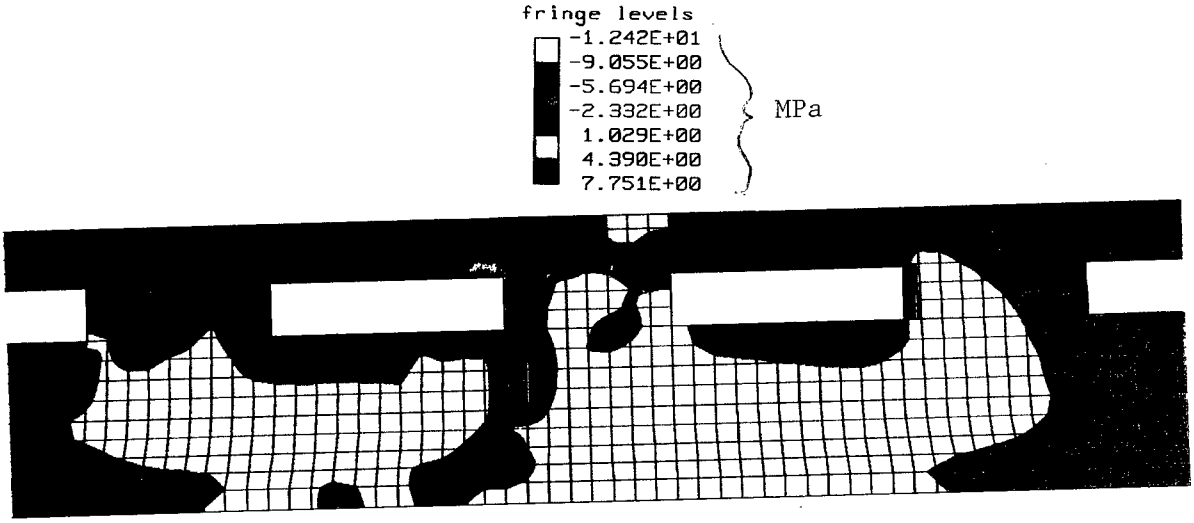

Figure A-47: Fringes of Y-stress (Simulation 6-1) (MPa)

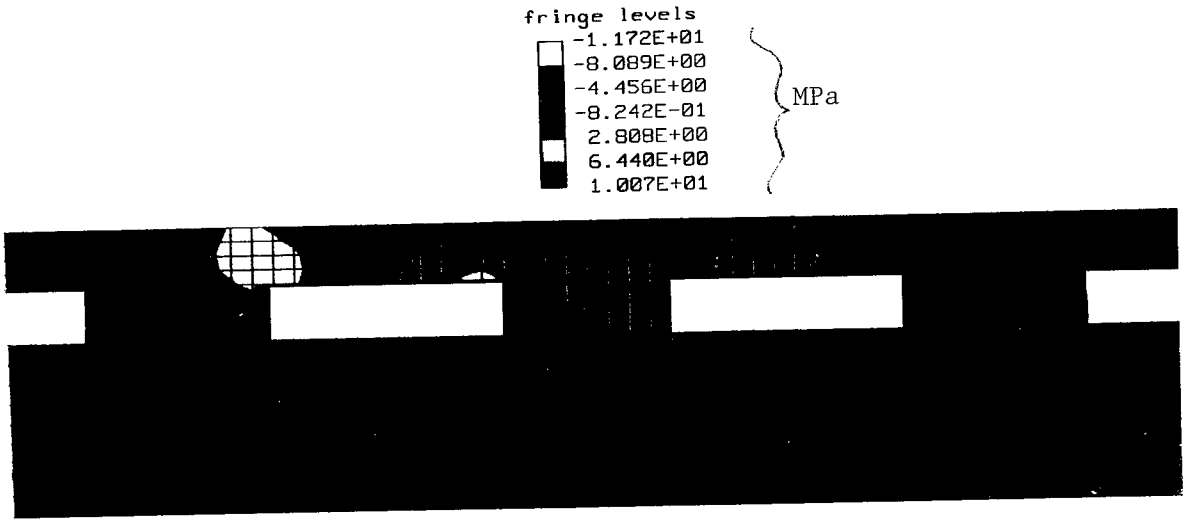

Figure A-48: Fringes of Z-stress (Simulation 6-1) (MPa)

APPENDIX B

SUMMARY OF AESTHETIC BRIDGE BARRIERS

The following pages represent a survey of aesthetic rails performed between May 1996 and July 1996. This material was presented at a July 3rd meeting between the Florida Department of Transportation and the FAMU-FSU College of Engineering. The Florida Department of Transportation was represented by Dr. Moussa Issa, Dr. Mohsen Shahawy, and Mr. Jerry Potter. FAMU-FSU College of Engineering was represented by Dr. Jerry Wekezer and Mr. Chris Gilbert. Results of this conference are presented in Chapter 2.

B.1 Conceptual Analysis of an Aesthetic Bridge Barrier

The highway profession is currently in the process of upgrading the performance of the bridge railing systems on the highways around the United States. Research has allowed for the development of rails that will withstand ever-increasing loads from larger and larger vehichles; however, the issue of aesthetics has been placed towards the bottom of the priority list. The objective of this research is the development of new, efficient, and aesthetic bridge barriers utilizing finite element methods for computer simulation. These barriers may represent some past attempts that have failed, modifications to a current barrier, or a completely new concept.

The barriers present within are a collection of both past and current efforts that are considered to be aesthetic. It is very difficult to define "aesthetic"; however, in Florida bridge rail aesthetics are primarily viewed as a rail that allows visibility of the natural beauty of our state. All of the rails presented are ranked on a performance level scale of 1 to 3. This scale is set forth in the 1989 AASHTO publication *Guide Specifications for Bridge Railings*[35] and the 1981publication *NCHRP Report 230*[36]; however, the two reports differ on tests to be performed to attain a particular performance level. Most new bridges are constructed for a performance level 2 application. This level of performance has a strength test with an 18,000-lb single-unit truck striking the rail at 50 mph at a 15-degree angle according to *Guide Specifications for Bridge Railings*[35]. At the same time, some rails that were tested according to *NCHRP Report 230*[36] show performance level 2 rails without performing the 18,000-lb truck test. This will be the cause of the discrepancy in the barrier summaries and for future research the most current publication will take precedent.

Any of the rails presented could be a potential candidate for further research. It is the researcher's recommendation to examine the Texas T411, the Modified Kansas Corral Bridge Rail, and a modification of the standard New Jersey Barrier currently used. All of these barriers are constructed of reinforced concrete and are very aesthetic in that visibility is not restricted. The Texas T411 and the Modified Kansas rail were selected based on the aesthetics of the rail, the New Jersey shape was selected due to its popularity in the highway industry. The Florida Department of Transportation has the ultimate decision as to which barriers shall be modeled and the researcher is open to fresh ideas.

B.2 Texas Type T411 Aesthetic Bridge Rail

The Texas Type T411 guard rail was developed around 1990 and was testes at the Texas Transportation Institute. The bridge rail is an aesthetic rail constructed of reinforced concrete. The dimensions of the guard fence are 32 in. high by 12 in. thick with 8 in. by 18 in. high openings spaced at 18 in. center to center. A photograph of the rail at the Texas Transportation Institute used for the full scale crash tests can be viewed in Figure 1. It is interesting to note that the pilasters of the rail (what appears to be very strong), are actually composed of 10.5 in. by 13 in. by 21 in. Styrofoam blocks. For this reason the pilasters can be considered to behave in a manner similar to the openings, as they have no significant structural strength.

The bridge rail was designed for a concrete with compressive strength 3,600 psi and reinforcing steel with a yield strength of 60,000 psi. Based on these materials, the dimensions of the top beam are a nominal 7 in. wide by 11 in. thick. This provides an ultimate capacity of 20.0 kip-ft. The posts are 10 in. by 10 in. with an ultimate moment capacity of 26.9 kip-ft.

The rail was crash tested in accordance with *NCHRP Report 230*[36] for a service level 2 application. Two crash tests were performed on the rail; Test 10 with a 4,500-lb vehicle striking at 60 mph at 25 degrees (see Figure 2) and Test S13 with an 1,800-lb vehicle at 60 mph at 20 degrees. The Texas T411 performed adequately with all the requirements of *NCHRP Report 230*[36]. Details of the results can be viewed in the *Transportation Research Record 1258*[14]. On interesting not from the tests is the fact that the vehicle remained against the rail with exit angles of 0 and 5.9 degrees for each of

the two respective tests. This exit angle is extremely important in order to determine the final location of the vehicle after the crash.

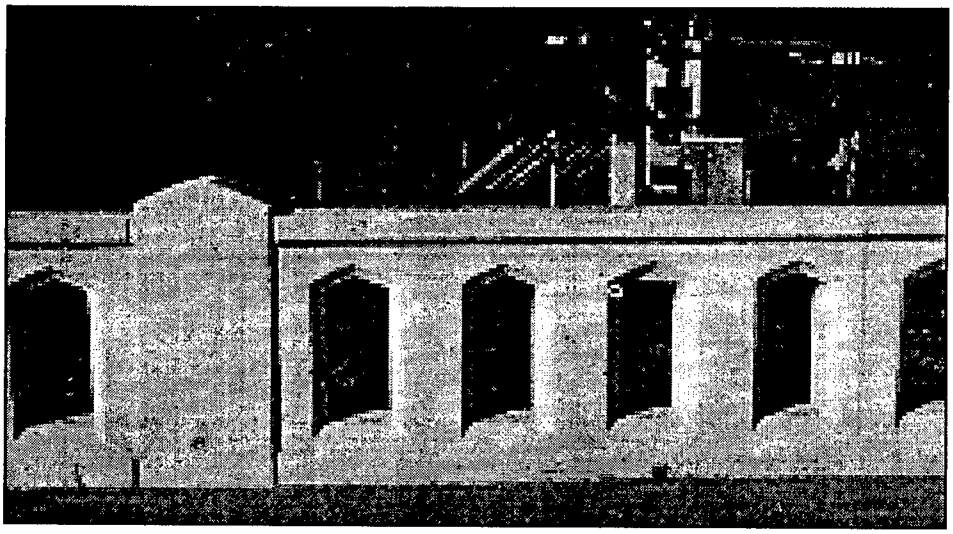

Figure B-1: Photograph of Texas T411 Bridge Barrier [14]

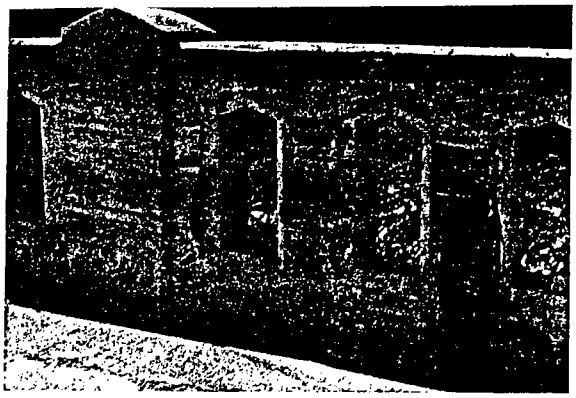

Damage to rail at point of impact.

Vehicle after Test 1185-1.

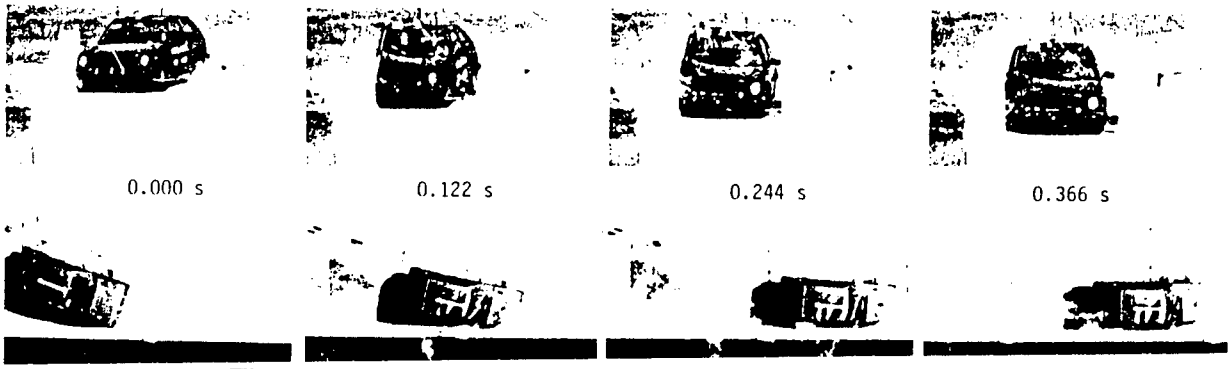

Figure B-2: Full Scale Crash Test of 1980 Honda Civic [14]

B.3 Federal Lands Highways Modified Kansas Corral Bridge Railing

The Kansas Corral Bridge Railing was developed and tested in the mid-1980s. Alterations were made to the design to provide a continuous beam rail and increased shear resistance of the posts. This version became know as the Modified Kansas Corral Bridge Rail. A division of the Federal Highway Administration known as the Federal Lands Highways Division made further aesthetic improvements to the rail to develop the present model called the Federal Lands Highways Modified Kansas Corral Bridge Rail.

This rail system is composed of a beam and post setup as can be seen in the photograph in Figure B-3 with a view of the posts in Figure B-4. The rail is 27 in. high with a 10 in. by 10 in. rail which projects approximately 5 in. inside the post to facilitate vehicle-rail interaction. The rail has a vertical slope of 1 to 10 and is reinforced with number 3 stirrups spaced at 3.5 in. The post is reinforced with number 4 reinforcing steel. This rail includes a 6 in. high curb to supply the connection between the bridge deck and the railing. The end of the rail is a vertical wall to be used in conjunction with a w- or three-beam rail for transition.

This railing is a good choice due to the open nature of the post and rail setup. The rail has performed satisfactorily to the requirements of AASHTO performance level 1 criteria.

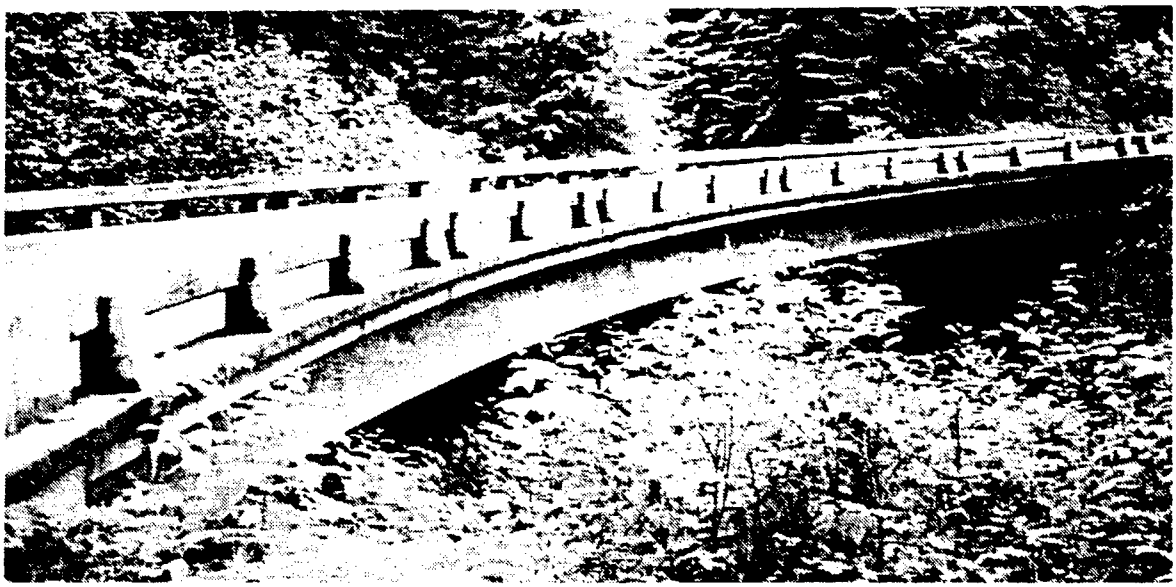

Figure B-3: Federal Lands Highways Modified Kansas Corral Bridge Railing [17]

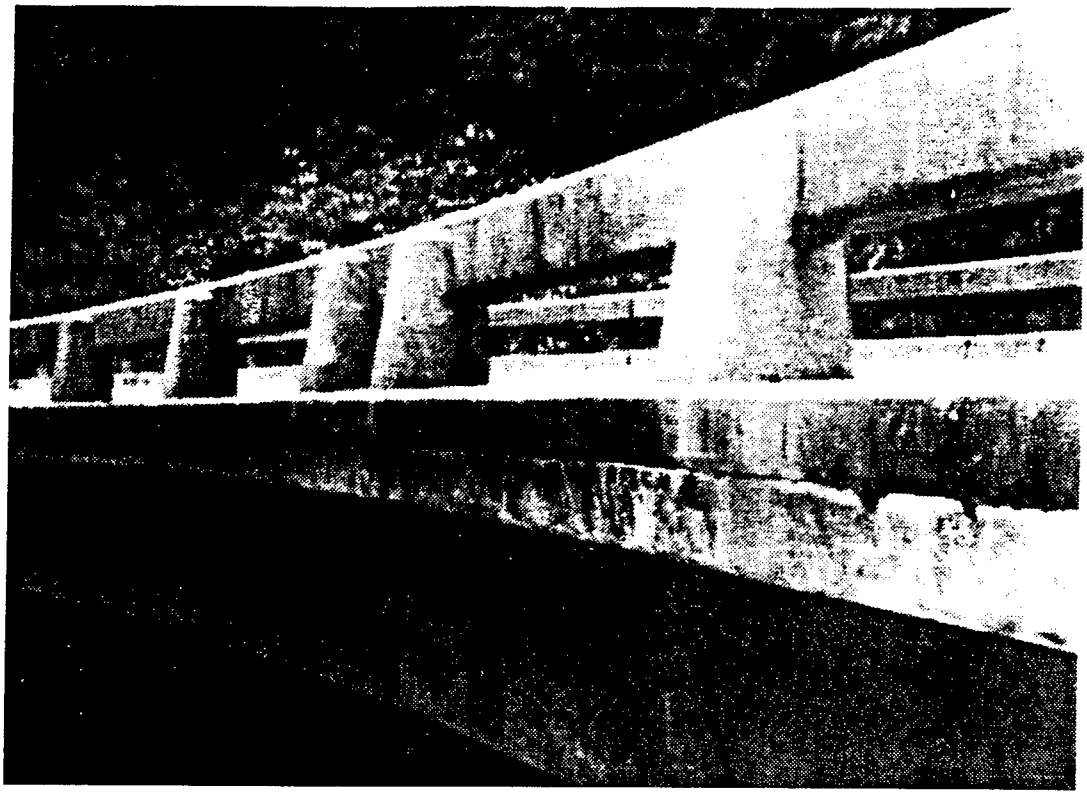

Figure B-4: View of Posts [17]

B.4 Texas C202 and Modified Texas C202 Bridge Rail

The standard Texas C202 bridge rail was altered in 1980 to attempt a design that would contain and redirect an 80,000-lb van-type tractor trailer for 50 mph, 15 degree-angle impacts. According to *NCHRP Report 230*[36], the rail must also be able to redirect a 1,800-lb automobile and a 4,500-lb automobile. A cross section of the modified rail can be seen in Figure B-5 along with a photograph in Figure B-6.

The rail is a beam and post design constructed of reinforced concrete. The rail is 13 in. wide and 23 in. tall with overall height of the concrete at 36 in. The posts are 13 in. high, 7 in. thick, and 60 in. long with 60 in. between each post. Details of the reinforcement can be seen in Figure B-5. The steel rail on top of the concrete is a standard Texas C4 rail. All reinforcing steel in the post and the rail are grade 40. The concrete has a compressive strength of 3,000 psi.

The rail was crash tested in accordance with *NCHRP Report 230*[36] for a service level 3 application. The Modified C202 performed adequately with all the requirements of *NCRP Report 230*[36]. Details of the results can be viewed in the *Transportation Research Record 1258*[27].

For the purposes of this project, the modified rail may be overdesigned and the standard Texas C202 rail should be considered. The cross section view can be viewed in Figure 6a.

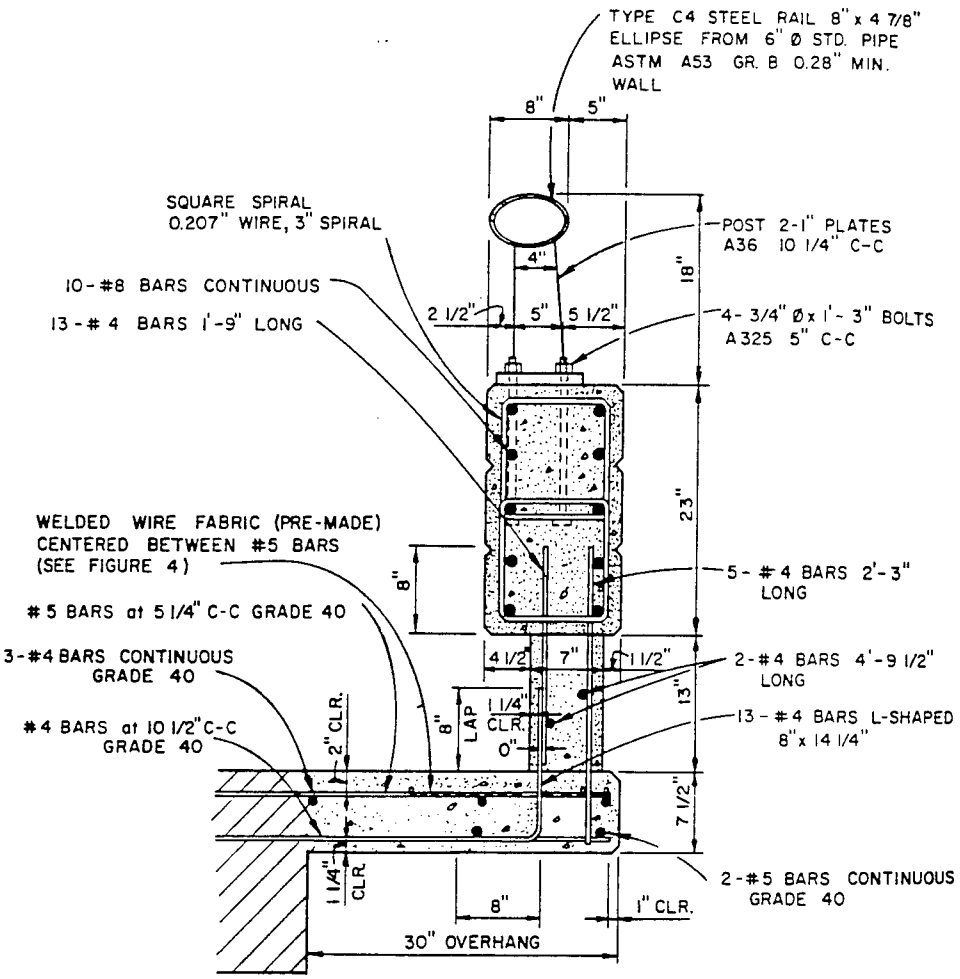

Figure B-5: Cross Section of Modified Texas C202 Rail [27]

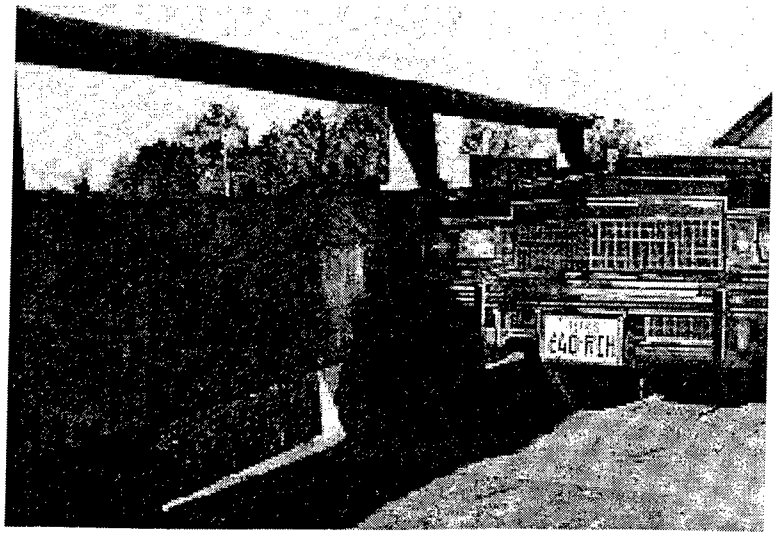

Figure B-6: Modified Texas C202 Rail [27]

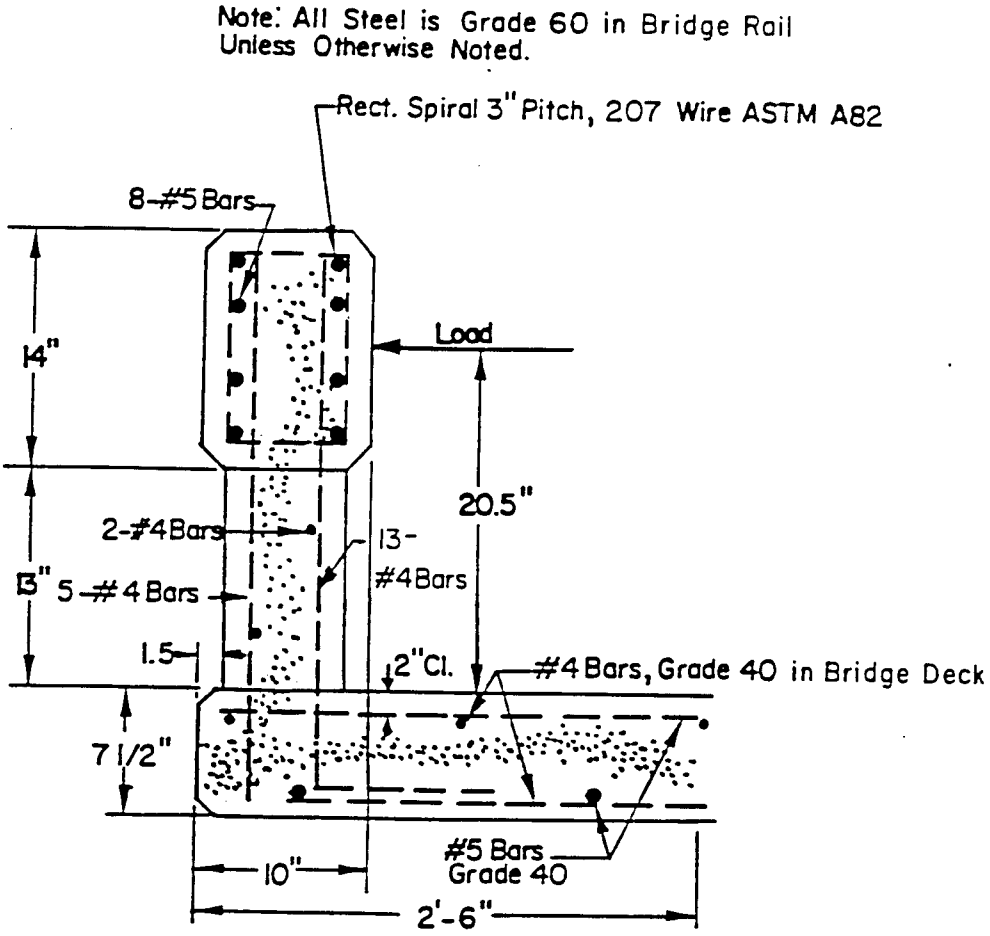

Figure B-7: Texas C202 Bridge Rail [27]

B.5 Modified T5 Rail

The modified T5 rail has a modified Texas Type C4 metal rail 18 in. tall mounted on top. This makes a combination bridge rail 50 in. tall that is designed to retain 80,000-lb trucks/trailers striking at 15 degrees and 50 mph. A cross section of the modified rail can be seen in Figure B-8 along with a photograph in Figure B-9.

The modified T5 rail consists of a concrete safety shaped parapet 32 in. high. The concrete parapet was thickened to 10.5 in. at the top and 20 in. at the bottom and contains a large amount of reinforcing steel. The metal rail mounted on top of the modified T5 concrete rail was a standard Texas Type C4 metal traffic rail. The rail was crash tested in accordance with *NCHRP Report 230*[36] for service level 3 application. The barrier met all the requirements specified by *NHCHRP Report 230*[36]. Details of the results can be viewed in the *Transportation Research Record 1065*[21].

For the purposes of this project, the modified T5 rail may be over designed and a reduced design of the rail should be considered. The Florida Department of Transportation currently uses a similar sidewalk barrier rail (see figure 8a) and a bicycle barrier rail (see figure 8b). Further modifications of either of these rails might include optimizing the concrete rail by adjusting the thickness and the height and the thickness of the concrete portion of the barrier.

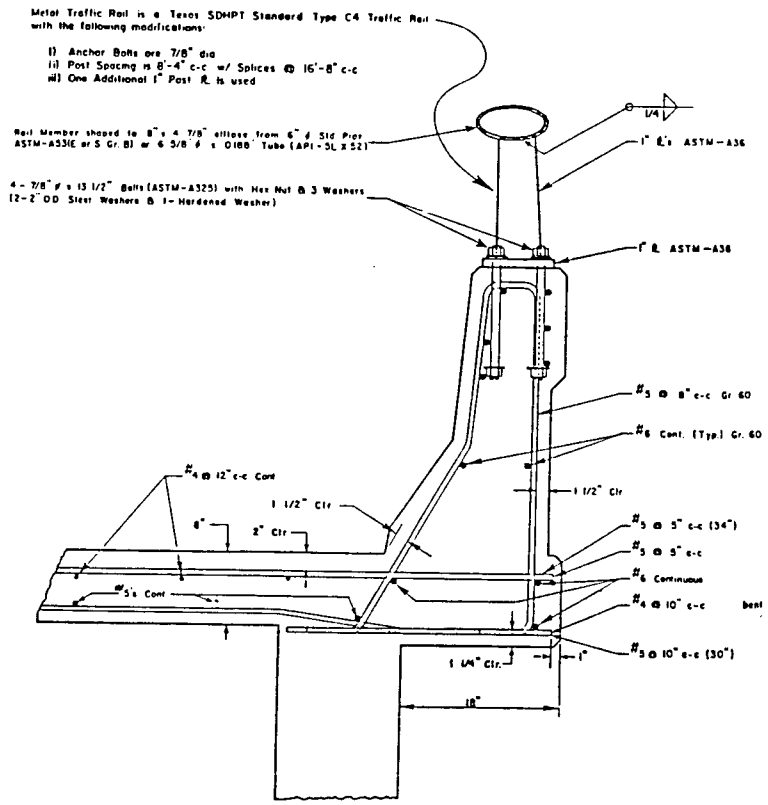

Figure B-8: Cross Section of Modified T5 Rail [21]

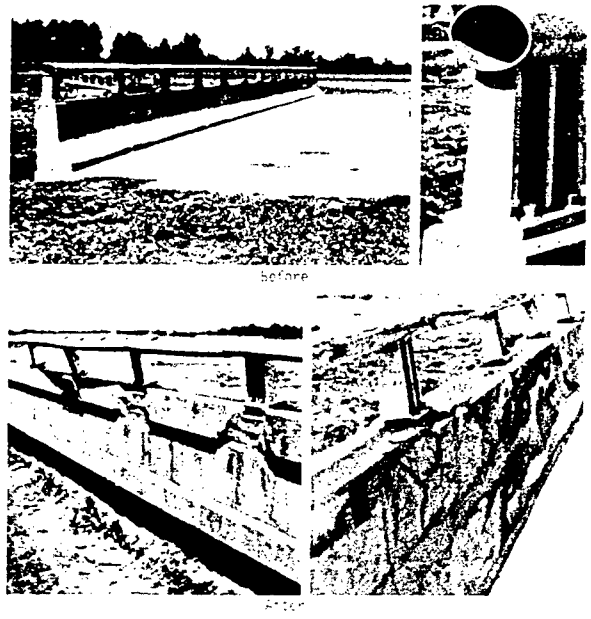

Figure B-9: Modified T5 Bridge Rail [21]

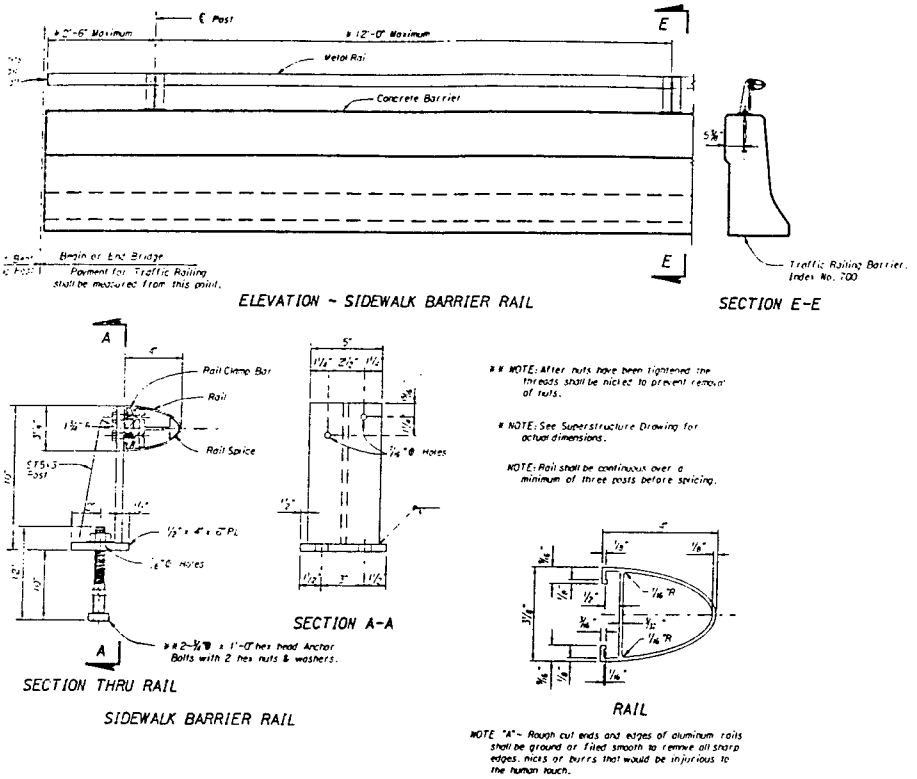

Figure B-10: FDOT Sidewalk Barrier Rail

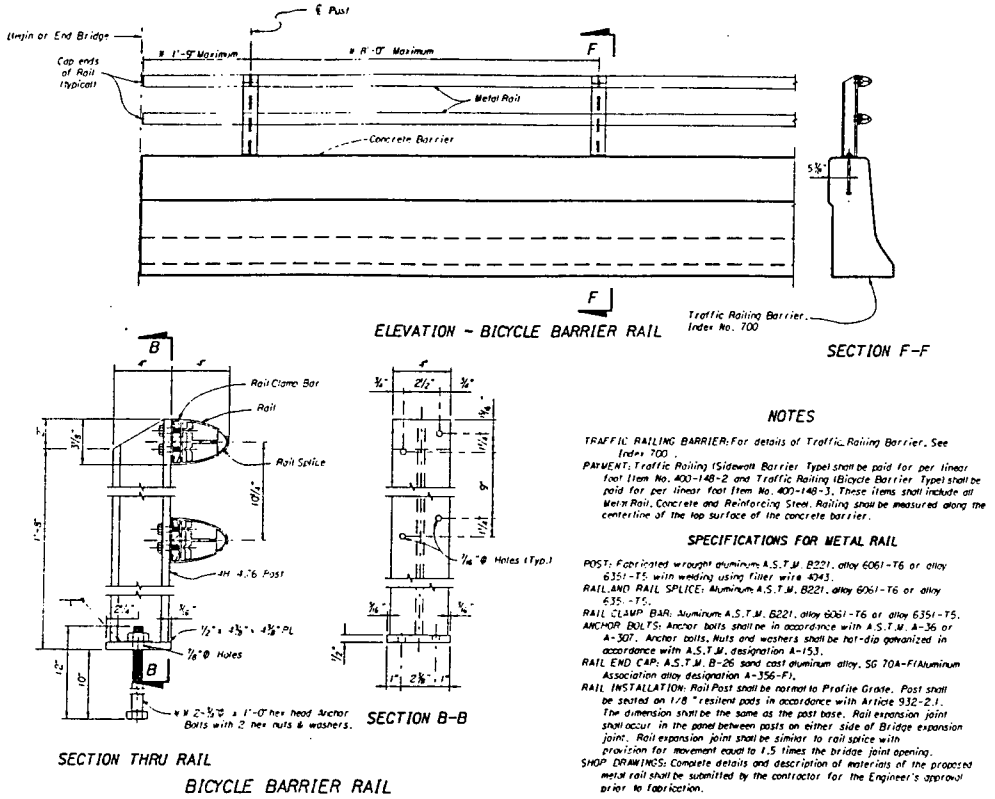

Figure B-11: FDOT Bicycle Barrier Rail

B.6 Illinois 2399-1 Metal Railing

This rail was adapted from an existing design used by Illinois as a retrofit railing; however, it can also be used for new construction. This rail was designed for a 5600-lb. lineload distributed uniformly over a 42 in. rail length at 29 in. Above the road. The posts are W6 X 25 rolled shapes at left, 3 in. on center. This rail was designed to be used in conjunction with a 7 in. curb yielding a total geometric height of the railing at 32 in. The cross section view can be seen in Figure B-12 with a photograph in Figure B-13. Three full scale crash tests were performed on the prototype railing:

(1) 1800-lb automobile striking at 60 mph and 20 degrees

(2) 5400-lb pickup truck striking at 65 mph and 20 degrees

(3) 18000-lb single-unit truck striking at 50 mph and 15 degrees

The rail performed acceptable in all three tests. All tests were performed according to *NCHRP Report 230*[36] and the rail is adequate for service level 2 application. Details of the crash tests can be viewed in the *Transportation Research Record 1258*[28].

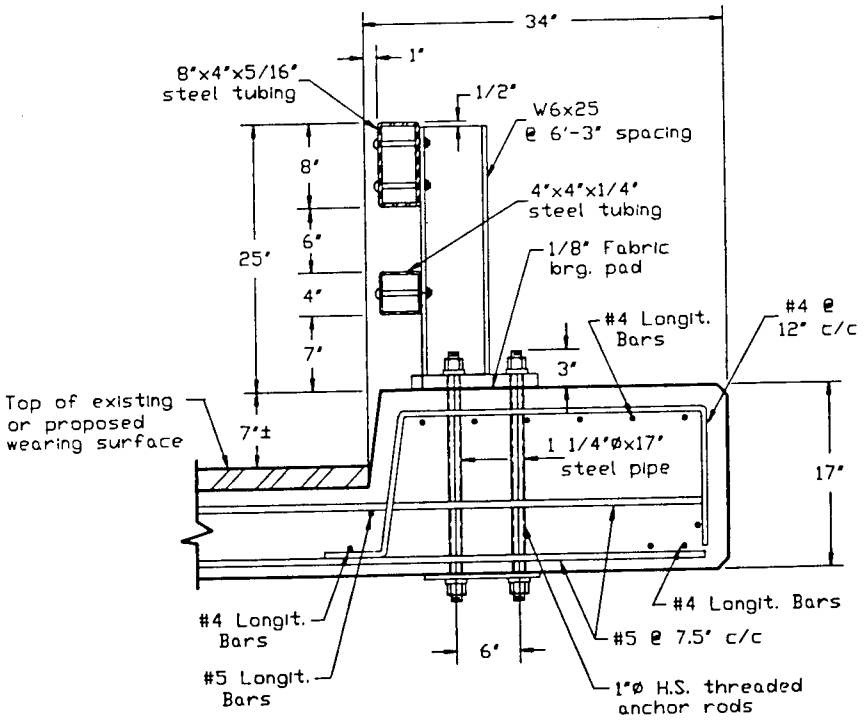

Figure B-12: Cross Section View of Illinois 2399-1 Rail [28]

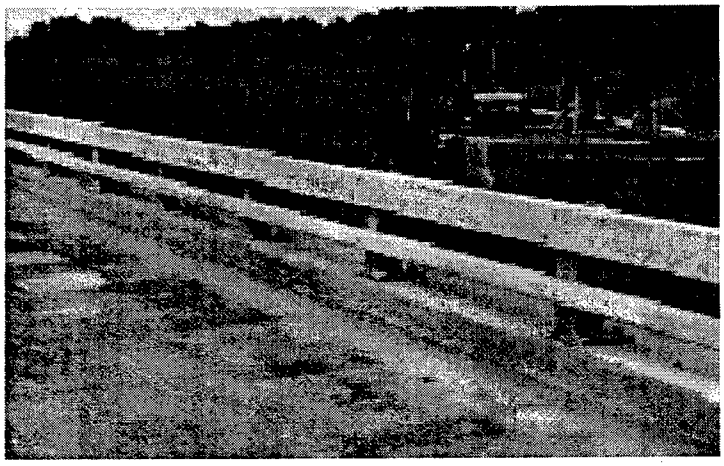

Figure B-13: Illinois 2399-1 Metal Rail [28]

B.7 Wyoming Tube-Type Bridge Rail

The Wyoming tube-type bridge rail is a low profile streamlined rail that is aesthetically pleasing and allows the traveling public views of the surrounding areas from the bridge deck. The rail has minimal maintenance costs due to the fact that replacement rail posts, rails, and associated hardware can be stockpiled to expedite repairs. Years of experience have shown that there has never been any penetration or vaulting over the rail, even when struck by tractor semi-trailers.

The rail consists of fabricated posts with two TS6 X 2 X 0.25 tube type beams. The metal rail sits on top of a 6 in. high curb with a total height of 29 in. Two crash tests were conducted on this rail system:

(1) Test S13- 1800-lb vehicle striking the bridge rail at 60 mph at 20 degrees

(2) Test 10- 4500-lb vehicle striking the rail at 60 mph at 25 degrees

The rail was crash tested in accordance with *NCHRP Report 230*[36] for a service level 2 application. The rail performed adequately in all tests. Details of the results can be viewed in the *Transportation Research Record 1258*[28]. A photograph of the rail can be seen in Figure B-14.

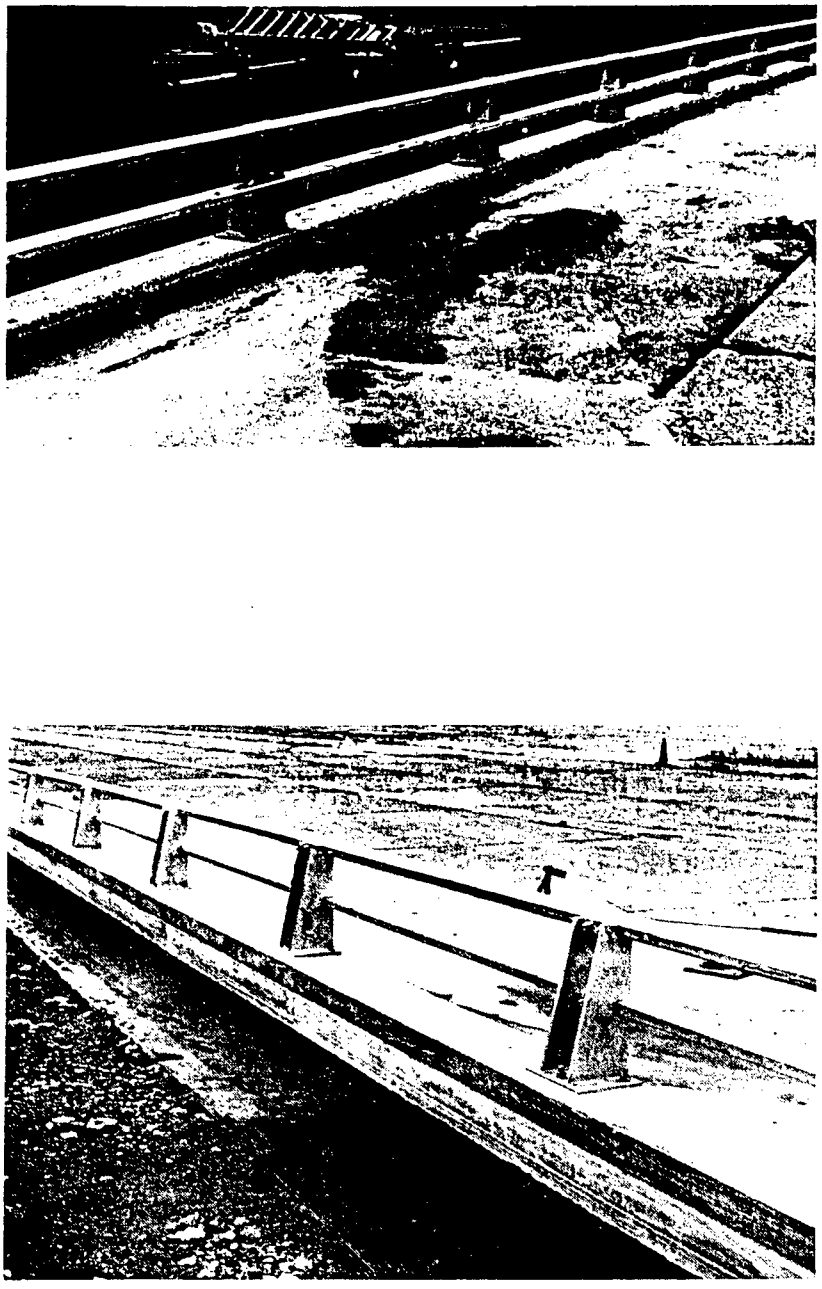

Figure B-14: Wyoming Tube-Type Bridge Rail [28]

B.8 BR27D and BR27C Bridge Railings

The BR27D and the BR27C bridge rails consists of concrete parapets with metal railings mounted on top. The concrete parapet serves to transfer the load to the bridge deck, while the rails allow visibility through the rail. These rails were developed for use in urban areas where truck traffic is minimum.

B.8.1 BR27D Bridge Railing

The rail is constructed of two A500 rails (grade B, TS4 X 3 X 0.25 in.) attached to posts (A500 grade B, TS4 X 4 X 0.1875 X 24 in.) mounted atop an 18 in. reinforced concrete parapet. The posts are spaced at 6 ft. 7 in. on center. Detailed elevations of the bridge railings are shown in Figure B-15 and photographs of the completed bridge railing installations are shown in Figure B-16. The rail was tested for performance level 1 application. Two crash tests were performed:

(1) 1800-lb automobile striking at 60 mph and 20 degrees

(2) 5400-lb pickup truck striking at 65 mph and 20 degrees

The rail performed adequately in both tests.

B.8.2 BR27C Bridge Railing

The rail is constructed of one A500 rail (grade B, TS4 S 3 X 0.25 in.) attached to posts (8500 grade B, TS4 X 4 X 0.1875 X 18 in.) mounted atop a 24 in. reinforced concrete parapet. The posts are spaced at 6 ft. 7 in. on center. Detailed elevations of the

bridge railings are shown in Figure B-17 and photographs of the completed bridge railing installations are shown in Figure B-18. The rail was tested for performance level 2 application. Three crash tests were performed:

(1) 1800-lb. automobile striking at 60 mph and 20 degrees

(2) 5400-lb. pickup truck striking at 65 mph and 20 degrees

(3) 18,000-lb. single unit truck striking at 50 mph and 15 degrees

The rail performed adequately in both test. Details of all the crash tests can be viewed in the *Transportation Research Record 1468*[25].

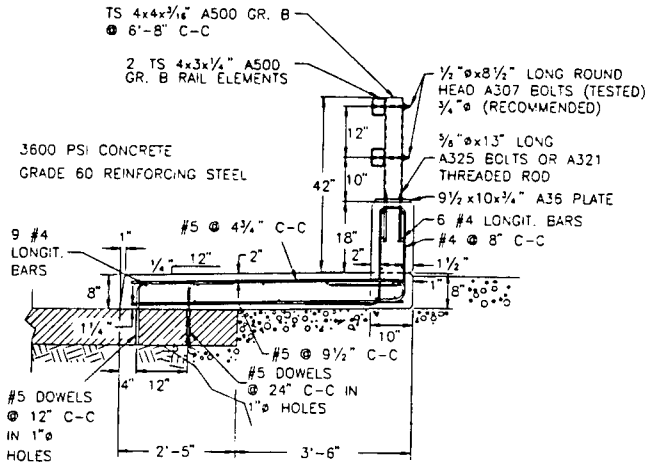

Figure B-15: Cross Section of BR27D Bridge Rail [25]

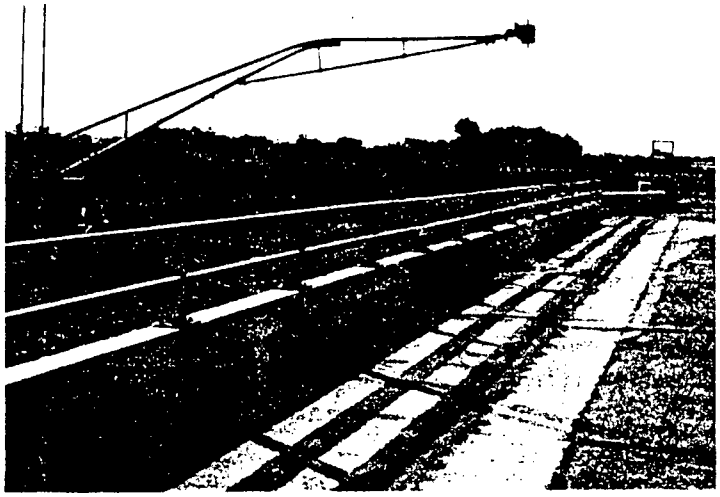

Figure B-16: BR27D Bridge Rail [25]

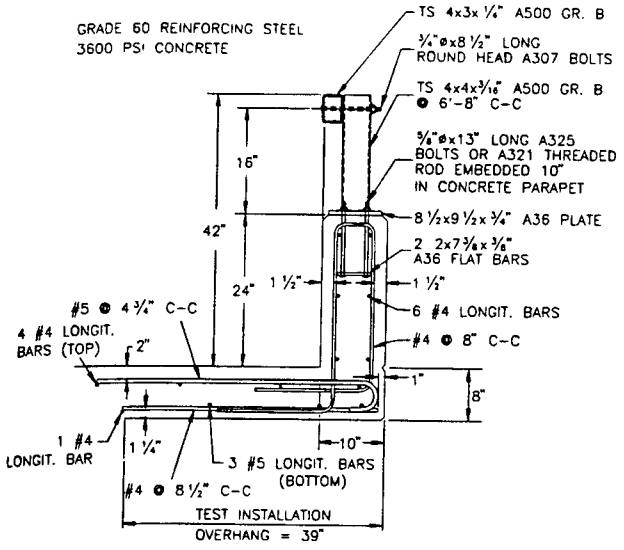

Figure B-17: Cross Section of BR27C Bridge Rail [25]

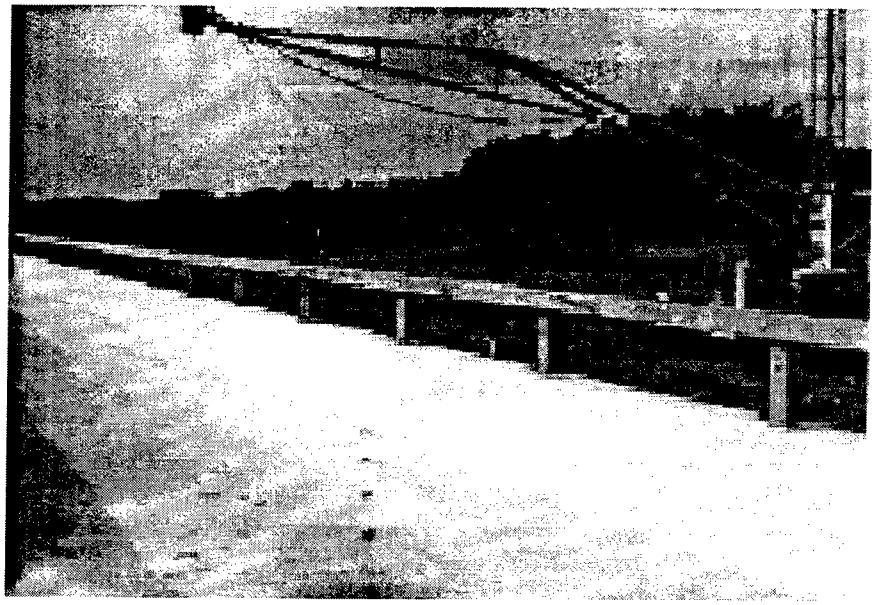

Figure B-18: BR27C Bridge Rail

APPENDIX C

LS-DYNA3D INPUT DECK MODIFICATIONS

Many times, access to important functions of LS-DYNA3D is often impossible from the preprocessors PATRAN or LS-INGRID, therefore some parameters still need to be added directly to the LS-DYNA3D keyword input deck. The following sections describe details of those manual modifications that must be made to the input file in order to facilitate a proper computer simulation.

C.1 Automatic Contact

LS-DYNA3D contains an automatic contact feature (type 13 slide surface) which does not require explicit definition of contact surfaces. The first and second items in the automatic contact card represent the static and dynamic coefficients of friction. Reasonable values for these coefficients must be assumed due to the fact that only one contact surface can be defined with the automatic contact feature. For the purposes of this project, the most critical contact is between the front body panels of the vehicle and the reinforced concrete bridge barrier. These values can vary from 0.2 to 0.5 [34] depending upon a variety of parameters such as:

- Guardrail material (i.e. concrete, steel, aluminum, etc.)
- Vehicle bumper material (i.e. steel, aluminum, etc.)
- Angle of impact

While the automatic contact is very user-friendly and saves initial input time, the long-term computational price is high. Several features of LS-DYNA3D which work well with other slide surfaces, are not available because only one contact surface can be defined when using this feature. The cards can be seen below:

Card 1

Variable	SSID	MSID	SSTYP	MSTYP	SBOXID	MBOXID	SPR	MPR

Card 2

Variable	FS	FD	DC	VC	VDC	PENCHK	BT	DT

Card 3

Variable	SFS	SFM	SST	MST	SFST	SFMT	FSF	VSF

Figure C-1: Card Format for *CONTACT_AUTOMATIC_SINGLE_SURFACE Option [1]

- SSID - Slave set ID.
- MSID - Master set ID.
- SSTYP - Slave segment or node set type. (EQ 2 = part set ID)
- MSTYP - Master segment set type. (EQ 0 = segment set ID)
- SBOXID - Slave nodes/segments (EQ 0 = Parts as defined by SSID are taken)
- MBOXID - Master segments (EQ 0 = Segments as defined by MSID are taken)
- SPR - Slave side in printed and binary force interface file (EQ 0 = No file)

- MPR - Master side in printed and binary force interface file (EQ 0 = No file)
- FS - Static coefficient of friction (0<FS<1)
- FD - Dynamic coefficient of friction (0<FD<1)
- DC - Exponential decay coefficient
- VC - Coefficient for viscous friction
- VDC - Viscous damping coefficient in percent of critical
- PENCH - Small penetration check (EQ 0 = Turned off)
- BT - Birth Time (Contact surfaces become active at this time)
- DT - Death Time (Contact surfaces deactivated at this time)
- SFS - Scale factor on default slave penalty stiffness
- SFM - Scale factor on default master penalty stiffness
- SST - Optional thickness for slave surface (Only applies to shells)
- MST - Optional thickness for master surface (Only applies to shells)
- SFST - Scale factor for slave surface thickness (Only applies to shells)
- SFMT - Scale factor for master surface thickness (Only applies to shells)
- FSF - Coulomb friction factor (μ_{sc} = FSF * μ_c)
- VSF - Viscous friction factor

The relationship between the coefficients of friction and the decay coefficients are shown in the following equations:

$$\mu = FD + (FS - FD)e^{-DC*Vrel} \qquad \text{(C-1)}$$

While it is difficult to obtain a single value for static and dynamic friction coefficients, Warner [38] reports a coefficient of friction for a pickup truck sliding on side on concrete as 0.3 to 0.4. For our case, the specific values are taken as follows:

FS = 0.35

FD = 0.30

It should be noted that if no value is input for DC, the default value is zero. A zero value for DC will make the previous equation equal to the static friction coefficient. This nonzero value provides a smooth transition between the static and the dynamic coefficients of friction. Plaxico [18] reports a decay coefficient of 0.000266, which is followed for our case. The effect of the decay coefficient can be seen in Figure C-2.

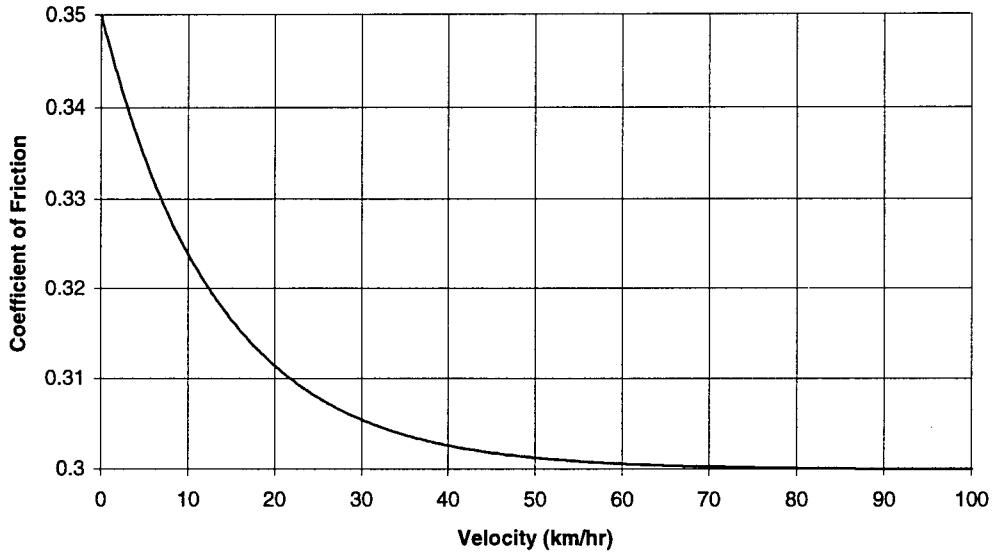

Figure C-2: Friction versus velocity

Analyzing Figure C-2, one can see that when the velocity is zero, the coefficient of friction is approximately the value for static friction and as the velocity increases, the coefficient of friction approaches the value for dynamic friction.

At a latter point in the research, it was discovered that contact type 5a could also be used to produce results similar to those obtained with contact type 13. Contact type 5a is defined with the *CONTACT_AUTOMATIC_NODES_TO_SURFACE option. The

card for this option is exactly the same as for contact type 13 (see Figure C-1) with the exception of one addition card which can be seen below:

Card 4

Variable	ISYM	EROSOP	IADJ					

Figure C-3: Card Format for *CONTACT_AUTOMATIC_NODES_TO_SURFACE Option [1]

- ISYM - Symmetry Plane Option (EQ 0 = off)
- EROSOP - Erosion/Interior node option (EQ 0 = no erosion of nodes)
- IADJ - Adjacent material treatment for solid elements (EQ 0 = solid element faces are included only for free boundaries).

In order to increase computational time, this contact was utilized between the barrier and parts of the vehicle observed to come into contact with the barrier. Contact type 13 was still used between the parts of the truck model. This increased the speed of the calculations due to the fact that every part of the vehicle was not searching for contact with the barrier.

C.2 Ground-Tire Interaction

LS-DYNA3D allows for the definition of a rigidwall with orthotropic friction. This option is especially useful in specifying friction between the tire and the ground where the frictional forces are substantially higher in a direction transverse to the rolling direction. The effect of the ground surface is described with the

*RIGIDWALL_PLANAR-ORTHO function and for visual effects the ground is modeled additionally with several shell finite elements, which do not take part in the contact. The card for this function can be seen below:

Card 1

Variable	NSID	NSIDEX	BOXID					

Card 2

Variable	XT	YT	ZT	XH	YH	ZH	FRIC	

Card 3

Variable	SFRICA	SFRICB	DFRICA	DFRICB	DECAYA	DECAYB		

Card 4

Variable	NODE1	NODE2	D1	D2	D3			

Figure C-4: Card Format for *RIGIDWALL_PLANAR_ORTHO Option [1]

- NSID - Nodal Set ID containing slave nodes.
- NSIDEX - Nodal Set ID containing nodes that exempted as slave nodes.
- BOXID - All nodes in box are included as slave nodes to rigid wall.
- XT - X-coordinate of tail of any outward drawn normal vector, n, originating on wall (tail) and terminating in space (head)
- YT - Y-coordinate of tail of normal vector n
- ZT - Z-coordinate of tail of normal vector n
- XH - X-coordinate of head of normal vector n
- YH - Y-coordinate of head of normal vector n
- ZH - Z-coordinate of head of normal vector n

- FRIC - Interface friction. (0<FRIC<1)
- SFRICA - Static friction coefficient in local a-direction, μ_{sa}
- SFRICB - Static friction coefficient in local b-direction, μ_{sb}
- DFRICA - Dynamic friction coefficient in local a-direction, μ_{ka}
- DFRICB - Dynamic friction coefficient in local b-direction, μ_{kb}
- DECAYA - Decay constant in local a-direction, d_{va}
- DECAYB - Decay constant in local b-direction, d_{vb}
- NODE1 - Node 1, alternative to definition with vector d below
- NODE2 - Node 2
- D1 - X-component of vector, alternative of definition with nodes above
- D2 - Y-component of vector
- D3 - Z-component of vector

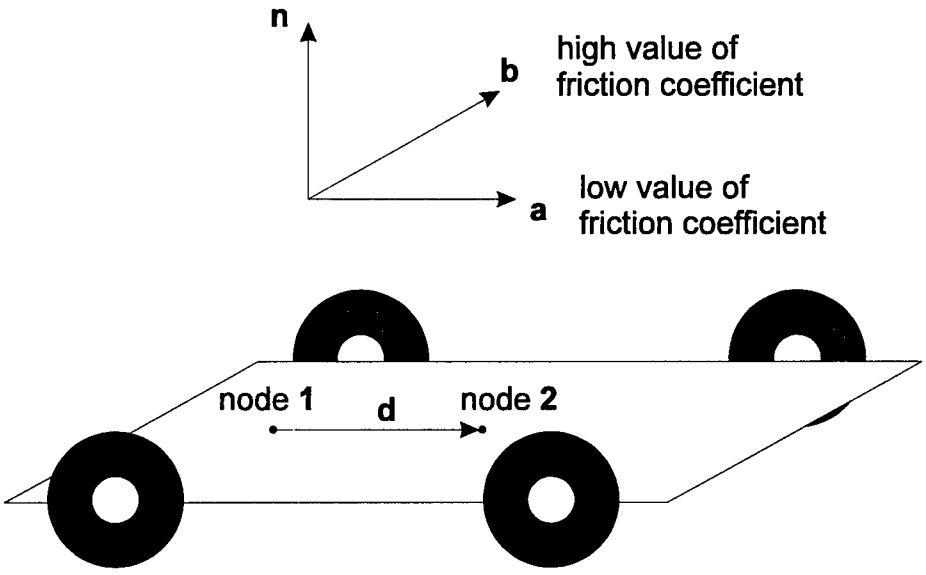

Figure C-5: Definition of orthotropic friction vectors [1]

There are two methods for defining the vector **d**. If the vector is defined by specifying two nodes, the local coordinate system will rotate with the body which contains the nodes (the vehicle). If the x, y, and z coordinates of the vector **d** are specified, the vector is fixed and the local coordinate system is stationary. For our case, nodes were specified at the front and the rear of the drive shaft to define the vector **d**. The local frictional directions are determined such that **b** = **n** x **d** and that **a** = **b** x **n.** If **n** is the normal vector to the wall and **d** is in the plane of the wall, **a** is in the direction of **d**. (see Figure C-5)

The relationship between the coefficients of friction and the decay coefficients are shown in the following equations:

$$\mu_a = \mu_{ka} + (\mu_{sa} - \mu_{ka})e^{-d_{va}V_{relative,a}} \tag{C-2}$$

$$\mu_b = \mu_{kb} + (\mu_{sb} - \mu_{kb})e^{-d_{vb}V_{relative,b}} \tag{C-3}$$

This relationship is identical to the relationship for the automatic contact friction. As stated previously, if d_{va} or d_{vb} equal zero, then the friction is equal to the static friction. The same decay coefficients are used as in the automatic contact feature, i.e. $d_{va} = d_{vb} =$ 0.000266.

There are a variety of parameters which may affect the value of the coefficients of friction between the tire and the ground surface which are as follows:

- Type and quality of tires.
- Road surface properties. (i.e. concrete, asphalt, etc.)
- Roadway weather conditions.

For this reason, it is again difficult to determine single values for the coefficients of friction. Limpert [37] recommends a transverse coefficient of friction between bias ply tires and concrete pavement as 0.9 to 0.6 depending upon road conditions, while Plaxico [18] suggests a transverse friction coefficient of friction of 0.2. Based on [18] and [37], average values for static and dynamic friction were taken as:

$$\mu_{sb} = 0.6$$

$$\mu_{kb} = 0.5$$

The values for the longitudinal coefficients of friction were set to zero in order to simulate the tires rolling freely; however, it should be noted that the tires do not actually roll on the ground surface, they merely serve to transport the vehicle as they "slide" across the ground.

The *RIGIDWALL_PLANAR_ORTHO Option [1], must be used in conjunction with the *SET_NODE_OPTION. This option allows the user to input the set of nodes which are not permitted to pass through the rigidwall (ground). For our case, the nodes corresponding to the bottom half of the tire are defined. The card for this function can be seen in the following figure:

Card 1

Variable	SID	DA1	DA2	DA3	DA4			

Card 2

Variable	NID1	NID2	NID3	NID4	NID5	NID6	NID7	NID8

Figure C-6: Card Format for *SET_NODE Option [1]

- SID - Node set I.D.
- DA1- Normal failure force. (Not used in our case.)
- DA2- Shear failure force. (Not used in our case.)
- DA3- Exponent for normal force. (Not used in our case.)
- DA4- Exponent for shear force. (Not used in our case.)
- NID1 TO NIDN - Nodes permitted from penetrating the rigidwall.

Once again, it is important to remember that the ground surface is for presentation purposes only, thus a linear elastic material model is assigned as these shell elements are not included in contact with any other elements.

C.3 Gravity

Gravity is represented in the simulations by applying a constant load curve to the entire system. The load curve is defined using the *DEFINE_CURVE function. The card for this function can be seen in below:

Card 1

Variable	LCID	SIDR	SFA	SFO	OFFA	OFFO	DATTYP	

Figure C-7: Card Format for *DEFINE_CURVE Option [1]

- LCID - Load curve ID. A unique number should be assigned to each separate load curve.
- SIDR - Stress initialization by dynamic relaxation (EQ.0 = No dynamic relaxation)
- SFA- Scale factor for abcissa value
- SFO - Scale factor for ordinate value
- OFFA - Offset for abcissa values

- OFFO - Offset for ordinate values
- DATTYP - Data type (1 for general XY data)

The curve is a constant applied acceleration of $y = 9.81 m/s^2$ at all times (see Figure C-8).

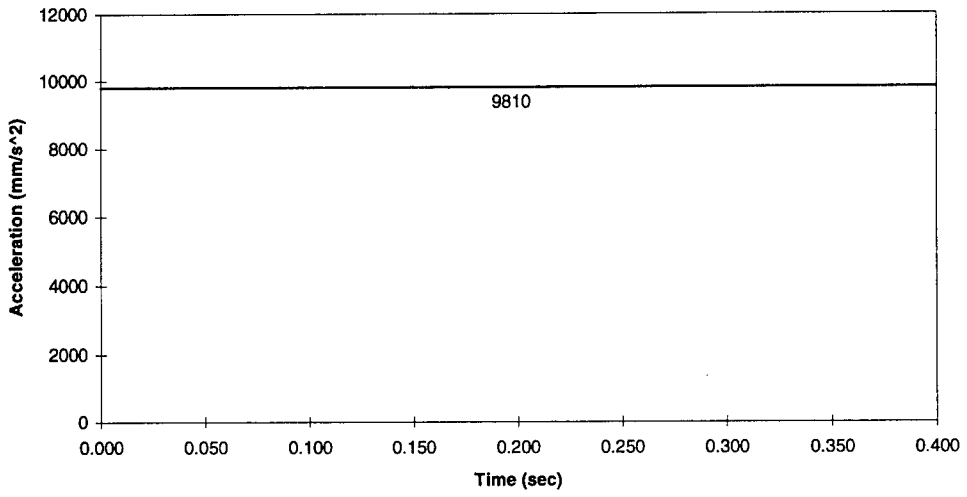

Figure C-8: Gravity Load Curve

The gravity load curve is applied to the system with the *LOAD_BODY_(OPTION) function. The card can be seen below:

Card 1

Variable	LCID	SF	LCIDDR					

Figure C-9: Card Format for *LOAD_BODY_(DIRECTION) Option [1]

- LCID - Load Curve ID.
- SF - Load Curve scale factor.
- LCIDDR - Load Curve ID for dynamic relaxation phase.

C.4 Accelerometer Definition

In order to obtain valid results, which could potentially be compared to full-scale crash test results, it is imperative to have a common point of reference for evaluation of displacements, velocities, and accelerations with respect to time. To accomplish this, an accelerometer is defined at the center of gravity of the vehicle. This was performed with the *ELEMENT_SEATBELT_ACCELEROMETER function. The card for this function can be seen below:

Card 1

Variable	SBACID	NID1	NID2	NID3				

Figure C-10: Card Format for *ELEMENT_SEATBELT_ACCELEROMETER Option [1]

- SBACID - Accelerometer ID. A unique number has to be used.
- NID1 - Node 1 ID.
- NID2 - Node 2 ID.
- NID3 - Node 3 ID.

This accelerometer outputs accelerations and velocities of node 1 to all output files in local instead of global coordinates. The local coordinate system is represented by three nodes as follows:

- local **x** from node 1 to node 2
- local **z** perpendicular to the plane containing nodes 1, 2, and 3 ((**z** = **x** x **a**), where **a** is from node 1 to node 3)
- local **y** = **z** x **x**

The material for the accelerometer is defined with the *MAT_RIGID function. In the LS-DYNA3D manual, this is material number 20. All parts belonging to this material are considered to be part of a rigid body. This material model has a low computational price. The cards for this material can be seen below:

Card 1

Variable	MID	RO	E	PR	N	COUPLE	M	ALIAS

Card 2

Variable	CMO	CON1	CON2					

Card 3

Variable	LCO or A1	A2	A3	V1	V2	V3		

Figure C-11: Card Format for *MAT_RIGID Option [1]

- MID - Material Identification. Unique number.
- RO - Mass density.
- E - Young's Modulus.
- PR - Poisson's Ratio.
- N - EQ. 0 - Normal LS-DYNA3D rigid body updates.
- COUPLE - Coupling Option (if available) (EQ = 0 Default)
- M - Coupling Option Flag. (EQ 0 = normal LS-DYNA3D rigid body updates)
- ALIAS - VDA surface alias name.
- CMO - Center of Mass constraint option. (EQ = +1.0 constraints applied in global directions.
- CON1 - First constraint parameter. (EQ = 0 No constraints)

- CON2 - Second constraint parameter. (EQ = 0 No constraints)
- A1 - Local coordinate system number for output. (Optional)
- A2 - Default to 0. (Optional)
- A3 - Default to 0. (Optional)
- V1 - Default to 0. (Optional)
- V2 - Default to 0. (Optional)
- V3 - Default to 0. (Optional)

This accelerometer element should be created at the center of gravity of the vehicle and assigned a rigid material and all nodes should be part of the same rigid body. The local axis for node 1 will then rotate with the body.

C.5 Strain Rate Hardening Effects

As stated in Chapter 5, strain rate hardening effects have a substantial influence in the performance of concrete materials in LS-DYNA3D. Based on the results presented in Chapter 5, strain rate hardening effects were included in both the concrete barrier and the steel elements in the truck model. These effects can be seen in Figure C-12. These two curves were defined in LS-DYNA3D with the use of the *DEFINE_CURVE option (see Figure C-7).

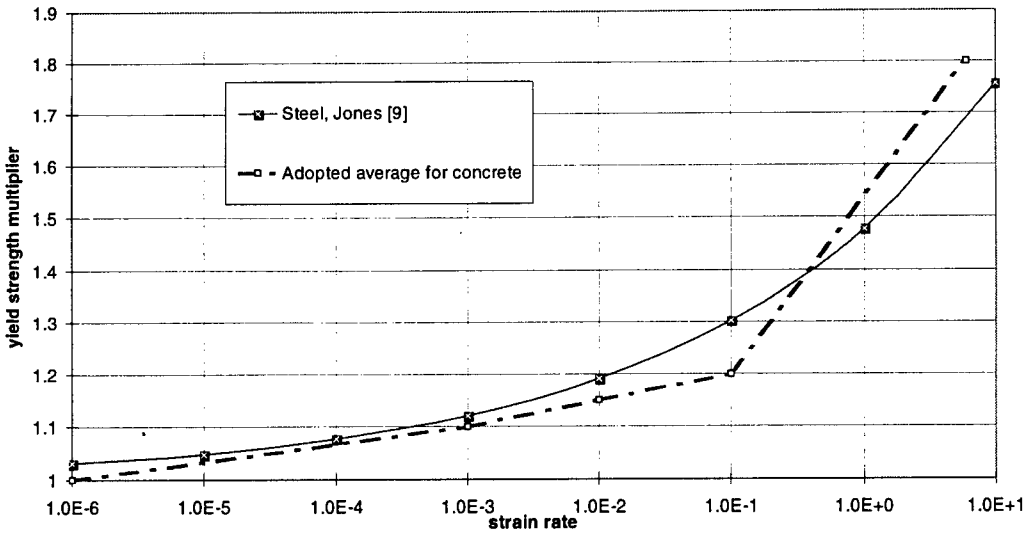

Figure C-12: Yield strength multiplier versus strain rate

APPENDIX D

LS-DYNA3D EXAMPLE INPUT DECK

```
*KEYWORD
*TITLE
ft6m16s100a25.fdot   * this is a new version FEB 13, 97
$                      changed part numbering : now accelerometer is part 44!
$    strain rate effect included
$    friction coeff. for truck-barrier contact : stat=.35,   dyn=.3
$    friction coeff. for truck-ground contact : stat=.6,   dyn=.5
*CONTROL_TERMINATION
3.000E-01       0 0.000E+00       0 0.000E+00
*CONTROL_TIMESTEP
5.000E-03 0.000E+00       0 0.000E+00 0.000E+00       0   0
*CONTROL_SHELL
0.000E+00       0       0       0       2       0
*CONTROL_DAMPING
      0 0.000E+00 0.000E+00 0.000E+00 0.000E+00       0 0.000E+00       0
*CONTROL_CONTACT
0.000E+00 0.000E+00       0       0       0       0       0       0
      0       0       0
*CONTROL_OUTPUT
      0       0       0       0 0.000E+00       0
*CONTROL_ENERGY
      0       0       0       0
*DATABASE_BINARY_D3PLOT
3.000E-03
*CONTROL_CPU
0.000E+00
*MAT_PIECEWISE_LINEAR_PLASTICITY
      1 7.850E-09 2.100E+05 3.000E-01 6.150E+02 0.000E+00 5.000E+08 0.000E+00
4.040E+01 5.000E+00 0.000E+00 0.000E+00
0.000E+00 4.000E-03 3.000E-02 1.500E-01 3.000E-01 4.000E-01 1.000E+01 0.000E+00
0.000E+00 6.150E+02 7.000E+02 7.900E+02 8.400E+02 8.600E+02 8.000E+02 0.000E+00
*MAT_PIECEWISE_LINEAR_PLASTICITY
      2 7.850E-09 2.100E+05 3.000E-01 6.150E+02 0.000E+00 5.000E+08 0.000E+00
4.040E+01 5.000E+00 0.000E+00 0.000E+00
0.000E+00 4.000E-03 3.000E-02 1.500E-01 3.000E-01 4.000E-01 1.000E+01 0.000E+00
0.000E+00 6.150E+02 7.000E+02 7.900E+02 8.400E+02 8.600E+02 8.000E+02 0.000E+00
*MAT_PIECEWISE_LINEAR_PLASTICITY
      3 7.850E-09 2.100E+05 3.000E-01 6.150E+02 0.000E+00 5.000E+08 0.000E+00
4.040E+01 5.000E+00 0.000E+00 0.000E+00
0.000E+00 4.000E-03 3.000E-02 1.500E-01 3.000E-01 4.000E-01 1.000E+01 0.000E+00
```

Title Information - Dollar Sign at beginning of line indicates remark.

Total Duration of Simulation

Timestep for Calculations

Timestep for Creation of Plot Files

First 37 Materials Represent Vehicle

Bumper

Frame

```
0.000E+00 6.150E+02 7.000E+02 7.900E+02 8.400E+02 8.600E+02 8.000E+02 0.000E+00
*MAT_PIECEWISE_LINEAR_PLASTICITY
     4 7.850E-09 2.100E+05 3.000E-01 6.150E+02 0.000E+00 5.000E+08 0.000E+00
4.040E+01 5.000E+00 0.000E+00 0.000E+00
0.000E+00 4.000E-03 3.000E-02 1.500E-01 3.000E-01 4.000E-01 1.000E+01 0.000E+00
0.000E+00 6.150E+02 7.000E+02 7.900E+02 8.400E+02 8.600E+02 8.000E+02 0.000E+00
*MAT_PIECEWISE_LINEAR_PLASTICITY
     5 7.850E-09 2.100E+05 3.000E-01 6.150E+02 0.000E+00 5.000E+08 0.000E+00
4.040E+01 5.000E+00 0.000E+00 0.000E+00
0.000E+00 4.000E-03 3.000E-02 1.500E-01 3.000E-01 4.000E-01 1.000E+01 0.000E+00
0.000E+00 6.150E+02 7.000E+02 7.900E+02 8.400E+02 8.600E+02 8.000E+02 0.000E+00
*MAT_PIECEWISE_LINEAR_PLASTICITY
     6 7.850E-09 2.100E+05 3.000E-01 6.150E+02 0.000E+00 5.000E+08 0.000E+00
4.040E+01 5.000E+00 0.000E+00 0.000E+00
0.000E+00 4.000E-03 3.000E-02 1.500E-01 3.000E-01 4.000E-01 1.000E+01 0.000E+00
0.000E+00 6.150E+02 7.000E+02 7.900E+02 8.400E+02 8.600E+02 8.000E+02 0.000E+00
*MAT_PIECEWISE_LINEAR_PLASTICITY
     7 7.850E-09 2.100E+05 3.000E-01 6.150E+02 0.000E+00 5.000E+08 0.000E+00
4.040E+01 5.000E+00 0.000E+00 0.000E+00 } Tires
0.000E+00 4.000E-03 3.000E-02 1.500E-01 3.000E-01 4.000E-01 1.000E+01 0.000E+00
0.000E+00 6.150E+02 7.000E+02 7.900E+02 8.400E+02 8.600E+02 8.000E+02 0.000E+00
*MAT_ELASTIC
     8 4.410E-09 2.100E+05 3.000E-01 } Engine and Transmission
*MAT_PIECEWISE_LINEAR_PLASTICITY
     9 7.850E-09 2.100E+05 3.000E-01 6.150E+02 0.000E+00 5.000E+08 0.000E+00
4.040E+01 5.000E+00 0.000E+00 0.000E+00
0.000E+00 4.000E-03 3.000E-02 1.500E-01 3.000E-01 4.000E-01 1.000E+01 0.000E+00
0.000E+00 6.150E+02 7.000E+02 7.900E+02 8.400E+02 8.600E+02 8.000E+02 0.000E+00
*MAT_PIECEWISE_LINEAR_PLASTICITY
    10 7.850E-09 2.100E+05 3.000E-01 6.150E+02 0.000E+00 5.000E+08 0.000E+00
4.040E+01 5.000E+00 0.000E+00 0.000E+00
0.000E+00 4.000E-03 3.000E-02 1.500E-01 3.000E-01 4.000E-01 1.000E+01 0.000E+00
0.000E+00 6.150E+02 7.000E+02 7.900E+02 8.400E+02 8.600E+02 8.000E+02 0.000E+00
*MAT_PIECEWISE_LINEAR_PLASTICITY
    11 7.850E-09 2.100E+05 3.000E-01 6.150E+02 0.000E+00 5.000E+08 0.000E+00
4.040E+01 5.000E+00 0.000E+00 0.000E+00
0.000E+00 4.000E-03 3.000E-02 1.500E-01 3.000E-01 4.000E-01 1.000E+01 0.000E+00
0.000E+00 6.150E+02 7.000E+02 7.900E+02 8.400E+02 8.600E+02 8.000E+02 0.000E+00
*MAT_PIECEWISE_LINEAR_PLASTICITY
    12 7.850E-09 2.100E+05 3.000E-01 6.150E+02 0.000E+00 5.000E+08 0.000E+00
4.040E+01 5.000E+00 0.000E+00 0.000E+00 } Hood
0.000E+00 4.000E-03 3.000E-02 1.500E-01 3.000E-01 4.000E-01 1.000E+01 0.000E+00
0.000E+00 6.150E+02 7.000E+02 7.900E+02 8.400E+02 8.600E+02 8.000E+02 0.000E+00
*MAT_PIECEWISE_LINEAR_PLASTICITY
    13 7.850E-09 2.100E+05 3.000E-01 6.150E+02 0.000E+00 5.000E+08 0.000E+00
4.040E+01 5.000E+00 0.000E+00 0.000E+00} Passenger Side Front Panel
0.000E+00 4.000E-03 3.000E-02 1.500E-01 3.000E-01 4.000E-01 1.000E+01 0.000E+00
0.000E+00 6.150E+02 7.000E+02 7.900E+02 8.400E+02 8.600E+02 8.000E+02 0.000E+00
*MAT_PIECEWISE_LINEAR_PLASTICITY
    14 7.850E-09 2.100E+05 3.000E-01 6.150E+02 0.000E+00 5.000E+08 0.000E+00
4.040E+01 5.000E+00 0.000E+00 0.000E+00} Driver Side Front Panel
0.000E+00 4.000E-03 3.000E-02 1.500E-01 3.000E-01 4.000E-01 1.000E+01 0.000E+00
0.000E+00 6.150E+02 7.000E+02 7.900E+02 8.400E+02 8.600E+02 8.000E+02 0.000E+00
```

```
*MAT_PIECEWISE_LINEAR_PLASTICITY
      15 7.850E-09 2.100E+05 3.000E-01 6.150E+02 0.000E+00 5.000E+08 0.000E+00
 4.040E+01 5.000E+00 0.000E+00 0.000E+00
 0.000E+00 4.000E-03 3.000E-02 1.500E-01 3.000E-01 4.000E-01 1.000E+01 0.000E+00
 0.000E+00 6.150E+02 7.000E+02 7.900E+02 8.400E+02 8.600E+02 8.000E+02 0.000E+00
*MAT_PIECEWISE_LINEAR_PLASTICITY
      16 7.850E-09 2.100E+05 3.000E-01 6.150E+02 0.000E+00 5.000E+08 0.000E+00
 4.040E+01 5.000E+00 0.000E+00 0.000E+00
 0.000E+00 4.000E-03 3.000E-02 1.500E-01 3.000E-01 4.000E-01 1.000E+01 0.000E+00
 0.000E+00 6.150E+02 7.000E+02 7.900E+02 8.400E+02 8.600E+02 8.000E+02 0.000E+00
*MAT_PIECEWISE_LINEAR_PLASTICITY
      17 7.850E-09 2.100E+05 3.000E-01 6.150E+02 0.000E+00 5.000E+08 0.000E+00
 4.040E+01 5.000E+00 0.000E+00 0.000E+00
 0.000E+00 4.000E-03 3.000E-02 1.500E-01 3.000E-01 4.000E-01 1.000E+01 0.000E+00
 0.000E+00 6.150E+02 7.000E+02 7.900E+02 8.400E+02 8.600E+02 8.000E+02 0.000E+00
*MAT_PIECEWISE_LINEAR_PLASTICITY
      18 7.850E-09 2.100E+05 3.000E-01 6.150E+02 0.000E+00 5.000E+08 0.000E+00
 4.040E+01 5.000E+00 0.000E+00 0.000E+00
 0.000E+00 4.000E-03 3.000E-02 1.500E-01 3.000E-01 4.000E-01 1.000E+01 0.000E+00
 0.000E+00 6.150E+02 7.000E+02 7.900E+02 8.400E+02 8.600E+02 8.000E+02 0.000E+00
*MAT_ELASTIC
      19 1.475E-10 2.100E+05 3.000E-01
*MAT_ELASTIC
      20 1.475E-10 2.100E+05 3.000E-01
*MAT_PIECEWISE_LINEAR_PLASTICITY
      21 7.850E-09 2.100E+05 3.000E-01 6.150E+02 0.000E+00 5.000E+08 0.000E+00
 4.040E+01 5.000E+00 0.000E+00 0.000E+00
 0.000E+00 4.000E-03 3.000E-02 1.500E-01 3.000E-01 4.000E-01 1.000E+01 0.000E+00
 0.000E+00 6.150E+02 7.000E+02 7.900E+02 8.400E+02 8.600E+02 8.000E+02 0.000E+00
*MAT_PIECEWISE_LINEAR_PLASTICITY
      22 7.850E-09 2.100E+05 3.000E-01 6.150E+02 0.000E+00 5.000E+08 0.000E+00
 4.040E+01 5.000E+00 0.000E+00 0.000E+00
 0.000E+00 4.000E-03 3.000E-02 1.500E-01 3.000E-01 4.000E-01 1.000E+01 0.000E+00
 0.000E+00 6.150E+02 7.000E+02 7.900E+02 8.400E+02 8.600E+02 8.000E+02 0.000E+00
*MAT_PIECEWISE_LINEAR_PLASTICITY
      23 7.850E-09 2.100E+05 3.000E-01 6.150E+02 0.000E+00 5.000E+08 0.000E+00
 4.040E+01 5.000E+00 0.000E+00 0.000E+00 } Cab
 0.000E+00 4.000E-03 3.000E-02 1.500E-01 3.000E-01 4.000E-01 1.000E+01 0.000E+00
 0.000E+00 6.150E+02 7.000E+02 7.900E+02 8.400E+02 8.600E+02 8.000E+02 0.000E+00
*MAT_PIECEWISE_LINEAR_PLASTICITY
      24 7.850E-09 2.100E+05 3.000E-01 6.150E+02 0.000E+00 5.000E+08 0.000E+00
 4.040E+01 5.000E+00 0.000E+00 0.000E+00 } Cab Mounts
 0.000E+00 4.000E-03 3.000E-02 1.500E-01 3.000E-01 4.000E-01 1.000E+01 0.000E+00
 0.000E+00 6.150E+02 7.000E+02 7.900E+02 8.400E+02 8.600E+02 8.000E+02 0.000E+00
*MAT_PIECEWISE_LINEAR_PLASTICITY
      25 7.850E-09 2.100E+05 3.000E-01 6.150E+02 0.000E+00 5.000E+08 0.000E+00
 4.040E+01 5.000E+00 0.000E+00 0.000E+00 } Passenger Side Door
 0.000E+00 4.000E-03 3.000E-02 1.500E-01 3.000E-01 4.000E-01 1.000E+01 0.000E+00
 0.000E+00 6.150E+02 7.000E+02 7.900E+02 8.400E+02 8.600E+02 8.000E+02 0.000E+00
*MAT_PIECEWISE_LINEAR_PLASTICITY
      26 7.850E-09 2.100E+05 3.000E-01 6.150E+02 0.000E+00 5.000E+08 0.000E+00
 4.040E+01 5.000E+00 0.000E+00 0.000E+00 } Driver Side Door
 0.000E+00 4.000E-03 3.000E-02 1.500E-01 3.000E-01 4.000E-01 1.000E+01 0.000E+00
```

```
0.000E+00 6.150E+02 7.000E+02 7.900E+02 8.400E+02 8.600E+02 8.000E+02 0.000E+00
*MAT_PIECEWISE_LINEAR_PLASTICITY
     27 7.850E-09 2.100E+05 3.000E-01 6.150E+02 0.000E+00 5.000E+08 0.000E+00
4.040E+01 5.000E+00 0.000E+00 0.000E+00 } Bed
0.000E+00 4.000E-03 3.000E-02 1.500E-01 3.000E-01 4.000E-01 1.000E+01 0.000E+00
0.000E+00 6.150E+02 7.000E+02 7.900E+02 8.400E+02 8.600E+02 8.000E+02 0.000E+00
*MAT_ELASTIC
     28 7.850E-09 2.100E+05 3.000E-01 } Drive Shaft
*MAT_ELASTIC
     29 7.850E-09 2.100E+05 3.000E-01
*MAT_ELASTIC
     30 7.850E-09 2.100E+05 3.000E-01
*MAT_ELASTIC
     31 7.850E-09 2.100E+05 3.000E-01
*MAT_ELASTIC
     32 7.850E-09 2.100E+05 3.000E-01
*MAT_RIGID
     33 7.850E-09 2.100E+05 3.000E-01 0.000E+00 0.000E+00 0.000E+00
4.040E+01 5.000E+00 0.000E+00 0.000E+00
0.000E+00 0.000E+00 0.000E+00 0.000E+00 0.000E+00 0.000E+00 0.000E+00 0.000E+00
*MAT_RIGID
     34 7.850E-09 2.100E+05 3.000E-01 0.000E+00 0.000E+00 0.000E+00
4.040E+01 5.000E+00 0.000E+00 0.000E+00 } Driver Side Rotar
0.000E+00 0.000E+00 0.000E+00 0.000E+00 0.000E+00 0.000E+00 0.000E+00 0.000E+00
*MAT_RIGID
     35 7.850E-09 2.100E+05 3.000E-01 0.000E+00 0.000E+00 0.000E+00
4.040E+01 5.000E+00 0.000E+00 0.000E+00
0.000E+00 0.000E+00 0.000E+00 0.000E+00 0.000E+00 0.000E+00 0.000E+00 0.000E+00
*MAT_RIGID
     36 7.850E-09 2.100E+05 3.000E-01 0.000E+00 0.000E+00 0.000E+00
4.040E+01 5.000E+00 0.000E+00 0.000E+00 } Passenger Side Rotar
0.000E+00 0.000E+00 0.000E+00 0.000E+00 0.000E+00 0.000E+00 0.000E+00 0.000E+00
*MAT_RIGID
     37 7.850E-09 2.100E+05 3.000E-01 0.000E+00 0.000E+00 0.000E+00
4.040E+01 5.000E+00 0.000E+00 0.000E+00 } Accelerometer
0.000E+00 0.000E+00 0.000E+00 0.000E+00 0.000E+00 0.000E+00 0.000E+00 0.000E+00
*DEFINE_CURVE
     2      0 0.000E+00 0.000E+00 0.000E+00 0.000E+00 } Strain Rate Curve for Concrete
$    strain rate      yield strength multiplier      concrete
       1.00E-06          1.0E+00
       1.00E-03          1.1E+00
       1.00E-02         1.15E+00
       1.00E-01          1.2E+00
       6.00E+00          1.8E+00
*DEFINE_CURVE
     3      0 0.000E+00 0.000E+00 0.000E+00 0.000E+00 } Strain Rate Curve for Steel
$    strain rate      yield strength multiplier      steel
       1.00E-06          1.0E+00
       1.00E-05         1.037E+00
       1.00E-04         1.076E+00
       1.00E-03         1.120E+00
       1.00E-02         1.190E+00
       1.00E-01         1.301E+00
```

```
        1.00E+00        1.477E+00
        1.00E+01        1.756E+00
*EOS_TABULATED_COMPACTION
      1 0.000E+00 0.000E+00 1.000E+00
    0.000E+00    -4.125E-04    -6.800E-02    -1.000E-01

    0.000E+00     5.171E+00     2.149E+02     4.631E+02

    0.000E+00     0.000E+00     0.000E+00     0.000E+00

    1.254E+04     1.254E+04     1.254E+04     1.254E+04

*MAT_PSEUDO_TENSOR
$    mid      ro       g       pr
      38 2.400E-09 1.020E+04 1.800E-01
$   sigf      a0      a1      a2      a0f     a1f      b1      per
 2.586E+00 6.464E+00 3.333E-01 1.289E-02 2.586E+00 1.500E+00 1.250E+00 2.270E+00
$     er      prr     sigy    etan     lcp     lcr
 2.068E+05 3.000E-01 4.137E+02 7.584E+02 2.000E+00 3.000E+00
$    eps1     eps2     eps3     eps4     eps5     eps6     eps7     eps8
     0.0  8.62e-06  2.15e-05  3.14e-05  3.95e-05  5.17e-04  6.38e-04  7.98e-04
$    eps9    eps10    eps11    eps12    eps13    eps14    eps15    eps16
  9.67e-04  1.41e-03  1.97e-03  2.59e-03  3.27e-03  4.00e-03  4.79e-03    .909
$     es1      es2      es3      es4      es5      es6      es7      es8
    0.309    .543     .840     .975     1.00     .790     .630     .469
$     es9     es10     es11     es12     es13     es14     es15     es16
    0.383    .247     .173     .136     .114     .086     .056     .0
*MAT_ELASTIC
      39 7.850E-09 2.000E+10 3.300E-01
*SECTION_SHELL
       1       7 0.000E+00 0.000E+00 0.000E+00 0.000E+00
 2.700E+00 2.700E+00 2.700E+00 2.700E+00 0.000E+00
*SECTION_SHELL
       2       2 0.000E+00 0.000E+00 0.000E+00 0.000E+00
 3.100E+00 3.100E+00 3.100E+00 3.100E+00 0.000E+00
*SECTION_SHELL
       3       2 0.000E+00 0.000E+00 0.000E+00 0.000E+00
 4.700E+00 4.700E+00 4.700E+00 4.700E+00 0.000E+00
*SECTION_SHELL
       4       2 0.000E+00 0.000E+00 0.000E+00 0.000E+00
 4.700E+00 4.700E+00 4.700E+00 4.700E+00 0.000E+00
*SECTION_SHELL
       5       2 0.000E+00 0.000E+00 0.000E+00 0.000E+00
 3.700E+00 3.700E+00 3.700E+00 3.700E+00 0.000E+00
*SECTION_SHELL
       6       2 0.000E+00 0.000E+00 0.000E+00 0.000E+00
 3.700E+00 3.700E+00 3.700E+00 3.700E+00 0.000E+00
*SECTION_SHELL
       7       2 0.000E+00 0.000E+00 0.000E+00 0.000E+00
 3.700E+00 3.700E+00 3.700E+00 3.700E+00 0.000E+00
*SECTION_SOLID
       8       1
*SECTION_SHELL
```

Equation of State for Concrete Material

Concrete Material 16 smeared reinforcement

Elastic Material for ground. Presentation Purposes Only.

Bumper

Frame

Tires

Engine and Transmission

```
      9       2 0.000E+00 0.000E+00 0.000E+00 0.000E+00
 3.000E+00 3.000E+00 3.000E+00 3.000E+00 0.000E+00
*SECTION_SHELL
      10      2 0.000E+00 0.000E+00 0.000E+00 0.000E+00
 2.000E+00 2.000E+00 2.000E+00 2.000E+00 0.000E+00
*SECTION_SHELL
      11      2 0.000E+00 0.000E+00 0.000E+00 0.000E+00
 2.000E+00 2.000E+00 2.000E+00 2.000E+00 0.000E+00
*SECTION_SHELL
      12      7 0.000E+00 0.000E+00 0.000E+00 0.000E+00} Hood
 4.000E+00 4.000E+00 4.000E+00 4.000E+00 0.000E+00
*SECTION_SHELL
      13      2 0.000E+00 0.000E+00 0.000E+00 0.000E+00} Passenger Side Front Panel
 1.100E+00 1.100E+00 1.100E+00 1.100E+00 0.000E+00
*SECTION_SHELL
      14      2 0.000E+00 0.000E+00 0.000E+00 0.000E+00} Driver Side Front Panel
 1.100E+00 1.100E+00 1.100E+00 1.100E+00 0.000E+00
*SECTION_SHELL
      15      2 0.000E+00 0.000E+00 0.000E+00 0.000E+00
 7.500E-01 7.500E-01 7.500E-01 7.500E-01 0.000E+00
*SECTION_SHELL
      16      2 0.000E+00 0.000E+00 0.000E+00 0.000E+00
 7.500E-01 7.500E-01 7.500E-01 7.500E-01 0.000E+00
*SECTION_SHELL
      17      2 0.000E+00 0.000E+00 0.000E+00 0.000E+00
 1.100E+00 1.100E+00 1.100E+00 1.100E+00 0.000E+00
*SECTION_SHELL
      18      2 0.000E+00 0.000E+00 0.000E+00 0.000E+00
 1.000E+00 1.000E+00 1.000E+00 1.000E+00 0.000E+00
*SECTION_SOLID
      19      1
*SECTION_SOLID
      20      1
*SECTION_SHELL
      21      2 0.000E+00 0.000E+00 0.000E+00 0.000E+00
 1.500E+00 1.500E+00 1.500E+00 1.500E+00 0.000E+00
*SECTION_SHELL
      22      2 0.000E+00 0.000E+00 0.000E+00 0.000E+00
 1.500E+00 1.500E+00 1.500E+00 1.500E+00 0.000E+00
*SECTION_SHELL
      23      2 0.000E+00 0.000E+00 0.000E+00 0.000E+00} Cab
 2.500E+00 2.500E+00 2.500E+00 2.500E+00 0.000E+00
*SECTION_SHELL
      24      2 0.000E+00 0.000E+00 0.000E+00 0.000E+00 } Cab Mounts
 2.300E+00 2.300E+00 2.300E+00 2.300E+00 0.000E+00
*SECTION_SHELL
      25      2 0.000E+00 0.000E+00 0.000E+00 0.000E+00} Passenger Door
 2.500E+00 2.500E+00 2.500E+00 2.500E+00 0.000E+00
*SECTION_SHELL
      26      2 0.000E+00 0.000E+00 0.000E+00 0.000E+00 } Driver Door
 2.500E+00 2.500E+00 2.500E+00 2.500E+00 0.000E+00
*SECTION_SHELL
      27      2 0.000E+00 0.000E+00 0.000E+00 0.000E+00} Bed
```

```
3.500E+00 3.500E+00 3.500E+00 3.500E+00 0.000E+00
*SECTION_BEAM
     28       2 0.000E+00 0.000E+00 0.000E+00 0.000E+00
 1.508E+03 4.800E+06 4.800E+06 9.650E+06 7.539E+02 0.000E+00
*SECTION_BEAM
     29       2 0.000E+00 0.000E+00 0.000E+00
 4.524E+02 1.629E+04 1.629E+04 3.257E+04 4.072E+02 0.000E+00
*SECTION_BEAM
     30       2 0.000E+00 0.000E+00 0.000E+00
 2.000E+03 1.042E+06 1.070E+06 3.347E+05 1.667E+03 0.000E+00
*SECTION_BEAM
     31       2 0.000E+00 0.000E+00 0.000E+00
 4.524E+02 1.629E+04 1.629E+04 3.257E+04 4.072E+02 0.000E+00
*SECTION_BEAM
     32       2 0.000E+00 0.000E+00 0.000E+00
 4.524E+02 1.629E+04 1.629E+04 3.257E+04 4.072E+02 0.000E+00
*SECTION_SHELL
     33       2 0.000E+00 0.000E+00 0.000E+00 0.000E+00
 1.000E+00 1.000E+00 1.000E+00 1.000E+00 0.000E+00
*SECTION_SOLID
     34       1
*SECTION_SHELL
     35       2 0.000E+00 0.000E+00 0.000E+00 0.000E+00
 1.000E+00 1.000E+00 1.000E+00 1.000E+00 0.000E+00
*SECTION_SOLID
     36       1
*SECTION_SOLID
     37       0
*SECTION_SOLID
     38       0
*SECTION_SHELL
     39       2 0.000E+00 0.000E+00 0.000E+00 0.000E+00
 0.000E+00 0.000E+00 0.000E+00 0.000E+00 0.000E+00
*PART
MAT.-TYPE: 24    ** LINEAR ISOTROPIC PLAST. **  SHELL: S/R CO-ROTATIONAL HUGHES
     1       1       1       0
*PART
MAT.-TYPE: 24    ** LINEAR ISOTROPIC PLAST. **  SHELL: BELYTSCHKO-TSAY
     2       2       2       0
*PART
MAT.-TYPE: 24    ** LINEAR ISOTROPIC PLAST. **  SHELL: BELYTSCHKO-TSAY
     3       3       3       0
*PART
MAT.-TYPE: 24    ** LINEAR ISOTROPIC PLAST. **  SHELL: BELYTSCHKO-TSAY
     4       4       4       0
*PART
MAT.-TYPE: 24    ** LINEAR ISOTROPIC PLAST. **  SHELL: BELYTSCHKO-TSAY
     5       5       5       0
*PART
MAT.-TYPE: 24    ** LINEAR ISOTROPIC PLAST. **  SHELL: BELYTSCHKO-TSAY
     6       6       6       0
*PART
MAT.-TYPE: 24    ** LINEAR ISOTROPIC PLAST. **  SHELL: BELYTSCHKO-TSAY
```

Drive Shaft

Driver Side Rotar

Passenger Side Rotar

Accelerometer

Concrete Barrier

Ground

Bumper

Frame

```
     7      7      7      0 } Tires
*PART
MAT.-TYPE: 1    ** ELASTIC - STEEL **        SOLID: CONSTANT STRESS
     8      8      8      0} Engine and Transmission
*PART
MAT.-TYPE: 24   ** LINEAR ISOTROPIC PLAST. ** SHELL: BELYTSCHKO-TSAY
     9      9      9      0
*PART
MAT.-TYPE: 24   ** LINEAR ISOTROPIC PLAST. ** SHELL: BELYTSCHKO-TSAY
    10     10     10      0
*PART
MAT.-TYPE: 24   ** LINEAR ISOTROPIC PLAST. ** SHELL: BELYTSCHKO-TSAY
    11     11     11      0
*PART
MAT.-TYPE: 24   ** LINEAR ISOTROPIC PLAST. ** SHELL: S/R CO-ROTATIONAL HUGHES
    12     12     12      0 } Hood
*PART
MAT.-TYPE: 24   ** LINEAR ISOTROPIC PLAST. ** SHELL: BELYTSCHKO-TSAY
    13     13     13      0 } Passenger Front Panel
*PART
MAT.-TYPE: 24   ** LINEAR ISOTROPIC PLAST. ** SHELL: BELYTSCHKO-TSAY
    14     14     14      0 } Driver Door Panel
*PART
MAT.-TYPE: 24   ** LINEAR ISOTROPIC PLAST. ** SHELL: BELYTSCHKO-TSAY
    15     15     15      0
*PART
MAT.-TYPE: 24   ** LINEAR ISOTROPIC PLAST. ** SHELL: BELYTSCHKO-TSAY
    16     16     16      0
*PART
MAT.-TYPE: 24   ** LINEAR ISOTROPIC PLAST. ** SHELL: BELYTSCHKO-TSAY
    17     17     17      0
*PART
MAT.-TYPE: 24   ** LINEAR ISOTROPIC PLAST. ** SHELL: BELYTSCHKO-TSAY
    18     18     18      0
*PART
MAT.-TYPE: 1    ** ELASTIC - STEEL **        SOLID: CONSTANT STRESS
    19     19     19      0
*PART
MAT.-TYPE: 1    ** ELASTIC - STEEL **        SOLID: CONSTANT STRESS
    20     20     20      0
*PART
MAT.-TYPE: 24   ** LINEAR ISOTROPIC PLAST. ** SHELL: BELYTSCHKO-TSAY
    21     21     21      0
*PART
MAT.-TYPE: 24   ** LINEAR ISOTROPIC PLAST. ** SHELL: BELYTSCHKO-TSAY
    22     22     22      0
*PART
MAT.-TYPE: 24   ** LINEAR ISOTROPIC PLAST. ** SHELL: BELYTSCHKO-TSAY
    23     23     23      0 } Cab
*PART
MAT.-TYPE: 24   ** LINEAR ISOTROPIC PLAST. ** SHELL: BELYTSCHKO-TSAY
    24     24     24      0 } Cab Mounts
*PART
```

```
MAT.-TYPE: 24   ** LINEAR ISOTROPIC PLAST. ** SHELL: BELYTSCHKO-TSAY
    27     25     25     0 } Passenger Door
*PART
MAT.-TYPE: 24   ** LINEAR ISOTROPIC PLAST. ** SHELL: BELYTSCHKO-TSAY
    28     26     26     0 } Driver Door
*PART
MAT.-TYPE: 24   ** LINEAR ISOTROPIC PLAST. ** SHELL: BELYTSCHKO-TSAY
    31     27     27     0 } Bed
*PART
MAT.-TYPE: 1    ** ELASTIC - STEEL **       BEAM: BELYTSCHKO-TSAY
    34     28     28     0 } Drive Shaft
*PART
MAT.-TYPE: 1    ** ELASTIC - STEEL **       BEAM: BELYTSCHKO-TSAY
    35     29     29     0
*PART
MAT.-TYPE: 1    ** ELASTIC - STEEL **       BEAM: BELYTSCHKO-TSAY
    36     30     30     0
*PART
MAT.-TYPE: 1    ** ELASTIC - STEEL **       BEAM: BELYTSCHKO-TSAY
    38     31     31     0
*PART
MAT.-TYPE: 1    ** ELASTIC - STEEL **       BEAM: BELYTSCHKO-TSAY
    39     32     32     0
*PART
MAT.-TYPE: 20   ** RIGID **             SHELL: BELYTSCHKO-TSAY
    40     33     33     0
*PART
MAT.-TYPE: 20   ** RIGID **             SOLID: CONSTANT STRESS
    41     34     34     0 } Driver Side Rotar
*PART
MAT.-TYPE: 20   ** RIGID **             SHELL: BELYTSCHKO-TSAY
    42     35     35     0
*PART
MAT.-TYPE: 20   ** RIGID **             SOLID: CONSTANT STRESS
    43     36     36     0 } Passenger Side Rotar
*PART
MAT.-TYPE: 20   ** RIGID **     SOLID: CONSTANT STRESS * accelerometer
    44     37     37     0 } Accelerometer
*PART
material 16s * concrete * SOLID: CONSTANT STRESS *  EOS 1
    45     38     38     1 } Concrete Barrier
*PART
material ..elastic * ground (model just for graphic presentation purposes)
    46     39     39     0 } Ground
*NODE
    1 1.205869629E+03 5.410858154E+02 8.883851562E+03     0     0 } Nodal Coordinates.
    2 1.208535400E+03 4.998131409E+02 8.885750000E+03     0     0
    3 1.204216431E+03 4.574236145E+02 8.878021484E+03     0     0
    4 1.191199951E+03 5.463658447E+02 8.854274414E+03     0     0
    5 1.189111938E+03 5.040981750E+02 8.849803711E+03     0     0
    6 1.184834839E+03 4.638894348E+02 8.840641602E+03     0     0
    7 1.181720459E+03 5.704509888E+02 8.828259766E+03     0     0
    8 1.172962524E+03 5.165388184E+02 8.816743164E+03     0     0
```

```
    9 1.173195435E+03 4.676535339E+02 8.798336914E+03     0     0
   10 1.137846191E+03 5.050289001E+02 8.776362305E+03     0     0
*ELEMENT_SOLID
  7000     8  7034  7035  7000  7038  7048  7049  7053  7052
  7001     8  7035  7036  7040  7000  7049  7050  7054  7053
  7002     8  7036  7037  7041  7040  7050  7051  7055  7054
  7003     8  7038  7000  7043  7042  7052  7053  7057  7056
  7004     8  7000  7040  7044  7043  7053  7054  7058  7057
  7005     8  7040  7041  7045  7044  7054  7055  7059  7058
  7006     8  7042  7043  7046  7001  7056  7057  7061  7060
  7007     8  7043  7044  7002  7046  7057  7058  7062  7061
  7008     8  7044  7045  7047  7002  7058  7059  7063  7062
  7009     8  7048  7049  7053  7052  7064  7065  7069  7068
  7010     8  7049  7050  7054  7053  7065  7066  7070  7069
*ELEMENT_BEAM
  2649    38  1875  1912  22098
  2650    38  2082  1624  22098
  2651    38  1911  1869  22098
  2652    38  1629  2084  22098
  6500    36  6500  6501  22098
  6501    36  6501  6502  22098
  6502    36  6502  6503  22098
  6503    36  6503  6504  22098
  6504    36  6504  6505  22098
  6505    36  6506  6507  22098
*ELEMENT_SHELL
     1     1     1     2     5     4
     2     1     2     3     6     5
     3     1     4     5     8     7
     4     1     5     6     9     8
     5     1     8     9    10    11
     6     1    11    10    13    12
     7     1     9    14    15    10
     8     1    10    15    16    13
     9     1     3    21    22     6
    10     1     6    22    14     9
*ELEMENT_SHELL_THICKNESS_BETA
 35133    46 35166 35167 35175 35174
2.00000000E+00 2.00000000E+00 2.00000000E+00 2.00000000E+00 0.00000000E+00
 35134    46 35167 35168 35176 35175
2.00000000E+00 2.00000000E+00 2.00000000E+00 2.00000000E+00 0.00000000E+00
 35135    46 35168 35169 35177 35176
2.00000000E+00 2.00000000E+00 2.00000000E+00 2.00000000E+00 0.00000000E+00
 35136    46 35169 35170 35178 35177
2.00000000E+00 2.00000000E+00 2.00000000E+00 2.00000000E+00 0.00000000E+00
 35137    46 35170 35171 35179 35178
2.00000000E+00 2.00000000E+00 2.00000000E+00 2.00000000E+00 0.00000000E+00
 35138    46 35171 35172 35180 35179
2.00000000E+00 2.00000000E+00 2.00000000E+00 2.00000000E+00 0.00000000E+00
 35139    46 35172 35173 35181 35180
2.00000000E+00 2.00000000E+00 2.00000000E+00 2.00000000E+00 0.00000000E+00
 35140    46 35174 35175 35183 35182
2.00000000E+00 2.00000000E+00 2.00000000E+00 2.00000000E+00 0.00000000E+00
```

Cont.

} Solid Elements.

Cont.

} Beam Elements between first two nodes. Third Node defines orientation.

Cont.

} Shell Element defined between four nodes.

Cont.

} Thickness of shell elements.

```
 35141    46  35175  35176  35184  35183
2.00000000E+00 2.00000000E+00 2.00000000E+00 2.00000000E+00 0.00000000E+00
 35142    46  35176  35177  35185  35184
2.00000000E+00 2.00000000E+00 2.00000000E+00 2.00000000E+00 0.00000000E+00
 35143    46  35177  35178  35186  35185
```

Cont.

```
*DATABASE_HISTORY_NODE
  16077   16346   16761   16762
*CONSTRAINED_SPOTWELD
    304    1413
*CONSTRAINED_SPOTWELD
     57    1087
*CONSTRAINED_SPOTWELD
  13263   12282
*CONSTRAINED_SPOTWELD
  13262   12453
*CONSTRAINED_SPOTWELD
  13012   12014
*CONSTRAINED_SPOTWELD
  13011   12246
*CONSTRAINED_SPOTWELD
   3575    2764
*CONSTRAINED_SPOTWELD
   3577    2775
*CONSTRAINED_SPOTWELD
   3565    2631
*CONSTRAINED_SPOTWELD
   3563    2621
*INITIAL_VELOCITY_NODE
     1-1.174E+04 0.000E+00-2.518E+04
     2-1.174E+04 0.000E+00-2.518E+04
     3-1.174E+04 0.000E+00-2.518E+04
     4-1.174E+04 0.000E+00-2.518E+04
     5-1.174E+04 0.000E+00-2.518E+04
     6-1.174E+04 0.000E+00-2.518E+04
     7-1.174E+04 0.000E+00-2.518E+04
     8-1.174E+04 0.000E+00-2.518E+04
     9-1.174E+04 0.000E+00-2.518E+04
    10-1.174E+04 0.000E+00-2.518E+04
```

Intial Velocities. Nodes 1-35165 represent truck. All remaining nodes are barrier and ground with velocity equal zero.

Cont.

```
*CONSTRAINED_RIGID_BODIES
    40      41
    42      43
*CONSTRAINED_EXTRA_NODES_SET
    40       1
*SET_NODE_LIST
     1
   4000    4007    4029    4034    4042    4057    5003    5011
   5020    5024    5027    5028
*CONSTRAINED_EXTRA_NODES_SET
    41       2
*SET_NODE_LIST
     2
  23524   23525   23526   23527   23528   23529   23530   23531
  23532   23533
```

```
*CONSTRAINED_EXTRA_NODES_SET
    42      3
*SET_NODE_LIST
     3
   3500    3507    3529    3534    3542    3558    4503    4511
   4520    4524    4527    4528
*CONSTRAINED_EXTRA_NODES_SET
    43      4
*SET_NODE_LIST
     4
  24641   24642   24643   24644   24645   24646   24647   24648
  24649   24650
*CONSTRAINED_EXTRA_NODES_SET
    44      5
*SET_NODE_LIST
     5
  16191   16192   16196   16197
*ELEMENT_SEATBELT_ACCELEROMETER
     1   35158   35159   35160
*CONSTRAINED_NODAL_RIGID_BODY
     6      0
*SET_NODE_LIST
     6
   2720    2723    2725    2728    2731    2732   22000   22019
  22020   22105
*CONSTRAINED_NODAL_RIGID_BODY
     7      0
*SET_NODE_LIST
     7
   2733    2736    2738    2741    2744    2745   22001   22021
  22030   22169
*CONSTRAINED_NODAL_RIGID_BODY
     8      0
*SET_NODE_LIST
     8
   1833    1834    1835    1836    1837    1838    1839    1840
   1872    1873    1874    1875    1876    1877    1878    1902
  22011   22018   22214   22215
*CONSTRAINED_NODAL_RIGID_BODY
     9      0
*SET_NODE_LIST
     9
   2061    2062    2063    2064    2065    2066    2067    2068
   2080    2081    2082    2083    2084    2085    2086    2109
  22008   22009   22196   22197
*CONSTRAINED_NODAL_RIGID_BODY
    10      0
*SET_NODE_LIST
    10
  15135   15204   15205   15206   15207   15208   15209   15210
  15655   15656   15657   15658   15659   15660   15661   15662
*CONSTRAINED_NODAL_RIGID_BODY
    11      0
```

Accelerometer as defined in Chapter 7.4

```
*SET_NODE_LIST
     11
   15039   15040   15041   15042   15043   15044   15045   15046
   15550   15551   15678   15761   15762   15763   15764   15765
*CONSTRAINED_NODAL_RIGID_BODY
     12      0
*SET_NODE_LIST
     12
    7004    7006    7009    7012    8073    8083    8084    8089
    8100    8122    8187    8188    8189
*CONSTRAINED_NODAL_RIGID_BODY
     13      0
*SET_NODE_LIST
     13
    7014    7015    8180    8183    8184    8185    8186
*CONSTRAINED_NODAL_RIGID_BODY
     14      0
*SET_NODE_LIST
     14
    7018    7019    9005
*CONSTRAINED_NODAL_RIGID_BODY
     15      0
*SET_NODE_LIST
     15
    9004    9009    9011
*CONSTRAINED_NODAL_RIGID_BODY
     16      0
*SET_NODE_LIST
     16
   17050   17051   20118
*CONSTRAINED_NODAL_RIGID_BODY
     17      0
*SET_NODE_LIST
     17
   16000   17048   20121
*CONSTRAINED_NODAL_RIGID_BODY
     18      0
*SET_NODE_LIST
     18
   17073   20082   20083
*CONSTRAINED_NODAL_RIGID_BODY
     19      0
*SET_NODE_LIST
     19
   16490   20612   20613
*CONSTRAINED_NODAL_RIGID_BODY
     20      0
*SET_NODE_LIST
     20
   16488   16492   20616
*CONSTRAINED_NODAL_RIGID_BODY
     21      0
*SET_NODE_LIST
```

```
    21
   16512   20573   20574
*CONSTRAINED_NODAL_RIGID_BODY
    22      0
*SET_NODE_LIST
    22
   16514   20577   20578
*CONSTRAINED_NODAL_RIGID_BODY
    23      0
*SET_NODE_LIST
    23
   10562   10570   16509   16510
*CONSTRAINED_NODAL_RIGID_BODY
    24      0
*SET_NODE_LIST
    24
   10582   10584   16498   16511
*CONSTRAINED_NODAL_RIGID_BODY
    25      0
*SET_NODE_LIST
    25
   10061   10069   17069   17070
*CONSTRAINED_NODAL_RIGID_BODY
    26      0
*SET_NODE_LIST
    26
   10081   10083   16001   17057
*CONSTRAINED_NODAL_RIGID_BODY
    27      0
*SET_NODE_LIST
    27
   17013   20078   20079
*CONSTRAINED_NODAL_RIGID_BODY
    28      0
*SET_NODE_LIST
    28
    7003    7005    7007    7011    7013    8002    8012    8017
    8036    8178    8179    8181
*CONSTRAINED_NODAL_RIGID_BODY
    29      0
*SET_NODE_LIST
    29
   14112   14114   14118   14122   14126   14130   14540   14542
   14546   14550   14554   14558
*CONSTRAINED_NODAL_RIGID_BODY
    30      0
*SET_NODE_LIST
    30
   14113   14115   14119   14123   14131   14601   14603   14607
   14611   14619
*CONSTRAINED_NODAL_RIGID_BODY
    31      0
*SET_NODE_LIST
```

```
    31
    23      58    1011    1085    1355
*CONSTRAINED_NODAL_RIGID_BODY
    32       0
*SET_NODE_LIST
    32
   309     310    1418    1419
*CONSTRAINED_NODAL_RIGID_BODY
    33       0
*SET_NODE_LIST
    33
   250     251     270     271    1010    1091    1411    1412
  1414    1415
*CONSTRAINED_NODAL_RIGID_BODY
    34       0
*SET_NODE_LIST
    34
   252     265    1008    1088
*CONSTRAINED_NODAL_RIGID_BODY
    35       0
*SET_NODE_LIST
    35
     1       2       3      17      19      20      25    1242
  1356    1357    1359    1360
*DEFINE_CURVE                                                    } Gravity Load Curve
     1       0 0.000E+00 0.000E+00 0.000E+00 0.000E+00
  0.00000005E+00    9.81000000E+03
  4.00000006E-01    9.81000000E+03
*LOAD_BODY_Y
     1 1.000E+00       1 } Gravity Applied in Y-Direction
*RIGIDWALL_PLANAR_ORTHO
    36                   } Rigidwall Representing Ground
  0.000   0.000   0.000  0.00000  1.00000  0.00000  0.00000
  0.000   0.600   0.000  0.50000  0.00000  0.00000
  6522    7000
*SET_NODE_LIST } Nodes which cannot pass through ground (tires)
    36
  23014   23018   23022   23158   23162   23166   23680   23684
  23688   23824   23828   23832   24131   24135   24139   24275
  24279   24283   24797   24801   24805   24940   24945   24949
*CONTACT_AUTOMATIC_SINGLE_SURFACE                    } Automatic Contact Card
     1       0       2       0       0       0       0       0
3.500E-01 3.000E-01 2.660E-04 0.000E+00 0.000E+00       0 0.000E+00 0.000E+00
1.000E+00 1.000E+00 0.000E+00 0.000E+00 0.000E+00 0.000E+00
*SET_PART
     1      38 } Parts to be included in automatic contact
     1       2       3       4       5       6       7       8
     9      10      11      12      13      14      15      16
    17      18      19      20      21      22      23      24
    27      28      31      34      35      36      38      39
    40      41      42      43      44      45
*END
```

APPENDIX E

BUDGET SUMMARY

The following is a summary of expenditures for the project entitled "Conceptual Analysis of an Aesthetic Bridge Barrier". The Florida Department of Transportation budget number is WPI-0510750 and the Florida State University budget number is 6120-524-39.

BUDGET SUMMARY FOR D.O.T STUDENT RESEARCH/CLERICAL-TECHNICAL ASSISTANT/P.I SALARIES (FSU- 6120-524-39)

STUDENT (MS)	APPOINTMENT PERIOD	APPOINTMENT AMOUNT ENCUMBRANCE	AMOUNT DISPERSED	AMOUNT REMAINING
Gilbert, Christ (2/28/96-6/23/98)	4/29/96-8/23/96	$7,140.00	$3,706.50	$3,433.50
(6/24/96-10/22/96)	8/26/96- 12/31/96	$3,864.00	$4,662.00	$2,635.50
(10/22/96-2/5/97)	1/6/97-4/22/97	$3,234.00	$2,831.64	$3,037.86
(2/6/97-4/4/97)	1/6/97-4/22/97	Same as above	$1,730.40	**$1,307.46 (Subtotal)**
Kreja, Ireneusz (6/24/96-10/22/96	8/17/96-4/22/97	$20,503.68	$8,934.08	$11,569.60
(10/23/96-2/5/97)	8/17/96-4/22/97	Same as above.	$6,847.04	$4,722.56
(2/6/97-4/4/97	Same as above	Same as above	$4,633.60	**88.96 (Subtotal)**
TOTAL		**$34,741.68**	**$33,345.26**	**$1,396.42**

Clerical/Technical Assistant	APPOINTMENT PERIOD	APPOINTMENT AMOUNT ENCUMBRANCE	AMOUNT DISPERSED	AMOUNT REMAINING
Johnnye B. Morris (6/24/96-10/22/96)	07/1/96-4/22/97	$3,440.00	$1,135.68	$2,304.32
(10/23/96-2/5/97)	Same as above.	Same as above	$1,135.82	$1,168.50
(2/7/97-4/4/97)	Same as above	Same as above	$ 649.04	$ 519.46
TOTAL		**$3,440.00**	**$2,920.54**	**$ 519.46**

Principal Investigator	APPOINTMENT PERIOD	APPOINTMENT AMOUNT ENCUMBRANCE	AMOUNT DISPERSED	AMOUNT REMAINING
Jerry W. Wekezer (6/24/96-10/22/96)	06/4/96-8/5/97	$16,153.83	**$16,153.83**	$0.00
TOTAL		$16,153.83	**$16,153.83**	$0.00

APPENDIX F

CONTEST FLYER

$$$$$$$$$$$$$$$$$$$$$$$$$$$$$$$$$$$$

ATTENTION!

The Civil Engineering Department of the FAMU/FSU College of Engineering and the Florida Department of Transportation are currently offering $300 to the best concept of a design of an aesthetic bridge barrier. Entries should be neat sketches and consist of a front view and a side view preferably on AutoCAD. All entries should be submitted by November 22, 1996 in CEB Rm 129b (Civil Engineering Office) or directed to Dr. Moussa Issa (Mail Station 80). If you have any questions please direct them to Chris Gilbert in CEB Rm 129b (904) 487-6381 or e-mail him at gilbert@eng.fsu.edu. All entries should be submitted in a sealed envelope with the contestants name, phone number, and e-mail address on the envelope and back of drawing. Shown below are some examples of aesthetic bridge barriers to get you started. Good Luck!

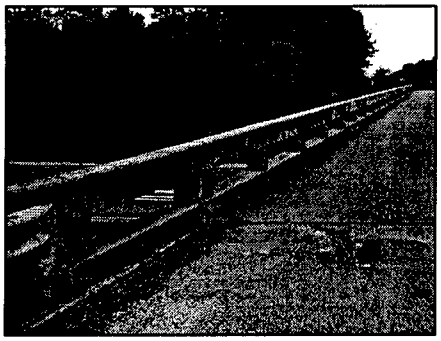

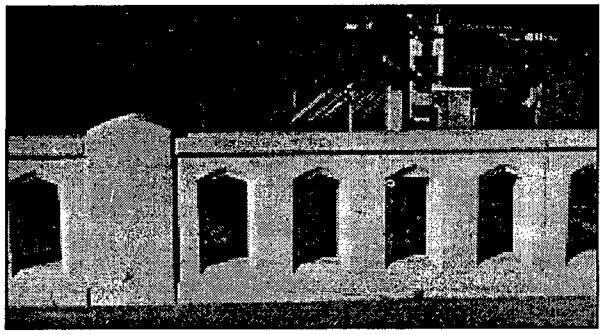

Reproduced by NTIS

National Technical Information Service
Springfield, VA 22161

This report was printed specifically for your order from nearly 3 million titles available in our collection.

For economy and efficiency, NTIS does not maintain stock of its vast collection of technical reports. Rather, most documents are printed for each order. Documents that are not in electronic format are reproduced from master archival copies and are the best possible reproductions available. If you have any questions concerning this document or any order you have placed with NTIS, please call our Customer Service Department at (703) 487-4660.

About NTIS

NTIS collects scientific, technical, engineering, and business related information — then organizes, maintains, and disseminates that information in a variety of formats — from microfiche to online services. The NTIS collection of nearly 3 million titles includes reports describing research conducted or sponsored by federal agencies and their contractors; statistical and business information; U.S. military publications; audiovisual products; computer software and electronic databases developed by federal agencies; training tools; and technical reports prepared by research organizations worldwide. Approximately 100,000 *new* titles are added and indexed into the NTIS collection annually.

For more information about NTIS products and services, call NTIS at (703) 487-4650 and request the free *NTIS Catalog of Products and Services*, PR-827LPG, or visit the NTIS Web site **http://www.ntis.gov**.

NTIS
Your indispensable resource for government-sponsored information—U.S. and worldwide

U.S. DEPARTMENT OF COMMERCE
Technology Administration
National Technical Information Service
Springfield, VA 22161 (703) 487-4650